SOFT COMPUTING ASSISTED MODELLING OF SYMMETRIC AND ASYMMETRIC COLD FLAT ROLLING PROCESSES

A Thesis Submitted in Partial Fulfillment of the Requirements

for the Degree of

DOCTOR OF PHILOSOPHY

by

Prashant P. Gudur

(Roll No. 04610303)

Department of Mechanical Engineering,

Indian Institute of Technology Guwahati,

Guwahati–781039,

INDIA

August 2008

Department of Mechanical Engineering,
Indian Institute of Technology Guwahati,
Guwahati-781039,
INDIA

CERTIFICATE

It is certified that the work contained in the Thesis entitled "**Soft Computing Assisted Modelling of Symmetric and Asymmetric Cold Flat Rolling Processes**" submitted by **Mr. Prashant P. Gudur** to the Indian Institute of Technology Guwahati for the award of the degree of Doctor of Philosophy has been carried out under my supervision in the Department of Mechanical Engineering, Indian Institute of Technology Guwahati. This work has not been submitted elsewhere for the award of any other degree or diploma.

21-08-2008

Dr. U.S. Dixit

Professor and Head,
Department of Mechanical Engineering,
Indian Institute of Technology Guwahati,
Guwahati– 781039,
INDIA

Dedicated to.....

My family.....

Acknowledgement

This thesis is the result of four years of work whereby I have been accompanied and supported by many people. It is a pleasant aspect that I have now the opportunity to express my gratitude for all of them.

I would like to express my sincere gratitude towards my supervisor, Prof. U.S. Dixit, for his guidance and encouragement during the research work. My thesis would not have been in the present shape without his invaluable support, advice and motivation. I would like to thank my doctoral committee members, Prof P.S. Robi, Dr. A.K. Singh and Prof. A.D. Sahasrabudhe for their valuable suggestions, and encouragement during the period of my research work. I am grateful to the head of the mechanical engineering department, Prof. U.S. Dixit for extending various facilities during the tenure of my doctoral programme. I would like thank Dr. S.R.M. Prasanna of Electronics department and Mr. D.K. Sarma (AWS, IIT Guwahati) for providing moral support during the thesis writing stage. Their help is immensely acknowledged.

I owe my thanks to all my friends especially Milind Salunkhe, Vadiraja, Ashok Alwal, Shounak Basak, Mahadevan, Manoj Sinha, Sandeep Gunjal, Chandrakant Maheshwari, Ajinaath Kamble, Sachin Singh, Tapan Mishra, Imran-Ur-Rehmaan, Bittagopal Mondal, Rajesh Kanna, Shiv Shankar and Jayana. I would like to express my thanks to all other research scholars and friends from Siang hostel, IIT Guwahati for their supports, advice and many helps. I would like to thanks Prof. Jois and Mrs. Jois, Prof. Pradeep Yammiyavar and Mrs. Yammiyavar, Mrs. Sahasrabudhe and other family friends for their support during my stay in IIT Guwahati.

I will be always grateful to my parents (Mr. Pralhad B. Gudur and Mrs. Pratibha P. Gudur) and my brother (Pramod) for their support. They have been a source of encouragement for me throughout my life. I would like to thank my wife (Rajni) for her endless support, patience and motivation during my thesis work. Lastly, I will be always grateful to Almighty.

21st August 2008

Prashant P. Gudur

IIT Guwahati

Synopsis

In the cold flat rolling process, a plate or sheet is passed between two counter-rotating rigid rolls in order to reduce its thickness, keeping the temperature during the process less than the recrysallization temperature of the material. In general, rolling process can be divided into two major types– symmetric rolling and asymmetric rolling. In symmetric rolling process, due to the geometric and parametric symmetry about the mid-plane of the sheet, the product that emerges from the roll mills is expected to be flat. The flatness of the rolled product is one of the major quality attributes. Thus, it becomes important to maintain the symmetric rolling conditions to obtain a flat product. However, in practice, geometric and parametric symmetry at the mid-plane of the sheet cannot be ensured, which leads to produce curvature in the rolled product. The limiting of the curvature in the rolled product is important from the point of view of quality. On the other hand, there are situations where asymmetric rolling may be desirable for producing the curved sheets and/or for reducing the roll force and roll torque. In the present study, symmetric and asymmetric cold flat rolling processes are modelled.

The well established methods used for modelling the rolling process are slab method, slip-line method, upper bound method and finite element method (FEM). Among these, FEM is preferred to other methods due to several advantages. However, tedious calculations and large computational time makes FEM unsuitable for online prediction. In recent years, there has been an emergence of soft computing for analyzing the rolling process. Neural network (NN), fuzzy set theory, genetic algorithm (GA) fall in the category of soft computing techniques. These techniques are more suitable for online prediction due to lesser complexity and faster execution.

In the neural network modelling of cold flat rolling process, a number of researchers trained neural networks either using experimental data or data obtained

by running FEM code [Gunasekera *et al*., 1998; Dixit and Chandra, 2003]. These trained networks have the capability to predict roll force and roll torque. However, they do not predict stress, strain and strain-rate fields, which are very much required for the optimization of the process. In view of this, the present work is an attempt to use neural networks in conjunction with FEM for the faster and detailed analysis of cold flat rolling process. Here, the neural networks have been employed for predicting the complete velocity field and location of the neutral point. In order to have faster training, neural networks based on radial basis function [Ham and Kostanic, 2001] have been used in the present work. The data required for training of neural networks are generated from a rigid-plastic finite element code [Dixit and Dixit, 1996]. The dependency of velocity field on the input parameters was determined by studying the traditional statistical tools. Neglecting the parameters having very little influence on the velocity field, size of the NN model can be reduced considerably. Strain hardening parameters b and n can be excluded from the input parameters of neural network modelling for velocity prediction as the statistical analysis reveals that velocity field is insensitive to strain hardening parameters. The well trained neural networks provide a highly accurate guess for the velocity field and location of the neutral point, which is further refined by the finite element code. The post-processor of the FEM code computes roll force, roll torque, strain distribution *etc*. This procedure provides highly accurate solution with reduced computational time and is suitable for on line control or optimization. Requirement of the huge amount of dataset is considered as one of the drawbacks of neural network modelling. Hence, in the present work, attention has been paid to develop a scheme, which requires less number of training and testing data.

Mamdani fuzzy model and Takagi-Sugeno fuzzy model are two models that are widely used in the modelling based on fuzzy set theory. Modelling of the rolling process using fuzzy models is a lesser investigated field. Moreover, no work has been reported for the fuzzy set based prediction of roll force and roll torque in the cold rolling process. In the present work, the roll force and roll torque in a cold flat rolling process are modelled using first order Takagi-Sugeno fuzzy models. The fuzzy models are constructed based on the algorithm of Ŝkrjanc *et al*. [2005]. The

fuzzy models predict the most likely, lower and upper estimates of the roll force and roll torque. Although the fuzzy models can be constructed using experimental data, in the present work the required data is generated by radial basis function neural networks. The neural networks in turn are trained by a finite element method based code. It is demonstrated that coefficients of the linear crisp function used to represent the output variables in the fuzzy inference system can be used for assessing the sensitivity of these variables with respect to the process variables.

An approximate method is proposed to estimate the roll force and roll torque for another material based on these values for one material (*i.e*. reference material). The approximate method will be highly useful for a quicker estimate of roll force and roll torque. In the modern production scenario, where a wide variety of the rolled sheets made of different materials are produced by the same organization, this method is an economical way to get an estimate of roll force and roll torque for a new material based on FEM or experimental data of a reference material. An algorithm to detect and suppress the outliers in the data is also proposed. The effectiveness of the proposed algorithm is demonstrated through an example.

The finite element analysis of cold flat rolling has been carried out by a number of researchers using updated Lagrangian and flow formulations. In the flow formulations, the major difficulty is the accurate estimation of pressure field. This difficulty has been addressed by many researchers in the past [Maniatty, 1994; Hashemolhosseini *et al*., 2002]. In the mixed pressure-velocity finite element formulation, Dixit and Dixit [1996] have suggested an approximate method to modify the pressure field. In the present work, momentum equations are solved to obtain the pressure in the rigid-plastic finite element analysis. A finite difference method is used to solve the momentum equations. These finite difference equations require the values of Levy-Mises coefficient and strain-rate components. They are obtained as a function of spatial coordinates using radial basis function neural network models. The results obtained from the present approach are compared with the model of Dixit and Dixit [1996] and the experimental results available in the literature. It is observed that the proposed method provides a better agreement with

the experimental results than the model of Dixit and Dixit. Thus, the present model makes an improvement over the existing FEM flow formulations.

In an asymmetric rolling of sheet, the work rolls radii, angular velocities, friction at the upper and lower roll-work interface and the surface roughness of the upper and lower rolls may be different. Due to these differences, rolled product gets curvature. There are some engineering applications in which the curvature in the rolled product is desirable. For these applications, a greater understanding of the relationship between the process parameters and the strip curvature is needed. In this work, analysis of asymmetric cold rolling process is carried out using a slab method based model [Salimi and Kadkhodaei, 2004; Salunkhe, 2006]. Effect of strain hardening behaviour of the material and roll deformation is studied in this work. The performance of the model is validated with experimental as well as analytical results available in the literature. Neural network model is constructed for quicker analysis of the sensitivity of curvature towards the friction coefficient.

Considering the uncertainties in the experimental results available in the literature, Dixit and Dixit [1996] treated material and process parameters as fuzzy parameters for the validation of their FEM model. However, their study does not include the estimation of the curvature of the rolled product due to uncertain frictional condition. The present work estimates the undesired curvature generated due to uncertain frictional condition at upper and lower roll-work interface. A methodology is proposed to control the curvature by operating the upper and lower roll at different speeds.

The important contributions of the present thesis are summarized below:

1. Velocity field is insensitive to the strain hardening parameters. Thus, strain hardening parameters can be ignored in the neural network modelling of the velocity field. The information obtained from NN model may be provided as a guess to the rigid-plastic finite element code. This procedure reduces the computational time required by FEM code for

finding out the velocity and pressure fields as well other parameters. This approach is beneficial for online prediction and control.

2. Takagi-Sugeno (TS) fuzzy models can be used for studying the dependency of roll force and roll torque on the process variables in the analysis of cold flat symmetric rolling process. Outliers in the modelling data can be effectively identified and suppressed using the methodology discussed in the present work.

3. A method for more accurate estimation of pressure is developed in the mixed pressure-velocity flow formulation of symmetric cold flat rolling process. Results of the present method are validated with experimental and analytical results available in the literature. The performance of the proposed method suggests improvement over the existing FEM formulations.

4. Asymmetry in the process conditions leads to produce curvature to the rolled product. However, it reduces roll force and roll torque as compared to the symmetric rolling process. Sensitivity of the curvature towards the different friction coefficient at lower and upper roll can be studied using NN modelling. In actual practise, even in symmetric rolling process, the uncertain frictional conditions at work-roll interface may lead to produce undesirable curvature. This undesirable curvature can be controlled by operating upper and lower roll at different speeds.

References

- Dixit, U.S. and Chandra, S., (2003), A neural network based methodology for the prediction of roll force and roll torque in fuzzy form for cold flat rolling process, International Journal of Advanced Manufacturing and Technology, **22**, pp. 883–889.

- Dixit, U.S. and Dixit, P.M., (1996), A finite element analysis of flat rolling and applications of fuzzy set theory, International Journal of Machine Tools and Manufacture, **36**, pp. 947–969.
- Gunasekera, J.S., Jia, Z., Malas, J.C. and Rabelo, L., (1998), Development of a neural network model for a cold rolling process, Engineering Applications of Artificial Intelligence, **11**, pp. 597–603.
- Ham, F., Kostanic, I., (2001), Principles of neurocomputing for science and engineering, (Mcgraw-Hill, New York).
- Hashemolhosseini, H., Dalayeli, H. and Farzin, M., (2002), Correction of hydrostatic pressure obtained by finite element flow formulation using moving least square method, Journal of Material Processing Technology, **125/126**, pp. 588–593.
- Maniatty, A.M, (1994), Predicting residual stresses in steady-state forming processes, Computing Systems in Engineering, **5**, pp. 171–177.
- Salimi, M. and Kadkhodaei, M., (2004), Slab analysis of asymmetrical sheet rolling, Journal of Material Processing Technology, **150**, pp. 215–222.
- Salunkhe, M.A., (2006), Analysis of cold flat asymmetric rolling process, M. Tech. Thesis, Indian Institute of Technology Guwahati.
- Ŝkrjanc, I., Blažič, S. and Agamennoni, O., (2005), Interval fuzzy model identification using l_∞–norm, IEEE Transactions on Fuzzy Systems, **13**, pp. 561-568.

Contents

Synopsis ..... **i**

Contents ..... **vii**

List of Figures ..... **xi**

List of Tables ..... **xv**

Nomenclature ..... **xvii**

1 Introduction **1**

1.1 Rolling Processes 1

1.2 Soft Computing Techniques 4

1.3 Objective and Organization of Thesis 6

2 Literature Survey **9**

2.1 Introduction 9

2.2 Research on Symmetric Rolling Process 10

2.2.1 One-dimensional Models 10

2.2.2 Slip-line Method Based Models 16

2.2.3 Upper Bound Theory Based Models 17

2.2.4 Finite Element Method Based Models 19

2.2.5 Models Based on Visio-plasticity Technique 25

2.2.6 Experimental and Theoretical Investigation of Friction at Roll-work Interface 25

2.2.7 Soft Computing Technique 29

2.3 Research on Asymmetric Rolling Process 37

2.3.1 Experimental Research 37

2.3.2 Theoretical Research 39

2.4 Detailed Objectives of the Present Thesis 45

3 Neural Network Assisted Finite Element Modelling 49

3.1 Introduction 49

3.2 Finite Element Formulation 50

3.3 Prediction of Velocity Field by Neural Networks 56

3.3.1 Study of Data 59

3.3.2 Neural Network (NN) Modelling 65

3.3.3 Prediction of the Parameters Using Trained Neural Network and FEM 68

3.4 Results and Discussion 68

3.4.1 Validation of the Neural Network Model 66

3.4.2 Prediction of Roll Force and Roll Torque 72

3.4.3 Comparison of Roll Pressure 73

3.4.4 Comparison of Equivalent Strain Contours 74

3.4.5 A Note on Computational Time 77

3.5 Summary 77

4 Prediction of Roll Force and Roll Torque Using RBF Neural Networks and Fuzzy Inference 79

4.1 Introduction 79

4.2 Problem Formulation 80

4.3 Data Generation Using RBF Neural Network 81

4.4 Fuzzy Inference Model for Prediction of Roll Force and Roll Torque 85

4.5 Result and Discussion 89

4.5.1 Roll Force and Roll Torque Prediction 89

4.5.2 Sensitivity Analysis for Roll Force and Roll Torque 93

4.6 Approximate Method for Prediction of Roll Force and Roll Torque for Another Material based on the Reference Material 95

4.7 Identification and Suppression of Outliers in the TS Model 98

4.8 Summary 100

5 Pressure Field Correction in FEM Flow Formulation with the Help of Finite Difference Method and Neural Networks 103

5.1 Introduction 103

5.2 Problem Formulation 104

5.3 Neural Network Modelling 109

5.4 Result and Discussion 111

5.4.1 Results with Fuzzy Parameters for Steel Material 112

5.4.2 Validation of the Model for Copper and Aluminium 118

5.4.3 Comparison with Slab Method 122

5.5 Summary 123

6 Neural Network and Fuzzy Set Applications in the Analysis of Curvature in an Asymmetric Rolling Porcess 125

6.1 Introduction 125

6.2 Slab Method Formulation 126

6.2.1 Roll Force, Roll Torque and Strip Curvature 131

6.3 Validation and Parametric Study of the Model 133

6.3.1 Roll Force and Roll Torque 133

6.3.2 Effect of Friction Mismatch on Roll Force and Roll Torque Prediction 136

6.3.3 Comparison of Roll Force and Roll Torque in Symmetric and Asymmetric Rolling 137

6.3.4 Power Dissipation for Different Speed Ratios 138

6.3.5 Strip Curvature Analysis 140

6.3.6 Effect of Roll Flattening on the Curvature 141

6.4 Neural Network Model for the Prediction of Curvature 141

6.4.1 Study of Effect of Strain Hardening on the Curvature 142

6.4.2 Neural Network Model 144

6.5 Effect of Frictional Asymmetry on the Curvature 146

6.5.1 Fuzzy Modelling of Parameters 147

6.5.2 Simulation with Fuzzy Material and Process Parameters 148

6.5.3 Control of Undesired Curvature 150

6.6 Summary 150

7 Conclusions and Scope for Future Work 153

7.1 Conclusions 153

7.2 Scope for Future Work 156

References 159

Appendix 183

Publications from the Present Thesis Work 201

List of Figures

1.1	A three-dimensional schematic representation of flat rolling process	2
1.2	A typical asymmetric flat rolling process	3
2.1	The forces acting on a slab on the exit side	10
2.2	Roll pressure distribution along the roll-work interface	11
2.3	Different friction models available in literature. (a) Coulomb's model, (b) Constant friction model (c) Wanheim and Bay's model	28
2.4	Flowchart showing some of the representative work in the modelling of symmetric rolling process	36
2.5	A typical cross shear zone in an asymmetric rolling process	37
2.6	The zone of cross shear and direction of the frictional stress on the slabs in an asymmetric rolling process	39
2.7	Flowchart showing some of the representative work in the modelling of asymmetric rolling process	44
3.1	The domains along with mesh and boundary conditions	52
3.2	A typical element (a) nodes for pressure approximation (b) nodes for velocity and geometry approximation	53
3.3	Schematic diagram of RBF neural network used in the present analysis	58
3.4	Locations of six nodes selected for data analysis	59
3.5	A general overview of the procedure that uses the NN predicted velocity field in the FEM model (NN assisted FEM model)	68
3.6	Errors in four-input NN prediction for horizontal velocity component	70
3.7	Errors in four-input NN prediction for vertical velocity component	70
3.8	Errors in three-input NN prediction for horizontal velocity component	71
3.9	Errors in three-input NN prediction for vertical velocity component	71
3.10	NN assisted FEM predictions *vs* FEM predictions for roll force	73
3.11	NN assisted FEM predictions *vs* FEM predictions for roll torque	73

3.12	Comparison of NN assisted FEM prediction *vs* FEM prediction for roll pressure distribution	74
3.13	Equivalent strain contours for high strain hardening material plotted by FEM model	75
3.14	Equivalent strain contours for high strain hardening material plotted by NN assisted FEM model	75
3.15	Equivalent strain contours for low strain hardening material plotted by FEM model	76
3.16	Equivalent strain contours for low strain hardening material plotted by NN assisted FEM model	76
4.1	A typical RBF neural network architecture used in the present analysis.	81
4.2	Flow chart illustrating the methodology adopted for NN model	84
4.3	Fuzzification of input variables for a typical cold rolling process	86
4.4	The TS fuzzy model predicted versus NN predicted roll force	90
4.5	The TS fuzzy model predicted versus NN predicted roll torque	90
4.6	The TS fuzzy model predicted versus FEM predicted roll force	91
4.7	The TS fuzzy model predicted versus FEM predicted roll torque	91
4.8	Lower, most likely and upper estimates of roll force	92
4.9	Lower, most likely and upper estimates of roll torque	93
5.1	Schematic representation of a rolled strip	106
5.2	The domain showing plastic boundaries and the points for finite difference approximation	107
5.3	The architecture of RBF model used in the present work	109
5.4	Training and testing data points selected from a typical element	110
5.5	Comparison of FEM and experimental results for roll force (Steel, $R/h_1 = 65$)	114
5.6	Comparison of FEM and experimental results for roll torque (Steel, $R/h_1 = 65$)	114
5.7	Comparison of roll pressure distribution for a typical case (Steel, $R/h_1 = 65$)	115
5.8	Comparison of FEM and experimental results for roll force (Steel, $R/h_1 = 130$)	116
5.9	Comparison of FEM and experimental results for roll torque (Steel, $R/h_1 = 130$)	117

5.10	Comparison of roll pressure distribution for a typical case (Steel, $R/h_1 = 130$)	117
5.11	Comparison of FEM and experimental results for roll force (Copper)	119
5.12	Comparison of FEM and experimental results for roll torque (Copper)	119
5.13	Comparison of FEM and experimental roll pressure distribution (Copper)	120
5.14	Comparison of FEM and experimental results for roll force (Aluminium)	120
5.15	Comparison of FEM and experimental results for roll torque (Aluminium)	121
5.16	Comparison of FEM and experimental roll pressure distribution (Aluminium)	121
5.17	Comparison of roll pressure distribution for different methods	123
6.1	The schematic diagram of asymmetric rolling	127
6.2	The strip curvature due to (a) difference in axial strains (b) difference in shear strains [Salunkhe, 2006]	132
6.3	Comparison of experimental and analytical roll force for speed mismatch, ($h_1 = 2$ mm)	134
6.4	Comparison of experimental and analytical roll force for speed mismatch, ($h_1 = 6$ mm)	135
6.5	Comparison of experimental and analytical roll force for different roll radius	135
6.6	Variation of roll force with reduction for different and same frictions on upper and lower rolls	136
6.7	Variation of roll torque with reduction for different and same frictions on upper and lower rolls	136
6.8	Comparison of symmetric and asymmetric roll force with different speed ratios	137
6.9	Comparison of symmetric and asymmetric roll torque with different speed ratios	138
6.10	Comparison of experimental, finite element analysis and present method for strip curvature index	140
6.11	A typical RBF neural network architecture used in the present analysis	144
6.12	Membership functions of b, n, σ_Y and f	147

List of Tables

3.1	Correlation analysis for velocity v_1 and v_2 (node: 1)	60
3.2	Correlation analysis for velocity v_1 and v_2 (node: 2)	61
3.3	Correlation analysis for velocity v_1 and v_2 (node: 3)	61
3.4	Correlation analysis for velocity v_1 and v_2 (node: 4)	61
3.5	Correlation analysis for velocity v_1 and v_2 (node: 5)	62
3.6	Correlation analysis for velocity v_1 and v_2 (node: 6)	62
3.7	ANOVA table for horizontal component of velocity, v_1 (Node: 6)	64
3.8	ANOVA table for vertical component of velocity, v_2 (Node: 6)	64
3.9	The p–values based on F–ratio for v_1 and v_2	64
3.10	Variation of testing error with β for a typical nodal velocity prediction	67
4.1	The final neural network parameters for roll force and roll torque prediction	85
4.2	The variation of the maximum approximation error in TS model with respect to number of modelling data for roll force and roll torque	89
4.3	Comparison of roll force expressions with the finite difference computed sensitivity values.	94
4.4	Comparison of roll torque expressions with the finite difference computed sensitivity values	95
4.5	Comparison of roll force predictions by the proposed approximate method with FEM	97
4.6	Comparison of roll torque predictions by the proposed approximate method with FEM	98
4.7	Performance of the proposed TS model and original TS model in the presence of outliers	100
5.1	The final network architecture for neural network modelling (Steel, $R/h_1 = 65$)	111

5.2	Fuzzy input parameters for two steels, Steel 1 with h_1 = 1 mm and Steel 2 with h_2 = 0.5 mm	113
6.1	Comparison of plastic deformation and frictional power for symmetric and asymmetric rolling	139
6.2	Effect of roll flattening on the strip curvature for a case of $R_u = R_l$ = 350 mm, $f_u = f_l = 0.14$, σ_Y = 169.9 MPa, h_1 = 4 mm and r =20 %.	141
6.3	Effect of strain hardening on the strip curvature	143
6.4	The final neural network parameters for radius of curvature prediction	145
6.5	Radius of curvature prediction for different friction and speed ratio ($R_u = R_l = 350$ mm, $r = 10$ %, $\sigma_Y = 169.9$ MPa, $h_1 = 7$ mm)	145
6.6	Radius of curvature prediction for different friction and speed ratio ($R_u = R_l = 350$ mm, $r = 15$ %, $\sigma_Y = 169.9$ MPa, $h_1 = 3.5$ mm)	145
6.7	Radius of curvature obtained due to friction mismatch at α-cut of 0.5 ($f_u = 0.085$, $f_l = 0.135$, $V_A = 1.0$)	148
6.8	Comparison of radius of curvature due to variation in flow stress at α-cut of 0.5 ($f_u = 0.085$, $f_l = 0.135$, b=0.05, n=0.26, $V_A = 1.0$)	149
6.9	Radius of curvature obtained due to friction mismatch at α-cut of 0.75. ($f_u = 0.0975$, $f_l = 0.1225$, $V_A = 1.0$)	149
6.10	Roll speed adjustment to minimize the curvature that causes due to friction mismatch, (f_u =0.085, f_l = 0.135, σ_Y = 169.9 MPa, b = 0.05, n = 0.26)	150

Nomenclature

a_i^j	Coefficients associated with the j^{th} input variables in the consequent part of IF-THEN rule
$A^j(i)$	Fuzzy subset corresponding to the j^{th} input variables that depends on i^{th} rule
b, n	Material hardening parameters
b_0	Bias
C	A constant dependent on the roll material used in Eq. (3.18)
c	Height of the curved strip
$\boldsymbol{c}_j$	RBF centre associated with j^{th} neuron
$d_{\max}$	Maximum Euclidean distance between the centers
d_p	FEM generated output for p^{th} data
E_r	Young's modulus of elasticity for the roll material
e_i	Difference between the nodal velocity value of FEM code and NN model
f	Coefficient of friction
f	Equivalent Coulomb's Coefficient of friction (used in Chapter 6)
f_u, f_l	Equivalent Coulomb's Coefficient of friction at upper and lower roll-work interface (used in Chapter 6)
F_r	Roll force per unit width of the strip
F_u, F_l	Roll force per unit width of the strip at the upper and lower rolls, respectively
h	Strip thickness at a distance x from the centre of the rolls
h_u, h_l	The vertical distance between the x axis and a point on the strip at the upper and the lower surfaces, respectively
h_1, h_2	Initial and final thickness of the strip

J	Total number of RBF centers
L	The projected contact length
l	arc of contact
l_0, l_1, l_2	Lengths of the neutral, upper and lower fibers of a curved strip
m	Number of neurons in the hidden layer
m, m_u, m_l	Friction factor , friction factors for upper and lower roll, respectively
N	Total number of nodes
N_R	Total number of rules in the TS model
o_p	Neural network predicted output for p^{th} data
P	Rolling power
P_p	Power required for plastic deformation
P_f	Power required to overcome friction at the roll-strip interface
P_t	Power required due to tensions
p	Pressure
p_{avi}, p_{avo}	Average pressures at inlet and exit
p_0	Pressure obtained by FEM
p_r	Pearson correlation coefficient
p_u, p_l	Normal contact pressures at the upper and the lower surfaces in the roll gap.
R	Undeformed roll radius
R'	Deformed roll radius
R_{curv}	Radius of curvature of a strip
R_{eq}	Equivalent roll radius
R_u, R_l	Radius of the upper and lower roll, respectively
r	Fractional reduction
r_1, r_2	Radius of curvature due to difference in normal strains and shear strains, respectively
rms_{err}^{f}	Root mean squared (*rms*) fractional error (Eq. 4.5)
S_{ij}	Deviatoric part of stress tensor

s_{xx1}, s_{yy1}	Deviatoric components of stress for upper surface, in x and y directions, respectively
s_{xx2}, s_{yy2}	Deviatoric components of stress for lower surface, in x and y directions, respectively
T	Roll torque per unit width of the strip
t	Time
t_b, t_f	Back tension and front tension, respectively
t_i	Component of traction vector
t_s, t_n	Interfacial shear and normal stress
U_1, U_2	Inlet and exit velocities of the strip
V_A	Ratio of the surface velocities of the lower roll to that of the upper roll
V_R	Angular velocity of the roll
V_u, V_l	Velocity of the upper and lower roll
v_n	Normal component of velocity
v_1, v_2	Horizontal and vertical component of velocity vector
w_i	Strength of the i^{th} fuzzy rule
w_j	Weights associated with the j^{th} neuron
x_i, x_j	Cartesian coordinates
x_{nu}, x_{nl}	The locations of the upper and the lower neutral points.
y_i	Output of the i^{th} IF-THEN rule in the TS model
$\hat{y}$	The aggregated output of the TS fuzzy model
ν_r	Poisson's ratio for roll material
μ	Membership grade
μ	Levy-Mises coefficient
λ, λ_1, λ_2	Maximum approximation error for computing most likely, lower and upper estimates of coefficients, respectively
$\varphi(.)$	A processing function
$\mathrm{d}\gamma_{xy1}$, $\mathrm{d}\gamma_{xy2}$	Incremental shear strains at a point on the upper and the lower surfaces of the strip, respectively

$d\lambda$	A constant in the flow rule
$d\varepsilon_{x1}, d\varepsilon_{x2}$	Incremental axial strains in x direction, for upper and lower surfaces, respectively
$\varepsilon_{x1}, \varepsilon_{x2}$	Axial strains at the upper and lower surfaces of the strip
$\tilde{\varepsilon}$	Equivalent plastic strain
$\tilde{\varepsilon}_f$	Final equivalent strain
$\dot{\tilde{\varepsilon}}$	Equivalent strain rate
$\dot{\varepsilon}_{ij}$	Strain rate tensor
α	Angle of contact
β	A constant factor multiplied for fine tuning of spread parameter
δ	Draft *i.e.* difference between the initial and final thickness of the strip
δ_{ij}	Kronecker's delta
ϕ	Angular position of the point on the surface
ψ	A parameter defined by Eq. (5.7)
σ	Spread parameter
σ_{ij}	Stress tensor
σ_u, σ_l	Normal axial stresses at the upper and the lower rolls, respectively
σ_Y	Flow stress in tension
$(\sigma_Y)_0$	Yield stress in tension
τ	Average shear stress on the vertical side of the element
τ_u, τ_l	Frictional shear stresses at the upper and lower interfaces

1

Introduction

1.1 Rolling Processes

Rolling is one of the most important metal forming processes. It plays an important role due to its versatility and high production rate in the manufacturing of various products with uniform cross sectional area. It is an efficient and economical method for the manufacturing of metal strips or plates. Rolling process was first developed in late 1500s and it accounts for about 90 percent of all metal working processes [Kalpakjian, 1989]. Most of the steel produced is rolled into strips, sheets, bars and other shapes such as I-beams or L-cross sections. In a rolling process, the material (*i.e.* ingot, billet, slab or sheet) is passed between a set of cylindrical work rolls that are usually supported by back-up rolls. The work rolls rotates in opposite directions. The space between the work rolls being less than the thickness of the entering material, the rolls grip the material, reduce its thickness and forces it through to the exit.

Different end-product shapes require different types of rolling processes. The various types of rolling processes that are mainly used in the industries are flat rolling, profile rolling, ring rolling, thread rolling, powder rolling, tube rolling *etc*. A variety of roll arrangements is found in the rolling mills like two-high, four-high, planetary mills *etc*. Among all these processes, the most basic and widely used process is flat rolling or simply rolling, where the rolled products are flat plates, strips or sheets. Figure 1.1 shows a schematic three-dimensional diagram of the flat rolling process. The figure shows counter rotating rigid work rolls, back-up rolls, metal strip being rolled and the rolling direction. The rigid work rolls which are smaller are supported by larger back-up rolls. The back-up rolls are used to minimize the deflection of work rolls.

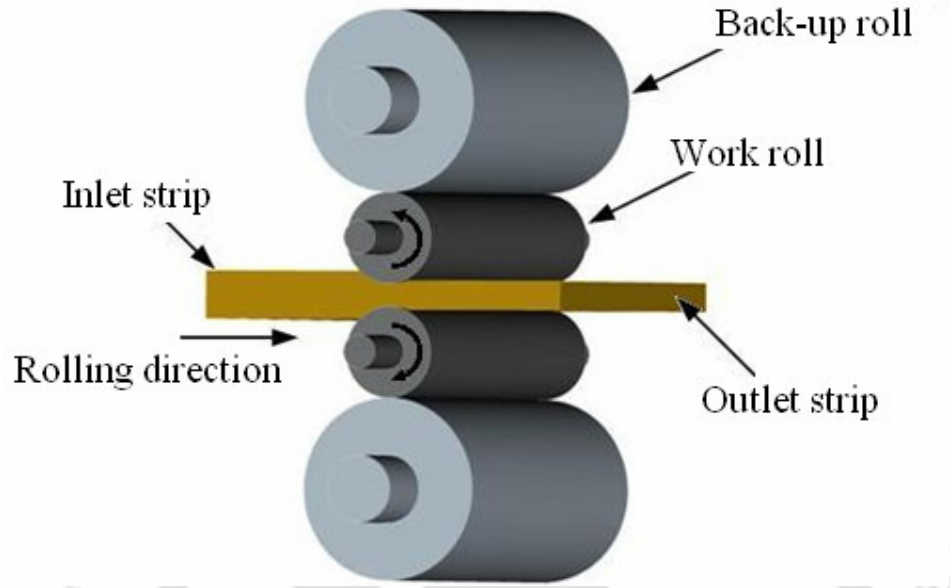

Figure 1.1. A three-dimensional schematic representation of flat rolling process

The rolling process can be classified into 3 categories– hot rolling, cold rolling and warm rolling. Hot rolling is defined as rolling of metals above their recrystalization temperature. In cold rolling process, temperature of the material is much lesser than its recrystalization temperature. Warm rolling is a process where the material is deformed at some intermediate temperature (above room temperature) but below the recrystalization temperature of the material. Compared to hot rolling, cold rolling process has certain distinct advantages:–

- In this process, no heating of the material is required.
- Better surface finish and superior dimensional control of the product is obtained.
- The products with improved strength properties may be obtained.
- Directional properties can be imparted to the products.

However, some disadvantages associated with cold rolling process are as follows:

- Higher forces are required for deformation.
- Heavier and more powerful equipment is required.
- Strain hardening occurs during the process.
- Undesirable residual stresses get produced in the product.

In general, flat rolling process can be divided into two major types– symmetric rolling and asymmetric rolling process. In symmetric rolling process, the geometric and parametric symmetry about the mid-plane of the sheet is maintained. Thus, the product that emerges from the rolling mills is expected to be flat. The flatness of the rolled product is one of the major quality features. Thus, it becomes important to maintain the symmetric rolling conditions to obtain a flat product. However, in actual practice, geometric and parametric symmetry at the mid-plane of the sheet cannot be ensured. If there are difference in the roll diameters, diffenrent frictional conditions at upper and lower roll, different rotational speeds or lubrication mismatch, the process is called as asymmetric rolling process. In this process, the strip that is being rolled has a tendency to obtain a curvature. The need for asymmetric rolling process depends on the application and requirement of the product. There are situations where asymmetric rolling may be desirable for producing the curved sheets and/or for reducing the roll force and roll torque. Figure 1.2 shows a typical asymmetric flat rolling process where asymmetry is caused due to different roll radius. The upper roll is smaller than lower roll. The back-up rolls are not shown in this figure.

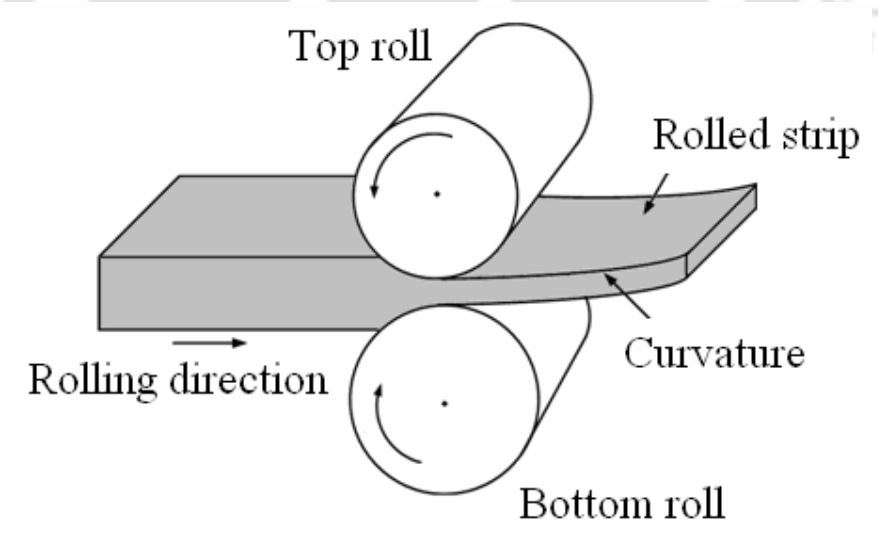

Figure 1.2. A typical asymmetric flat rolling process

The asymmetric rolling process requires lesser roll pressure, roll force and roll torque as compared to symmetric rolling process. Thus, controlled non-symmetry has the potential of raising the productivity of rolling mills. However, asymmetric rolling process is more complex than symmetric rolling process. In view of the complexity of the process, experimental investigations and the mathematical modelling of both symmetric and asymmetric rolling process has been an interesting and challenging research area since many years. The mathematical analysis of rolling process can be done using the established techniques like slab method, slip-line method, upper bound method and finite element method (FEM). Among these methods, FEM has been very effective tool in the modelling of rolling processes as it can easily incorporate non-homogeneity of deformation, process dependent material properties and different friction models. However, tedious calculations and large computational time makes FEM difficult for online control and optimization of the rolling processes.

1.2 Soft Computing Techniques

The mathematical modelling of rolling process using the techniques mentioned in the previous section are several decades old. A recently developed modelling technique is soft computing technique. Unlike conventional methodologies (hard computing techniques), soft computing techniques are tolerant of imprecision, uncertainty and partial truth. Soft computing techniques do not suffer from the brittleness and inflexibility of conventional algorithmic approaches. Soft computing is a general term covering a number of methodologies. Neural networks (NN), fuzzy set theory and genetic algorithms (GAs) form the part of soft computing techniques. Soft computing techniques rely more on the data than the physics of the process, although knowledge of the physics of the process may enhance the usefulness of the soft computing techniques. These techniques are more suitable for online prediction due to lesser complexity and faster execution.

One of the major soft computing techniques is neural network modelling. Neural networks get their motivation from biological nervous systems. The history of neural network (NN) modelling began in the early 1940s. McCulloch and Pitts

[1943] presented the concept of neurological network by suggesting the idea of mind-like machine. The incorporation of neural networks (NN) in the modelling of rolling process speeded up only in mid-1990s. Neural networks are a relatively new artificial intelligence technique that emulates the behavior of biological neural systems. These networks can 'learn' the complex relationships among the data. This feature makes the technique very useful in modelling the complex processes for which mathematical modelling is difficult or impossible. The most commonly used neural networks are multilayer perceptron (MLP) neural network and radial basis function (RBF) neural networks [Ham and Kostanic, 2001].

Fuzzy set theory derives its motivation from approximate reasoning. Zadeh [1965] introduced concept of fuzzy set as an extension of classical notion of set. In the classical set theory, membership of elements in a set is assessed in binary terms: an element either belongs or does not belong to the set. On the contrary, fuzzy sets are the set whose elements have degrees of membership that assumes a value between 0 and 1 inclusive. The main feature that separates fuzzy set based models from a black-box technique like neural network is that the fuzzy models are, to a certain degree, transparent to the interpretation and analysis [Setnes *et al*., 1998]. Usually, a fuzzy set based model is built by using an expert knowledge in the form of linguistic rules. In general, data acquired by experiments, mathematical modelling, NN modelling or any other suitable methods are used to develop the fuzzy models. In engineering applications, two types of fuzzy models are widely used: Mamdani fuzzy model and Takagi-Sugeno (TS) fuzzy model.

Genetic algorithms are widely used as search and optimization tools in modelling of engineering applications. Genetic algorithms are based on the nature's law of the 'survival of the fittest'. The name genetic algorithm is derived from the fact that they follow the principle of natural genetics. The concept of genetic algorithm was first developed by Holland [1975]. Since then, many variants of these algorithms have been developed. Two of the major categories of the genetic algorithms are: binary-coded and real-coded genetic algorithm. Genetic algorithms are extensively used due to their broader applicability and easy to use [Goldberg,

1989]. Compared to neural networks, fuzzy set theory and genetic algorithm has not been used extensively in the modelling of rolling processes.

In the modelling of the rolling processes, quicker estimations of parameters are important for online control and optimization. In an actual rolling mill, the material properties and process parameters may not be known precisely. Also, the mathematical modelling encompasses many approximations to ease the complexity of the process. In such situations, soft computing based models helps to alleviate the complexity of the process by considering the imprecision and uncertainty. Recently, Dixit and Dixit [2008] emphasized on the utilization of these soft computing techniques in the modelling of metal forming and machining processes. The authors mentioned that soft computing techniques and other established methods can be complementary to one another and at the same time any of these techniques can be applied separately depending on the nature of the problem.

1.3 Objective and Organization of the Thesis

The primary objective of the present thesis is to develop soft computing assisted models of symmetric and asymmetric cold flat rolling processes. The main focus of the methodologies developed is to assimilate soft computing techniques along with the previous established techniques to alleviate the complexity of the process and for faster prediction of the parameters. Thus, in this work the soft computing techniques have been used as complementary tools to traditional modelling methods.

The remaining chapters in the thesis are organized as follows:

- A brief review of literature in the symmetric as well as asymmetric flat rolling process and objectives of the present thesis are elaborated in Chapter 2.
- In Chapter 3, the neural network modelling of velocity field and location of neutral point in the cold flat rolling process is described. Analysis of neural network assisted finite element model is explained. The benefits of the proposed method are elaborated.

- In Chapter 4, Takagi-Sugeno (TS) fuzzy models for the prediction of roll force and roll torque are illustrated. The sensitivity analyses with the help of developed fuzzy models are carried out. Effect of outliers and its suppression is also discussed in the chapter.
- Chapter 5 deals with a novel approach developed for the estimation of pressure in the mixed pressure-velocity finite element formulation. Advancement of the proposed methodology is described by comparing the results of the proposed method against the experimental results as well as analytical results from the previous literature.
- Analysis of asymmetric rolling process using a slab method based model is explained in Chapter 6. The performance of the slab model is validated against experimental results available in the literature. Neural network modelling for the prediction of curvature is carried out for studying the sensitivity of curvature towards friction. Further, estimation and control of undesirable curvature generated due to uncertain frictional conditions in an actual rolling mill is also elaborated in the chapter.
- Conclusions and scope for future work are presented in Chapter 7 followed by references and appendices.

2

Literature Survey

2.1 Introduction

The cold flat rolling process is one of the most widely investigated processes. It can be divided into two major classes— symmetric rolling and asymmetric rolling. In symmetric rolling process, the rolling speed, roll diameters and friction at the roll-work interface are kept symmetrical with respect to central mid-thickness plane of the raw material. Due to this geometric and parametric symmetry, the product that emerges from the roll mills is flat. The flatness of the rolled product is one of the major quality attributes. Thus, it becomes important to maintain the symmetric rolling conditions to obtain a flat product. However, in practice, symmetry of process conditions cannot be ensured, which leads to produce curvature in the rolled product. The limiting of the curvature in the rolled product is important from the point of view of quality. On the other hand, there are some engineering applications in which the curvature in the rolled product is desirable. For these applications, a greater understanding of the relationship between the process parameters and strip curvature is needed. With clear quantitative understanding of the asymmetric rolling process, it is possible to set the process parameters for producing the sheets, strips or plates of desired curvature.

In this chapter, a review of existing literature in the area of symmetric and asymmetric rolling processes is presented in two different sections. Section 2.2 discusses the various approaches for mathematical modelling and experimental investigations for symmetric flat rolling process. Section 2.3 emphasizes on the experimental investigation and mathematical analyses carried out by several researchers for the analysis of asymmetric flat rolling process. Detailed objectives of the present work have been presented in Section 2.4.

2.2 Research on Symmetric Rolling Process

A number of theoretical models have been developed during the past several decades by making various assumptions to simplify the complex behaviour of the rolling process. The development of models suitable for the analysis of rolling relies heavily upon the use of these assumptions. The choice of assumptions depends upon the desired outputs of the model and the simplicity required. This section presents a review of the literature starting from simplified model of early days to present day computational models.

2.2.1 One-dimensional Models

The theoretical modelling of strip rolling can be traced back to 1920s. The pioneering work carried out by Karman [1925] was the beginning of the mathematical modelling of the rolling process. The theory of homogeneous deformation suggested by Karman is based on simplified equilibrium of forces acting on an infinitesimal small slab element in the deformation zone of strip as shown in Fig. 2.1. This method used by Karman is popularly known as the slab method.

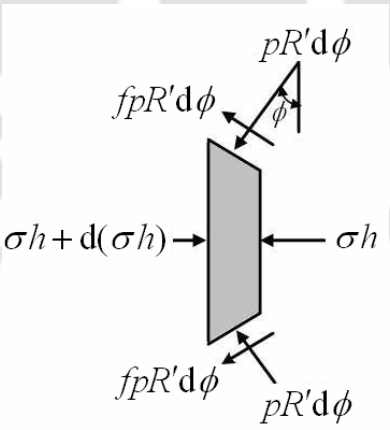

Figure 2.1. The forces acting on a slab on the exit side

Karman derived simple first order ordinary differential equations for the prediction of roll pressure and force in rolling. Karman's theory is based on the assumption that

'plane sections remain plane' during the rolling operation through the arc of contact. The first order ordinary differential equation of equilibrium may be written as

$$\frac{\mathrm{d}}{\mathrm{d}\phi}(h\sigma) = 2pR'(\sin\phi \pm \cos\phi), \tag{2.1}$$

where p is the roll pressure at the point, f is the coefficient of friction and σ denotes the mean horizontal stress over a vertical section specified by its angular coordinate ϕ. The upper sign applies to the exit side and the lower sign applies to the entry side of the neutral point. (The neutral point is the point at which the strip velocity is equal to roll velocity. Before the neutral point, the strip moves slower than the roll. After the neutral point, the strip moves faster than the roll. In some cases, instead of a neutral point, there is a small sticking region, in which the strip velocity is equal to the roll velocity.) The resultant compressive force acting over this section per unit width is $h\sigma$, where h is the local strip thickness and R' is the deformed roll radius. A typical roll pressure distribution at the roll-work interface is obtained using Karman's expression as shown in Fig. 2.2. The theory of Karman assumes that the tangential friction forces in the contact zone can exceed the resistance of the metal in simple shear.

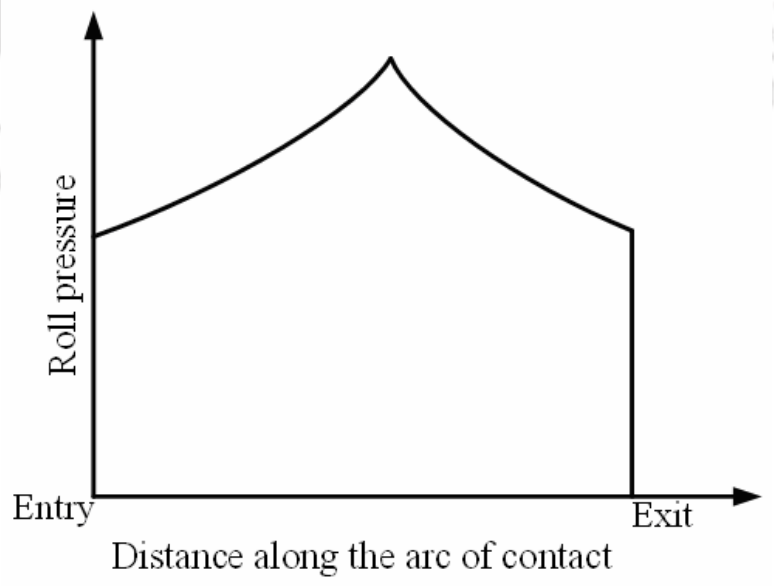

Figure 2.2. Roll pressure distribution along the roll-work interface

Siebel [1930] proposed a constant frictional force on the roll-strip interface. Nadai [1939] considered three assumptions while deriving solutions for Karman's equations. These assumptions are:–

1. A constant coefficient of friction.
2. A constant shearing stress.
3. A surface friction proportional to the velocity of slip.

Nadai showed that an increase in the coefficient of friction also increases the roll force and the slip. Tselikov [1939] adopted a different approach to the solution of Karman's equation (Eq. 2.1). The author considered angle ϕ to be constant and equal to half the entry angle. However, his assumption of constant angle ϕ is valid for only small contact angle occurring in the rolling of thin strip.

Orowan [1943] used a graphical-numerical method of computation in order to determine the roll pressure distribution. He assumed that slipping does not take place over the whole arc of contact and the plastic shear takes place in the rolled strip, when the surface of the strip sticks to the rolls with static friction. Orowan also introduced the inhomogeneous deformation by introducing a complicated adjusting factor into the computation. He relaxed the assumption of constant horizontal velocity of the material over any vertical cross-section. Orowan even abandoned the mathematical approximations such as $\sin\phi \simeq \tan\phi \simeq \phi$ and $1-\cos\phi = 0$ or $\frac{1}{2}\phi^2$.

Thus, Orowan's method avoided most of the assumptions used by Karman as well as other previous researchers. However, his model was based on the following assumptions:

- The deformation could be represented as plane strain.
- The arc of contact is circular although its radius may change and this is modelled by Hitchcock's formula.
- At the work-roll interface, there is Coulomb friction or sticking.
- The material is incompressible.
- The stress distribution through the strip thickness is like that in non-parallel compression of plates.

Subsequently, several authors simplified Orowan's model. The simplifications and assumptions were generally related to contact-arc form, friction model, yield criterion, and deformation type (homogeneous or inhomogeneous). Bland and Ford [1948] simplified Orowan's equations by making an assumption related to the small contact angle involved. The authors assumed that roll pressure equals the stress in the vertical direction. As the difference between the roll pressure and stress in the vertical direction is a function of the cosine of very small angles, the error is not large. The authors derived equations for roll force and torque, with and without front and back tensions. The approximate analyses for the effects of elastic entry and exit are developed by Bland and Ford [1952]. Ford *et al*. [1951] and Bland and Sims [1953] made considerable modifications to the simplified theory of Bland and Ford by allowing for a certain degree of variation of the yield stress in the plastic arc of contact in the deformation zone. Sims [1954] presented an analysis for calculating roll force and roll torque for hot rolling. The method was developed with the assumption of sticking throughout the arc of contact, and was experimentally verified using lead material. Alexander [1972] computerized Orowan's model and presented adequate predictions of roll force and roll torque. However, he did not include the inhomogeneity factor introduced by Orowan [1943] and felt the need of slip-line field solution for the accurate estimation of this factor. Venter and Abd-Rabbo [1980, 1982] presented a numerical solution of the non-homogenous Orowan's equation of equilibrium. The Authors reported that their model provides realistic advancement to the solution of the rolling problem and correlates with the results of Alexander [1972]. Roychoudhuri and Lenard's model [1984] is the refined model of Orowan [1943]. In their model, instead of Hitchcock's equation, elastic deformation of the roll is obtained using a two-dimensional theory of elasticity.

The roll force can be obtained by integrating the roll pressure along the arc of contact. However, in order to avoid the integration, Eklund [1933] had proposed the following equation (Eq. 2.2) based on the study of material flow during plastic deformation:

$$F_r = \bar{\sigma}\sqrt{\frac{D'\delta}{2}}\left(1+\frac{1.6f\sqrt{\frac{D'\delta}{2}}-1.2\delta}{h_1+h_2}\right), \tag{2.2}$$

where F_r is the roll force, $\bar{\sigma}$ is the mean plane strain yield strength, D' is the deformed roll diameter, $\delta=(h_1-h_2)$, is the draft, f is the coefficient of friction, and h_1 and h_2 are the initial and final strip thicknesses, respectively. The notations in Eq. (2.2) have been changed to correspond to this thesis. Eklund's method has been very popular in the early years due to the embodiment of the essential rolling variables and it was considered to be a convenient form for calculation of roll force. Later, Roberts [1965] proposed a simplified model assuming uniformity of pressure along the arc of contact. He proposed an equation for roll force as

$$F_r = \sigma_c L_e, \tag{2.3}$$

where σ_c is the average compressive yield strength and L_e is the effective (not the actual) length of the arc of contact. The effective length of the arc of contact L_e is equal to sum of three contributing parts:

$$L_e = l_P + l_E + l_F, \tag{2.4}$$

where, l_P is length associated with the actual plastic reduction of the strip, l_E is the length associated with the flattening of the work rolls by the normal roll force and l_F is the length associated with flattening due to frictional effects. More details of effective length calculations are provided in the book of Roberts [1978].

In early methods, work rolls were considered to remain rigid or without any elastic deformation. Hitchcock [1935] was the first one to establish a relationship between deformed roll radius R' and actual roll radius R in the form of following relation:

$$R' = R\left(1+\frac{16(1-\nu_r^2)}{\pi E_r}\frac{F_r}{\delta}\right), \tag{2.5}$$

where F_r is the roll force per unit width of the strip, ν_r and E_r are Poisson's ratio and Young's modulus of the roll material respectively, and δ is the draft. Since then, Hitchcock's formulae of roll deformation has been used by many researchers. Jortner *et al.* [1959, 1960] were one of the early researchers to establish the actual shape of the region of contact between the roll and strip surface and pressure distribution along it. Further, they reported that Hitchcock's formula is valid only if the pressure distribution between roll and the strip is of elliptical form.

Of late, the slab method has been replaced by more sophisticated methods. However, a few researchers have used the slab method with modified analysis of roll deformation for very thin strips or temper rolling analysis. These authors discussed the inappropriateness of Hitchcock's formula for rolling of thin and hard strips particularly at low reduction. Fleck and Johnson [1987] have relaxed the assumption that the rolls remain circular in foil rolling. Instead they assumed that, when the rolls deform, the roll profile includes a central flattened region. Fleck *et al.* [1992] refined the model of Fleck and Johnson [1987] by treating the rolls as elastic half-space. The contact length is split into a series of zones, according to whether the strip is plastic or elastic and whether there is slip between the roll and strip. Le and Sutcliffe [2001] discarded the assumption that the strip was absolutely flat in the central region and instead used Hooke's law for plane strain condition, to calculate the pressure profile in the central region. Interestingly, the strip profile was still predicted to be remarkably flat in that region. Recently, Chandra and Dixit [2004] used rigid-plastic finite element model for analyzing temper rolling process. The roll deformation is computed in an iterative manner using theory of elasticity solution considering roll as an elastic half space similar to that of Fleck *et al.* [1992]. The authors confirmed the observations of Le and Sutcliffe [2001] that in case of very small entry thickness, severe deformation is observed and deformed profile is no longer cylindrical. In addition to that, the authors reported that the number of pressure peaks increase with reduced entry thickness of the strip. In the review paper of theoretical analyses of rolling, Montmitonnet and Buessler [1991] have presented a review of theoretical analyses of rolling in Europe till 1990.

The most of the previous studies did not utilize extensive numerical computations due to lack of computing facilities at that time. Therefore, slab method based models had more mathematical simplifications than many other techniques like slip-line field theory, upper bound theory and finite element method.

2.2.2 Slip-line Field Based Models

The methods which can easily incorporate inhomogeneity of deformation during the rolling process are the slip-line method, upper bound method and the finite element method. The slip-line field is constructed by networking two kinds of slip-lines representing the maximum and minimum constant shear lines that are orthogonal to each other. The detailed review regarding the use of slip-line for rolling analysis has been carried out by Hartley *et al*. [1989].

In the beginning, Alexander [1955] presented a graphical slip-line field solution for hot rolling process. The slip-line field solutions for cold rolling were suggested by Firbank and Lancaster [1965, 1966 and 1967]. The authors determined local stress, velocity distribution, and pressure distribution. Firbank and Lancaster [1965] reported that the slip-line solutions are applicable to situations where reductions are very small so that it allows assuming the arc of contact is a straight line. Collins [1968] presented a matrix algebraic representation of slip-line geometries. He developed a novel computational procedure by approximating the linear operators using finite-dimensional matrices. Further, Collins [1969] presented a slip-line field solution that showed the presence of small rigid regions in the arc of contact. In this work, work hardening, which is very significant in cold rolling, was completely ignored. Graphical solutions were presented also by Crane and Alexander [1972] for some parameters in hot rolling of strip. Thorough numerical results for the thick strip rolling have been computed by Dewhurst *et al.* [1973] using the linear matrix approach of Collins [1968]. Nepershin [1999] modelled a symmetrical steady-state plane strain slab and strip hot rolling problem using the slip-line method for the rigid-plastic material. However, the main drawback of the slip-line method, which can lead to inaccurate estimation of the rolling parameters, is its inability to incorporate strain hardening effects with ease.

2.2.3 Upper Bound Theory Based Models

The upper bound method involves the construction of a kinematically admissible velocity field for a given deformation process. A kinematically admissible velocity field satisfies the continuity equations and velocity boundary conditions. The power calculated from a kinematically admissible velocity field is more than the actual power. Thus, one can have an estimation of upper bound of power. Johnson and Kudo [1960] demonstrated the use of upper bound solutions for the determination of temperature fields in the arc of contact region for hot rolling. The material has been assumed to be rigid-perfectly plastic. Green and Wallace [1962] developed an upper bound approach assuming that the material in the roll gap is rigid-perfectly plastic and the shear stress along the arc of contact attains the value of the shear yield stress in plane strain. It was extended by Green *et al*. [1964] to include the cases of slipping, and combined slipping and sticking. An upper bound method was proposed for the analysis of rolling by Avitzur [1964] by assuming a continuous velocity field. It provides an expression for torque and the position of the neutral point for a non-hardening material, but it does not provide important design parameters such as roll force and pressure distribution. Later on, Avitzur *et al*. [1987] analyzed the process of strip rolling using the upper bound technique by taking a velocity field that allows for tangential discontinuities. Two triangular velocity fields, one with triangles in linear rigid body motion and the other with triangles in rotational rigid body motion, are developed. The authors determined the total power as a function of four independent process parameters namely; thickness of the strip, reduction, friction and strip tension. The results of these two velocity fields are compared with the obtained solution from Avitzur's continuous velocity field [1964]. Further, Zhu and Avitzur [1988] and Avitzur *et al*. [1988] analyzed the central burst and split end defects in plane strain rolling by applying the upper bound method coupled with principle of minimum energy. They used the condition that the power required is less when cracks are present.

Lahoti *et al*. [1980] modeled the rolling process using upper bound method. They used Hill's [1963] kinematically admissible velocity field to derive expressions for the strain-rate components and equivalent strain-rate. The authors

used upper bound method for estimating the lateral spread, elongation, boundaries of the deformation zone, and the location of neutral plane. They also estimated the stresses, roll force and roll torque using slab method. Tirosh *et al*. [1985] developed a comprehensive upper bound solution for roll force and torque predictions. The authors considered the dynamic behaviour of visco-plastic material, the speed dependent energy dissipations, as well as the heat generation due to plastic work in their model. However, their model seems difficult to apply and their predictions for low rolling speeds do not agree well with experimental data. In general, the upper bound technique is able to provide the velocity, strain rate and strain fields but is unable to determine the stress distribution in the deforming material. Due to this, Marques and Martins [1990] analyzed the plane strain rolling process by dividing the deforming zone into several sub-domains. The study is based on a general kinematically admissible velocity field which is used along with the method of weighted residuals to determine the stress field. Doğruoğlu [2001] introduced a method to construct the kinematically admissible velocity field in the deformation zone. The author introduced elliptical flow lines to represent the flow of material in the deformation zone. Recently, in a three-dimensional deformation of the plate rolling process, Sezek *et al*. [2008] used an upper bound method. The authors used dual stream functions for deriving a kinematically admissible velocity field considering spread.

Limitations of using the upper bound method when there is Coulomb's friction at the interface have been observed by Drucker [1954]. Collins [1969] observed that the usual definition of a kinematically admissible velocity field is unnecessarily restrictive when the upper bound theorem is applied. He has also developed a generalized upper bound theorem which can be used to solve many problems of practical interest in the presence of Coulomb's friction. In the finite element analysis of cold rolling process, Dixit and Dixit [1996] used this generalized upper bound method for the accurate estimation of neutral point.

2.2.4 Finite Element Method Based Models

The finite element method (FEM) originated in the field of structural analysis. It has been rapidly expanding to a wider range of non-structural problems for which exact solutions cannot be found with the traditional techniques. As the finite element method together with high-speed computers is capable of predicting the detailed distribution of field variables, it is quite obvious that this method has been widely used for the analysis of metal forming processes in general and rolling process in particular. The models are considered to be two dimensional (plane strain) or three dimensional. Predominantly, finite element analysis of metal forming problems involves large strain, and inclusion of both material and geometric nonlinearities. The finite element method is expected to be used for simulating metal forming processes, because realistic boundary conditions and material properties can be taken into account. In most of the rolling analyses, the roll is modelled as a rigid or as an elastic body. For material behaviour, viscoplastic, rigid-plastic, elasto-visco-plastic or elastic-plastic model is used.

Finite element method (FEM) is preferred to other methods, as it is able to relax many of the simplifying assumptions; it can easily incorporate non-homogeneity of deformation, process-dependent material properties and different friction models. A number of researchers have employed finite element method for analyzing the rolling problem. Domanti and McElwain [1998] reviewed works of many previous researchers that are based on the finite element modelling as well as other techniques in the cold flat rolling of the metal products.

In the finite element method, the modelling of rolling process involves following steps:

- The strip to be rolled is divided into finite elements which are either triangular or quadrilateral in shape.
- The elements are interconnected at nodal points.
- The elemental equations are obtained by following a strategy that minimizes the error in the solution.
- The elemental equations are assembled to produce global equations.

- The global equations are solved for obtaining the values of primary variables at the nodes.
- The post-processing is carried out to calculate the desired qualities from the nodal values of primary variables.

In the finite element analysis, two widely used finite element based formulations are updated Lagrangian formulation and Eulerian or flow formulation. Some literature is also available on another hybrid model, which is termed as mixed or combined Eulerian-updated Lagrangian formulation [Abo-Elkhier, 1997].

In the updated Lagrangian formulation, the mesh moves and deforms in space, in accordance with the deformation history of the material [Shangwu *et al*. 2003]. In an early attempt, Tamano [1973] formulated an elastic-plastic material model which is suitable for small reduction skin-pass rolling. Thompson [1982] included elastic strain rates in a steady state, isothermal, analysis of viscoplastic flow of metal during rolling. The authors demonstrated that the inclusion of the elastic strain rates allows evaluation of the residual stresses in the strips. Liu *et al*. [1985] incorporated an elastic-plastic finite element model to solve a plane-strain rolling problem. The yielding is based on von-Mises criterion and plastic flow on the Prandtl-Reuss relationship. The effect of unloading is also included. Yarita *et al*. [1988] have analyzed the plane strain rolling process utilizing an elastic-plastic finite element model. They have attempted to predict the stress and strain distribution within the deformation zone using an updated Lagrangian code. Shivpuri and Chou [1989] included dynamic effect in the elastic-plastic finite element analysis of strip rolling. The authors observed that the elastic response of the roll has a major influence on roll force and roll torque results at high R/h_1 ratios (roll radius to half strip thickness), however, elastic response of the strip is of minor importance. Lindgren and Edberg [1990] used explicit as well as implicit finite element formulation in the simulation of rolling. The author reported that roll force prediction using both the formulations is in better agreement with the experimental results. Further, the authors discussed some of the advantages of explicit formulation over implicit formulation. Lee [1998] carried out a three-dimensional elastic-plastic finite element analysis of strip rolling. The material to be rolled is assumed to be an elastic-plastic

solid which undergoes large elastic and plastic strains during the rolling process. Despite the popularity of the updated Lagrangian formulation, it has some disadvantages as compared to the Eulerian formulation. In the large deformation analyses, finite element mesh may be completely distorted after a number of increments. Remeshing becomes inevitable which many times, is inefficient and computationally expensive [Gelton and Koter, 1982]. Few other advantages of Eulerian formulation over the updated Lagrangian formulation have been reported by Abo-Elkhier [1997] while modelling of strip cold rolling using Eulerian fixed mesh technique.

In Eulerian or flow formulation, the material to be rolled is considered as a rigid-plastic material behaving like a non-Newtonian fluid and a spatial description is used, whose independent variables are the present position occupied by the particle and present time. As this method fixes the attention on a given region of space, it is suitable for the steady state problems. In the past, researchers have assumed no slipping between the strip and the roll surfaces to provide a simple velocity boundary condition in plane-strain rolling. Employing this assumption, Tamano and Yangimoto [1975] calculated the stress and strain distributions in skin-pass rolling by the elastic-plastic finite element method. In their approach, the error in the stress due to the numerical integration accumulates significantly when a large deformation is simulated. Rao and Kumar [1979] analyzed a plane-strain problem using the finite element method. The incremental displacement method was used for the nonlinear analysis of the problem. The convergence of the method, the flow of the material under the rolls, the extent of deformation of the material and the pressure distribution on the rolls was studied. The application of the rigid-plastic formulation to the simulation of metal forming processes started about 1970s and is presented in the pioneer works of Lee and Kobayashi [1973] and Zienkiewicz and Godbole [1974] who considered the metal forming process (extrusion or punching) as a flow of plastic solid and developed a rigid-plastic finite element technique. Zienkiewicz *et al*. [1978] considered the rolled material to be rigid-visco-plastic and incompressible. They simulated the friction at the roll-work interface by introducing

a thin layer of elements whose yield strength is assumed to depend on the coefficient of friction and mean stress.

$$\sigma_y = - f \sigma_m , \tag{2.6}$$

where σ_y is the frictional stress (and also the assumed yield strength), f is the coefficient of friction and σ_m is the mean stress. The neutral point is not modelled in this method. Dawson and Thompson [1978] provided a model for plane strain rolling which is based upon an incompressible elasto-visco-plastic flow.

Atreya and Lenard [1979] developed a model that is a combination of a finite element method and slab method. The model describes the roll deformation with an elastic finite element programme while strip deformation is described with a slab model. As a result of this, their predictions of roll torque are in better agreement with experimental data than Orowan's, however, roll forces are better predicted by Orowan's theory. Mori *et al.* [1982] minimized a functional with respect to the position of neutral point in their formulation, thus making the analysis more realistic. The authors have used Coulomb's friction model in their formulation. Velocity-dependent frictional stress for the treatment of the neutral point problem was developed by Li and Kobayashi [1982]. Assuming the existence of rigid-plastic material and rigid roll, Li and Kobayashi have compared their predictions with the previously reported experimental results in the literature and observed that there is a good agreement between the FE based results and experimental results.

Shima *et al.* [1982] assumed a constant coefficient of friction and analysed plane-strain rolling by the rigid-plastic finite element methods and found the solution by obtaining the velocity field that minimizes the total power. Thompson and Berman [1984] developed a flow formulation using Eulerian reference frames with velocity as the prime field variable to study the steady state elastic-viscoplastic flow during rolling. Hwu and Lenard [1987] incorporated roll flattening and the variable coefficient of friction in the model of Li and Kobayashi [1982]. They found that the net effect of including the roll deformation causes an increase in predicted roll force and roll torque of approximately 20 per cent for the cases studied. A

comparison of predicted and experimental result indicates better agreement than in the case of Li and Kobayashi [1982].

Park and Kobayashi [1984] used the rigid-visco-plastic FE method to three-dimensional cases. Kim *et al*. [1991] combined the two-dimensional rigid-plastic finite element method with the slab method to extend the analysis for three-dimensional analysis of shape rolling. Similarly, analysis of cold flat rolling process using two-dimensional rigid-plastic finite element method has been extended to three-dimensional analysis by Iguchi and Yarita [1991]. The frictional boundary condition, which takes slipping and sticking into consideration, was applied to the rigid-plastic FEM analyses. Gratacos *et al*. [1992] considered the elastic deformation of the rolls in their finite element analysis for thin strip rolling. Hwang and Joun [1992] developed an approach based on the rigid-viscoplastic finite element method and employed a penalty algorithm to relax the contact boundary condition for the determination of the stress distributions at the roll-strip interface. Prakash *et al*. [1995] presented a FEM formulation in which the neutral point is found iteratively from the condition that the interfacial shear stress changes its sign at the neutral point. Using different friction models, mesh division and number of elements in the deformation zone, Jiang and Tieu [2001] focused on analysing the influence of friction variation on the convergence and results of simulation such as roll pressure, forward slip and spread by three-dimensional rigid–plastic finite element method.

In most of the previous FEM analyses, either the Lagrange multiplier or the penalty function method may be employed to enforce the condition of incompressibility. The selection of the proper value of the penalty parameter is important. As the pressure is divergence of the velocity times penalty constant, the accuracy of the former is very sensitive to the accuracy of the velocity field. Considering this fact, Dixit and Dixit [1996] employed mixed pressure-velocity formulation for analysing cold rolling process. However, in the mixed pressure-velocity finite element formulation, no pressure boundary conditions are employed and therefore the pressure field is computed up to additive spurious constants. The authors suggested an approximate method to modify the pressure field. In the past, there have been few attempts for improving the prediction of pressure field using

finite element method. Maniatty [1994] used a discontinuous pressure field which allows the unknown nodal pressures to be eliminated in a computationally efficient manner from the formulation, reducing the number of degrees of freedom to only the unknown nodal velocities. The pressure field is recovered at the end of the solution. This makes the algorithm computationally faster, however the accuracy of predicted pressure field cannot be ascertained. Hashemolhosseini *et al*. [2002] proposed a method of recovering the pressure field in metal forming by satisfying the stress equilibrium equations. The equilibrium equation is approximated using a least square method.

Shida and Awazuhara [1973] carried out experimental investigations using steel material to be rolled whereas Al-Salehi *et al*. [1973] conducted experiments using aluminium and copper strips. The experimental values of roll force, roll torque and roll pressure reported by these authors have been used as a benchmark for validating the FEM based models and other models. Among all the FEM based models, model of Dixit and Dixit [1996] is in a close agreement with the experimental results of Shida and Awazuhara [1973]. Further, Dixit [1997] compared the results of FEM model with the experimental results of Al-Salehi *et al*. [1973] and found in good agreement.

Dixit and Dixit [1997] discussed different approaches for determining the residual stress and difficulties associated with the methods. The authors proposed a simplified approach to find the longitudinal residual stress (stress in the direction of rolling) using the flow formulation. A parametric study has been carried out to show the influence of process parameters on the residual stress distribution pattern. However, previous researchers like Thompson [1982], and Malinowski and Lenard [1992] used updated Lagrangian formulation and Eulerian-updated Lagrangian formulation, respectively that are computationally expensive.

The finite element method (FEM) is widely used for analyzing complex rolling process. This method is capable of predicting quite accurate deformation behaviour such as stress distribution, roll force, and roll torque. However, analyses using FEM techniques can be computationally expensive and the time required for a fully converged solution restricts its wider application for optimization problems.

2.2.5 Models Based on Visioplasticity Technique

The visioplasticity method combines experiment and analysis. It is originated by Thomsen *et al*. [1954]. Once the velocity vectors have been determined from an actual test, strain rates are calculated and the stress distributions are obtained from the plasticity equations. The method has helped to obtain reliable solutions in detail for processes in which the experimental determination of the velocity vectors was possible [Kobayashi *et al*. 1989].

Thomson and Brown [1982] used visioplasticity approach in the analysis of cold rolling of aluminium specimens. The authors reported that the analysis by visioplasticity itself did not lead to a satisfactory stress field. However, when the visioplastic method is used to produce slip-line fields from directions of maximum shear strain rate, it gives satisfactory deformation and stress fields. The authors observed that slip-line field and profile of roll pressure are similar to that of Firbank and Lancaster [1965 and 1967] and Collins [1969].

Lately, Rodríguez-Rodríguez *et al*. [2001] studied the strain distribution in the samples of hot rolled steel by using visioplasticity. The authors used steel samples of different chemical composition. The samples were machined in a wedged shape to allow the variation of reduction in the height. It is observed that the strain distributions were affected by the chemical composition of the steel. The material that shows evidence of the higher values of strain was the one with the lower alloying content. The visioplasticity approach is developed to enable the complete stress history from a record of the deformation pattern. However, little work has been reported using visioplastic technique in the rolling processes.

2.2.6 Experimental and Theoretical Investigations of Friction at Roll-work Interface

The study of friction remains fundamental to the development of all rolling models. In fact, the process of rolling actually takes place due to friction. At the roll-work interface, both normal and shear stresses exists and the interface is not stationary but moves along with the strip as it passes between the rolls. In addition, the frictional force changes direction within a small contact region. A number of experimental

investigations have been carried out to indicate that the ratio of frictional force to normal force is not constant but varies along the contact length.

In the beginning, experimental investigation of friction at roll-work interface and roll pressure distribution curves were carried out by Siebel and Lueg [1933]. The authors used annealed aluminium as a material to roll. The authors obtained the results of pressure variation in the roll gap for copper, iron and aluminium strip. The authors used piezoelectric technique where pressure was transmitted through the transducers that were embedded in the roll. Rooyen and Backofen [1957] mounted two pressure-sensitive pins into the surface of the rolls. One pin was mounted radial to the roll and one at an oblique angle. This concept enables separation of the normal and frictional stresses. Experimental investigations were conducted by Al-Salehi *et al*. [1973] using smaller pin transducers to measure stresses along the arc of contact and mill mounted load and torque cells to measure roll loads and torque during cold rolling. The authors conducted a number of experiments on rolling of copper, aluminium and mild steel strips using 6.25 inch (15.875 cm) diameter rolls. It is reported that for certain conditions more than one pressure peak may occur. In his experimental work, Lenard [1991 and 1992] found that the average friction coefficient in dry rolling was strongly affected by the material yield strength, hardness and strain hardening exponent. The magnitude of the reduction and the relative velocity between the strip and the roll were also observed to affect the friction coefficient. Jeswiet and Cao [1994] carried out experimental investigations to measure normal and friction forces at the roll-work interface in dry cold rolling of aluminum. The authors discussed the effect of the degree of aspect ratio upon friction and normal forces.

Stephenson [1983] questioned the reliability and practical significance of measurements using embedded pins. He stated that the pressure pin tests are necessarily performed under conditions that are very different from actual production rolling which in turn may produce error in actual practice. An improved pin technique was developed by Tuncer and Dean [1987]. The authors used a conical pin fitting into a conical bore in the roll. The aim to adopt this method was to prevent the material from penetrating the roll at high pressure. Tieu and Liu [2004]

measured friction variation along the roll-work interface by using a sensors-roll. Four pin-transducers are embedded in the sensor roll. The authors demonstrated that the friction coefficient is not constant along the contact length of roll-work interface and the location of the single pressure peak does not precisely coincide with the location of the neutral point. Recently, Jeswiet *et al*. [2006] discussed the various methods that have been used to measure friction in rolling in the past. The authors discussed some of the recent sensor designs that may be used to measure friction.

In a simplified mathematical modelling of cold rolling process, Roberts [1976] described a method of calculating the coefficient of friction from roll force and strip material data. In most of the early mathematical modelling of rolling processes, either Coulomb's friction model or constant friction model is employed. Wanheim and Bay [1978] suggested an improved model for the frictional shear stress, assuming it to be a certain function of the roll pressure p and friction factor m. The authors reported that at low normal pressure *i.e.* $(p/\sigma_Y < 1.5)$, the friction stress is proportional to the normal stress whereas at high normal pressure *i.e.* $(p/\sigma_Y > 3)$, the friction stress is almost constant. The two range being combined via an intermediate transition region. Wanheim and Bay's friction model is applied by Christensen *et al*. [1986] and Zhang and Bay [1997] in the analysis of plate rolling and cross shear plate rolling, respectively. The appropriateness of Wanheim and Bay's friction model is ascertained by Richelsen [1991] who used finite element method for simulating the plane-strain rolling. The author showed the results for two different friction models *i.e*. Coulomb's model and Wanheim and Bay's friction model. He discussed the difference in the variation of frictional and normal stress for both friction models. Later on, Richelsen [1994] analyzed the combined contact and friction problem using an interface element, using a realistic friction model with a non-linear dependence of the frictional stress on the normal pressure.

In the analysis of foil rolling, Kumar and Dixit [2006] used Wanheim and Bay's model for the analysis of foil rolling process. The authors observed that friction model has great influence on qualitative and quantitative predictions of foil-rolling process. They observed that for high pressure, frictional shear stresses predicted by Wanheim and Bay's model are considerably lower than those predicted

by Coulomb's model. Based on the comparison with experimental data, the authors reported that Wanheim and Bay's model is more appropriate than Coulomb's model in the foil rolling problems. Figure 2.3 shows the three different friction models that are widely used in the analysis of rolling processes.

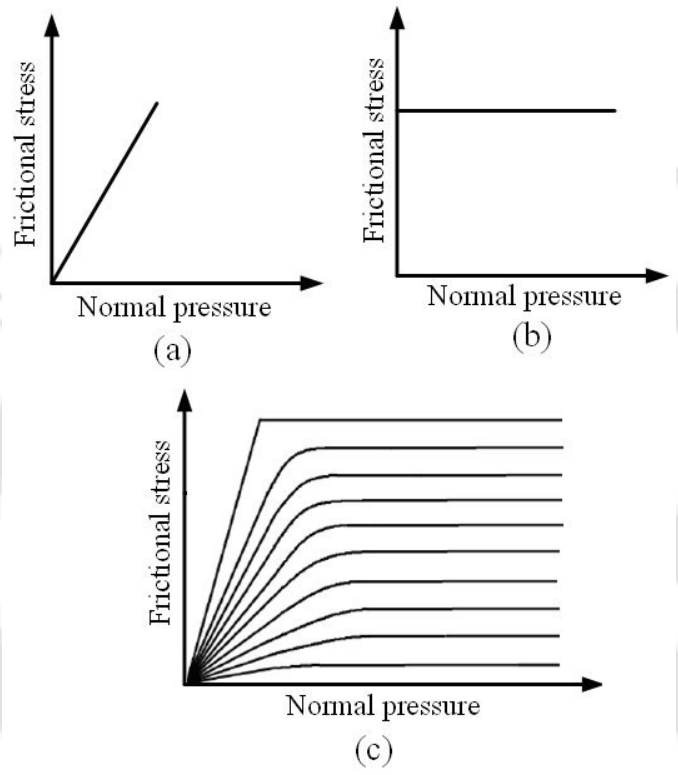

Figure 2.3. Different friction models available in literature. (a) Coulomb's model, (b) Constant friction model (c) Wanheim and Bay's model

Instead of assuming a constant coefficient of friction along the roll-work interface, Rao and Lee [1989] used experimentally measured velocity profile as an input to finite element model for analyzing strip rolling. The authors obtained the variation of the coefficient of friction in the contact region by taking the ratio of shear stress to normal pressure. They observed that coefficient of friction does not remain constant in the roll gap. In the experimental investigations, Rooyen and Backofen [1957], Al-Salehi *et al.* [1973] and Lim and Lenard [1984] also observed the varying friction at the roll-work interface.

In the past, various researchers demonstrated that the friction model plays an important role in determining the correct rolling mechanics and deformation distributions of the strip; also it affects the rolling pressure and the accuracy of on-line control models. Thus, it becomes evident to choose the realistic friction model for mathematical modelling of rolling processes.

2.2.7 Soft Computing Techniques

In engineering, algebraic and differential equations are used to create mathematical models of complex processes like rolling process. However, such approaches require accurate knowledge of the process and numerical calculations to emulate the process. The complexity of the problem itself may introduce uncertainties, which can make the modelling nonrealistic or inaccurate. Due to which, in recent years, there has been a large development of techniques for artificial intelligence that are used to analyze these complex processes. Techniques like artificial neural network (ANN), fuzzy set theory, genetic algorithm (GA) are known as soft computing techniques. Soft computing technique makes use of tolerance for imprecision, uncertainty and partial truth to achieve robustness, low cost and quicker solutions to the complex problems. The application of soft computing techniques is increasing with successful applications in lot of areas like engineering design, optimization, manufacturing system, process control, simulation and communication systems *etc*. In the recent years, many researchers have incorporated soft computing techniques for the analysis of rolling process.

The history of artificial neural network (ANN) modelling began in the early 1940s. McCulloch and Pitts [1943] laid the concept of neurological network by proposing the idea of mind-like machine. In the mid-1980s, these techniques became scientifically sound and capable of applications. The incorporation of neural networks (NN) in the modelling of rolling process speeded up only in mid-1990s. Pican *et al*. [1996] presented an artificial neural network for presetting the roll force in a temper mill. In their research, the authors replaced the existing mathematical model with a new connectionist model. Larkiola *et al*. [1996] integrated physical model and a NN model based on a back-propagation algorithm to a program

package in order to predict roll force in cold rolling. Cho *et al*. [1997] applied a corrective back propagation NN model to predict the roll force for a tandem cold mill. The network had used a set of additional inputs such as the chemical composition of the coil, coiling temperature, and the aggregated amount of processed strips of each roll. Gorni [1997] developed a NN model which predicts slab temperature in the plate rolling. The information obtained from thermometers installed inside special slabs, which are run through the furnace is used to learn the neural networks. The author mentioned that there is a lack of confidence some people feel about the performance of the NN model, as it is difficult to understand how, exactly, these models generate results. The author concluded that this reservation with the technology will be corrected in time and continuous use of these tools and its continuous development will increase the general confidence in these soft computing techniques.

Gunasekera *et al*. [1998] demonstrated a NN model based on a back propagation algorithm to predict the effects of important process parameters on roll force. The authors used a mathematical model based on the works of Gunasekera and Alexander [1987] to generate the training and testing data for the neural network. The authors reported that analysis of rolling process using the techniques like FEM is time-consuming and is not generally practical for the use in industry whereas a neural network based modelling is able to learn on-line, robust in the presence of noise, and behave smoothly to ensure process stability. Neural network based models can also be implemented in real-time optimizing process control that require critical control of process parameters during processing. Myllykoski *et al*. [1998] developed process models for optimization of rolling processes.

Nolle *et al*. [1997] proposed an approach using neural network and genetic algorithm for the optimization of roll profiles in strip rolling. However, such hybrid techniques require a large number of training data to develop the NN model. Lu [1998] applied a back propagation algorithm neural network in combination with a mathematical model to predict the roll force of finishing stands in a hot-strip mill. The author implemented genetic algorithm to optimize the neural network's structure and parameters. Chun *et al*. [1998] modelled a neural network using a

back-propagation learning algorithm, to predict the flow stress, roll force and roll torque obtained during the rolling of aluminium alloys. The authors ascertained that well trained NN models provide fast, accurate and consistent results, making them superior to other predictive techniques. Kusiak *et al*. [1999] incorporated NN model to predict the influence of various frictional conditions on the roll force and torque. The authors used experimental data for training the neural networks.

Lee and Lee [2002] proposed a long-term learning method using a neural network to improve the thickness error of a hot-rolling mill. They noted that the frequencies of lot changes are correlated with the large prediction errors of the rolling force. Thus, a corrective neural network on the lot change is more helpful than using the conventional method. In the algorithm, at the first-coil of the lot, the NN compensation is applied instead of using the conventional learning output. From second to last coils in a lot, the conventional learning output is used. Yang *et al*. [2003] developed NN model for prediction of roll force and roll torque. The authors developed a finite element based code for constructing the NN model. The authors used the FE model to generate the training data for developing the neural network (NN) models. The orthogonal design techniques have been implemented to set-up the rolling conditions for collecting the data for neural network modelling. Son *et al*. [2004] implemented genetic algorithm to optimize the architecture of a neural network. The authors reported that learning approach with the optimal structure of neural network could be applied to improve the accuracy of rolling force prediction in hot rolling mill.

On-line adaptable neural network is modelled by Lee and Choi [2004]. The authors proposed a learning scheme to improve the performance of NN model for roll force in a plate mill. Further, Son *et al*. [2005] incorporated the on-line learning method, which can be learned by new input data, to the prediction of roll force in hot-rolling mill. Power estimation is an important parameter for the design and scheduling of mills. Behzadipour *et al*. [2004] introduced a NN model to estimate power in both flat and shape rolling. The NN model was trained by obtaining the data based on Sims [1954] flat rolling model. Recently, Geerdes *et al*. [2008] presented physics-based and artificial neural networks-based hybrid temperature

prediction schemes for the prediction of temperature in a hot strip mill. The authors reported that using a feed forward NN model together with the heat transfer model helps to achieve better temperature predictions than using the heat transfer model alone in every instance.

The performance of neural network is assessed by its prediction accuracy, network architecture, number of data needed to train a NN model and important input parameters that makes more influence on the output variables *etc*. A systematic procedure has been explained by Dixit and Chandra [2003] who modelled a multilayer perceptron (MLP) network working on a back propagation algorithm for prediction of the roll force and the roll torque. The authors carried out effect of each input variable (factor) on the output variable to determine most influencing input variable. As a result, more representation of such input variables are supplied to the training dataset, as compared to the input variables whose influence on the output variable is less. Further, authors recommended a methodology that suggests adding more data to the training and testing dataset until the desired accuracy is obtained. Apart from training data size, size of testing dataset is equally important. A guideline regarding the size of testing data has been provided by Kohli and Dixit [2005].

Yang *et al*. [2004] used statistical tools to determine critical input parameters for the prediction of roll force. The determination of critical input parameters has been carried out by using analysis of variance (ANOVA). These methods give a clear indication of the key performance input variables that are sufficient to model with. Use of such statistical technique helps to overcome the drawback of this 'information overload' for modelling the complex processes as well as reducing the computational burden. All of the researchers mentioned above used multi-layer perceptron (MLP) neural network for modelling the roll force and roll torque and other variables. In their book, Ham and Kostanic [2001], the authors stated that a radial basis function (RBF) neural network takes lesser training time compared to a MLP neural network.

In the recent past, Samanta [2004] used radial basis function neural network for gear fault detection. The author used genetic algorithm based approach to

determine the optimum spread parameter. Further, RBFs were created, trained and tested using MATLAB through a simple iterative algorithm of adding more neurons in the hidden layer till the performance goal is reached. Sonar *et al*. [2005] applied the radial basis function neural network for predicting the surface roughness in a turning process for dry and wet turning of mild steel using high speed steel (HSS) and carbide tools. The application of radial basis function neural network is incorporated for predicting various parameters in natural circulation boiling water reactor by Garg *et al*. [2007]. The authors used two different types of artificial neural network *viz*. MLP network and RBF network in a systematic manner to overcome data scarcity in the NN modelling. Considering the limitation on the number of experimental data and inherent noise, Sarma and Dixit [2007] modelled MLP neural network based on experimental data. The authors used the trained MLP model to further train the RBF neural network for the prediction of the average surface roughness and tool life in the turning of grey cast iron. Basak *et al*. [2007] modelled radial basis function neural network for predicting the surface roughness and tool wear as functions of cutting speed, feed, and machining time. The authors used experimental data to train the NN model. Panda *et al*. [2008] compared the results of flank wear in drills obtained by RBF neural network and MLP neural network. The authors concluded that both networks can predict the drill flank wear reasonably well.

In the cold rolling process, Sbarbaro-Hofer *et al*. [1993] carried out the controlling of strip thickness in a rolling mill by employing a radial basis function neural network. However, no literature is available where roll force, roll torque and other parameters are modelled using RBF neural networks. All these parameters are very much required for the optimization of the rolling process.

Apart from neural networks, another soft computing technique which has gained equal attention of researchers is fuzzy-set theory. Fuzzy set theory derives its motivation from approximate reasoning. Zadeh [1965] introduced concept of fuzzy set as an extension of classical notion of set. In the classical set theory, membership of elements in a set is assessed in binary terms: an element either belongs or does not belong to the set. On the contrary, fuzzy sets are the set whose elements have

degrees of membership. The membership function assumes a value between 0 and 1 inclusive. The main feature that separates fuzzy set based models from a black-box technique like neural network is that the fuzzy models are, to a certain degree, transparent to the interpretation and analysis [Setnes *et al*., 1998]. Usually, a fuzzy set based model is built by using an expert knowledge in the form of linguistic rules. In general, data acquired by experiments, mathematical modelling, NN modelling or any other suitable methods are used to develop the fuzzy models.

In the analysis of cold rolling process, the material properties and friction coefficient are not known precisely. Hence, Dixit and Dixit [1996] treated them as fuzzy variables and computed the roll force, roll torque and pressure distribution *etc*. using fuzzy arithmetic. A fuzzy set based algorithm for controlling the thickness variations in the hot rolling is developed by Jung and Im [2000]. The method consists of controlling the thickness of outgoing strip by varying the rolling speed. Few other applications of fuzzy set theory like shape control for cold rolled strip [Jung and Im, 1997], shape control in producing thin cold rolled strip [Jung *et al*., 1996] and flatness control [Zhu *et al*., 2003] have been carried out in the past. The application of fuzzy set theory has been extended to the schedule design problem of tandem rolling by Dixit and Dixit [2000]. The authors considered the scheduling problem as an optimization problem, which minimizes the total specific power. Lately, Dixit *et al*. [2002] have used the concept of fuzzy set theory for presenting a systematic design procedure for designing a laboratory cold rolling mill.

In engineering analysis, attempts have been made in the past to incorporate the combinations of fuzzy set theory with other methods such as neural networks, genetic algorithm *etc*. Pratihar *et al*. [1999] described a technique based on fuzzy logic and genetic algorithms to solve the patch finding problems of a mobile robot. Nandi and Pratihar [2004] designed a genetic-fuzzy system to predict surface finish and power requirement in grinding. The authors presented a methodology which improves the performance of fuzzy logic controller. The knowledge base is optimized off-line using genetic algorithm. Zuperl *et al*. [2005] discussed the application of fuzzy adaptive control strategy to the problem of cutting force control in high speed end-milling operation. The research is concerned with the optimization

of a metal cutting process. Abburi and Dixit [2006] developed a knowledge based system for the prediction of surface roughness in a turning process. The authors used NN model and fuzzy set theory for this purpose. The trained neural network is used for generating the large amount of data that are fed to a fuzzy set based rule generation module.

Using genetic algorithm as a search tool, Wang *et al*. [2000] demonstrated an optimal rolling scheduling method. The method aims at achieving uniform power distribution, maximum safe level of strip tension, and good flatness in a tandem cold rolling mills. Chakraborty and Kumar [2003] minimized the time required for hot rolling of an ingot. The idea was to determine the minimum possible odd number of passes, so that the ingot leaves in the same direction as it entered. This ensures the necessary degree of reduction without violating the prescribed upper limits of the available torque and roll force. The problem was solved by using a number of variants of genetic algorithms, including a multipopulation island model and differential evolution, besides the simple genetic algorithms. Nandan *et al*. [2005] used a genetic algorithms-based multioptimization technique to identify the parameter settings and rolling schedules that would result in the optimum values of crown and flatness. Wang *et al*. [2005] introduced an intelligent searching mechanism using genetic algorithm to optimize the rolling schedule by assessing rolling constraints and the combined cost function of tension, shape, and power distribution. Most of the genetic algorithm based works in the rolling process are related to scheduling problems only.

In comparison to the neural networks, application of other soft computing techniques like fuzzy set theory, genetic algorithm *etc*. is still not common in the wide area of metal forming. Figure 2.4 shows some of the major contributions in the field of symmetric rolling process in the form of a chart.

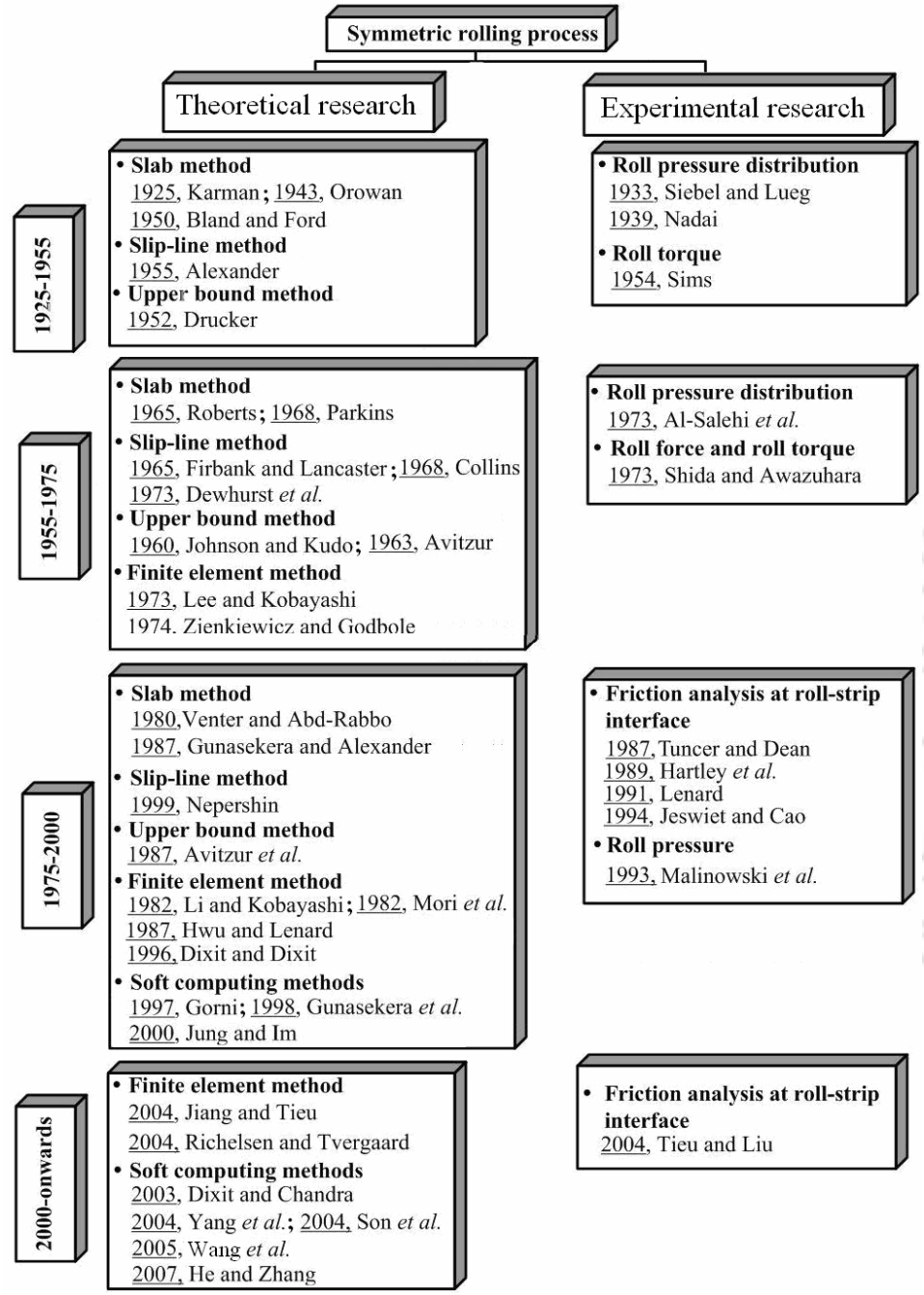

Figure 2.4. Flowchart showing some of the representative work in the modelling of symmetric rolling process

2.3 Research on Asymmetric Rolling Process

In a rolling process, if the roll radius, angular velocities of the upper and lower roll, friction conditions at the upper and lower roll-work interface and the surface roughness of the rolls are different, then the process may be termed as asymmetric rolling process. Due to these differences, two neutral points will be generated *i.e.* neutral point at upper roll-work interface and neutral point at lower roll-work interface. This leads to form a third deformation zone between backward-slip and forward-slip zones, known as the cross shear region. The strip to be rolled gets a curvature which some time is desirable. Figure 2.5 shows schematic diagram of asymmetric rolling process. The asymmetry is caused due to different peripheral speed of upper and lower roll.

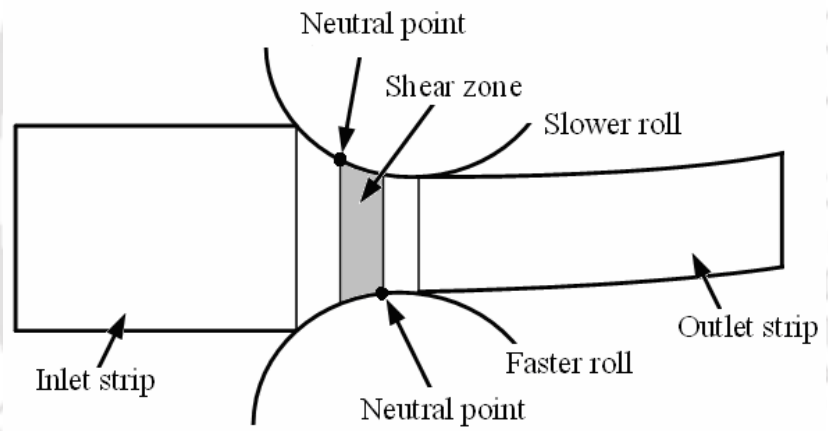

Figure 2.5. A typical cross shear zone in an asymmetric rolling process

In the recent years, asymmetric rolling process has become crucial due to the realization of improved surface properties of the product and lower energy requirement. The mechanics of asymmetric rolling of metal strip has been the subject of continuing interest to researchers. However, the experimental investigations as well as the mathematical analysis started very late due to the difficulty and complexity of the process as compared to symmetric rolling process.

2.3.1 Experimental Research

To study the asymmetric rolling process as well as sign and the magnitude of the curvature of the rolled strip, many researchers carried out experimental

investigations and mathematical analyses. In an early attempt, experiments were carried out by Chekmarev and Nefedov [1956]. Using 522 specimens of lead, steel and aluminium as a material to roll, the authors reported that under certain conditions, a 40% decrease in roll force is possible. Few experiments were carried out using twin-roll driven asymmetric rolling mill by Kennedy and Slamar [1958]. In their experimental investigations, steel strips were rolled and roll torque was monitored. The authors presented an empirical relation relating curvature (turn-up or turn-down) to speed ratio (peripheral speed of top roll to peripheral speed of bottom roll) and torque ratio (top spindle torque to bottom spindle torque). Buxton and Browning [1972] rolled strips of plasticine with aluminum work rolls. All the previous works on asymmetric rolling were focused on the decrease in the roll force and the measurement of the strip curvature to decide which way the rolled strip would curve.

Johnson and Needham [1966] rolled lead strips to simulate the hot rolling process. They investigated the influence of roll speed differentials, roll diameter differences and roll surface roughness differences on the roll force, roll torque and strip curvature. The authors reported that the direction of strip curvature varies with the peripheral roll velocity, reduction ratio and surface roughness. Tanaka *et al*. [1963] experimentally investigated the effect of non-symmetry of the rolling pass on the residual stress distribution and diameter of the curled strip. Reddy and Verduzco [1972] experimentally observed a more than 15% decrease in the roll force with roll speed mismatch in the asymmetric rolling process. Yamamoto *et al*. [1982] have performed cold strip rolling experiments by a two-high plaster rolling mill to obtain the roll force and torque by using the plasticine as test material. Pan and Sansome [1982] investigated the effect of roll speed mismatch on the roll force, roll torque and forward slip in a cold rolling process. Experiments were carried out using thin strip of aluminium, copper and mild steel. Their results showed that the roll speed mismatch can reduce the roll force by 40%.

In an experimental investigation of the strip curvature, Pospiech [1987] observed that in a friction mismatch case, as the reduction is increased, the curvature of the strip changes sign. The author further reported that lubrication mismatch can

have a significant effect on the curvature of the strip. The strip tends to wrap itself around when the reduction is high and the bottom roll is lubricated. Ghobrial [1989] proposed a photo-elastic experimental method to study the contact stresses during an asymmetric flat rolling. Hwang and Tzou [1997] conducted an experimental study on the effect of mismatching roll speed on the roll force, roll torque and forward slip using aluminium as a material to roll. Jeswiet and Greene [1998] carried out an experimental analysis of roll speed mismatch with increasing reduction on strip curvature. Their results agreed with previous studies, and they concluded that strip curvature changes direction with increased reduction.

2.3.2 Theoretical Research

The analysis of asymmetric rolling using mathematical modelling is first initiated by Siebel [1941] who used slab method to derive the equilibrium equations. Sachs and Klinger [1947] used the mechanics of single roll drive mills to develop the asymmetric rolling model. The authors developed a homogeneous deformation model using the slab method with Coulomb friction. They reported that the surface speed of the undriven roll should be lower than that of the driven roll. The authors realized that there exists a region identified as the region of cross shear (Fig. 2.6), where the frictional forces (τ_u and τ_l) on the driven and undriven rolls act on the strip in the opposite directions. The rolled strip at the exit obtains curvature due to this cross shear region.

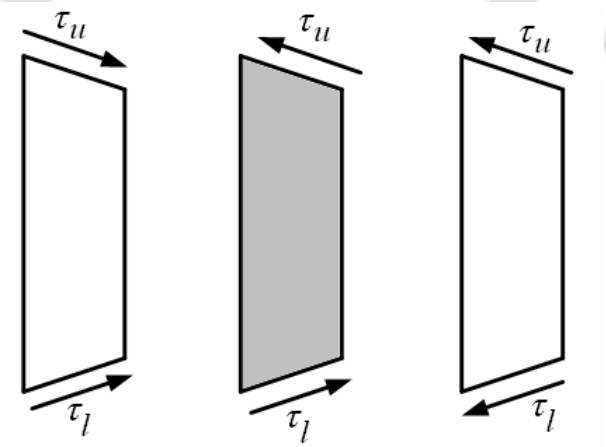

Figure 2.6. The zone of cross shear and direction of the frictional stress on the slabs in an asymmetric rolling process

Zorowski and Shutt [1963] developed a model for hot rolling using the theory of Orowan [1943] with sticking friction model. The theory proposed by Zorowski and Shutt [1963] generate symmetric normal pressure distributions on the rolls. Further, Holbrook and Zorowski [1966] extended the earlier model of Zorowski and Shutt [1963] to include non-symmetry of the roll pressure distribution. All of the above analytical models were developed for a single roll driven case and utilized the slab method to derive the governing equations. Mischke [1996] developed equations of equilibrium in asymmetric flat rolling and considered the entry angle of the strip in his slab method based formulation. In order to verify the experimental investigations, Hwang and Tzou [1997] developed a model based on slab method assuming constant friction factor between the rolls and the strip. Zhang and Bay [1997] reported that due to the shear zone formation in an asymmetric rolling, the friction hill of the pressure distribution along the contact arc will be cut off thereby lowering the roll force compared to symmetric rolling process. Salimi and Sassani [2002] used the slab method to find the curvatures of the strip for different asymmetric conditions. Gao *et al.* [2002] carried out the slab method based analysis of asymmetric rolling process with different coefficients of friction at the upper and lower roll-work interface. The authors reported that the shear deformation zone length increases with an increase in the friction coefficient ratio. The authors also observed that the roll pressure decreases with increase in the friction coefficient ratio. Salimi and Kadkhodaei [2004] used slab method to numerically calculate the roll force and torque in the asymmetric rolling process. The authors considered the non-uniformity of the normal and shear stresses in deriving the governing equations. The authors reported that this consideration plays an important role in the analysis and predicts the actual behavior of the deforming material. The authors compared the analytical roll force, torque and roll pressure with the experimental and analytical results of other investigators.

The use of slip-line method for the analysis of asymmetric rolling was initiated by Dewhurst *et al.* [1974]. The authors conducted analytical and experimental investigations for asymmetric hot rolling. A slip-line field for hot rolling of strip between unequal diameter rolls with different angular velocities is

constructed. The results obtained by slip-line field analysis are compared with experimental results. The experiments were carried out using pure lead strip as a material to be rolled. Strip curvature caused by differences in peripheral roll velocity and roll diameters was measured at different reductions. The authors reported that the rolled strip could bend either way depending on the geometry and relative speeds of the rolls. However, from the experiments, it is observed that the strip may bend towards the faster moving roll, contrary to the earlier experimental results of Johnson and Needham [1966]. Collins and Dewhurst [1975] extended the slip-line field analysis presented by Dewhurst *et al.* [1974] to investigate the effect of different roll radii and roll speed on curvature and roll torque. The authors reported that curvature of the rolled strip is very sensitive to changes in the roll geometry and it can be both positive and negative.

The analysis of asymmetric rolling using upper bound method has been carried out by a few researchers like Johnson and Needham [1966]. The researchers compared the strip curvature obtained by using the upper bound method and the experimental results. Further, Pan and Sansome [1982] compared the experimental results with the upper and lower bound models. In this analysis, the asymmetry was created due to speed mismatch between upper and lower rolls. Dyja and Pietrzyk [1983] analyzed the asymmetric rolling of a bimetallic strip using the upper bound method. Simplifying the geometry of the system by assuming linear contact surfaces both between plates and rolls and between plates, a velocity field is derived which depends on the ratio of the reductions of the dissimilar plates. The final thickness ratio is found as a function of rolling conditions (overall reduction, initial thickness, roll radius, yield stress ratio and friction) by minimizing the dissipated power. Kiuchi and Hsiang [1986] used an upper bound technique for calculating the curvatures in the rolled plates by rolls of different diameter and roll speed mismatch. The authors included the entry angle of the strip in the model as one cause of asymmetry. Their result of curvature due to diameter mismatch is in good agreement with the experimental results but show large discrepancies when their results due to speed mismatch are compared with the experimental results of some other investigators. Hwang and Chen [1996] analyzed asymmetric strip rolling process

using an upper bound method, which makes use of a stream function. The authors predicted roll force and strip curvature and found them to be in good agreement with the experimental results.

Shivpuri *et al*. [1988] are one of the early investigators who used finite element (FE) model for the analysis of asymmetric rolling process. An elastic-plastic FE model is used in the analysis. The asymmetry was considered due to roll speed mismatch. After comparing the results of FE model with previously reported experimental results, the authors concluded that the frictional non-symmetry and weight of the material emerging from the rolls at the exit plane could be responsible for unexpected additional curvature in the experimental results. Similarly, Cao *et al*. [1993] simulated the rolling process using an elastic-plastic plane strain FE model and the influence of roll speed mismatch with equal diameter rolls was investigated. Strip curvature was measured with increased reduction and the results were compared with the experimental investigations of Dewhurst *et al*. [1974]. A detailed study of asymmetric rolling was conducted by Park *et al*. [1993] using a FE simulation. The asymmetry was obtained due to roll speed mismatch. In addition, their investigations also considered the influence of rolling parameters such as reduction ratio, ingoing strip height, average roll speed and average strip temperature. Pietrzyk *et al*. [1993] performed an experimental study and a finite element simulation of various thicknesses of rolled copper strips using different roll diameters ratios. In the experiments, the influence of the degree of reduction on the curvature of the rolled copper strip was measured for different roll diameter ratios. All of the above mentioned researchers used roll speed mismatch for generating asymmetry.

Richelson [1997] studied the influence of different friction conditions at the roll-work interface on the strip curvature in the analysis of asymmetric rolling process. The author used elastic-visco-plastic FE model for the analysis. The result shows that below the recrystalization temperature of material, the rolled plate curves towards the roll with the highest friction coefficient. Park and Hwang [1997] performed an extensive analysis of front end bending in plate rolling using the finite element method. The aim of their work was to increase the knowledge about the

basic parameters of front end bending in plate rolling and to feed an empirical model for the prediction of the rolled stock curvature. An elastic-plastic finite element simulation was carried out by Lu *et al*. [2000], which shows the influence of different diameters of the working rolls and of the degree of reduction on the curvature. The authors reported that the bending of an asymmetrically rolled strip depends on its initial thickness, the degree of deformation and the average radius of the rolls. The authors also reported that the influence of the average roll radius is greater for thin strip than a thick strip. Knight *et al*. [2003] analyzed a plane strain FE model to investigate the effect of asymmetric factors and rolling parameters on the direction and severity of strip curvature. The authors ascertained that when differential interface friction is applied to the model, the predicted curvature is always towards the roll with the greatest friction. An increase in the magnitude of curvature is observed for increasing differential friction. Salunkhe [2006] employed the flow formulation for the analysis of asymmetric rolling process. The finite element formulation used by the author is similar to the one which Dixit and Dixit [1996] used for symmetric rolling process. The estimation of the positions of the upper and lower neutral points is a difficult task, owing to the asymmetry in the rolling process. Salunkhe introduced a penalty function optimization technique to determined the positions of the upper and lower neutral points. Lately, Philipp *et al*. [2007] developed a finite element model to simulate the front end bending. The work carried out by the authors focuses on the well known bending due to the speed mismatch of the rolls. The authors highlighted the influence of initial strip thickness on both the curvature of the strip and the neutral point.

The use of soft computing techniques in the analysis of asymmetric rolling process is still in a premature stage as compared to the analysis of symmetric rolling process. Recently, Kadkhodaei *et al*. [2007] have incorporated a genetic algorithm in the slab method based analysis of asymmetric rolling process. The amount of deflection of the plate at entry to the deformation region is predicted using genetic algorithm in the optimization based solution of the governing equations to ensure the free entry condition. The shear stresses are taken into account in applying the von-Mises yield criterion. The authors verified the various results of the proposed model

with the experimental and theoretical results of other investigators. However, the authors did not include the effect of strain hardening in their analysis. None of the literature is available which uses soft computing techniques like neural networks and fuzzy set theory for investigating different parameters like curvature of the strip and friction coefficient on the upper roll and lower roll *etc*. in the asymmetric rolling process. Figure 2.7 depicts some of the major works available in the literature for the analysis of the asymmetric rolling process.

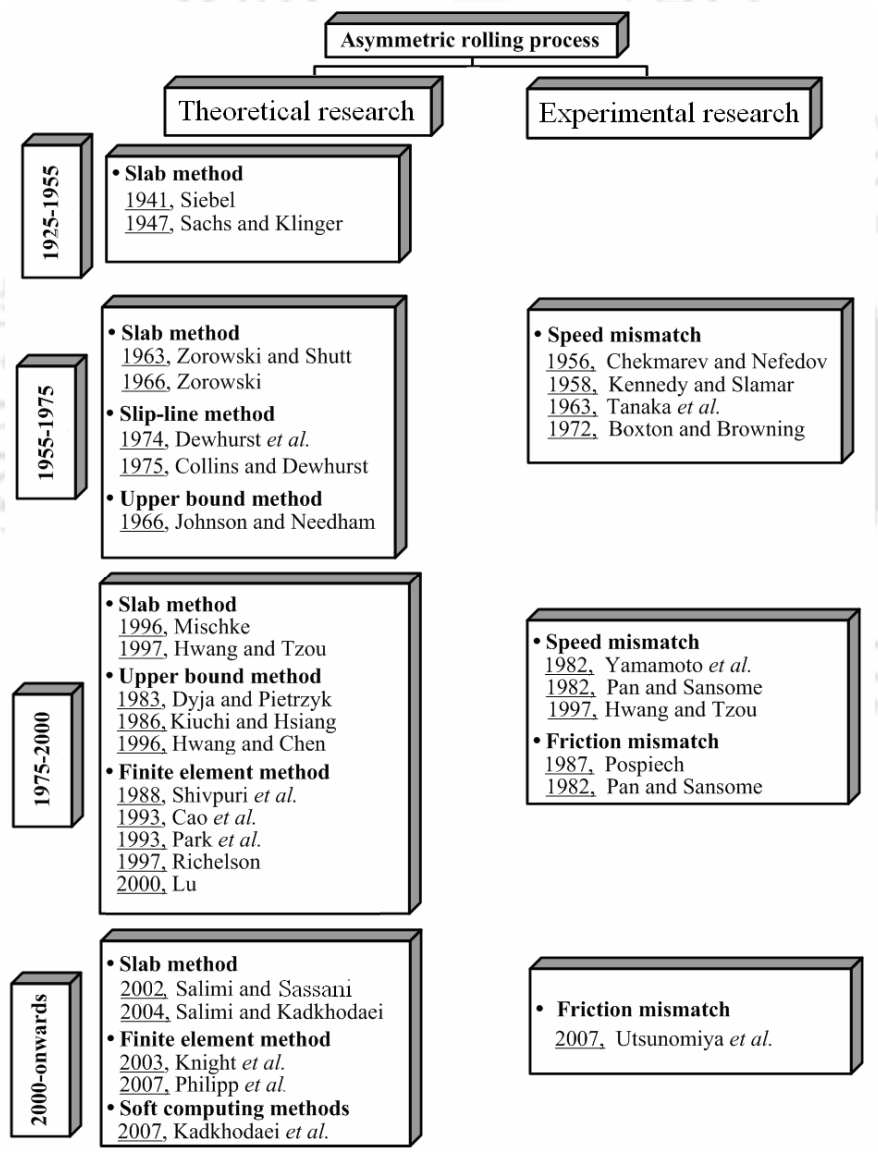

Figure 2.7. Flowchart showing some of the representative work in the modelling of asymmetric rolling process

2.4 Detailed Objectives of the Present Thesis

Literature survey reveals that many of the proposed techniques for the modelling of symmetric as well as asymmetric rolling processes are complicated due to non-linear nature of the problem. The proposed methods are inconvenient for faster prediction due to requirement of large computational time. Models based on soft computing techniques have faster predictability and the knowledge of functional relationship between the independent variables and dependent variables to construct the model is not necessary. Soft computing techniques do not suffer from the brittleness and inflexibility of the earlier proposed methods. In the present work, soft computing assisted modelling of symmetric and asymmetric cold flat rolling process is carried out. The soft computing techniques have been incorporated along with some established techniques to alleviate the complexity of the process and faster prediction.

Although, a number of attempts have been made earlier to incorporate the soft computing (particularly neural networks) based models for the prediction of roll force and roll torque only. However, these models do not provide other necessary information that is required for detailed analysis of cold rolling process. The aim of the present work is to develop a neural network assisted finite element model that gives detailed information of the process with reduced computational time. Requirement of the huge amount of dataset is considered as one of the drawbacks of NN modelling. Hence, a methodology will be presented, which requires less number of training and testing data in the NN models.

The dependency of roll force and roll torque on the process variables in the analysis of cold flat symmetric rolling process is an important issue. Thus, another objective of the present work is to model the roll force and roll torque using Takagi-Sugeno fuzzy models. It will be demonstrated that the coefficients associated with the linear expression of the TS fuzzy model can be used for the sensitivity analysis. Accuracy of the models based on soft computing techniques depends up on the accurate modelling data that are required for construction of these models. In these models, identification of outliers (faulty data) is an important task. A methodology

will be presented for the identification and suppression of the outliers present in the modelling data.

In the mixed pressure-velocity finite element formulation, accurate estimation of pressure is difficult. The present work focuses to develop a more accurate approach for prediction of pressure field. Finite difference method and neural networks will be incorporated for computing the variables required for the proposed approach. The benefits of the developed approach over the previously established approaches will be discussed.

In an actual rolling mill, any geometric and parametric asymmetry at the mid-thickness of the sheet in the rolling process leads to asymmetric rolling process. In this process, rolled sheet obtains curvature. The control of the curvature in the rolled product is important from the point of view of quality. On the other hand, there are situations where asymmetric rolling may be desirable for producing the curved sheets and/or for reducing the roll force and roll torque. Thus, another objective of the present thesis is to study the detailed investigations of the roll force, roll torque, power requirement and curvature in an asymmetric rolling process. A model based on slab method will be used for this analysis. Strain hardening and roll deformation will be incorporated in the proposed model which has not been studied in the previous literature, except in the preliminary work of Salunkhe [2006]. In this thesis, a more thorough study of the model developed by Salunkhe [2006] for asymmetric cold rolling of strain-hardening material with non-rigid rolls will be presented. Salunkhe [2006] has carried out inverse modelling of friction identification based on certain assumption. The appropriateness of these assumptions will be ascertained by with the help of neural network model.

It is observed by various researchers that the friction at the roll-work interface varies in actual rolling mills. This produces undesirable curvature to the rolled product. However, none of the researchers studied the curvature generation due to the uncertain frictional conditions at the mid-plane of the sheet. In the present thesis, the situation of uncertain frictional conditions at the upper and lower roll-work interface will be modelled to estimate the undesirable curvature. In the end, a

methodology based on speed mismatch of upper and lower rolls will be presented to control this undesired curvature.

3

Neural Network Assisted Finite Element Modelling

3.1 Introduction

The finite element analysis of the rolling process has attracted the attention of a number of researchers as it can easily incorporate non-homogeneity of deformation, process dependent material properties and different friction models. However, due to non-linear nature of the problem, the finite element analysis takes a lot of time and is not convenient for on-line prediction or optimization of the rolling process. Recently, there have been some applications of modelling the rolling process by means of neural networks. In most of the previous works, trained networks predict only roll force and roll torque. The input data for training the neural network have been obtained either through experiments or from finite element method (FEM) code.

In this chapter, neural network assisted finite element modelling for symmetric cold flat rolling process is described. Neural networks are introduced in the model to ensure the faster prediction. In the present work, neural networks are employed for the prediction of velocity field and location of neutral point. The neural networks are trained by using the data obtained from finite element based code. The well trained neural network provides a highly accurate guess of a complete velocity field and the location of neutral point, which may be employed for finding out the refined velocity and pressure field using the finite element based code. The refined velocity and pressure field is post-processed for computing roll force, roll torque, stress field, strain field and strain-rate fields.

The determination of important input parameters and requirement of the huge amount of dataset are important factors to be addressed in the neural network modelling. In the present work, statistical techniques are used to determine the

important input parameters and attention has been paid to develop a method, which requires a less number of training and testing data. The performance of the present neural network assisted finite element model has been validated against the finite element model of Dixit and Dixit [1996]. The present model indicates the promising application for on-line prediction and optimization.

3.2 Finite Element Formulation

The finite element model used in the present work is based on the rigid-plastic finite element formulation [Dixit and Dixit, 1996]. It is briefly described in this section. The index notations are employed to represent the expressions and equations used in the formulation. For the steady-state plane strain rolling process, a mixed pressure-velocity formulation is used. In the present work, friction is modelled as Coulomb's model, although Dixit and Dixit [1996] have used Wanheim and Bay's model. It has been observed that in the case of thick strip rolling both the models provide approximately same results, albeit in the case of foil rolling there is a large difference in prediction of various parameters by both models [Kumar and Dixit, 2006].

For the steady-state rolling process, the Eulerian form of the continuity and momentum equations is

$$\frac{\partial v_i}{\partial x_i} = 0, \tag{3.1}$$

$$-\frac{\partial p}{\partial x_i} + \frac{\partial S_{ij}}{\partial x_j} = 0, \tag{3.2}$$

where v_i is the velocity vector at the point with Cartesian coordinate x_i, p is the negative of hydrostatic stress or pressure and S_{ij} is the deviatoric stress component. In rigid-plastic material, the pressure p is given by

$$p = -\frac{\sigma_{kk}}{3}, \tag{3.3}$$

and the deviatoric part S_{ij} of the stress tensor σ_{ij} is related to $\dot{\varepsilon}_{ij}$ by the relation [Malvern, 1969]:

$$S_{ij} = 2\mu\dot{\varepsilon}_{ij}. \tag{3.4}$$

In Eulerian formulation, the strain-rate tensor $\dot{\varepsilon}_{ij}$ which is normally used as a measure of deformation is given by

$$\dot{\varepsilon}_{ij} = \frac{1}{2}\left(\frac{\partial v_i}{\partial x_j} + \frac{\partial v_j}{\partial x_i}\right). \tag{3.5}$$

For rigid-plastic material, the plastic strain-rate tensor is the same as the strain-rate tensor. For material yielding according to von-Mises criterion, the proportionality factor μ is given by [Malvern, 1969]:

$$\mu = \frac{\sigma_Y}{3\tilde{\dot{\varepsilon}}}. \tag{3.6}$$

In the above expression, $\tilde{\dot{\varepsilon}}$ is the equivalent strain rate is defined as

$$\tilde{\dot{\varepsilon}} = \sqrt{\frac{2}{3}\dot{\varepsilon}_{ij}\dot{\varepsilon}_{ij}}\ , \tag{3.7}$$

and σ_Y is the flow stress in uniaxial tension or compression. In general, σ_Y is a function of temperature and strain-rate. The temperature rise and strain rates in a typical cold rolling operation are quite small. Thus, the effect of temperature and strain-rate may be neglected. However, the effect of strain hardening may be included by a power law. Hence, for most of the metals, dependence of flow stress on $\tilde{\varepsilon}$ is given as

$$\sigma_Y = (\sigma_Y)_0\left(1+\frac{\tilde{\varepsilon}}{b}\right)^n. \tag{3.8}$$

Here, $(\sigma_Y)_0$, b and n are uniaxial yield stress, strain hardening parameters respectively. When the loading is proportional, the flow stress of an isotropic strain

hardening material can be expressed in terms of the equivalent plastic strain $\tilde{\varepsilon}$ which can be obtained by integrating $\dot{\tilde{\varepsilon}}$ along the particle path:

$$\tilde{\varepsilon} = \int_0^t \dot{\tilde{\varepsilon}} \, \mathrm{d}t. \tag{3.9}$$

The detailed procedure followed for constructing particle paths and integrating the strain rates is given by Dixit and Dixit [1995] and is briefly described in Appendix A.

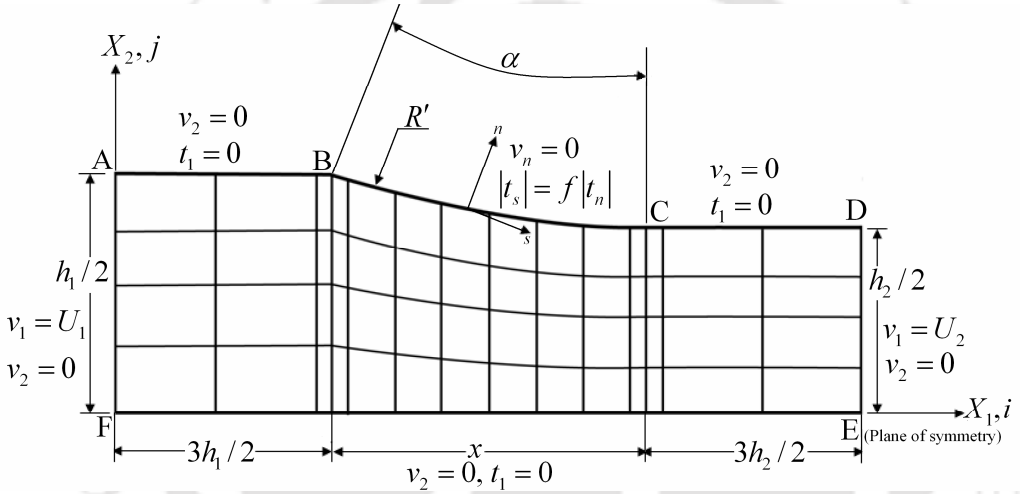

Figure 3.1. The domains along with mesh and boundary conditions

In the pre-processing stage, mesh generation is done as shown in Fig. 3.1. Because of sharp change in the boundary conditions at B and C, smaller size of elements is taken near these points. More number of elements is chosen for deformation region as compared to inlet and exit region. Figure 3.2 (a) and (b) shows a typical quadrilateral element in natural coordinates that are selected to discretize the domain. For pressure, bi-linear approximation is chosen and for approximation of velocity components and geometry, bi-quadratic approximation is chosen. Thus, the pressure is approximated using four noded quadrilateral Lagrangian elements while velocity components are approximated using nine noded quadrilateral Lagrangian elements. For a strip of 56 elements, 75 nodes for pressure and 261 nodes for velocity components are chosen.

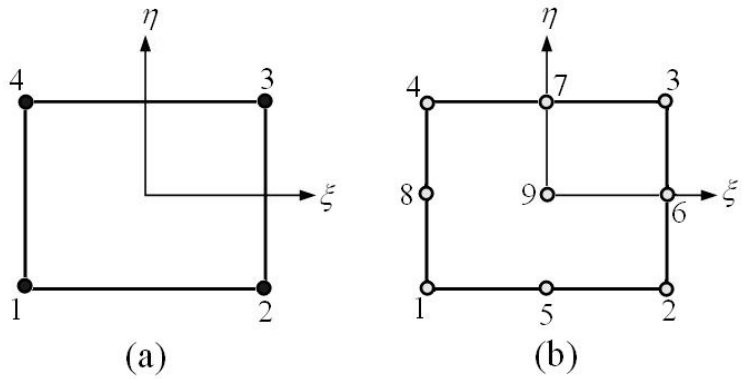

Figure 3.2. A typical element (a) nodes for pressure approximation (b) nodes for velocity and geometry approximation

The boundary conditions along AF and DE are given as

$$\begin{aligned} v_1 = U_1, v_2 = 0 \quad \text{on AF}, \\ v_1 = U_2, v_2 = 0 \quad \text{on DE}, \end{aligned} \tag{3.10}$$

where v_1 and v_2 are the components of velocity in x_1 and x_2 direction, respectively. The inlet and exit velocities U_1 and U_2 respectively, along AF and DE are related as

$$U_1 = U_2(1-r), \tag{3.11}$$

where r is the fractional reduction given by

$$r = \frac{h_1 - h_2}{h_1}, \tag{3.12}$$

and the roll velocity corresponding to U_2 is obtained as the velocity at the neutral point (a point where shear stress changes its sign). The neutral point, in this formulation is found by minimizing the total power with respect to the position of neutral point which is based on the generalized upper bound theorem [Collins, 1969].

On the plane of symmetry FE and on the surface AB and CD, the following boundary conditions are used.

$$v_2 = 0, \; t_1 = 0, \tag{3.13}$$

where t_1 is the traction component in longitudinal direction. On the roll-work interface (boundary BC), the normal component of velocity, $v_n = 0$. This leads to

$$v_2 + v_1 \tan\phi = 0 \quad \text{on BC}, \tag{3.14}$$

where ϕ is the angular position of the point on the interface. The frictional traction t_s is related to normal traction t_n by Coulomb's friction mode subjected to a limit on its maximum value as

$$|t_s| = \begin{cases} f|t_n| & \text{if} \quad f|t_n| \le \dfrac{\sigma_Y}{\sqrt{3}}, \\ \dfrac{\sigma_Y}{\sqrt{3}} & \text{if} \quad f|t_n| > \dfrac{\sigma_Y}{\sqrt{3}}, \end{cases} \tag{3.15}$$

where f is the coefficient of friction and t_s and t_n are the tangential and normal components of stress vector $\boldsymbol{t}$ defined as

$$t_i = \sigma_{ij} n_j . \tag{3.16}$$

Here, n_j is the unit normal to the surface. The roll deformation is estimated using Hitchcock's formula [Hitchcock, 1935]. According to this formula, the ratio of the radius of the deformed arc of contact R' to roll radius R is given by

$$\frac{R'}{R} = \left(1 + \frac{F_r}{C\delta}\right), \tag{3.17}$$

where F_r is the roll force per unit width and $\delta = (h_1 - h_2)$ is the draft (difference in the initial and final thickness of the strip). The constant C that depends on material of the roll, is given by

$$C = \frac{\pi E_r}{16(1-\nu_r^{\,2})}, \tag{3.18}$$

where E_r and ν_r are the Young's modulus of elasticity and Poisson's ratio respectively, of the roll material. In this work, C has been taken as 46 GPa, a typical

value for the steel rolls. In the present work, Hitchcock's formula has been used in view of its simplicity, although it may lead to error when used for rolling analysis of a hard and thin strip.

Following the standard Galerkin formulation [Reddy, 2006], the global equations after application of all the boundary condition are obtained in the following form [Appendix B]:

$$[K]\{\Delta\} = \{F\}, \tag{3.19}$$

where $[K]$ is the global coefficient matrix, $\{F\}$ is the global right hand side vector and $\{\Delta\}$ is the global vector of nodal values of pressure and velocity (unknown primary variables). A typical nodal velocity component or the location of neutral point can be expressed as a function $g(R/h_1, f, r, b, n)$ of five input (material and process) parameters.

Once the solution is obtained in the form of nodal velocities v_i and pressure, the secondary variables *viz*. roll force, roll torque, strain field *etc*. can be computed. The roll force per unit width F_r is given by

$$F_r = \int_0^l (t_n \cos\phi - t_s \sin\phi)\mathrm{d}s, \tag{3.20}$$

where l is the arc of contact. The roll torque per unit width T is computed by following relationship

$$T = \frac{PR}{V_R}, \tag{3.21}$$

where, V_R is the angular velocity of the roll and P is the total power. The total power P consists of the following three parts:

(i) Power required for plastic deformation (P_p) :

The power dissipated due to plastic deformation is given by

$$P_p = \int_A S_{ij}\dot{\varepsilon}_{ij}\mathrm{d}x_1\mathrm{d}x_2. \tag{3.22}$$

(ii) Power required to overcome friction at the roll-work interface (P_f):

The power dissipated due to friction is given by

$$P_f = \int_0^l | t_s | | \Delta v_s | \, \mathrm{d}s \,, \tag{3.23}$$

where Δv_s is the relative velocity with respect to the velocity of neutral point along the interface and l is the arc of contact. The shear stress t_s is calculated from Eq. (3.15).

(iii) Power required due to tensions (P_t):

The power required in the presence of front and back tensions is

$$P_t = (t_b - t_f)\frac{h_1}{2}U_1 \,. \tag{3.24}$$

The roll pressure or interfacial normal stress t_n is calculated using Eq. (3.16).

3.3 Prediction of Velocity Field by Neural Network

Artificial neural systems, or neural networks, are physical cellular systems that can acquire, store, and utilize experiential knowledge. Neural network techniques have been found capable of learning from a dataset to describe the non-linear and interaction effects with great success. Artificial neural networks are basically connectionist systems, in which various nodes called neurons are interconnected. A typical neuron receives one or more input signals and provides an output signal depending on the processing function of the neuron. This output is transferred to connected neurons in varying intensities, the signal intensity being decided by the weights. Artificial neural networks draw their inspiration from biological neural network. Neural networks can be used for finding out the relationship between independent and dependent variables. For this purpose, a set consisting of input and output vector pairs is needed. From this set, some pairs are used for the training of the network that is used for adjusting the parameters of the network in order to minimize the predicted error. After that the network is tested or cross-validated with the remaining pairs. A properly fitted network should provide very less amount of

training as well as testing error. Different types of networks have been used for finding out the relation between output as well as input vector. The two most common being multi-layer perceptron (MLP) neural network and radial basis function (RBF) neural network [Ham and Kostanic, 2001].

A multi-layer perceptron (MLP) neural network is a feed-forward neural network with one or more hidden layers. Typically a network consists of an input layer, one or more hidden layer, and an output layer. The input signals are propagated in a forward direction on a layer-by-layer basis. A feed-forward neural network has a sequence of layers consisting of a number of neurons in each layer. The output of neurons of one layer becomes input to neurons in the succeeding layer. Presence of hidden layer is needed in order to provide complexity to network architecture for modelling non-linear functional relationship. During the training process, the network adjusts its weights to minimize the error between the predicted and actual outputs. Most common algorithm available for adjusting the weights is back propagation algorithm. The training process involves two passes. In the forward pass, the input signals propagate from the network input to output. In the reverse pass, the calculated error signals propagate backward through the network where they are used to adjust the weights.

Unlike multi-layer perceptron neural network, RBF neural network is a network having three layers– input layer, one hidden layer, and output layer. The input layer consists of neurons, corresponding to the elements of input vector. These neurons send the values of independent variables to the neurons of succeeding hidden layer. Each neuron of the hidden layer is assigned a fixed center, which is of the same dimension as the input vector. The centers are chosen from the training dataset. A neuron of the hidden layer receives input vector and emits the output, which is a function of the Euclidian distance of the input vector and the center associated with that particular neuron. This function is a radial basis functions having radial symmetry. Some of the available functions are multiquadrics, inverse multiquadrics, Gaussian and thin plate splines [Ham and Kostanic, 2001]. In the present work, a Gaussian function (bell-shaped) of the following form is used:

$$\varphi(x) = \exp(-x^2 / \sigma^2), \tag{3.25}$$

where x is the Euclidian distance between the center and input vector, σ is known as the spread parameter, which controls the domain of influence of the radial basis function.

The weighted addition of the outputs of neurons of the hidden layer is sent to the output neuron, which processes it by adding a constant term called bias termed as b_0. Thus the output of the RBF neural network is approximated as

$$f(x) = \sum_{j=1}^{m} w_j \varphi_j \left(\| \boldsymbol{x} - \boldsymbol{c}_j \|_2 \right) + b_0 , \tag{3.26}$$

where $\boldsymbol{x} = \{R/h_1, f, r, b, n\}^{\mathrm{T}}$ is the input vector, $\varphi_j(\cdot)$ is the processing function of the j^{th} node in the hidden layer, $\|.\|_2$ denotes Euclidean norm, w_j are the weights associated with the j^{th} node in the hidden layer, m is the number of neurons in the hidden layer and $\boldsymbol{c}_j$ are the RBF centers obtained from the input vector space. For fixed centers and spread parameter, applying Eq. (3.26) for each training data provides a linear system of equations with m unknowns w_j and one unknown b_0, which can be solved using least square method. Hence, the training procedure takes much less time compared to a multi-layer perceptron network.

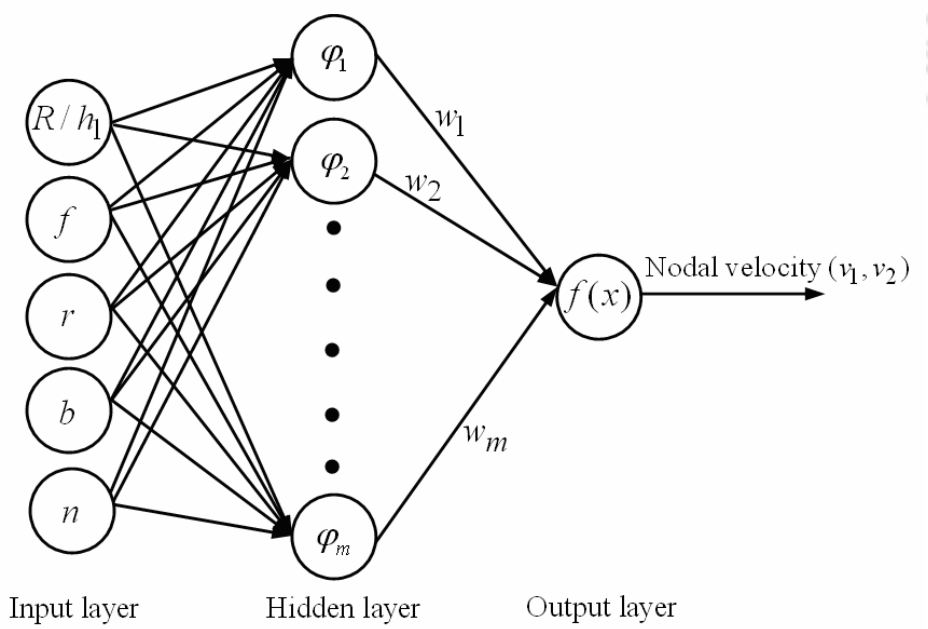

Figure 3.3. Schematic diagram of RBF neural network used in the present analysis

Due to faster training procedure, the present work employs RBF neural networks for the estimation of nodal velocities as a function of R/h_1, f, r, b and n. The number of nodal variables, also corresponding to neurons in the output layer, in a typical problem is quite large; hence the reduction of training time is of prime importance. Also, the number of neurons in the hidden layer should be kept as small as possible in order to have less prediction time. Thus, before deciding the architecture of the network, a thorough study of the data was carried out in order to understand the dependence of nodal velocities on the five-input variables. This is described in the next subsection.

3.3.1 Study of Data

The upper half of a portion of a metal strip constructed with a mesh of 56 elements consists of 261 nodes for velocity field with 2 degrees of freedom. The study was carried out for six different nodes in the plastic zone. The nodes are selected to represent the entire domain in the plastic zone. These nodes are shown by black dots in Fig. 3.4.

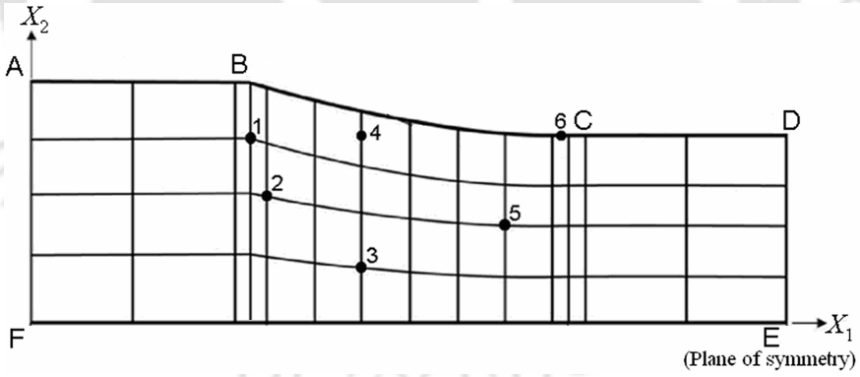

Figure 3.4. Locations of six nodes selected for data analysis.

The range of the input variables for the present analysis is taken as follows:

$$R/h_1 : 10-100,\ f : 0.04-0.14,\ r : 0.04-0.24,\ b : 0.02-0.08,\ n : 0.001-0.6$$

For studying the influence of input parameters on the nodal velocity for 2^5 =32 dataset obtained by finite element based code, the data was studied using SPSS V 12.0.1 (Statistical Package for the Social Sciences) software. The correlation

analyses and analysis of variance is carried out on the selected nodes in the deformation region to find out critical input variables, which may be significant for predicting velocity field.

3.3.1.1 Correlation Analysis

The Pearson's correlation coefficient (p_r) is one of the statistical techniques to analyze the relationship between the variables. It is also known as Pearson product-moment correlation coefficient. The correlation coefficient (p_r) reflects the degree of linear relationship between the two variables. It is obtained by dividing the covariance of the two variables by the product of their standard deviations. The covariance is the measure of how much two random variables vary together. If two variables tend to vary together, then the covariance between the two variables will be positive. On the other hand, if they vary in the opposite direction, then the covariance between the two variables will be negative. Correlation coefficient ranges from +1 to -1. A correlation coefficient of +1 depicts a perfect positive linear relationship between the variables. A correlation coefficient of -1 indicates an exact negative linear relationship between the two variables whereas correlation coefficient of 0 means that there is no linear relationship between the two variables.

In the present study, the dependence of nodal velocities on the five-input parameter is studied by carrying out correlation analysis. Tables 3.1–3.6 show results of correlation analysis for node 1–6 respectively.

Table 3.1. Correlation analysis for velocity v_1 and v_2 (node: 1)

Parameter	R/h_1	f	r	b	n	v_1	v_2
R/h_1	1	0.000	0.000	0.000	0.000	0.001	0.381*
f	0.000	1	0.000	0.000	0.000	0.001	0.191
r	0.000	0.000	1	0.000	0.000	-1.00**	-0.235
b	0.000	0.000	0.000	1	0.000	-0.003	0.250
n	0.000	0.000	0.000	0.000	1	0.002	-0.266
v_1	0.001	0.001	-1.00**	-0.003	0.002	1	--
v_2	0.381*	0.191	-0.235	0.250	-0.266	--	1
** Correlation is significant at the 0.01 level (2-tailed).							

Table 3.2. Correlation analysis for velocity v_1 and v_2 (node: 2)

Parameter	R/h_1	f	r	b	n	v_1	v_2
R/h_1	1	0.000	0.000	0.000	0.000	0.019	0.240
f	0.000	1	0.000	0.000	0.000	-0.011	0.153
r	0.000	0.000	1	0.000	0.000	-0.998**	-0.573**
b	0.000	0.000	0.000	1	0.000	-0.03	0.060
n	0.000	0.000	0.000	0.000	1	0.015	-0.243
v_1	0.019	-0.011	-0.998**	-0.03	0.015	1	--
v_2	0.240	0.153	-0.573**	0.060	-0.243	--	1
** Correlation is significant at the 0.01 level (2-tailed).							

Table 3.3. Correlation analysis for velocity v_1 and v_2 (node: 3)

Parameter	R/h_1	f	r	b	n	v_1	v_2
R/h_1	1	0.000	0.000	0.000	0.000	-0.045	0.798**
f	0.000	1	0.000	0.000	0.000	-0.050	-0.042
r	0.000	0.000	1	0.000	0.000	-0.994**	-0.253
b	0.000	0.000	0.000	1	0.000	0.009	-0.036
n	0.000	0.000	0.000	0.000	1	-0.001	0.163
v_1	-0.045	-0.050	-0.994**	0.009	0.001	1	--
v_2	0.798**	-0.042	-0.253	-0.036	0.163	--	1
** Correlation is significant at the 0.01 level (2-tailed).							

Table 3.4. Correlation analysis for velocity v_1 and v_2 (node: 4)

Parameter	R/h_1	f	r	b	n	v_1	v_2
R/h_1	1	0.000	0.000	0.000	0.000	0.066	0.815**
f	0.000	1	0.000	0.000	0.000	0.071	0.017
r	0.000	0.000	1	0.000	0.000	-0.989**	-0.50**
b	0.000	0.000	0.000	1	0.000	-0.004	-0.005
n	0.000	0.000	0.000	0.000	1	-0.015	0.048
v_1	0.066	0.071	-0.989**	-0.004	-0.015	1	--
v_2	0.815**	0.017	-0.50**	-0.005	0.048	--	1
** Correlation is significant at the 0.01 level (2-tailed).							

Table 3.5. Correlation analysis for velocity v_1 and v_2 (node: 5)

Parameter	R/h_1	f	r	b	n	v_1	v_2
R/h_1	1	0.000	0.000	0.000	0.000	-0.085	0.434**
f	0.000	1	0.000	0.000	0.000	0.100	0.093
r	0.000	0.000	1	0.000	0.000	-0.981**	-0.681**
b	0.000	0.000	0.000	1	0.000	-0.023	0.061
n	0.000	0.000	0.000	0.000	1	-0.022	-0.014
v_1	-0.085	0.100	-0.981**	-0.023	-0.022	1	--
v_2	0.434**	0.093	-0.681**	0.061	-0.014	--	1
** Correlation is significant at the 0.01 level (2-tailed).							

Table 3.6. Correlation analysis for velocity v_1 and v_2 (node: 6)

Parameter	R/h_1	f	r	b	n	v_1	v_2
R/h_1	1	0.000	0.000	0.000	0.000	0.630**	0.75**
f	0.000	1	0.000	0.000	0.000	-0.216	0.011
r	0.000	0.000	1	0.000	0.000	0.608**	-0.566**
b	0.000	0.000	0.000	1	0.000	0.018	-0.026
n	0.000	0.000	0.000	0.000	1	-0.220	0.039
v_1	0.630**	-0.216	0.608**	0.018	-0.220	1	--
v_2	0.75**	0.011	-0.566**	-0.026	0.039	--	1
** Correlation is significant at the 0.01 level (2-tailed).							

The correlation analysis shows that for node 1 (Table 3.1), the horizontal and vertical component of velocity v_1 and v_2 respectively, makes significant correlation with reduction r and R/h_1. For node 2 (Table 3.2), the horizontal and vertical component of velocity v_1 and v_2 respectively, makes significant correlation with reduction r only. For node 3, the horizontal component of velocity v_1 makes significant correlation with r and vertical component of velocity v_2 makes significant correlation with R/h_1. At node 4, reduction makes significant correlation with v_1 and v_2 whereas R/h_1 makes significant correlation for v_2. Similar results

are obtained for node 5. For node 6, it is observed that significant correlation occurs for R/h_1 and r for both v_1 and v_2. It is observed that at all these nodes, strain hardening coefficient b and n does not make any correlation with both v_1 and v_2. Thus, strain hardening coefficient b and n are found insignificant in determination of velocity components.

3.3.1.2 Analysis of Variance(*ANOVA*)

Like correlation analysis, the data obtained from an experiment involving several levels of one or more factors can be analyzed by the technique of analysis of variance (ANOVA). This technique enables us to break down the variance of the measured variables into portions caused by the several factors. The variation components will be those associated with factor effect (main effect or interaction effect) and that associated with random variation, referred as residual. This residual can be seen as the amount of variance one would expect if none of the factors had any effect. The *F*–ratio is used to asses the significance of the effect. If the *F*–ratio is large, we say effect is significant *i.e*. the variation it causes can not be attributed to chance or randomness. The critical value (*p*–values) for variance tests is found from the *F*-tables for some pre-specified level of significance.

In the present analysis, the analysis of variance is carried out for horizontal component as well as vertical component of velocity (v_1 and v_2) for all six nodes. Table 3.7 and 3.8 shows the details of the ANOVA tables for node 6. The *p*–values of v_1 and v_2, up to 3 decimal, based on *F*–ratio for all 6 nodes are shown in Table 3.9. The *p*–value provides an objective measure of the strength of evidence, which the parameter supplies against the null hypothesis that the parameter is significant for prediction of velocity. A smaller *p*–value means the parameter is significant for determining the velocity. In most of the engineering applications, 5% significance level is commonly used. Table 3.9 shows that parameters R/h_1, r and f may be considered significant even at 1% significance level. For nodes 1 and 2, n is found significant at 10% significance level. On the other hand, strain hardening parameter b is not found significant even at 10% significance level. Thus, the strain hardening does not seem to have influence on the velocity distribution. By finite element

analysis of wire drawing process, Dixit and Dixit [1995] had also observed the same.

Table 3.7. ANOVA table for horizontal component of velocity, v_1 (Node: 6)

			Sum of squares	df	Mean square	F-ratio	p-value
Velocity v_1	Main effects	(Combined)	26.751	5	5.350	22.768	0.000
		R/h_1	13.036	1	13.036	55.475	0.000
		f	1.527	1	1.527	6.497	0.017
		r	12.162	1	12.162	51.756	0.000
		b	0.010	1	0.010	0.043	0.837
		n	0.016	1	0.016	0.069	0.795
	Model		26.751	5	5.350	22.768	0.000
	Residual		6.110	26	0.235		
	Total		32.861	31	1.060		

Table 3.8. ANOVA table for vertical component of velocity, v_2 (Node: 6)

			Sum of squares	df	Mean square	F-ratio	p-value
Velocity v_2	Main effects	(Combined)	43.596	5	8.719	43.230	0.000
		R/h_1	27.860	1	27.860	138.129	0.000
		f	0.006	1	0.006	0.031	0.861
		r	15.626	1	15.626	77.472	0.000
		b	0.032	1	0.032	0.159	0.693
		n	0.073	1	0.073	0.360	0.554
	Model		43.596	5	8.719	43.230	0.000
	Residual		5.244	26	0.202		
	Total		48.840	31	1.575		

Table 3.9. The p–values based on F–ratio for v_1 and v_2

Nodes	R/h_1		f		r		b		n	
	v_1	v_2	v_1	v_2	v_1	v_2	v_1	v_2	v_1	v_2
1	0.769	0.021	0.713	0.232	0.002	0.143	0.173	0.120	0.270	0.099
2	0.068	0.105	0.253	0.293	0.001	0.000	0.737	0.678	0.140	0.100
3	0.015	0.000	0.008	0.682	0.003	0.019	0.620	0.729	0.971	0.120
4	0.005	0.000	0.003	0.767	0.001	0.000	0.855	0.928	0.437	0.400
5	0.004	0.001	0.001	0.418	0.000	0.000	0.397	0.596	0.419	0.904
6	0.000	0.000	0.017	0.861	0.001	0.000	0.837	0.693	0.795	0.554

Since the analysis of variance suggests that parameter n is significant at 10% significance level for nodes 1 and 2, it was decided to develop one type of network

models with R/h_1, f, r and n as input parameters and other type of networks with R/h_1, f and r as the input parameters for prediction of horizontal and vertical component of velocity (v_1 and v_2).

3.3.2 Neural Network (NN) Modelling

Two types of RBF network architectures were tried out for the prediction of velocity field and location of neutral point. The first network was trained by 24 datasets, out of which 16 datasets correspond to the corners of four-dimensional input space (R/h_1, f, r and n) and 8 datasets are randomly chosen. Neural networks behave poorly in extrapolation. Thus it is essential to include the data corresponding to the corners of the input space in the training dataset. This ensures that neural networks have to interpolate only during the prediction. The second network having three-dimensional input (R/h_1, f and r) space was trained in the similar way with total 16 datasets.

The size of testing (or cross-validation dataset) is very important from the viewpoint of reliability of the network. A guideline regarding this has been provided in [Kohli and Dixit, 2005]. It is briefly explained here. Suppose that in the validation data, the percentage of data having an error greater than a prescribed value is p_f. The network is always fitted in such way so that in no prediction, the error is more than the prescribed value. For a testing data size of k, the probability that in this dataset, all of the predictions fall within the limit is given by

$$P_0 = \left(1 - \frac{p_f}{100}\right)^k . \tag{3.27}$$

Using this expression, one can find the testing dataset size k, if P_0 and p_f are known. For example, if the requirement is that, in general, 75% of the time the prediction error should come out to be less than the prescribed value and the probability that a network will have poorer predictive capability is 0.1. Then, putting p_f = 25 and P_0 = 0.1 into the expression Eq. (3.27) gives k = 8. Hence, in the present work, 8 random testing datasets were chosen for testing the NN models.

The dimensional values of variables lie in different ranges. Hence, normalization has been carried out for these input variables such that their values lie from 0.1 to 0.9. In the present work, NEWRB function from MATLAB toolbox was used for training of the network. The function uses an algorithm that starts with zero neurons in the hidden layer and keeps on adding the input vector with greatest error as center in successive runs till the error goal is achieved. Based on the testing error, the error goal of a sum-squared error of 0.0001 was found to provide a very good performance. The first network that was trained by 24 datasets required 22 neurons in the hidden layer to achieve the error goal of 0.0001, whilst the network trained by 16 datasets needed 15 neurons in the hidden layer to reach the error goal.

Spread parameter is another important parameter for constructing an RBF neural network. The following simple relationship is available in the literature [Haykin, 1996] to calculate the spread parameter:

$$\sigma = \frac{d_{\max}}{\sqrt{J}}, \tag{3.28}$$

where $d_{\max}$ is maximum Euclidean distance between the centers and J is the number of center. As this relation is a heuristic relation, to fine tune the value of spread parameter, the value calculated by Eq. (3.28) is multiplied by a constant factor β. A number of numerical experiments were carried out to find out the optimum β. Table 3.10 shows the sensitivity of testing errors with β for a typical nodal velocity (at node 4 of Fig. 3.4) in the deformation zone. Although the variation of percentage root mean squared fractional error and maximum percentage error (effective error) is not unimodal with β, both error measures provide minimum value at β =1.5. Observation of the sensitivity of testing errors with β for about 25 nodal velocities, led to the conclusion that the errors are the least for β =1.5. Thus, in the present work, the optimum β is taken as 1.5.

Table 3.10. Variation of testing error with β for a typical nodal velocity prediction

β	% rms_{err}^{f} fractional error	Effective error
0.5	5.22	8.32
0.75	2.06	7.70
1	1.19	2.51
1.25	4.07	4.86
1.5	1.10	2.09
1.75	1.61	3.40
2	2.07	4.02

Once the network is trained for the best possible architecture with least effective error, the velocity field (horizontal component of velocity and vertical component of velocity) for any given input data can be found out. Similarly, an RBF neural network for predicting location of neutral point is also modelled. Here, the output neuron corresponds to arc length from exit to neutral point divided by the total arc length. It was observed that this ratio does not depend significantly on hardening parameters. Similar procedure is adapted to train and test the model for predicting the location of neutral point.

3.3.3 Prediction of the Parameters Using Trained Neural Network and FEM

As already mentioned, a number of neural networks are trained for predicting the components of velocity at different nodes. One network predicts the location of neutral point. The network predicted complete velocity field as well as the location of neutral point is supplied as the initial guess to the finite element code. At the beginning, no roll flattening is considered and the pressure and modified velocity fields are computed. The post-processing module of the finite element code calculates the roll force, knowing which the deformed roll radius is calculated using Hitchcock's formula. With the deformed roll radius, finite element code is run again to obtain new pressure and velocity fields as well as deformed roll radius. This procedure is repeated till the roll radius converges with 1% accuracy. Due to the accurate guess of velocity field and location of neutral point, only 2-3 iterations of finite element code are needed to converge. After that, secondary variables *viz*. roll

force, roll torque, roll pressure *etc*. are calculated as described earlier in Section 3.2. A general overview of the entire methodology is shown in Fig. 3.5.

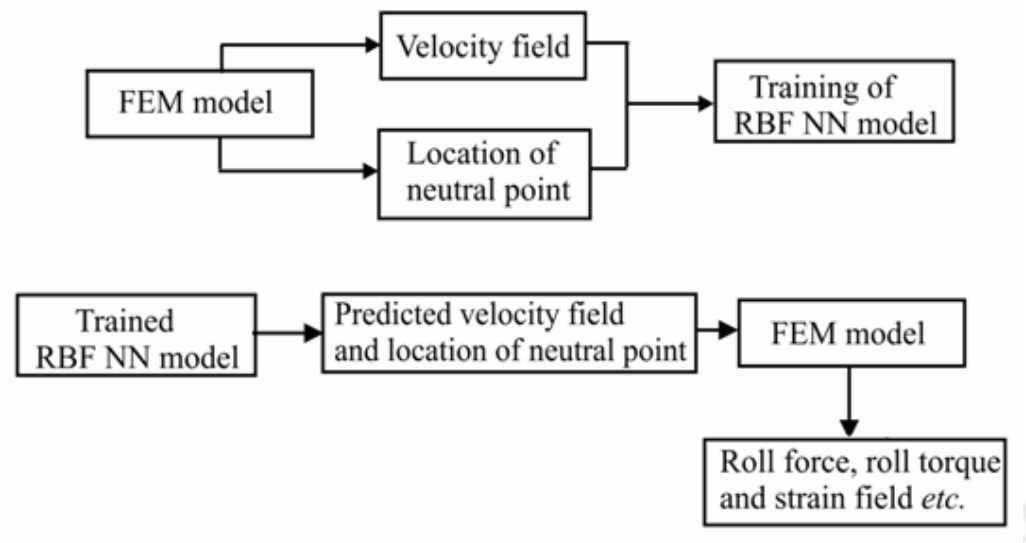

Figure 3.5. A general overview of the procedure that uses the NN predicted velocity field in the FEM model (NN assisted FEM model)

3.4 Results and Discussion

In the present work, radial basis function neural networks have been implemented for the modelling of cold flat rolling process, which predicts the velocity field and location of neutral point. From the result of statistical analyses (correlation analysis and analysis of variance) carried out in the present work, it has been observed that strain hardening parameters have little effect on determination of the velocity field. The results of statistical analyses are further strengthened by carrying out error analysis. In the first model, strain hardening parameter b is excluded whereas in the second model b and n are excluded.

3.4.1 Validation of the Neural Network Model

Two different types of neural network models are studied. The neural network model with four-input parameter was trained with 24 training datasets and 8 testing datasets. The performance of the neural network was assessed using 32 random validation datasets that were not used in the construction of the model. These

validation datasets were generated within the same range of the process parameters that are used for generating training and testing datasets.

3.4.1.1 Error Analysis

The performance of the neural network modelling has been checked for three different error criteria, which are termed as Error1, Error2 and Error3.

$$\text{Error1} = \sum_{i=1}^{N} \frac{|e_i|}{N}, \tag{3.29}$$

$$\text{Error2} = \sqrt{\frac{\sum_{i=1}^{N} e_i^2}{N}}, \tag{3.30}$$

$$\text{Error3} = \max |e_i|, \tag{3.31}$$

where e_i is the difference between the nodal velocity value of FEM code and NN model and N is the total number of nodes (261 nodes in the present case) in the finite element mesh.

In the error analysis of first NN model of four-input parameters for velocity prediction, Fig. 3.6 shows the three errors plotted for the prediction of the validation datasets. Here, the non-dimensional horizontal exit velocity is taken as 1. The Error 1 and Error 2 are less than 2% and the maximum error (Error 3) is less than 7% for the horizontal components of velocity (v_1). Similarly, Figure 3.7 shows the errors in the network prediction for validation datasets of vertical component of velocity (v_2). From the Figs. 3.6 and 3.7, it is observed that the neural network model predicts accurate velocity field for the given input parameter.

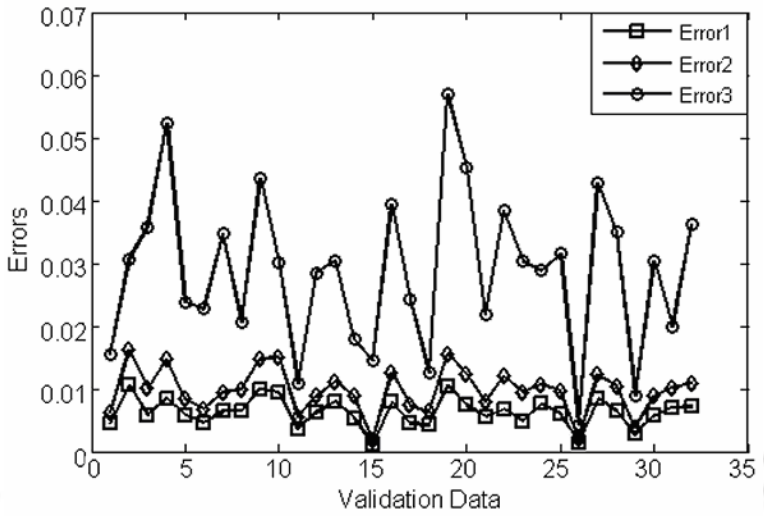

Figure 3.6. Errors in four-input neural network prediction for horizontal velocity component

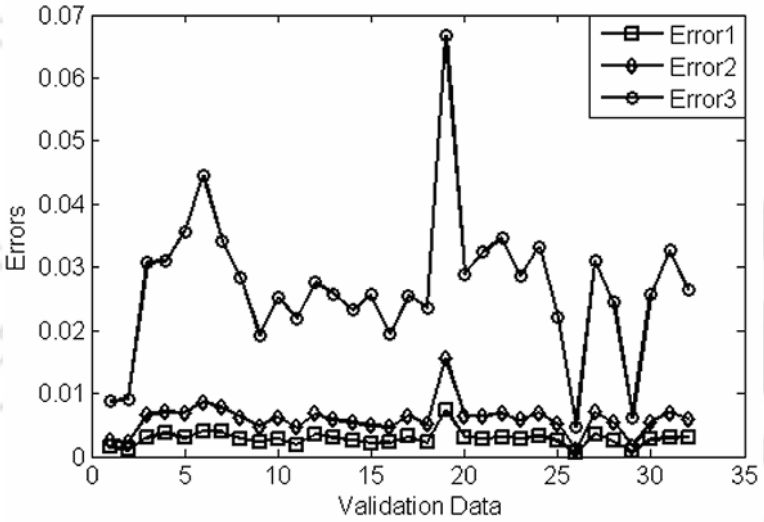

Figure 3.7. Errors in four-input neural network prediction for vertical velocity component

The second network has been modelled with three-input parameters. Thus, the strain hardening behaviour is excluded in the modelling of the velocity field. It is observed that the non-inclusion of strain hardening parameters does not deteriorate the prediction capability of the network the prediction of velocity field, as apparent from Figs. 3.8 and 3.9.

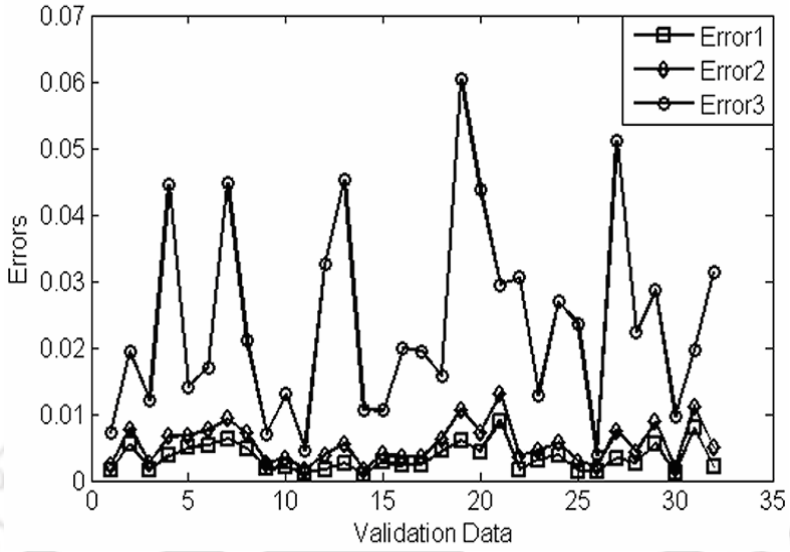

Figure 3.8. Errors in three-input neural network prediction for horizontal velocity component

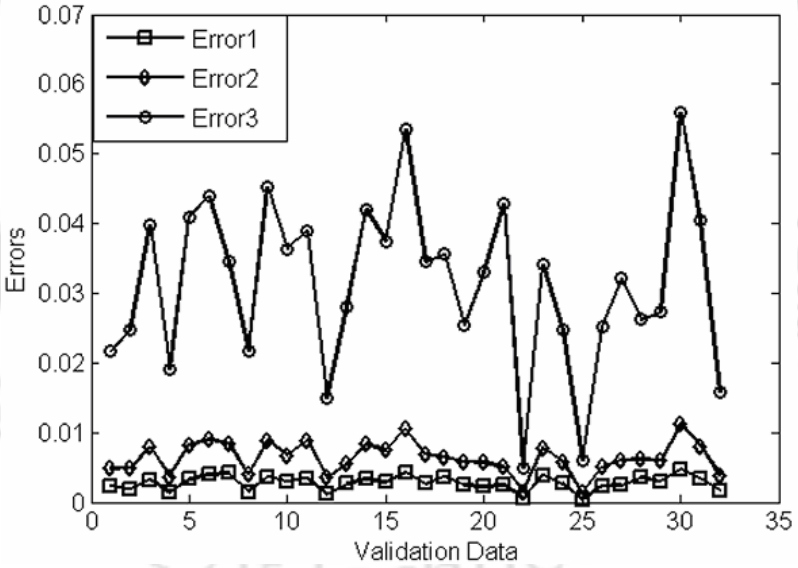

Figure 3.9. Errors in three-input neural network prediction for vertical velocity component

The statistical analysis led to the conclusion that strain hardening parameter n is of minor influence on the prediction of the velocity field. However, after fitting the networks and error analysis, it is observed that strain hardening parameter n can be excluded from the input parameters of neural network model along with b, leaving only three parameters *viz.* R/h_1, f, r required for obtaining the velocity

field. This also reduces the requirement of training data as the requirement of training datasets increases with increasing number of input neurons.

Similarly, validation of the neural network model for predicting the location of the neutral point is also carried out by using 32 unseen datasets. Here, a maximum of 10% deviation from that of FEM results is observed. This much accuracy in the prediction of neutral point is enough for providing a suitable guess to FEM code. Taking this guess, FEM calculates very accurate location of the neutral point in only 2-3 iterations.

3.4.2 Prediction of Roll Force and Roll Torque

The performance of the present model is validated by comparing the results of the roll force, roll torque with the results of finite element model of Dixit and Dixit [1996]. The neural network predicted velocity field of the present model is used to calculate the roll force F_r, roll torque T and equivalent strain $\tilde{\varepsilon}$ by providing this velocity field as a guess in the finite element code. The refined velocity and pressure fields are obtained by carrying out 2-3 iterations of finite element code.

Figure 3.10 and 3.11 compares the roll force and roll torque obtained by NN assisted FEM with those obtained by the FEM code directly. A solid line passing through the origin and inclined at 45^o is drawn in the figures. For perfect prediction, all points should lie on this line. It is observed that predicted values of roll force and roll torque are almost same as obtained by FEM code alone. The maximum deviation in roll force prediction is 3% and in roll torque prediction 2%. NN assisted FEM takes about one tenth of the time taken by the FEM code. It is estimated that if a refined mesh with 4 times the velocity nodes is used, the NN assisted FEM will take less than 1/40 times the time taken by the unassisted FEM code. Although the refinement of this order is not required just for roll torque and force prediction, it may be desirable when a highly accurate stress field needs to be predicted for optimizing the process.

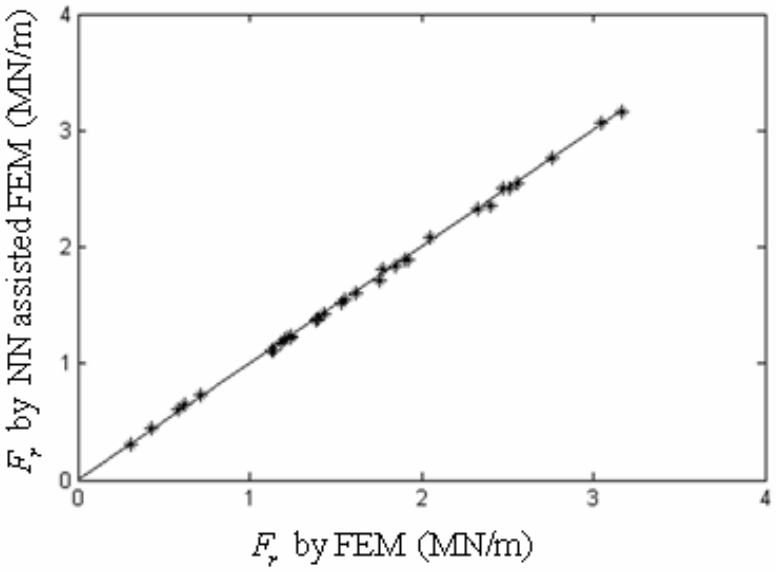

Figure 3.10. NN assisted FEM predictions *vs* FEM predictions for roll force

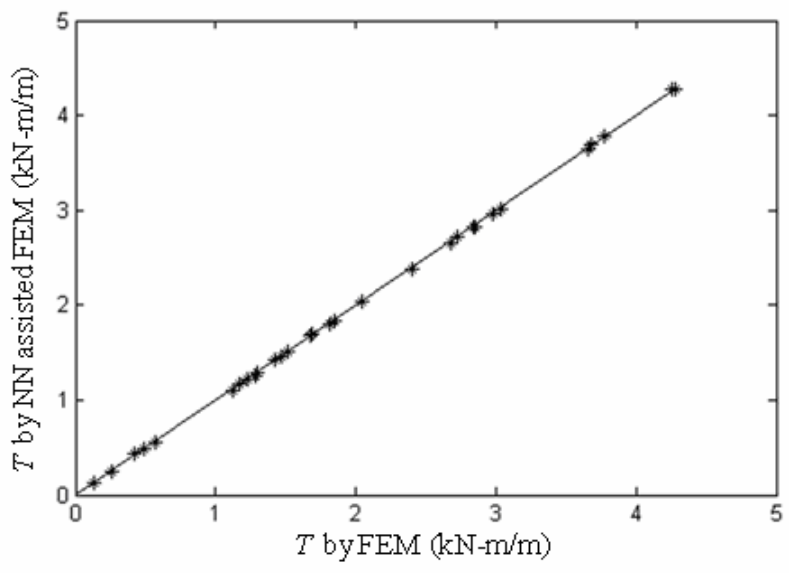

Figure 3.11. NN assisted FEM predictions *vs* FEM predictions for roll torque

3.4.3 Comparison of Roll Pressure Distribution

Comparison of roll pressure distribution obtained by the present method and from Dixit and Dixit [1996] for a typical case is carried out. The non-dimensionalized roll pressure distribution, $t_n/(\sigma_Y)_0$ for both models is plotted in Fig. 3.12. The material

to be rolled is considered as steel and material properties are shown in the figure. It is observed that in both the models, a pressure peak is observed which is coincident with the position of the neutral point. Moreover, both models predict similar profile of roll pressure distribution.

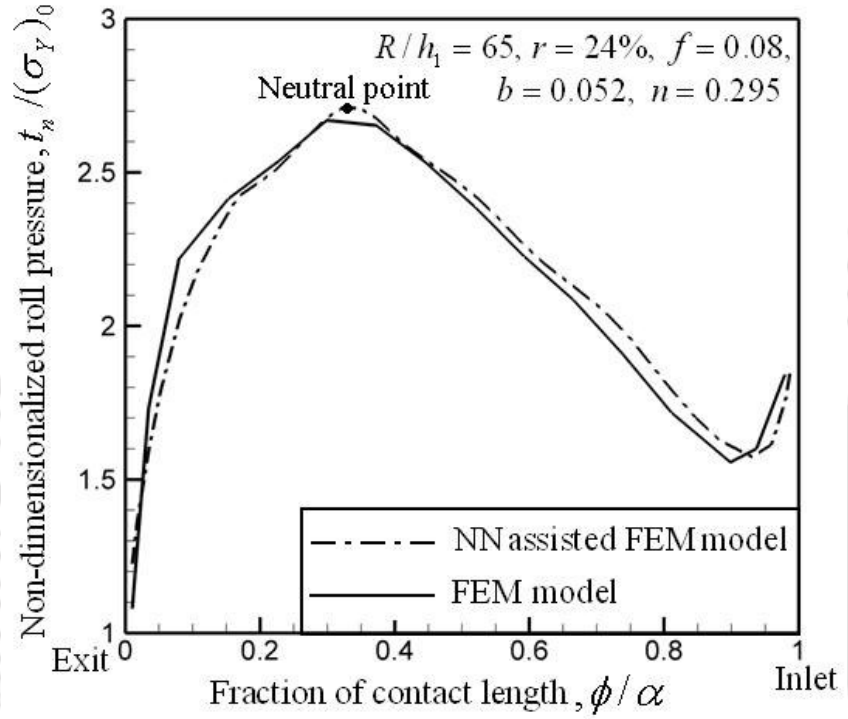

Figure 3.12. Comparison of NN assisted FEM prediction *vs* FEM prediction for roll pressure distribution

3.4.4 Comparison of Equivalent Strain Contours

The contours of equivalent strains were plotted to exhibit the deformation pattern. The equivalent strain is obtained by integrating the equivalent strain rate along the constructed particle path line (Eq. 3.9). In the non-dimensionalized version, the semi-exit thickness and the exit velocity will be unity. The contours have been plotted for a typical case of process variables *i.e.* $R/h_1 = 65,\ f = 0.08,\ r = 14\%$. The strain hardening parameters b and n have been chosen to represent two cases–high strain hardening material and low strain hardening material.

3.4.3.1 High Strain Hardening Material

In the fhe first case, the material hardening parameters b and n are considered as 0.02 and 0.6 respectively. Thus for a high strain hardening material, the equivalent strain contours are discussed during the rolling process. Contours in Fig. 3.13 have been obtained by running FEM code till all nodal velocities converges to within 0.01% accuracy. On the other hand, contours in Fig. 3.14 have been obtained by NN assisted FEM code, in which FEM code refines the NN predicted velocity field by carrying out 2-3 iterations. It is seen that both the contours are similar. There is about 10% difference in the maximum strain. This difference can further be reduced if a few more iterations of NN assisted FEM code is carried out.

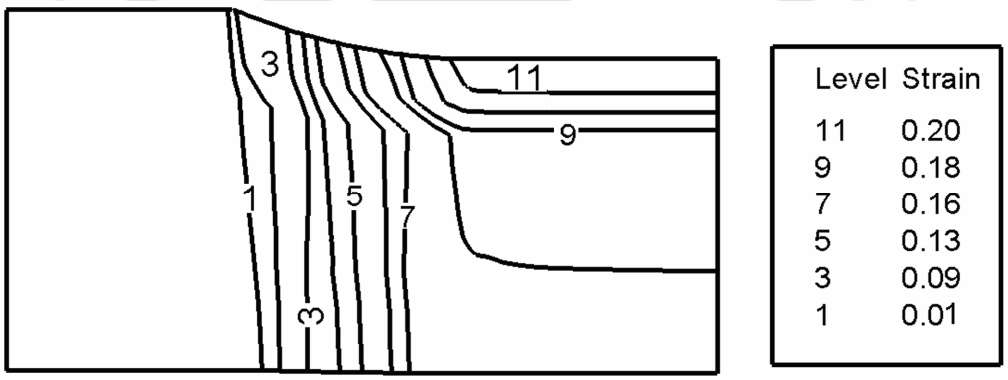

Figure 3.13. Equivalent strain contours for high strain hardening material plotted by FEM model

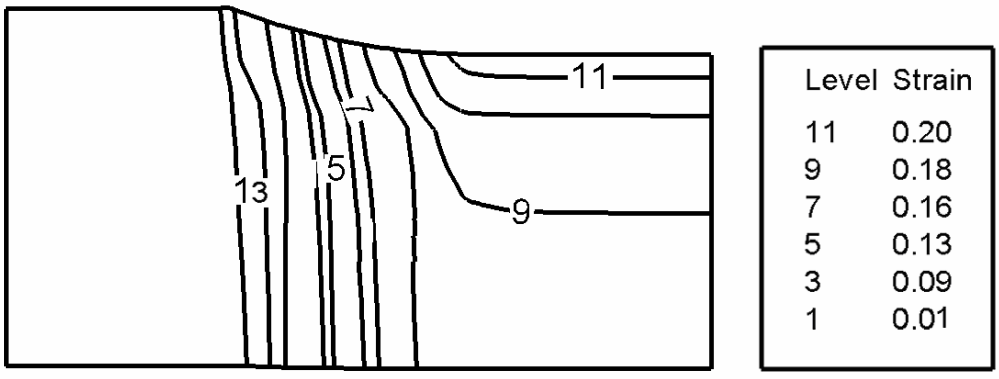

Figure 3.14. Equivalent strain contours for high strain hardening material plotted by NN assisted FEM model

3.4.3.2 Low Strain Hardening Material

In the second case, the material hardening parameters *b* and *n* are considered as 0.08 and 0.001 respectively. The other parameters are kept same as that of previous case.

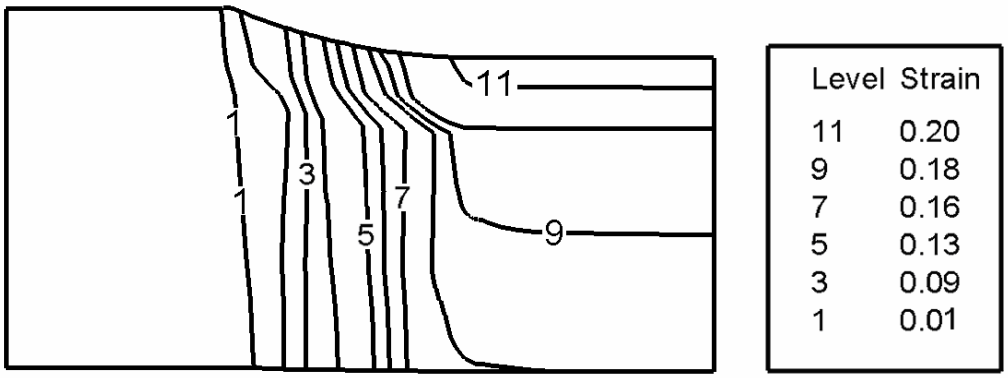

Figure 3.15. Equivalent strain contours for low strain hardening material plotted by FEM model

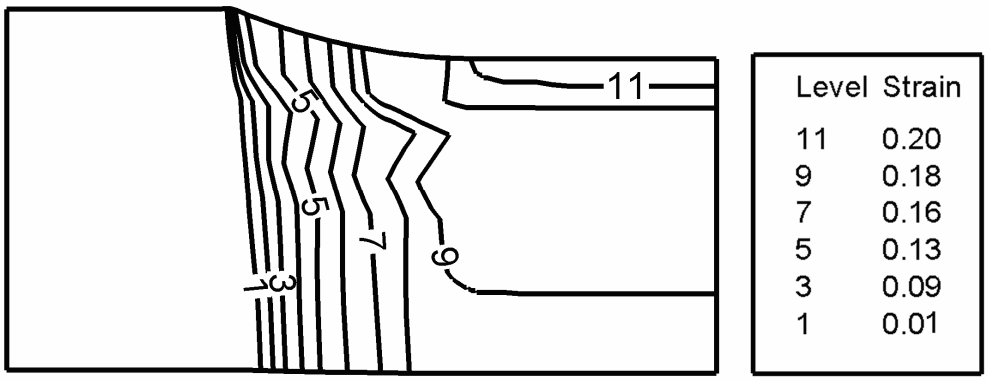

Figure 3.16. Equivalent strain contours for low strain hardening material plotted by NN assisted FEM model

Figure 3.15 and 3.16 shows the equivalent strain contours of the low strain hardening material. Here also the contours obtained by finite element model and NN assisted finite element model are almost similar. In this case of low strain hardening material, the deviation in maximum strain prediction is 5%. One interesting observation is that strain distribution pattern as well as the magnitudes of strain is same for low as well as high strain hardening materials, as clearly seen by comparing Fig. 3.13 and 3.15. Thus, it can be stated that the strain distribution pattern is governed purely by kinematical and friction conditions of the rolling

process and strain hardening does not have an appreciable effect on the strain distribution pattern.

3.4.5 A Note on Computational Time

In the present NN assisted FEM model, it is observed that the time required for prediction of velocity by a neural network model was less than 5 seconds. Finite element code would have required about 30 minutes for the same task, in a Pentium IV processor with a compiler that optimizes the code. The above computation time is for the mesh shown in Fig. 3.1. The computational effort required to solve the system of linear equations is of the order of N^3 *i.e.* $O(N^3)$ where N is the number of equations to be solved. As for a refined mesh, major computational time goes in solving the system of linear equations, the computational time vary as $O(N^3)$, where N is the number of velocity nodes. On the other hand, the computational time required to predict the velocity by a neural network will be at most $O(N^2)$. This is because the maximum number of hidden neurons in a network is N for N velocity nodes. Therefore, the computational time for the fitted network will be at most $O(N)$. As, the number of fitted network are approximately proportional to N, the total computational time to predict velocity at all nodes will be $O(N^2)$. For a refined mesh of 112 elements, computational time required for prediction of velocity by a finite element code alone will be much higher whereas a neural network model requires less than 25 seconds for prediction of velocity. Thus the proposed methodology helps to reduce the computational in a significant manner.

3.5 Summary

In this work, RBF neural network have been used for predicting the velocity field and neutral point location in the cold flat rolling process. The significant input parameters were determined by studying the traditional statistical tools to determine the effect of the parameters on the velocity field. Neglecting the parameters having very little influence on the velocity field, size of the NN model can be reduced

considerably. It has been found out that the strain hardening parameters b and n can be excluded from the input parameters of neural network modelling for obtaining the velocity field.

The required training, testing and validation data have been obtained from rigid-plastic finite element code. The trained network provides the predicted velocity field and the location of neutral point as guess values which are further refined and post-processed in the finite element code to calculate required parameters such as roll force, torque and equivalent strain. This procedure requires only 2-3 iterations of the finite element code for calculation of roll force, roll torque and equivalent strain *etc*. The predicted values are sufficiently close to those obtained by FEM code alone. With this procedure, the computational time is reduced by a factor of about 10 for the chosen mesh. The reduction in the computational time will be even more significant for a refined mesh. Also, in the case of elasto-plastic FEM analysis, where the computational time is generally of the order of ten times the rigid-plastic FEM analysis, the incorporation of the methodology proposed here will reduce the computational time by a factor of more than 100. Thus, the neural network assisted FEM has a potential of providing a highly accurate results with less computational time.

4

Prediction of Roll Force and Roll Torque Using RBF Neural Network and Fuzzy Inference

4.1 Introduction

Recently, some researchers have started exploring the possibility of utilizing soft computing techniques (particularly neural network and fuzzy set theory) for modelling the metal forming processes. There has been considerable focus on neural networks in the recent past as it is widely applicable and easy to use as an approximator for problems with highly nonlinear and complex data. The neural networks have been used in the past for the prediction of roll force and roll torque. However, very few attempts have been made in the past to incorporate the fuzzy set theory in the modelling and control of the rolling process.

This chapter discusses the implementation of Takagi-Sugeno (TS) fuzzy inference for the prediction of roll force and roll torque. The fuzzy inference model based on the algorithm of Ŝkrjanc *et al*. [2004] is developed. The required data for fuzzy inference modelling is generated by a radial basis function neural networks. A study on the sensitivity of the roll force and roll torque with respect to the process variables is carried out using the coefficients of the crisp functions of the TS fuzzy inference. An approximate method to estimate the roll force and roll torque for another material based on these values for reference material is proposed. In the modern production scenario, where a wide variety of rolled sheets made of different materials are produced by the same organization, this method is an economical way to get the roll force and roll torque data for a new material based on FEM or experimental data of a reference material.

The usefulness of the soft computing techniques is mainly dependent on the accuracy of modelling data (data required for construction of models using soft

computing techniques). Presence of outliers in the modelling data may deteriorate the accuracy of prediction. In the present work, an algorithm is proposed for detection and suppression of the outliers in the modelling data.

4.2 Problem Formulation

In the cold flat rolling process, if the width of the strip is at least five times the arc of contact between the roll and strip, the process may be assumed as a plane-strain deformation process. The process variables for the estimation of roll force and roll torque are roll radius R, initial strip thickness h_1, final strip thickness h_2, coefficient of friction f and material to be rolled. In cold flat rolling, at a moderate speed, the temperature and strain-rate effects may be neglected. Considering the strain-hardening effect by a power law, the flow stress is expressed in Eq. (3.8). The relation between the process variables and the output can be expressed as

$$F_r = (\sigma_Y)_0 \, h_1 \beta_1 (R/h_1, f, r, b, n), \tag{4.1}$$

$$T = (\sigma_Y)_0 \, h_1^2 \beta_2 (R/h_1, f, r, b, n), \tag{4.2}$$

where F_r is the roll force and T is the roll torque per unit width respectively. In the above relations, percentage reduction r is defined in Section 3.2 (Eq. 3.12).

For the purpose of present analysis, the range of process variables is taken as follows:

$$R/h_1 : 10-100, \;\; f : 0.04-0.14, \;\; r : 4-24\,\%, \;\; b : 0.02-0.08, \;\; n : 0.001-0.6$$

The roll force and roll torque corresponding to the input variables are obtained using the FEM based code [Dixit and Dixit, 1996]. These input-output datasets are used for the training of radial basis function (RBF) neural network. The details of the data generation are explained in Section 4.3.

4.3 Data Generation Using RBF Neural Network

The large amount of data generation from experiments or FEM based code is a costly affair. To overcome this, input-output datasets required for TS fuzzy model is generated with the help of neural networks. In the present work, a radial basis function (RBF) neural network is used. The architecture of the RBF neural network used for the roll force and roll torque prediction is shown in Fig. 4.1.

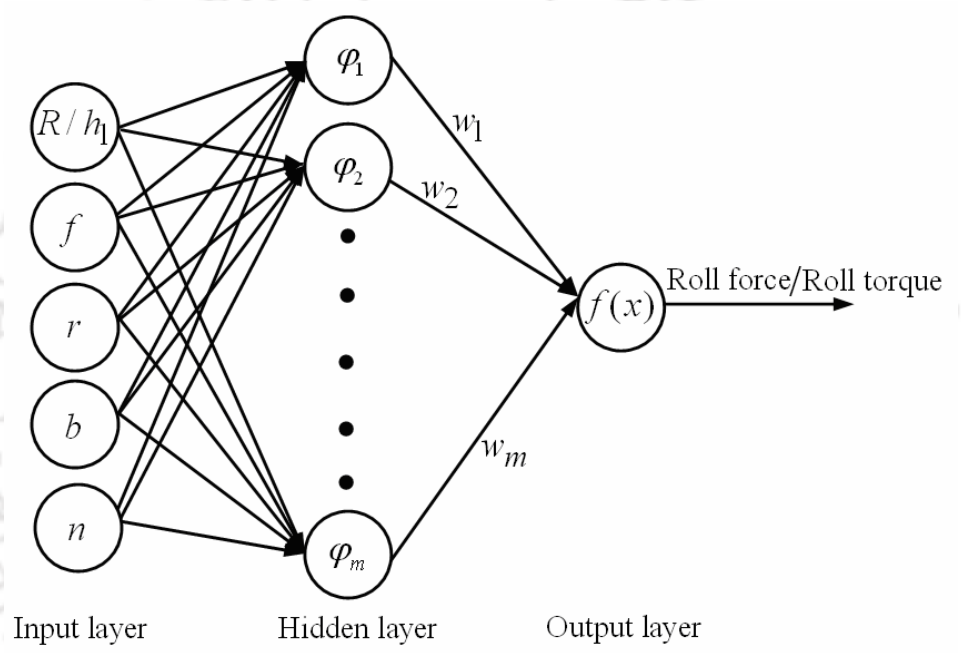

Figure 4.1. A typical RBF neural network architecture used in the present analysis

Separate neural networks are used for the prediction of roll force and roll torque. The detailed information about the functioning of the RBF neural network is explained in Ham and Kostanic [2001]. The radial basis function used in this work is a Gaussian function discussed in Subsection 3.3. The weighted addition of the outputs of neurons of the hidden layer is sent to the output neuron, which processes it by adding a constant term b_0 called bias. Thus the output of the RBF neural network is approximated as

$$f(\boldsymbol{x}) = b_0 + \sum_{j=1}^{m} w_j \varphi_j(\| \boldsymbol{x} - \boldsymbol{c}_j \|_2), \tag{4.3}$$

where $\boldsymbol{x} = \{R/h_1, f, r, b, n\}^T$ is the input vector, $\varphi_j(.)$ is the processing function of the j^{th} neuron in the hidden layer, $\|.\|_2$ denotes Euclidean norm, w_j are the associated weights, m is the number of neurons in the hidden layer and $\boldsymbol{c_j}$ are the RBF centers obtained from the input vector space. For fixed centers and spread parameter, applying Eq. (4.3) for each training data provides a linear system of equations with m unknowns w_j and one unknown b_0, which can be solved using the least square method. Hence, the training procedure takes lesser computational time, as compared to multi-layer perceptron neural network.

The procedure for choosing the training and testing data is similar to that of Dixit and Chandra [2003]. It is briefly explained here. During the data generation, first the corner data corresponding to a five-dimensional input space are generated. Thus, 2^5 =32 corner data are generated for five-input variables models. This is done considering the fact that neural network behaves poorly in extrapolation. In order to ensure that the neural network need not extrapolate, it is necessary to include the data corresponding to the corners of the input space in the training dataset. In addition to the corner datasets, the input variable, which has a high influence on the output variable, should find more representation in the training dataset, as compared to the input variables whose influence on the output variable is less. This has been ensured by choosing the data based on the effect of each input variable (factor). The effect of factor for an input variable can be calculated as [Dieter, 1995]

$$\text{Effect of factor} = \frac{\sum \text{Response at high level} - \sum \text{Response at low level}}{\text{Half the number of runs in the experiment}}, \qquad (4.4)$$

In the present work, the minimum value amongst the effects of factor is scaled to 2. The scaled effects of R/h_1, r, n, f and b are 7, 6, 4, 2 and 2 respectively. Hence, 5 additional level of R/h_1, 4 additional levels for r and 2 additional levels for n are generated. The input variable R/h_1 is having two levels as 10 and 100. Additional five levels for R/h_1 correspond to 25, 40, 55, 70 and 85. The other input variables corresponding to additional levels of R/h_1 are generated randomly in their

respective range. The procedure is repeated for other input variables as well. Thus, with 32 corner data, another 11 data are added to training dataset. Eight data are generated randomly for testing the network. The dimensional values of the input variables lie in different ranges. Hence, normalization has been carried out for these input variables such that their values lie from 0.1 to 0.9. In the present work, the MATLAB function NEWRB is used for the training of the network. The details of the function NEWRB are explained in Subsection 3.3.2.

The performance of the neural network is checked by determining the percentage root mean squared (*rms*) fractional error for training and testing datasets. The percentage root mean squared fractional error is given as

$$\% \, rms_{err}^{f} = \sqrt{\sum_{p=1}^{N} \frac{(d_p - o_p)^2}{N (d_p)^2}} \times 100 , \tag{4.5}$$

where d_p is the desired output (FEM generated), o_p is the neural network predicted output for a particular pattern (p) and N is the total number of data. The maximum of training and testing root mean squared fractional error is called as effective error.

Spread parameter and the mean squared error goal are the important parameters for constructing an RBF neural network. Spread parameter is calculated using Eq. (3.28). However, to fine-tune the value of spread parameter, the value calculated by Eq. (3.28) is multiplied by a suitable constant factor β. The performance of the network is evaluated by varying the error goal from 0.01 to 0.0001. This range of error goal is divided into 6 steps in a geometric progression and the network is trained using five different values of β (β = 1.0, 1.25, 1.5, 1.75 and 2.0) at each value of error goal. The best network is chosen based on the least value of effective error. If the maximum percentage error in prediction for the testing dataset is less than a prescribed value (5% in present case), the training of network is considered as complete. On the other hand, if prediction for some testing data provides an error more than the prescribed value, the data are transformed to the training dataset. Two fresh data are added to the testing dataset in lieu of each

transferred data and the whole procedure is repeated till the desired accuracy is obtained. This entire methodology is illustrated by means of a flow chart (Fig. 4.2).

The final network and design parameters are shown in Table 4.1. The constructed neural network for the roll force or roll torque is used further to generate data in the learning process of Takagi-Sugeno (TS) fuzzy model which is described in the next section.

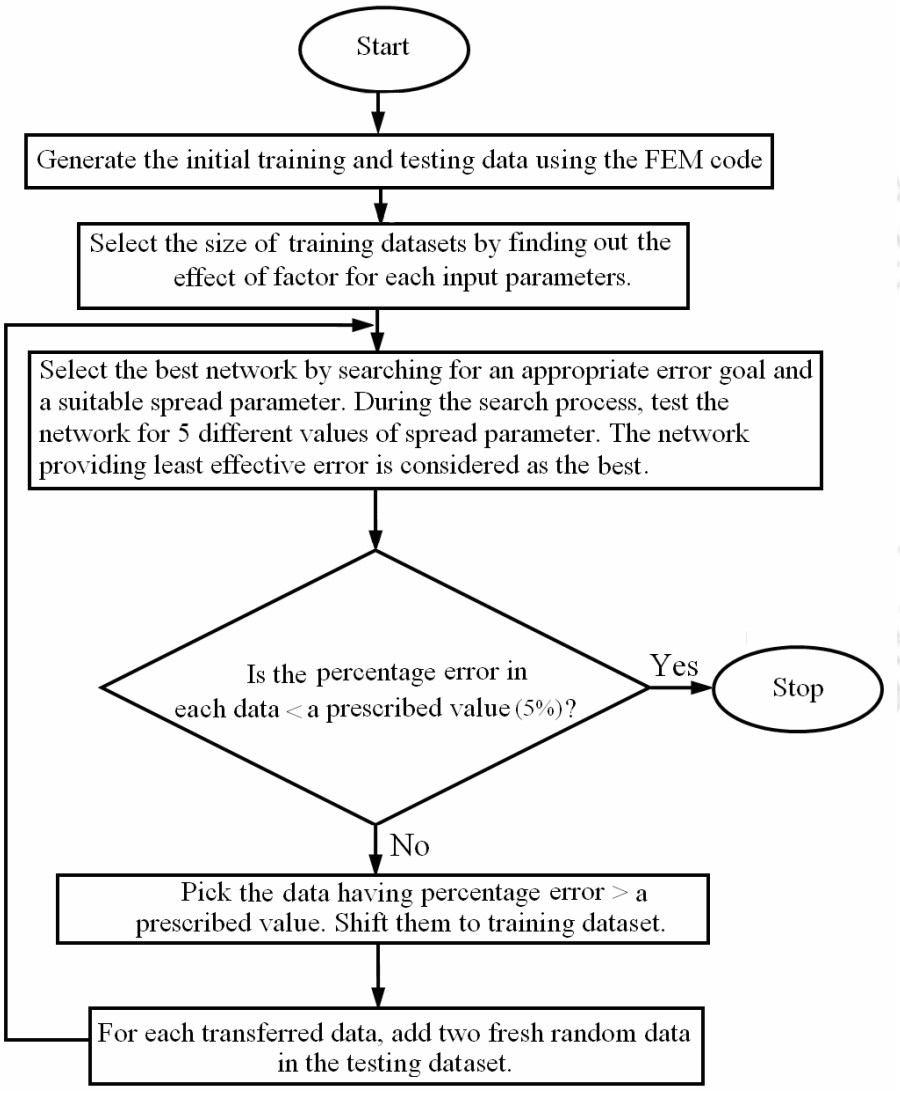

Figure 4.2. Flow chart illustrating the methodology adopted for NN model

Table 4.1. The final neural network parameters for roll force and roll torque prediction

Network parameters	For roll force prediction	For roll torque prediction
Error goal	0.0001	0.0001
β	1.5	1.5
Number of centers	49	47
Number of training data	55	55
Number of testing data	30	30
$\% \ rms_{err}^{f}$ (training)	0.2509	0.7730
$\% \ rms_{err}^{f}$ (testing)	2.8906	3.4804

4.4 Fuzzy Inference Model for Prediction of Roll Force and Roll Torque

The main feature that separates fuzzy inference models from black-box techniques like neural networks is that the fuzzy models are, to a certain degree, transparent to the interpretation and analysis [Setnes *et al*., 1998]. In general, two types of fuzzy models that are widely used in engineering applications are Mamdani fuzzy model and Takagi-Sugeno fuzzy model.

Ebrahim Mamdani of London University built one of the first fuzzy systems to control a steam engine and boiler combination in 1976. Hence the model is known as Mamdani fuzzy model. The author applied a set of fuzzy rules supplied by experienced human operators. The Mamdani-style fuzzy inference process is performed in four steps *i.e*. fuzzification of the input variables, rule evaluation, aggregation of the rule outputs and finally defuzzification. Unlike Mamdani fuzzy model, in a Takagi–Sugeno (TS) fuzzy model, the output of each fuzzy IF-THEN inference rule is represented as a crisp analytical function. In most of the practical TS fuzzy systems, linear functions are used as the output of the fuzzy IF-THEN inference rule [Ying, 1998].

In the present work, the TS fuzzy model is generated using the methodology of Ŝkrjanc *et al*. [2004]. Two separate fuzzy inference models are generated for the prediction of the roll force and the roll torque. The input datasets having five-input variables *viz*., R/h_1, f, r, b and n are fuzzified. The partial belonging of a variable to

different fuzzy subsets can be described numerically by a membership function (MF). The membership function assumes a value between 0 and 1 inclusive. Although there are various ways to construct a membership function, triangular and trapezoidal membership functions are used here, due to their simplicity and other beneficial properties [Pedrycz, 1994]. In general, there are n^m fuzzy rules where n and m are the numbers of fuzzy subsets for each variable and input variables respectively. Increasing the number of fuzzy subsets may improve the accuracy of the prediction of the model, but it increases the total number of rules as well as the computational time. This is ascertained by constructing a fuzzy model with a test function of $u = x^2 + y^2 + z^2$. In this model, x and y are treated as input parameters and u is treated as output. The number of fuzzy subsets has been varied from 2 to 4. It is observed that as the number of subsets increases, the accuracy of the model increases. At the same time, number of rules and the computational time also increase. Thus, in order to maintain the accuracy and reasonable computational time, in the present study, each input variable is divided into 3-fuzzy subsets, *i.e.*, low (L), medium (MD) and high (H) as shown in Fig. 4.3. This makes the total number of rules 3^5=243.

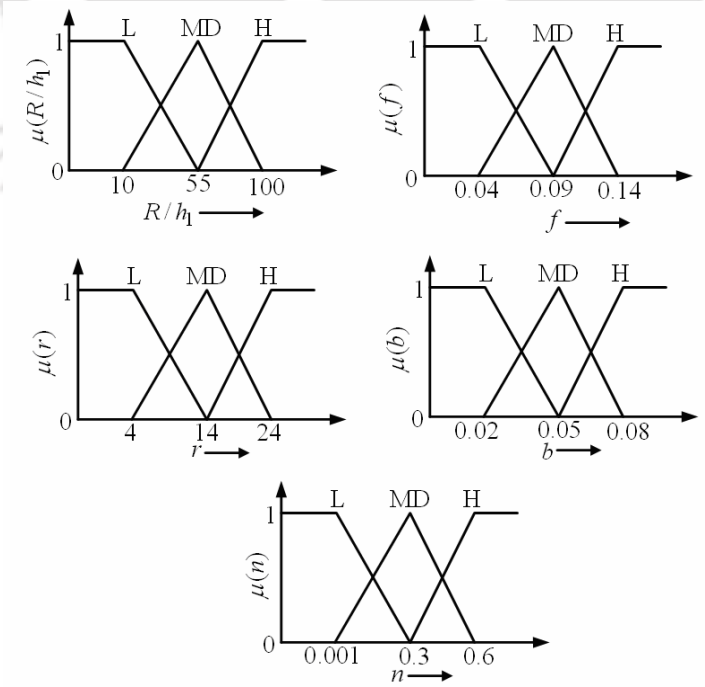

Figure 4.3. Fuzzification of input variables for a typical cold rolling process

The representation of IF-THEN rules in the TS fuzzy model is given as

$$\begin{aligned} R_i : \text{IF } x_1 \text{ is } A^1(i) \text{ and } x_2 \text{ is } A^2(i) \text{ .....and } x_k \text{ is } A^k(i), \\ \text{THEN } \quad y_i = a_i^0 + a_i^1(x_1) + a_i^2(x_2) + \text{.....} + a_i^k(x_k). \end{aligned} \tag{4.6}$$

where R_i is the i^{th} rule, vector $\boldsymbol{x} = [x_1, x_2, \ldots . x_k]$ represents the set of k input variables like $[R/h_1, f, r, b, n]$ and $A^j(i)$ is the fuzzy subset corresponding to the j^{th} input variable. Note that depending on the rule, $A^j(i)$ can be low (L), medium (MD) or high (H). The output of the i^{th} IF-THEN rule is y_i, which is assumed to be a linear function of the input variables. The coefficients associated with the input variables in the linear functions are denoted as a_i^j, where subscript denotes the rule number and superscript denotes the associated input variable. The aggregated output of the TS fuzzy model, $\hat{y}$ is expressed by a weighted average of the rule consequents:

$$\hat{y} = \frac{\sum_{i=1}^{N_R} w_i y_i}{\sum_{i=1}^{N_R} w_i}, \tag{4.7}$$

where w_i is the strength of the i^{th} fuzzy rule and N_R is the total number of rules. The strength of a fuzzy rule can be evaluated using a suitable T-norm operator. Here, the strength of the rule is taken as the product of the membership grades of the input values of the variables in the corresponding fuzzy subsets.

The coefficients a_i^j of Eq. (4.6) can be obtained by minimizing the maximum approximation error (λ) between the actual output and the fuzzy model output over the given input-output datasets. For this, the following linear programming (LP) model is solved:

$$
\begin{aligned}
&\text{Minimize } \lambda, \\
&\text{subject to,} \\
&o_p - \hat{y}_p \le \lambda, \qquad p = 1,\ 2, \ldots\ldots m, \\
&-o_p + \hat{y}_p \le \lambda, \qquad p = 1,\ 2, \ldots\ldots m, \\
&\qquad\qquad\qquad\qquad \lambda \ge 0, \\
&a_i^j \ge 0, \qquad\qquad i = 1, 2, \ldots\ldots N_R, \quad j = 1, 2, \ldots\ldots 5.
\end{aligned}
\tag{4.8}
$$

where the subscript p represents the p^{th} input-output pattern and m is the total number of patterns in the dataset. The actual output of the p^{th} data is o_p. The maximum approximation error is termed as λ. The design variables of the problem are a_i^j and λ. The LINPROG function from the MATLAB optimization toolbox is used to solve this linear programming problem.

The method described above has been extended to the prediction of lower and upper estimates of the roll force and the roll torque based on the model described in [Škrjanc *et al.*, 2004]. The maximum approximation error for computing the coefficients for lower and upper prediction are termed as λ_1 and λ_2 respectively. The coefficients for lower and upper estimates are obtained by solving the following LP models:

$$
\begin{aligned}
&\text{Minimize } \lambda_1, \\
&\text{subject to,} \\
&o_p - \hat{y}_p \le \lambda_1, \qquad p = 1,\ 2, \ldots\ldots m, \\
&o_p - \hat{y}_p \ge 0, \qquad p = 1,\ 2, \ldots\ldots m, \\
&\qquad\qquad\qquad\qquad \lambda_1 \ge 0, \\
&a_i^j \ge 0, \qquad\qquad i = 1, 2, \ldots\ldots N_R, \quad j = 1, 2 \ldots\ldots 5.
\end{aligned}
\tag{4.9}
$$

and

$$
\begin{aligned}
&\text{Minimize } \lambda_2, \\
&\text{subject to,} \\
&-o_p + \hat{y}_p \le \lambda_2, \qquad p = 1,\ 2, \ldots\ldots m, \\
&o_p - \hat{y}_p \le 0, \qquad p = 1,\ 2, \ldots\ldots m, \\
&\qquad\qquad\qquad\qquad \lambda_2 \ge 0, \\
&a_i^j \ge 0, \qquad\qquad i = 1, 2, \ldots\ldots N_R, \quad j = 1, 2, \ldots\ldots 5.
\end{aligned}
\tag{4.10}
$$

4.5 Results and Discussion

The accurate learning of a TS model is highly dependent on the size of the data used for modelling. If the model learns from a large number of data, it is expected to be more reliable. As the TS model with five-input variables has total 243 rules, the total number of coefficients in the consequent functions becomes 1458. The minimum size of dataset should be much more than the total number of coefficients in the TS fuzzy model.

In the present analysis, the objective of the TS fuzzy inference model is to minimize the maximum approximation error λ. A less value of λ ensures the correct learning of the model and evaluation of the coefficients. Table 4.2 shows the effect of modelling data on λ. Based on the observation from Table 4.2, the TS fuzzy modelling has been carried out with 3000 uniformly distributed NN generated data.

Table 4.2. The variation of the maximum approximation error in TS model with respect to number of modelling data for roll force and roll torque

Number of modelling data	Maximum approximation error, λ	
	Roll force (MN/m)	Roll torque (kN-m/m)
1500	1.8452	2.1034
2000	1.4259	1.6319
2500	1.1037	1.2103
3000	0.9476	1.0341
3500	0.9418	1.0289

4.5.1 Roll Force and Roll Torque Prediction

The performance of the present TS fuzzy model is validated with 50 random data that have not been previously used for constructing the model. The percentage root mean squared (*rms*) fractional error defined by Eq. (4.5) is used for evaluating the performance of the model. The $\%\ rms_{err}^{f}$ for the roll force and the roll torque is 2.3740 and 2.8951 respectively, for the case of validation data.

4.5.1.1 Comparison with NN Model

The TS model prediction for roll force and roll torque versus NN predicted roll force and roll torque is shown in Figs. 4.4 and 4.5 respectively. A solid line passing

through the origin and inclined at 45° is drawn in the figure. For perfect prediction, all points should lie on this line. In order to get an idea about the percentage error in prediction, the dotted lines representing ±5% accuracy lines are drawn. From Fig. 4.4, it is observed that all the prediction for validation datasets lie within ±5% accuracy for roll force prediction. For the roll torque prediction, a few predictions lie just outside the ±5% accuracy line (Fig. 4.5).

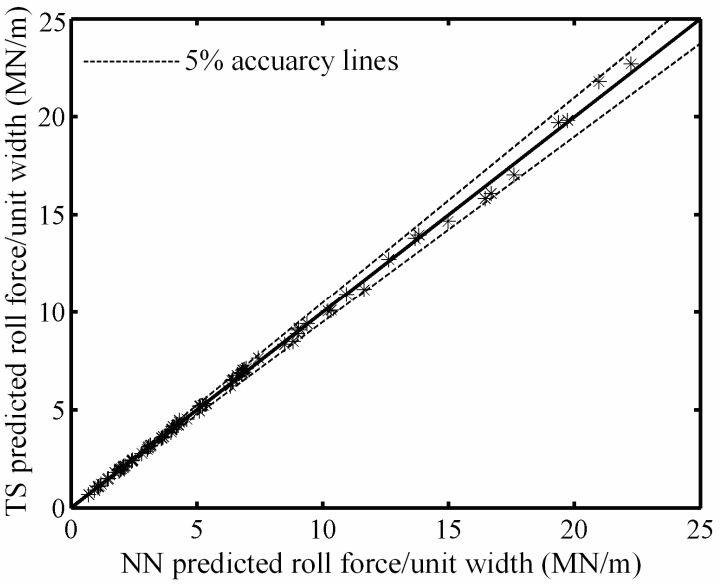

Figure 4.4. The TS fuzzy model predicted versus NN predicted roll force

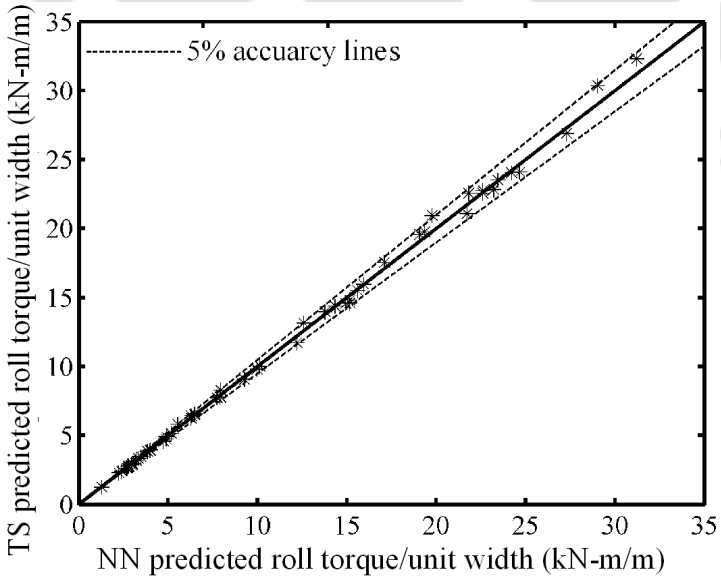

Figure 4.5. The TS fuzzy model predicted versus NN predicted roll torque

4.5.1.2 Comparison with FEM Model

The accuracy of the present TS model is further ascertained by comparing the results with the FEM based predictions of roll force and roll torque.

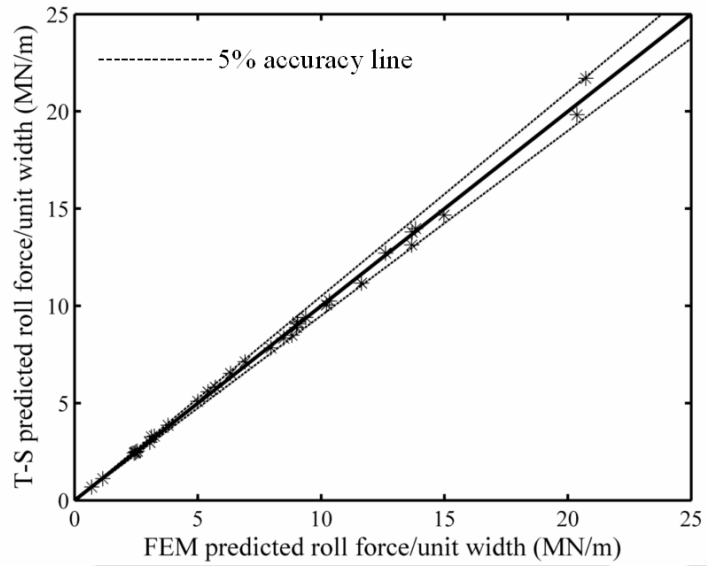

Figure 4.6. The TS fuzzy model predicted versus FEM predicted roll force

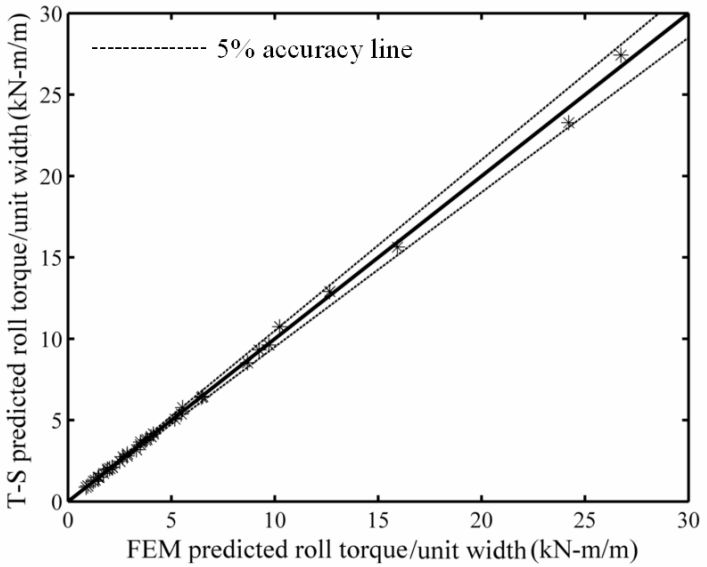

Figure 4.7. The TS fuzzy model predicted versus FEM predicted roll torque

For this investigation, 30 random data that are not seen previously by TS model are chosen. Using Eq. (4.5) for evaluating the performance of the model, it is observed that $\%\ rms_{err}^{f}$ for the roll force and the roll torque is 2.4084 and 2.9280 respectively.

Figure 4.6 and 4.7 shows that TS model based predictions of roll force and roll torque are in good agreement with the FEM based results.

4.5.1.3 Lower and Upper Estimation of Roll Force and Roll Torque

The results are also generated for the prediction of lower and upper estimates along with the most likely estimate of roll force and roll torque using validation data. Figures 4.8 and 4.9 provide a visual depiction of the results. It is seen that NN predicted values lie between the lower and upper estimates of roll force and roll torque. It is also observed that, in most of the cases, NN predicted values of roll force and roll torque are in close agreement with the most likely values that are predicted by TS model. The prediction of lower and upper estimates of roll force and roll torque is helpful where the TS model is constructed with the experimental data. The experimental results in a complex process like rolling have a scatter. In such cases, the results cannot be meaningfully represented by a single curve. The results characterized by a range of lower and upper estimates give a realistic visualization of the process.

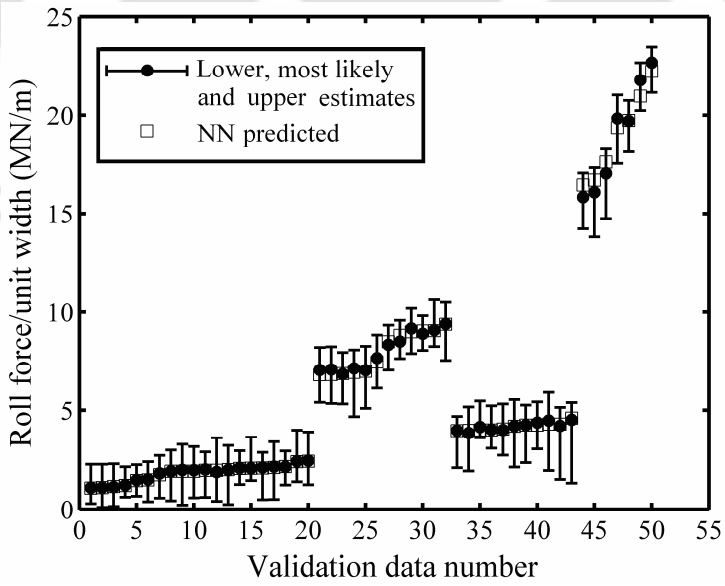

Figure 4.8. Lower, most likely and upper estimates of roll force

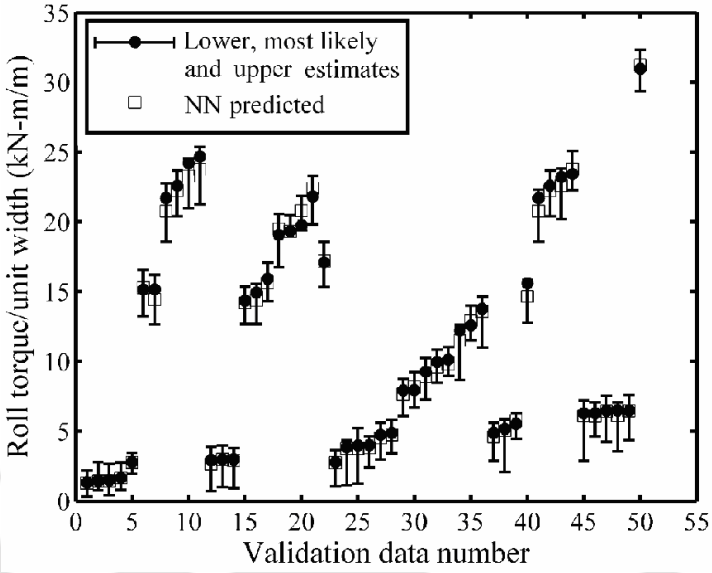

Figure 4.9. Lower, most likely and upper estimates of roll torque

4.5.2 Sensitivity Analysis for Roll Force and Roll Torque

After successfully implementing TS fuzzy inference model for the prediction of roll force and roll torque, the linear functions representing the roll force and roll torque for any given set of input variables are studied from the point of view of sensitivity analysis. The coefficients of the functions are expected to provide the sensitivity coefficients corresponding to the process variables.

It is observed that for five-input variables model, although the roll force and roll torque prediction is fairly accurate, the coefficients of the functions are different than sensitivity values calculated using a finite difference scheme. It is envisaged that increasing the number of modelling data will increase the accuracy of sensitivity values calculated through the coefficients of linear functions. Here, for the preliminary understanding of the sensitivity, a TS fuzzy model with a lower dimension *i.e*. with three-input variable is analyzed. The material to be rolled is steel with the material hardening parameters b and n as 0.052 and 0.295, respectively [Dixit and Dixit, 1996]. The TS fuzzy model with 3^3=27 fuzzy rules reduces the coefficients to 108, as against a TS model with five-input variables that would have provided the 1458 coefficients with 243 rules. For a three-input variable model, the maximum approximation errors λ for roll force and roll torque predictions come

out to be 0.1853 and 0.2341 respectively. Table 4.3 and 4.4 show the predicted linear functions of roll force and roll torque obtained from the TS fuzzy inference model for 8 corner and 4 random data.

The partial derivatives of roll force and roll torque with respect to R/h_1, f and r is calculated from a finite difference scheme using the data obtained from the FEM based code [Dixit and Dixit, 1996]. A quadratic approximation with three points is made for the estimation of the partial derivatives. With this scheme, if h is the difference between x coordinates of two nearest points, the partial derivative of the function f with respect to x is given by

$$\frac{\partial f}{\partial x} = \frac{4f(x+h) - 3f(x) - f(x+2h)}{2h}. \tag{4.11}$$

The optimum value of h to be used in the above equation is computed using a standard procedure as explained in Appendix C. The step size is obtained as 10, 0.02 and 4 for the partial derivatives of roll force and roll torque with respect to R/h_1, f and r respectively.

Table 4.3. Comparison of roll force expressions with the finite difference computed sensitivity values.

Case (R/h_1-f-r)	Roll force expressions	Results using finite difference scheme		
		$\frac{\partial F_r}{\partial (R/h_1)}$	$\frac{\partial F_r}{\partial f}$	$\frac{\partial F_r}{\partial r}$
10-0.04-4	$0.0811+0.0066(R/h_1)+0.5078f+0.0302r$	0.0068	0.7050	0.0335
10 -0.04-24	$0.4514+0.0160(R/h_1)+0.7721f+0.0112r$	0.0183	0.7625	0.0115
10-0.14-4	$0.0706+0.0030(R/h_1)+0.3249f+0.0430r$	0.0034	0.2575	0.0579
10-0.14-24	$0.0553+0.0535(R/h_1)+0.1265f+0.0149r$	0.0662	0.1150	0.0156
100-0.04-4	$0.2381+0.0038(R/h_1)+2.0519f+0.1071r$	0.0042	1.9425	0.1114
100-0.04-24	$0.1346+0.0121(R/h_1)+0.9365f+0.0945r$	0.0138	1.0450	0.0942
100-0.14-4	$0.2315+0.0018(R/h_1)+0.8848f+0.2046r$	0.0028	0.9337	0.1842
100-0.14-24	$0.0020+0.0140(R/h_1)+0.0045f+0.1784r$	0.0188	8.19	0.1963
70-0.10-14	$0.0010+0.0112(R/h_1)+3.3561f+0.0736r$	0.0154	3.5525	0.0809
40-0.06-24	$0.2045+0.0358(R/h_1)+0.5785f+0.0209r$	0.0336	0.5725	0.0232
50-0.08-16	$0.0718+0.0215(R/h_1)+4.2460f+0.0275r$	0.0237	4.6825	0.0314
84-0.04-18	$0.1523+0.0090(R/h_1)+5.0565f+0.0879r$	0.0101	4.5525	0.0813

Table 4.4. Comparison of roll torque expressions with the finite difference computed sensitivity values

Case (R/h_1-f-r)	Roll torque expressions	Results using finite difference scheme		
		$\frac{\partial T}{\partial (R/h_1)}$	$\frac{\partial T}{\partial f}$	$\frac{\partial T}{\partial r}$
10-0.04-4	$0.0536+0.0024(R/h_1)+0.6929f+0.0055r$	0.0025	0.0155	0.0065
10-0.04-24	$0.1905+0.0280(R/h_1)+1.0567f+0.0038r$	0.0371	1.0775	0.0277
10-0.14-4	$0.0330+0.0032(R/h_1)+0.3057f+0.0023r$	0.0047	0.020	0.0242
10-0.14-24	$0.0040+0.0741(R/h_1)+0.0870f+0.0001r$	0.0793	1.0275	0.0350
100-0.04-4	$0.1342+0.0015(R/h_1)+1.9307f+0.1327r$	0.0026	1.7633	0.2627
100-0.04-24	$0.3594+0.0424(R/h_1)+1.2062f+0.1106r$	0.0510	1.1202	0.1810
100-0.14-4	$0.1035+0.0010(R/h_1)+0.4902f+0.2315r$	0.0018	0.5025	0.3013
100-0.14-24	$0.0008+0.0595(R/h_1)+0.0032f+0.2131r$	0.0550	17.605	0.2575
50-0.08-16	$0.2951+0.0299(R/h_1)+0.7560f+0.0218r$	0.0315	0.6857	0.0278
70-0.10-14	$0.2301+0.0121(R/h_1)+0.3544f+0.1210r$	0.0173	0.3987	0.1258
30-0.10-16	$0.1068+0.0548(R/h_1)+0.2243f+0.0057r$	0.0613	0.4837	0.0063
80-0.08-24	$0.1069+0.0660(R/h_1)+7.0055f+0.0215r$	0.0587	6.7853	0.0236

A comparison of finite difference calculated partial derivatives with the coefficients in the expressions for roll force and roll torque predicted by fuzzy inference reveals that the coefficients obtained from fuzzy inference can fairly represent the partial derivatives of the output variables (Tables 4.3 and 4.4). Thus, the TS fuzzy inference is a suitable tool for the prediction of roll force, roll torque and their partial derivatives. It is expected that increasing the number of modelling data and fuzzy subset in TS fuzzy inference will further improve the accuracy of the derivative predictions.

4.6 Approximate Method for Prediction of Roll Force and Roll Torque for Another Material based on the Reference Material

In Subsection 4.5.2, a TS model was constructed specific to a particular material. This may seem to be a limitation in the situations where a variety of metals are rolled and one would like to have prediction for a general material. A simple procedure to estimate the roll force and roll torque for a general material based on the results of a reference material is proposed in this work. The proposed method along with the results is explained in this section.

It is already explained in Chapter 3 that the velocity distribution in a rolling process does not depend significantly on the material. We may obtain the roll force and roll torque for a hypothetical non-hardening material of unit flow stress. Assume that the rolling process is discretized into a number of strain increments. Now, for a general material, whose behaviour is governed by Eq. (3.8), at each strain increment the incremental torque and force will be multiplied by σ_Y. If the final equivalent strain is $\tilde{\varepsilon}_f$, the average multiplying factor may be obtained as

$$K = \frac{\int_0^{\tilde{\varepsilon}_f} (\sigma_Y)_0 \left(1+\frac{\tilde{\varepsilon}}{b}\right)^n \mathrm{d}\tilde{\varepsilon}}{\tilde{\varepsilon}_f} = (\sigma_Y)_0 \frac{b\left[\left(1+\frac{\tilde{\varepsilon}_f}{b}\right)^{n+1} - 1\right]}{(n+1)\tilde{\varepsilon}_f}. \tag{4.12}$$

Thus, the multiplying factor depends on the material parameters and $\tilde{\varepsilon}_f$. The average $\tilde{\varepsilon}_f$ as a function of R/h_1, f and r is obtained by a trained radial basis function neural network. The training data for the network is generated by FEM for the rolling of any material. The neural network model is constructed using the methodology explained in Section 4.3. Now suppose for a particular material, we get multiplying factor as K_1, roll torque as T_1 and roll force as F_{r1}. If the multiplying factor for the other material is K_2, the roll torque and roll force for this material are given by

$$T_2 = \left(\frac{K_2}{K_1}\right) T_1, \tag{4.13}$$

$$F_{r2} = \left(\frac{K_2}{K_1}\right) F_{r1}. \tag{4.14}$$

This method is expected to give fairly accurate results for the rigid rolls. In the presence of roll deformation, the roll force prediction may be less accurate due to different deformed radii of the rolls in the two cases. The effect of roll deformation on roll torque is lesser in case of cold rolling, in which friction is less. For the rolling of strips of moderate thickness and hardness, using Hitchcock's formula (Eq. 3.17), the roll force is approximated by modifying Eq. (4.14) as

$$F_{r2} = \left(\frac{K_2}{K_1}\right)\frac{\left(1+\frac{F_{r2}h_1}{Cr}\right)}{\left(1+\frac{F_{r1}h_1}{Cr}\right)}F_{r1}. \qquad (4.15)$$

Using this methodology and the results of Section 4.5.2, the roll force and roll torque are computed for random values of hardening parameters, keeping $(\sigma_Y)_0 = 324$ MPa only. Table 4.5 shows that roll force is predicted within an accuracy of 8.5% for all cases. Similarly, Table 4.6 shows that the roll torque is predicted within an accuracy of 5%. Hence, this simplified method can be fruitfully used on shop floor. However, the method should be used with caution for the rolling of a drastically different material that may produce a significantly different roll deformation pattern.

Table 4.5. Comparison of roll force predictions by the proposed approximate method with FEM

R/h_1	f	r	b	n	Roll force/width (MN/m)		% deviation
					Approx. method	FEM	
40	0.06	10	0.02	0.6	2.5917	2.6524	2.2884
			0.055	0.07	0.9889	0.9152	8.0528
			0.07	0.1	1.0001	0.9238	8.2593
25	0.05	17	0.04	0.001	0.8721	0.8235	5.9016
			0.065	0.25	1.1388	1.1212	1.5697
			0.03	0.02	0.899	0.8429	6.6555
48	0.11	9	0.075	0.04	1.0493	1.0015	4.7728
			0.065	0.09	1.0913	1.0646	2.5079
			0.025	0.15	1.2531	1.2251	2.2855
30	0.14	20	0.08	0.5	2.1493	2.1807	1.4399
			0.05	0.05	1.3179	1.2547	5.0370
			0.02	0.6	5.2874	5.4217	2.4770
90	0.06	8	0.06	0.08	1.433	1.3938	2.8124
			0.035	0.25	1.7419	1.7258	0.9329
			0.07	0.001	1.3584	1.2948	4.9119
65	0.08	24	0.02	0.1	2.5166	2.472	1.8042
			0.045	0.01	2.0152	1.9876	1.3886
			0.06	0.001	1.9858	1.9293	2.9285
82	0.13	10	0.045	0.26	2.1261	2.1089	0.8155
			0.064	0.15	1.8243	1.7845	2.2303
			0.058	0.45	2.4323	2.4682	1.4545
78	0.11	19	0.031	0.04	2.281	2.1985	3.7525
			0.056	0.067	2.3204	2.2541	2.9413
			0.075	0.41	3.4729	3.4858	0.3700

Table 4.6. Comparison of roll torque predictions by the proposed approximate method with FEM

R/h_1	f	r	b	n	Roll torque/width (kN-m/m)		% deviation
					Approx. method	FEM	
40	0.06	10	0.02	0.6	2.0458	1.9836	3.1357
			0.055	0.07	0.9058	0.8687	4.2707
			0.07	0.1	0.9054	0.8778	3.1442
25	0.05	17	0.04	0.001	0.8535	0.8367	2.0079
			0.065	0.25	1.0713	1.0678	0.3278
			0.03	0.02	0.8671	0.8595	0.8842
48	0.11	9	0.075	0.04	0.9913	0.9712	2.0696
			0.065	0.09	1.0257	1.0050	2.0597
			0.025	0.15	1.1485	1.1321	1.4486
30	0.14	20	0.08	0.5	2.1879	2.2248	1.6586
			0.05	0.05	1.4838	1.451	2.2605
			0.02	0.6	4.3745	4.5821	4.5307
90	0.06	8	0.06	0.08	1.562	1.6106	3.0175
			0.035	0.25	1.8625	1.913	2.6398
			0.07	0.001	1.5235	1.5408	1.1228
65	0.08	24	0.02	0.1	4.1394	4.2319	2.1858
			0.045	0.01	3.4165	3.4785	1.7824
			0.06	0.001	3.4709	3.4345	1.0598
82	0.13	10	0.045	0.26	2.4158	2.4886	2.9253
			0.064	0.15	2.1404	2.2057	2.9605
			0.058	0.45	2.6765	2.7886	4.0199
78	0.11	19	0.031	0.04	3.7846	3.8305	1.1983
			0.056	0.067	3.8413	3.8826	1.0637
			0.075	0.41	5.301	5.3817	1.4995

4.7 Identification and Suppression of Outliers in the TS model

The efficient and accurate prediction of output variables based on soft computing techniques like neural networks or fuzzy models depends on the accuracy of the modelling data. It is not uncommon to have outliers in the dataset. An outlier is an observation that lies outside the overall pattern of a distribution. In the present work, the following methodology is proposed for identification and suppression of the outliers:

- Based on the results of TS fuzzy inference model, a rule base consisting of Mamdani inference type rules are generated. In Mamdani style inference, the rule output is a fuzzy variable instead of a crisp expression. Here, the

method suggested by Chen and Black [1997] is employed for developing the rule base.

- Each modelling data is checked against the rule base as follows. For each set of input variables, the rule base predicts an output in the form of a fuzzy subset such as Low (L), medium (M) or high (H). If the output variable has a membership grade in fuzzy subset equal to 0, the data is considered to be a total outlier and is removed. If the membership grade of the output variables is between 0 to 0.5, the data is considered as a partial outlier and its effect on modelling is reduced by a factor of 2μ, where μ is the membership grade of the output variable. Thus, after removing the total outliers, the following linear programming model is solved:

$$\begin{aligned} &\text{Minimize } \lambda, \\ &\text{subject to,} \\ &o_p - \hat{y}_p \le \lambda / \max(1,\, 2\mu_p), \qquad p = 1,\, 2, \ldots\ldots m, \\ &-o_p + \hat{y}_p \le \lambda / \max(1,\, 2\mu_p), \qquad p = 1,\, 2, \ldots\ldots m, \\ &\qquad\qquad \lambda \ge 0, \\ &a_i^j \ge 0, \qquad i = 1, 2 \ldots\ldots N_R, \quad j = 1, 2, \ldots\ldots 5. \end{aligned} \tag{4.16}$$

where μ_p is the membership grade associated with the output variable of p^{th} modelling data.

To test the effectiveness of the proposed algorithm, for constructing a three-input variable (R/h_1, f, r) inference, 1% faulty data (consisting of data with errors from 5-30% in a uniform random fashion) were introduced in a total of 3000 modelling data. The maximum approximation error λ came out to be 1.5165 MN/m for roll force and 2.1137 kN-m/m for roll torque. After constructing the TS fuzzy inference by solving Eq. (4.8), a Mamdani style fuzzy rule base is created. Each rule provides the output as one fuzzy subset amongst L, MD and H. Using the rule base, the proposed procedure is followed to construct the modified TS fuzzy inference by solving Eq. (4.16) that provided λ as 0.8769 MN/m for roll force and 1.0963 kN-m/m for roll torque. To further assess the performance of the proposed procedure, two sets of 50 random data (different from modelling data) with 1% faulty data were

chosen. Table 4.7 shows advantages of the proposed methodology for suppression of outliers for both sets of data.

Table 4.7. Performance of the proposed TS model and original TS model in the presence of outliers

	$\% \, rms_{err}^{f}$			
	Set # 1		Set # 2	
	Original TS model	Modified TS model	Original TS model	Modified TS model
Roll force	8.677	2.723	7.3606	2.8355
Roll torque	9.573	3.278	9.1214	3.5210

4.8 Summary

In this work, a Takagi-Sugeno (TS) fuzzy model is used to model the cold rolling process. The data required for construction of fuzzy modelling is generated using radial basis function neural networks. A linear programming method is used to obtain the coefficients associated with the linear expressions of the TS fuzzy inference model. It is demonstrated that TS fuzzy inference can predict roll force, roll torque and their derivates with respect to the process variables with a reasonable accuracy. Compared to neural network model, the fuzzy inference model is simpler to construct as it does not require proper selection of network parameters, such as spread parameter and goal in RBF neural network. It is also shown that fuzzy inference models can easily be constructed to predict lower and upper estimates along with most likely estimates of the output parameter. The only disadvantage of the fuzzy inference model is the requirement of a huge dataset for accurate prediction of the output variables along with their sensitivity with respect to the process variables. This disadvantage may be overcome by generating the modelling data for fuzzy inference by a trained neural network, as done in this work.

This thesis also proposes an approximate method to estimate the roll force and roll torque for another material based on these values for one material. The approximate method will be highly useful for a quicker estimation. In the modern production scenario, where a wide variety of rolled sheets made of different materials are produced by the same organization, this method is an economical way

to get the roll force and roll torque data for a new material based on FEM or experimental data of a reference material.

A simple methodology for the detection and suppression of the outliers is proposed in this chapter. It is showed by an illustration that the presence of outliers deteriorates the performance of the TS model considerably. An algorithm is proposed in the present work to suppress the effect of outliers. The proposed methodology can also be extended to predict the lower and upper estimates in the presence of outliers.

5

Pressure Field Correction in FEM Flow Formulation with the Help of Finite Difference and Neural Networks

5.1 Introduction

In the finite element analyses of cold flat rolling process, flow formulation has been extensively used considering the material as rigid-plastic. As the material remains incompressible during plastic deformation, a penalty parameter has been used by several researchers to introduce an artificial compressibility. Choosing a proper value of penalty parameter is important in these formulations. The hydrostatic stress being the divergence of the velocity times the penalty parameter, its accuracy is very sensitive to the accuracy of the velocity field. Considering this fact, Dixit and Dixit [1996] employed mixed pressure-velocity formulation, where pressure is the negative of hydrostatic stress. It can be shown that the mixed pressure-velocity formulation is the same as the Lagrange multiplier formulation, where the Lagrange multiplier turns out to be the hydrostatic stress [Reddy, 2006]. In the mixed pressure-velocity finite element formulation, no pressure boundary conditions are employed and therefore the pressure field is computed up to additive spurious constants. Dixit and Dixit [1996] have suggested an approximate method to modify the pressure field.

Dixit and Dixit compared results of their model with the experimental results of Shida and Awazuhara [1973] and observed a good agreement between the FEM results and the experimental results. However, some deviation was present particularly for roll torques. Dixit and Dixit attributed this deviation to the uncertainty associated with the values of material and process parameters. It is to be mentioned that none of the other rigid-plastic FEM analyses available in literature

provide better agreement with the experimental results of Shida and Awazuhara [1973] than the model of Dixit and Dixit [1996].

The major difficulty in the flow formulation is the estimation of hydrostatic stress accurately. In this thesis, a mixed pressure-velocity finite element flow formulation is used for obtaining the velocity field during the rolling process. The hydrostatic stress is obtained by solving the momentum equations using a finite difference method. Neural network models based on a radial basis function are constructed for prediction of Levy-Mises coefficient and strain-rate components. The trained neural network model provides the values of Levy-Mises coefficient and strain-rate components as a function of spatial coordinates. These neural networks predicted values are used in the finite difference equations. The proposed method is compared with a mixed pressure-velocity finite element method and experimental results available in the literature. It is observed that the proposed method provides a better agreement with the experimental results than the model of Dixit and Dixit [1996].

5.2 Problem Formulation

In the present study, only the steady-state part of the process is considered, and hence an Eulerian formulation is used. A two-dimensional plane-strain problem is considered. In the present analysis, the velocity field is obtained using the formulation of Dixit and Dixit [1996]. The finite element formulation for a rigid-plastic formulation is already explained in Chapter 3. In this formulation, in order to express stress as a function of strain rate in a convinent form, the Cauchy stress and strain-rate tensor is decomposed into two parts:

$$\sigma_{ij} = -p\delta_{ij} + S_{ij}, \tag{5.1}$$

where p is the pressure (Eq. 3.3), S_{ij} is the deviatoric stress (Eq. 3.4) and δ_{ij} is Kronecker's delta. The continuity and momentum equations (neglecting inertia terms) are expresses as (Eq.3.1 and 3.2)

$$\frac{\partial v_i}{\partial x_i} = 0\,, \tag{5.2}$$

$$\sigma_{ij,j} = 0\,. \tag{5.3}$$

For the present analysis, the upper half of a portion of metal strip is considered. A mesh consisting of 56 elements along with the boundary conditions is shown in Fig. 3.1. Boundary conditions are described in Section 3.2. The roll velocity corresponds to the velocity at the neutral point. The neutral point is found by minimizing the total power with respect to the position of neutral point. The roll deformation is estimated using Hitchcock's formula [1935]. No boundary condition is imposed on pressure. However, in the absence of front and back tension, Dixit and Dixit [1996] modified the pressure using the following equations:

$$p = p_0 - p_{avo} e^{2a\psi} \quad \text{from neutral point to exit} \tag{5.4}$$

$$p = p_0 - p_{avi} e^{2a(\psi_o - \psi)} \quad \text{from neutral point to inlet} \tag{5.5}$$

where p_0 is the pressure obtained by FEM and p_{avi} and p_{avo} are the average pressures at the inlet and exit boundaries, respectively. This correction ensures that average modified pressure at the inlet and exit boundaries are zero. Dixit and Dixit [1996] used this correction as a condition imposed on pressure in absence of tensions. In Eqs. (5.4 and 5.5),

$$a = f\sqrt{\frac{R'}{h_2}}\,, \tag{5.6}$$

$$\psi = \tan^{-1}\left(\sqrt{\frac{R'}{h_2}}\,\phi\right), \tag{5.7}$$

where R' is the deformed roll radius, ϕ is the angular position of the point at the roll-work interface (*i.e.* the angle between the lines joining the center of deformed arc with the exit point and the particular point on the roll-work interface), ψ_0 is the

value of ψ when ϕ is equal to the angle of contact α and f is the coefficient of friction. Figure 5.1 shows the nomenclatures used in the above equations.

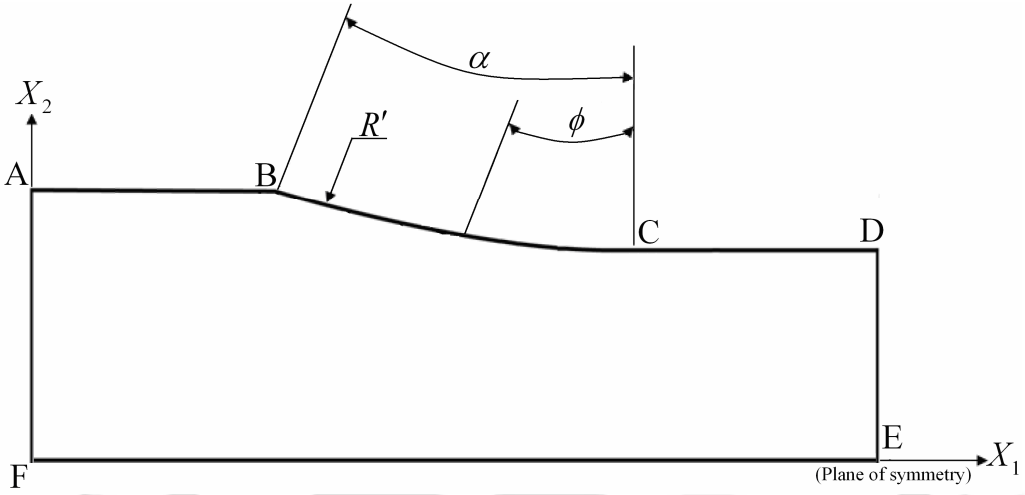

Figure 5.1. Schematic representation of a rolled strip

In the present formulation, the pressure field is obtained by satisfying the momentum equations. In unabridged form, after substituting the values of p and S_{ij}, the momentum equations can be re-written as

$$\frac{\partial}{\partial x_1}\left(-p+2\mu\frac{\partial v_1}{\partial x_1}\right)+\frac{\partial}{\partial x_2}\left\{\mu\left(\frac{\partial v_1}{\partial x_2}+\frac{\partial v_2}{\partial x_1}\right)\right\}=0, \tag{5.8}$$

$$\frac{\partial}{\partial x_1}\left\{\mu\left(\frac{\partial v_1}{\partial x_2}+\frac{\partial v_2}{\partial x_1}\right)\right\}+\frac{\partial}{\partial x_2}\left(-p+2\mu\frac{\partial v_2}{\partial x_2}\right)=0. \tag{5.9}$$

A finite forward difference approximation of Eq. (5.8) is given by

$$\frac{\left(-p+2\mu\frac{\partial v_1}{\partial x_1}\right)_{m+1,n}-\left(-p+2\mu\frac{\partial v_1}{\partial x_1}\right)_{m,n}}{\left\{(x_1)_{m+1,n}-(x_1)_{m,n}\right\}} + \left\{\frac{\left\{\mu\left(\frac{\partial v_1}{\partial x_2}+\frac{\partial v_2}{\partial x_1}\right)\right\}_{m,n+1}-\left\{\mu\left(\frac{\partial v_1}{\partial x_2}+\frac{\partial v_2}{\partial x_1}\right)\right\}_{m,n}}{\left\{(x_2)_{m,n+1}-(x_2)_{m,n}\right\}}\right\}=0. \tag{5.10}$$

Equation 5.10 is obtained by applying a forward difference formula at a typical point (m, n) shown in Fig. 5.2. With this equation, knowing the value of pressure at the point (m, n), the pressure at the next point in the horizontal line may be computed as

$$(p)_{m+1,\,n} = (p)_{m,\,n} + \left(2\mu\frac{\partial v_1}{\partial x_1}\right)_{m+1,\,n} - \left(2\mu\frac{\partial v_1}{\partial x_1}\right)_{m,\,n} + \left\{\frac{\left\{\mu\left(\frac{\partial v_1}{\partial x_2}+\frac{\partial v_2}{\partial x_1}\right)\right\}_{m,\,n+1} - \left\{\mu\left(\frac{\partial v_1}{\partial x_2}+\frac{\partial v_2}{\partial x_1}\right)\right\}_{m,\,n}}{\{(x_2)_{m,\,n+1} - (x_2)_{m,\,n}\}}\right\}\{(x_1)_{m+1,\,n} - (x_1)_{m,\,n}\} \tag{5.11}$$

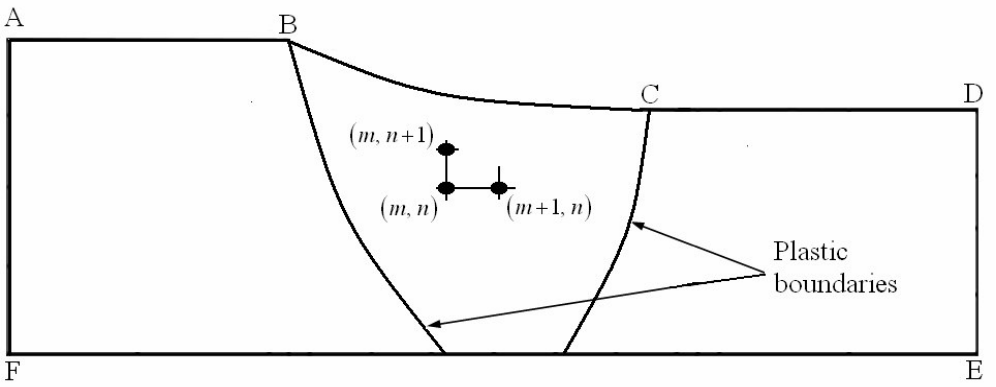

Figure 5.2. The domain showing plastic boundaries and the points for finite difference approximation

In the present formulation, the pressure along the line of symmetry is found using Eq. (5.11). For computational convenience, an approximation is made. At the line of symmetry FE shown in Fig. 5.2, the rate of change of shear stress with respect to the vertical direction is assumed zero. The shear stress is necessarily zero at the line of symmetry and it has been observed numerically that shear stress is nearly zero near to the axis of symmetry. Moreover, considering the typical plastic boundaries in a rolling process, it is seen from Fig. 5.2 that the length of plastic zone at the axis of symmetry is much smaller compared to roll-work contact length. Therefore, this approximation does not introduce any significant error. Thus, on the line of symmetry,

$$(p)_{m+1,\,n} = (p)_{m,\,n} + \left(2\mu\frac{\partial v_1}{\partial x_1}\right)_{m+1,\,n} - \left(2\mu\frac{\partial v_1}{\partial x_1}\right)_{m,\,n}. \tag{5.12}$$

With this approximation, even the coarse finite difference grid produces reasonably accurate results. Due to narrow plastic zone at the line of symmetry, the computation of rate of change of shear stress along vertical direction introduces the large amount of numerical errors that keep accumulating in the computed pressure values along the horizontal direction. Hence, it is better to make this approximation along the line of symmetry. In the absence of back tension, the pressure at the inlet surface is taken as zero. In the presence of back tension, the pressure at the inlet would be one third of the back tension per unit width of the strip divided by strip thickness, with a negative sign.

The finite difference approximation of Eq. (5.9) along with the continuity equation provides

$$\left\{\frac{\left\{\mu\left(\frac{\partial v_1}{\partial x_2}+\frac{\partial v_2}{\partial x_1}\right)\right\}_{m+1,\,n} - \left\{\mu\left(\frac{\partial v_1}{\partial x_2}+\frac{\partial v_2}{\partial x_1}\right)\right\}_{m,n}}{\left\{(x_1)_{m+1,n} - (x_1)_{m,n}\right\}}\right\} + \frac{\left(-p-2\mu\frac{\partial v_1}{\partial x_1}\right)_{m,\,n+1} - \left(-p-2\mu\frac{\partial v_1}{\partial x_1}\right)_{m,\,n}}{\left\{(x_2)_{m,\,n+1} - (x_2)_{m,\,n}\right\}} = 0. \tag{5.13}$$

With the help of this equation, knowing the pressure at the point (m, n), the pressure at the next point (m, n+1) in the vertical line is computed as

$$(p)_{m,\,n+1} = (p)_{m,\,n} + \left(2\mu\frac{\partial v_1}{\partial x_1}\right)_{m,\,n} - \left(2\mu\frac{\partial v_1}{\partial x_1}\right)_{m,\,n+1} + \left\{\frac{\left\{\mu\left(\frac{\partial v_1}{\partial x_2}+\frac{\partial v_2}{\partial x_1}\right)\right\}_{m+1,\,n} - \left\{\mu\left(\frac{\partial v_1}{\partial x_2}+\frac{\partial v_2}{\partial x_1}\right)\right\}_{m,\,n}}{\left\{(x_1)_{m+1,\,n} - (x_1)_{m,\,n}\right\}}\right\}\left\{(x_2)_{m,\,n+1} - (x_2)_{m,\,n}\right\}. \tag{5.14}$$

The method consists of first computing the pressure values at various points on the line of symmetry using Eq. (5.12) and then computing the pressures at various vertical lines emanating from these points. For obtaining the Levy-Mises coefficient μ and velocity gradients as a function of the coordinates (x_1, x_2), the neural network modelling is used. Details of the neural network modelling are explained in next section.

5.3 Neural Network Modelling

In this work, radial basis function (RBF) neural networks have been used [Ham and Kostanic, 2001] as they require much less time in training compared to multi-layer perceptron networks. For modelling of $\dot{\varepsilon}_{11}, \dot{\varepsilon}_{12}$ and σ_Y as a function of x_1 and x_2, three separate radial basis function neural networks are used. The Levy-Mises coefficient μ is calculated from these neural networks using Eq. (3.6). The architecture of the radial basis function neural network used for the present analysis is shown in Fig. 5.3. It consists of one input layer having neurons corresponding to x_1 and x_2 coordinates, one hidden layer having a number of neurons that process the input using the radial basis functions and one output layer corresponding to the parameter being modelled. The details of the radial basis function neural network are already explained in Chapter 3.

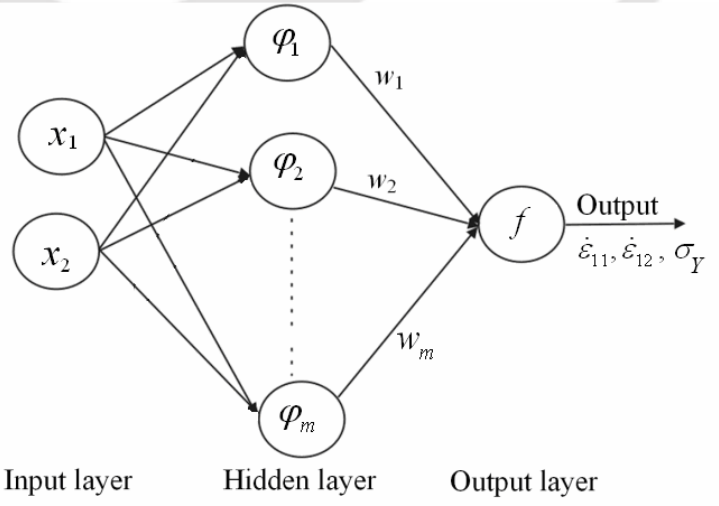

Figure 5.3. The architecture of RBF model used in the present work

In this work, the radial basis function associated with each neuron in the hidden layer is a Gaussian function (bell-shaped) is given by Eq. (3.25). The final output of the RBF neural network is

$$f(x_1, x_2) = \sum_{j=1}^{m} w_j \varphi_j \left(\sqrt{(x_1 - c_{1j})^2 + (x_2 - c_{2j})^2} \right) + b_0, \tag{5.15}$$

where $\varphi_j(.)$ is the processing function of the j^{th} neuron in the hidden layer, w_j is the weight associated with that neuron, m is the number of neurons in the hidden layer, b_0 is bias (a constant term) and c_{1j}, c_{2j} are the coordinates of the center associated with the j^{th} neuron which are chosen to lie within the domain. For fixed centers and spread parameter, applying Eq. (5.15) for each training data provides a linear system of equation having m unknowns w_j and one unknown b_0 that can be solved using the least square method. Hence, the training procedure takes much less time compared to the time for training the multi-layer perceptron networks.

The network is trained by taking the results of FEM corresponding to 2×2 Gauss point formula as well as the center of the element. Thus with the mesh consisting of 56 elements, 280 training data are obtained. The trained network is cross-validated with 2 points along the horizontal center line of each element. With 56 elements, the number of cross-validation data (testing data) becomes 112. Figure 5.4 shows the selection of training data and cross-validation data for a typical element in natural coordinates.

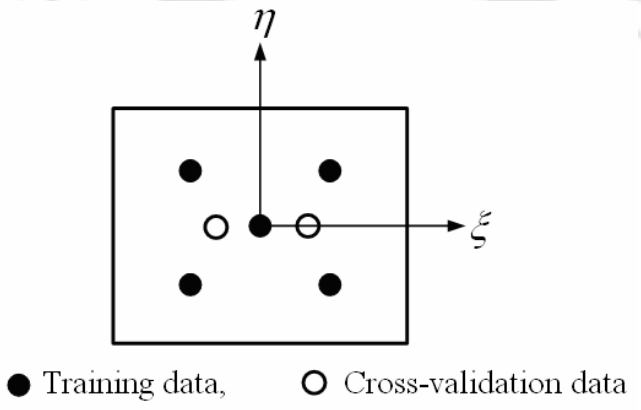

Figure 5.4. Training and testing data points selected from a typical element

The MATLAB function NEWRB is used for training of the network. The details of the NEWRB function are explained in Chapter 3 (Section 3.3.2). The selection of spread parameter is based on a simple heuristic relationship (Eq. 3.28). Since Eq. (3.28) is a heuristic relation, spread parameter is fine tuned by multiplying a constant factor β as explained in Section 3.3.2. The optimum β that provides the least percentage root mean squared fractional error in the prediction for cross validation points was found to be 0.5. Thus, in the present work, β is taken as 0.5. It is to be mentioned that the value of optimum β depends on the values of input and output parameters of NN model. Thus, the value of optimum β may differ from one NN model to other NN model.

The performance of the neural networks is checked by determining the percentage root mean squared (*rms*) fractional error for training and testing points. The percentage root mean squared fractional error is calculated as given in Eq. (4.5). Table 5.1 shows the final network architecture for a typical case of 24 % reduction. The trained networks are used for the computation of Levy-Mises coefficient and strain-rate components required in the finite difference equations.

Table 5.1. The final network architecture for neural network modelling (Steel, $R/h_1 = 65$)

Network parameters	$\dot{\varepsilon}_{11}$	$\dot{\varepsilon}_{12}$	σ_Y
Error goal	0.0001	0.0001	0.0001
β	0.5	0.5	0.5
Number of centers	266	272	269
Number of training data	280	280	280
Number of testing data	112	112	112
$\%\ rms_{err}^{f}$ (training)	0.0027	0.0024	0.1390
$\%\ rms_{err}^{f}$ (testing)	0.5744	0.4203	1.2182

5.4 Results and Discussion

The proposed methodology needs to be validated with the experimental results. So far no experimental data measuring the hydrostatic stress inside the material during its rolling is available in the literature. However, the experimental results of roll

torque roll force and roll pressure distribution have been reported in the literature. These results are compared with the present model to assess its accuracy.

5.4.1 Results with Fuzzy Parameters for Steel Material

Several authors including Dixit and Dixit [1996] and Li and Kobayashi [1982] used the experimental results of Shida and Awazuhara [1973] and Al-Salehi *et al*. [1973] for validation of their models. In this work, the roll force and roll torque values are compared with the experimental results of Shida and Awazuhara [1973] and Al-Salehi *et al*. [1973] and finite element results of Dixit and Dixit [1996].

The inherent variations in the experimental investigation causes scatter in the experimental data and a large deviation with the FEM results. Due to this, Dixit and Dixit [1996] considered the material and the process parameters as fuzzy parameters. Also, it is observed experimentally and analytically that the value of the friction coefficient varies in the roll gap instead of being constant [Rooyen and Backofen, 1957; Al-Salehi *et al*., 1973; Lim and Lenard, 1984 and Rao and Lee, 1989]. Thus, Dixit and Dixit [1996] considered the input parameters *i.e*. initial values of yield strength $(\sigma_Y)_0$, strain hardening coefficients b and n, and coefficient of friction f to be four fuzzy parameters which are characterized by their membership functions. Standard methods are available in the textbook for constructing the membership function. Dixit and Dixit considered a linear triangular membership function. In this process of determining the fuzzy parameters, parameters are divided into three subsets such as low, most likely and high. A triangular membership function is given by

$$\mu(x)=\begin{cases}0 & x\le l'\\ \dfrac{x-l'}{m-l'} & l'\le x\le m\\ \dfrac{h'-x}{h'-m} & m\le x\le h'\\ 0 & x\ge h'\end{cases} \tag{5.16}$$

where

$$l' = \begin{cases} m - 2(m-l) & m > 2(m-l) \\ 0 & m \le 2(m-l) \end{cases}$$

and

$$h' = m + 2(h-m)$$

Here, l, m and h are fuzzy subsets of a parameter respectively. The value of μ is 0.5 at $x = l$ and h. The value of μ is 1 at $x = m$.

Table 5.2. Fuzzy input parameters for two steels, Steel 1 with h_1 = 1 mm and Steel 2 with h_2 = 0.5 mm

Parameters	Low (l)		Most likely (m)		High (h)	
	Steel 1	Steel 2	Steel 1	Steel 2	Steel 1	Steel 2
$(\sigma_Y)_0$, MPa	291.6	322.2	324	358	356.4	393.8
f	0.06	0.06	0.08	0.08	0.14	0.14
b	0.0416	0.0352	0.052	0.044	0.0624	0.0528
n	0.236	0.24	0.295	0.3	0.354	0.36

The values of the fuzzy parameters for two different materials are shown in Table 5.2. Dixit and Dixit assumed that the variations in yield stress and hardening coefficients may go up to $\pm 10\%$ and $\pm 20\%$, respectively. While updating the parameters, the equivalent Coulomb's coefficient of friction has been taken as 0.14. The finite element model with the fuzzy parameters provides the roll force and roll torque as a band bounded by the upper and lower limit curves for each membership grade. Dixit and Dixit [1996] observed that almost all experimental data is contained in the band of 0.5 membership grade. However, it is noted that the experimental values of roll torque lies only in the upper half of the band unlike the experimental values of roll force. This indicates that the model of Dixit and Dixit [1996] is unable to provide the same order of accuracy for roll force and roll torque even after updating of the material and process parameters. In the present analysis, corresponding to the upper limit of 0.5 membership grade which corresponds to the high estimate of the parameters, the finite element computations are carried out by

the present model and are compared with the model of Dixit and Dixit [1996] as well as the experimental results of Shida and Awazuhara [1973] for roll force and roll torque. Figure 5.5 and 5.6 shows the comparison for roll force and roll torque prediction respectively.

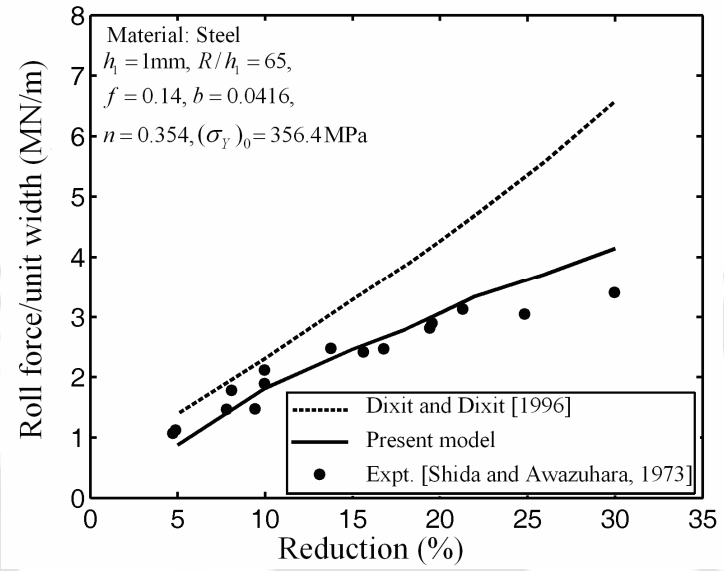

Figure 5.5. Comparison of FEM and experimental results for roll force (Steel, $R/h_1 = 65$)

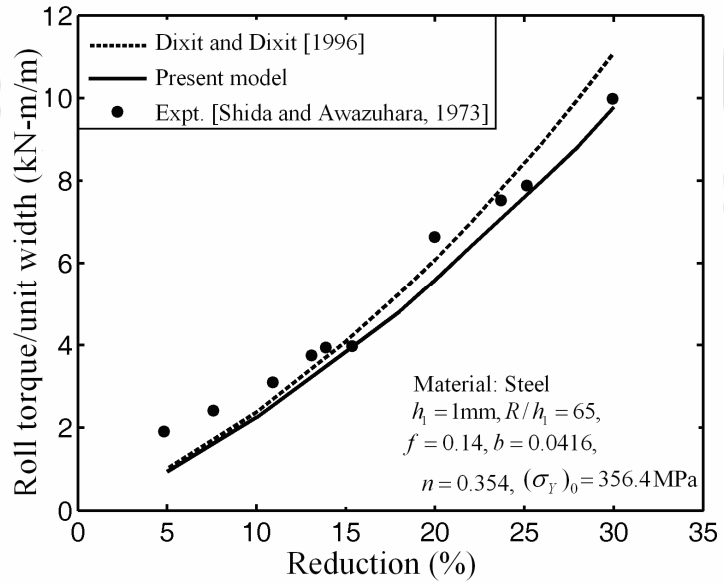

Figure 5.6. Comparison of FEM and experimental results for roll torque (Steel, $R/h_1 = 65$)

It is observed from Figs. 5.5 and 5.6 that the results obtained by the model of Dixit and Dixit [1996] is in a good agreement with the experimental roll torque values but over predicts the roll force. On the other hand, the present model predicts both the roll force and roll torque with a close agreement with that of experimental results. The only difference in the present model and the model of Dixit and Dixit is the method of obtaining the pressure. Thus, the method proposed in this work for the computation of pressure seems to be better.

The roll pressure distribution for a typical case of 24% reduction is compared with that of Dixit and Dixit [1996]. The experimental roll pressure distribution for steel is not reported in the literature. Figure 5.7 shows the pressure distribution for the two models after updating the parameters. Although, the profile of roll pressure distribution is similar in both the models, it is observed that Dixit and Dixit model predicts higher values of the non-dimensionalized roll pressure as compared to the present model.

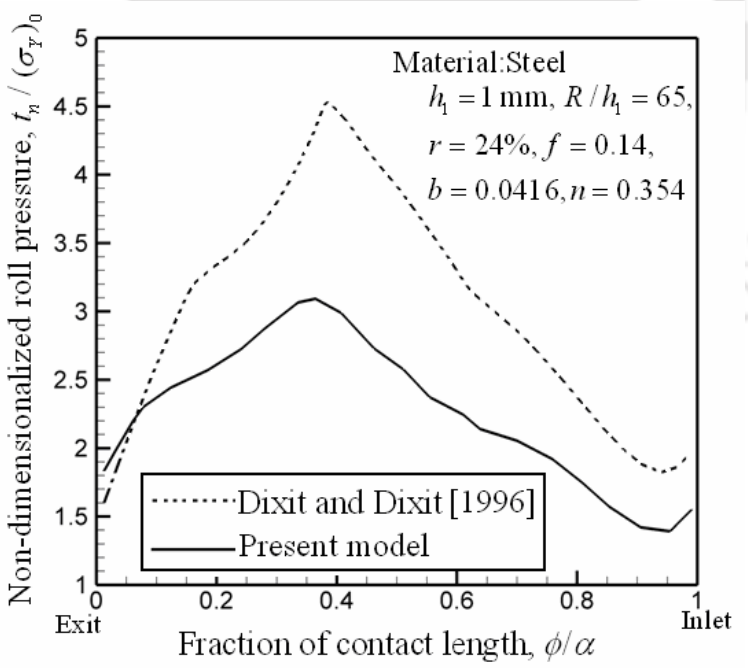

Figure 5.7. Comparison of roll pressure distribution for a typical case (Steel, $R/h_1 = 65$)

The accuracy of the present model is further assessed by carrying out the computations for the second set of material and process parameters for different reductions. Like previous set, the material to be rolled is considered as steel but with different initial strip thickness ($h_1 = 0.5\,\text{mm}$). For this set, the results are not reported in the paper of Dixit and Dixit [1996]. The results presented in Fig. 5.8 and 5.9 have been generated by running the code developed by Dixit [1997] for comparison with the present model. Figure 5.8 shows that after updating the material and process parameters, Dixit's model over predicts the roll force by a large amount when compared with the experimental results of Shida and Awazuhara [1973]. On the other hand, the present model shows good agreement with the experimental results of Shida and Awazuhara [1973]. Figure 5.9 shows the comparison for roll torque prediction. Considering the scatter present in the experimental results of roll torque, it is concluded that roll torque predicted by the present model is in fair agreement with the experimental values.

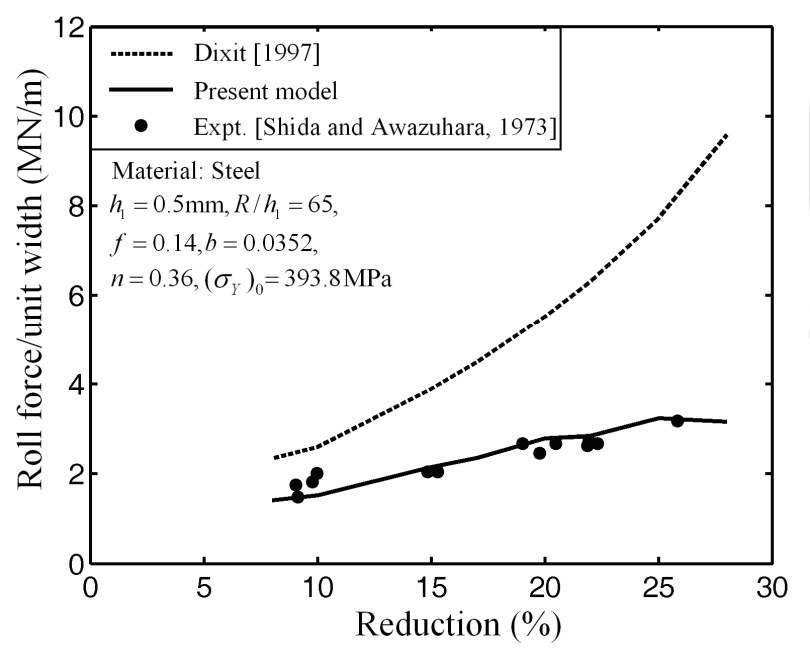

Figure 5.8. Comparison of FEM and experimental results for roll force (Steel, R/h_1 = 130)

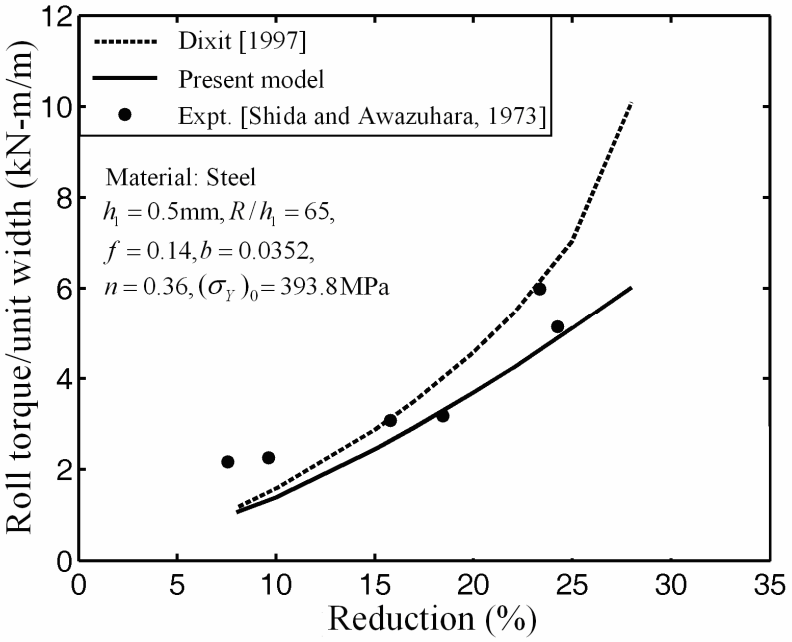

Figure 5.9. Comparison of FEM and experimental results for roll torque (Steel, $R/h_1 = 130$)

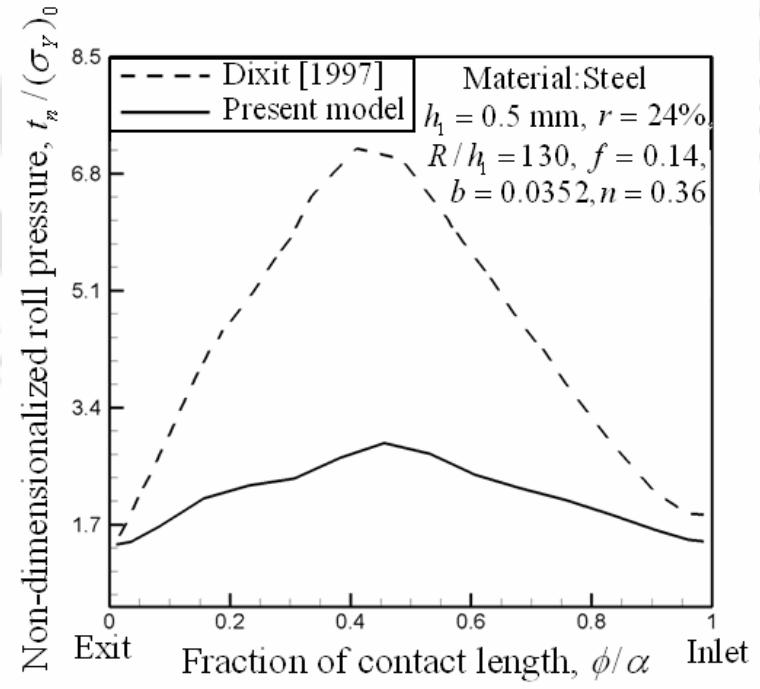

Figure 5.10. Comparison of roll pressure distribution for a typical case (Steel, $R/h_1 = 130$)

Figure 5.10 shows the roll pressure distribution for a second set of material and process parameter ($h_1 = 0.5$ mm). Similar to the results reported in Fig. 5.7, the roll pressure distribution obtained by the present model and by the model of Dixit [1997] differ in magnitude for the second set of material and process parameters.

Figures 5.5-5.6 and Figs. 5.8-5.9 show that present model and Dixit and Dixit model differs largely for roll force prediction. This is due to the method of obtaining pressure in the present model. However, there is a lesser deviation in both the models for roll torque prediction. This may be attributed to the method of roll torque computation. In both the models, roll torque is computed by dividing the total power with the angular velocity (V_R) of the roll, where the total power consist of power required for plastic deformation, power required to overcome friction at the roll-work interface and power required due to front and back tension (Eqs. 3.21-3.24). The pressure plays a minor role here.

5.4.2 Validation of the Model for Copper and Aluminium

The present model is further validated for rolling of copper and aluminium also. In these simulations, the values of roll force, roll torque and roll pressure distribution are compared with the experimental results of Al-Salehi *et al.* [1973] and model of Dixit [1997].

5.4.2.1 Results for Copper

Figure 5.11 shows that Dixit's model [1997] provides slightly higher values of the roll force compared to the present model for rolling of copper strip. Figure 5.12 shows that the predicted values of roll torque from the present model and Dixit's model are almost similar. In this case, no updating of the material or the process parameters has been done. The comparison of roll pressure distribution for the rolling of copper is shown in Fig. 5.13. The general shapes of FEM generated curves are similar to the experimental pressure distribution curve. However, the similarity of roll pressure distribution with the experimental result is more pronounced for the present model than the model of Dixit [1997].

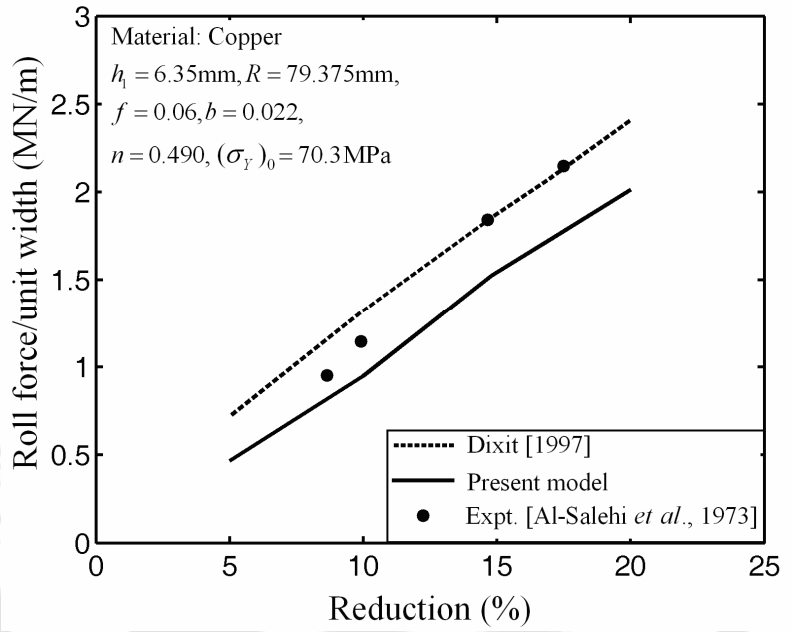

Figure 5.11. Comparison of FEM and experimental results for roll force (Copper)

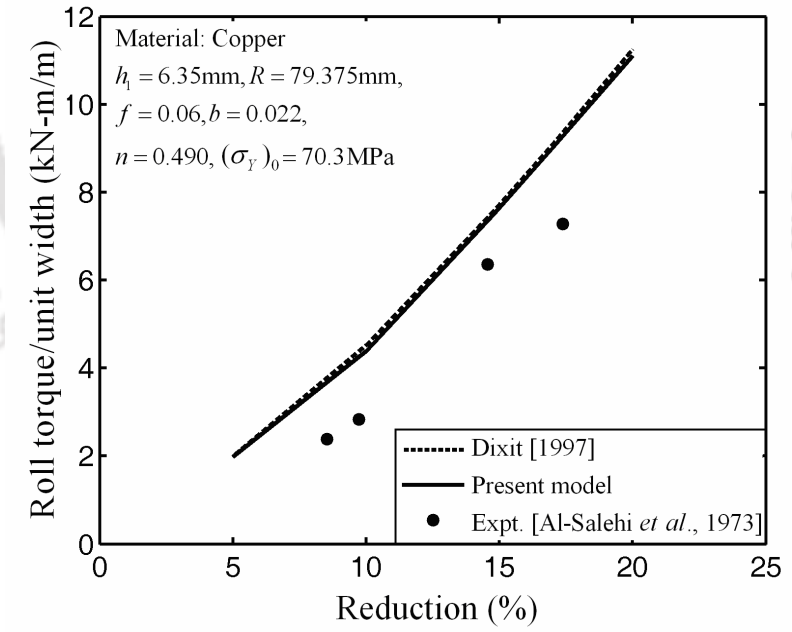

Figure 5.12. Comparison of FEM and experimental results for roll torque (Copper)

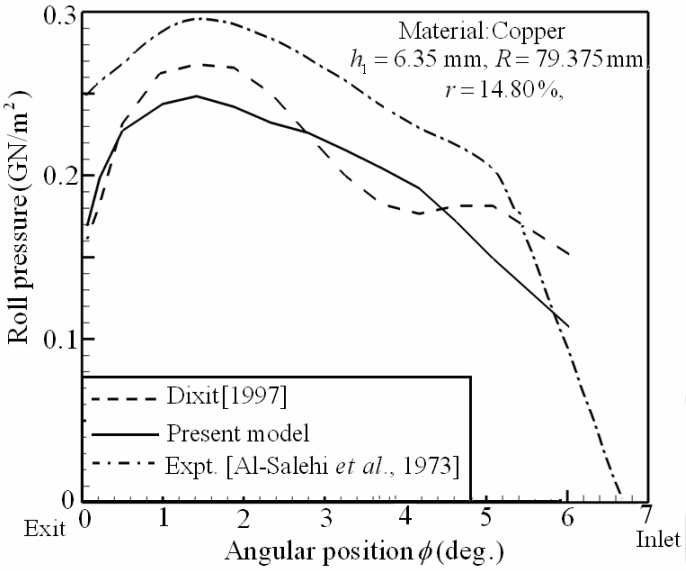

Figure 5.13. Comparison of FEM and experimental roll pressure distribution (Copper)

5.4.2.2 Results for Aluminium

The results are also generated for aluminium. The values of roll force and roll torque are compared with the experimental results of Al-Salehi *et al.* [1973] and finite element model of Dixit [1997]. Figure 5.14 and 5.15 shows that the present model is in fairly good agreement with the finite element model of Dixit [1997]. Like copper, no updating of the material or the process parameters has been done for aluminium.

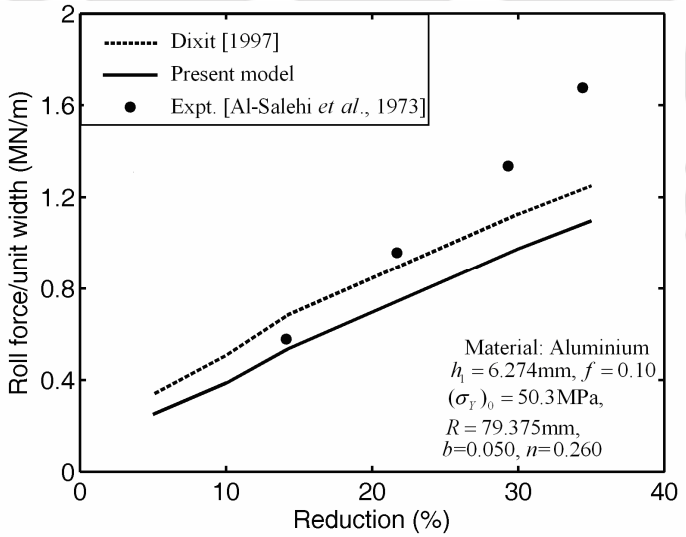

Figure 5.14. Comparison of FEM and experimental results for roll force (Aluminium)

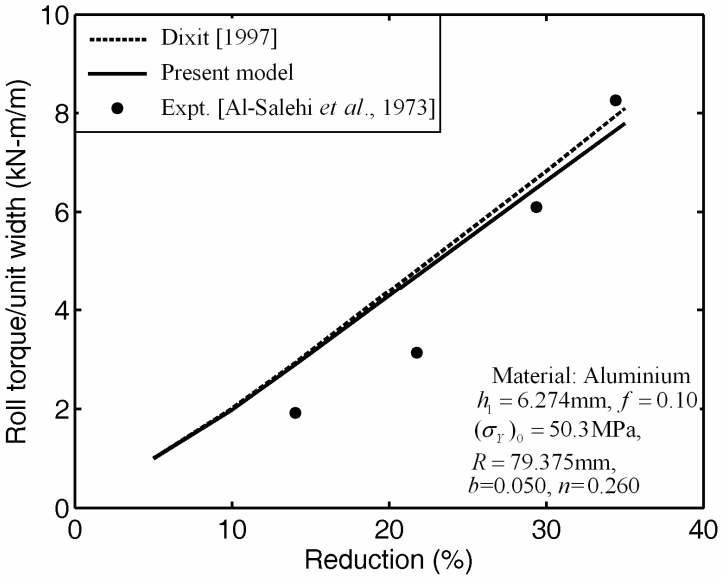

Figure 5.15. Comparison of FEM and experimental results for roll torque (Aluminium)

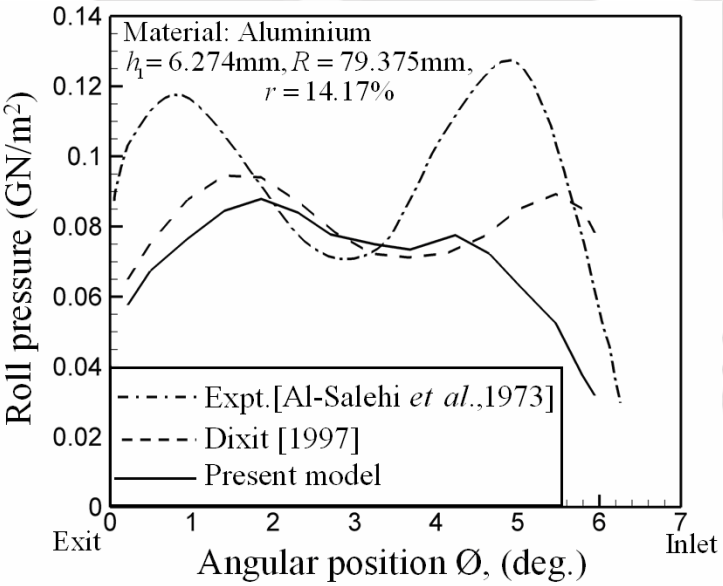

Figure 5.16. Comparison of FEM and experimental results for roll pressure distribution (Aluminium)

Figure 5.16 shows the roll pressure distribution for aluminium. It is observed that the results of the present model and Dixit's model [1997] are in a reasonable agreement. The profile of roll pressure distribution is found similar in both the finite element models. The pressure distribution obtained by the present model differs with the experimental pressure distribution in magnitude. It is reported in Ref. [Al-Salehi

et al., 1973] that, in the case of aluminium, the roll force calculated from the normal pressure distribution is 20% higher than that measured from load cell. Thus, considering the uncertainties in the experimental results for aluminium, the agreement may be treated as a fair agreement with the finite element models.

One interesting observation is that in the case of the results presented for steel (Figs. 5.5–5.10), there is a significant difference between the results of the present model and the model of Dixit and Dixit [1996], whilst both models differ only slightly for the results presented for copper and aluminium (Figs. 5.11–5.17). This is due to the fact that R/h_1 ratio is much smaller in the latter cases (copper and aluminium). As R/h_1 ratio decreases, the contribution of the hydrostatic term (pressure) decreases in comparison to the deviatoric term in the thickness direction normal stress at the roll-work interface. Thus, the error in the computation of the pressure becomes less significant as R/h_1 ratio decreases. That is why for low R/h_1 ratio, both model differs only slightly whereas for higher R/h_1 ratio, difference in the results of both model due to pressure computation is more significant.

5.4.3 Comparision with Slab Method

The roll pressure distribution from the present model has also been compared with the roll pressure distribution obtained using a slab method code [Salunkhe, 2006]. A high R/h_1, low reduction and low friction are chosen to make the rolling process amenable to slab method model. For this comparison, it is assumed that the performance of FE model with high R/h_1, low reduction and low friction will be closer to that of a slab method based model.

It can be observed from Fig. 5.17 that the pressure distribution obtained by the slab method is closer to the present model than the model of Dixit [1997]. The pressure distribution obtained by Dixit's model is far away from the slab method pressure distribution and has a valley near the inlet. Like slab method, the pressure distribution by the present model does not contain any valley. Thus, from Fig. 5.17, it is concluded that the present model provides a realistic pressure distribution.

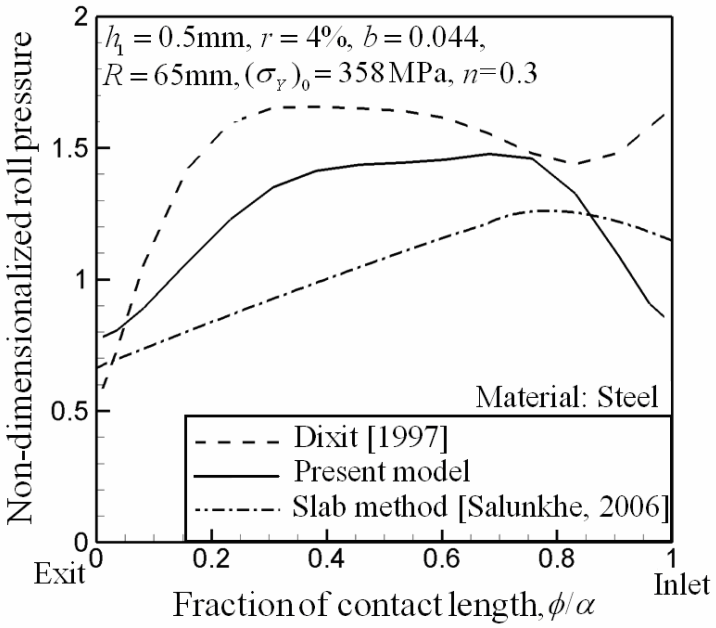

Figure 5.17. Comparison of roll pressure distribution for different methods

5.5 Summary

In the present work, cold flat rolling process is analyzed using finite element method and finite difference method assisted by neural network models. First, the velocity field is obtained by a rigid-plastic mixed pressure-velocity finite element flow formulation. After that the pressure field is obtained using a finite difference method. For obtaining the pressure field, radial basis function neural network modelling is incorporated. Three different neural network models are constructed for obtaining Levy-Mises coefficient and strain-rate components required in the finite difference equations for pressure computations. For a more accurate prediction of the pressure field, the following procedure may be adopted. If the finite difference computed pressure field is significantly different from the pressure field obtained by FEM, the fresh location of neutral point is obtained using the finite element code with modified pressure. With fresh location of the neutral point, the new velocity field is obtained. The new velocity field is used for finding out the pressure field by the finite difference method. In case, the new finite difference computed pressure field is different than the previous pressure field, the procedure is repeated. Thus, the

velocity and pressure fields are obtained from finite element method-finite difference method (FEM-FDM) based procedure in an iterative manner. It was observed that with 56 elements, the finite element predicted velocity field is quite accurate. The finite difference modified pressure field does not give rise to a significantly different velocity field by FEM due to weak coupling of pressure and velocity. Thus, in the present work, the iterative procedure was not found necessary. A few computations were carried out with the refined mesh (112 elements) in order to ascertain the appropriateness of 56 elements in the finite element model.

A comparison of the proposed methodology is carried out with the experimental results and finite element models available in the literature. It is observed that for a high roll radius to thickness ratio, the results obtained from the present model differ with the model of Dixit and Dixit [1996], and are closer to the experimental results of Shida and Awazuhara [1973]. At a low roll radius to thickness ratio, the hydrostatic stress plays less significant role in the computation of roll pressure and roll force distribution and the proposed model is closer to Dixit [1997] than experimental results of Al-Salehi *et al*. [1973].

The comparison of roll pressure distribution is carried out. In the comparison, the set of process parameters for which the slab method is justified, the present model is found closer to the slab method than Dixit's model. Thus, the present model discussed in this thesis makes an improvement over the existing rigid-plastic FEM flow formulations available in the literature.

6

Neural Network and Fuzzy Set Applications in the Analysis of Curvature in an Asymmetric Rolling Process

6.1 Introduction

In general, rolling process can be divided into two major types– symmetric rolling and asymmetric rolling. It is already discussed in Chapter 1 that in a symmetric rolling process, due to the geometric and parametric symmetry about the mid-plane of the sheet, the product that emerges from the rolling mills is expected to be flat. The flatness of the rolled product is one of the major quality attributes. Thus, it becomes important to maintain the symmetric rolling conditions to obtain a flat product. However, practically it is difficult to ensure the geometric and parametric symmetry at the mid-plane of the sheet. This may lead to produce curvature in the rolled product. The limiting of the curvature in the rolled product is important from the point of view of quality. On the other hand, there are situations where asymmetric rolling may be desirable for producing the curved sheets and/or for reducing the roll force and roll torque. Thus, it becomes important to have broader knowledge of asymmetric rolling process in order to maintain the quality of the rolled sheets.

In the present thesis, a slab method model developed by Salunkhe [2006] is used to study various aspects of asymmetric rolling process with the help of neural network and fuzzy set theory. Salunkhe [2006] included the strain hardening behaviour of the material and roll deformation in the model. Instead of Coulomb's model, Wanheim and Bay's friction model [Appendix D] is employed in his model. He compared the results of roll force and roll torque model with the analytical model of Salimi and Kadkhodaei [2004] only. The author did not validate the performance of the model with a number of experimental results available in the literature. He

also did not elaborate on the suitability of various assumption made. A rigorous study of the effect of strain hardening and roll deformation on the curvature was also not carried out in his work.

In the present thesis, a more detailed study of various parameters has been carried out. The performance of the slab model is validated by comparing the results with different experimental results and analytical results available in the literature. Instead of using soft computing techniques for prediction of roll force and roll torque, attention is paid to the analysis of curvature using neural networks and fuzzy set theory in this chapter. Roll force and roll torque prediction with the help of soft computing tools can be carried out in a manner similar to symmetric rolling. Here, a neural network model is developed for the prediction of curvature. The developed model may be used for prediction of curvature for a given sets of data and to carry out sensitivity analysis of the curvature with respect to friction at the upper and lower roll-work interface.

In the past, several researchers observed experimentally and analytically that the value of the coefficient of friction varies in the roll gap instead of being constant. This characteristic is elaborated in Section 5.4.1. The uncertain frictional condition at the upper and lower roll-work interface leads to create asymmetry in the rolling process. The present work also investigates the curvature generated due to uncertain frictional condition at the upper and lower roll-work interface. In order to simulate this uncertainty, the coefficient of friction at upper and lower roll-work interface is treated as fuzzy. A strategy based on controlling the roll velocity is suggested for minimizing the undesirable curvature generated due to uncertain frictional conditions. The results indicate a good potential of the proposed method.

6.2 Slab Method Formulation

The slab method model [Salimi and Kadkhodaei, 2004; Salunkhe, 2006] used in the present work is briefly explained here. Figure 6.1 shows an asymmetric rolling process. It is assumed that the speed of lower roll is higher than that of upper roll ($V_l > V_u$). Now, in an asymmetric rolling process, due to asymmetric conditions, two

neutral points will be generated *i.e.*, neutral point at upper roll-work interface and neutral point at lower roll-work interface. This leads to form three zones in the roll gap. In zone I, the strip velocity is lower than the speeds of both the rolls and the frictional stresses on the upper and the lower surfaces are in the forward direction. In zone II, the strip velocity is more than the speed of the upper roll and less than the speed of the lower roll. This zone is known as cross shear zone. In this zone, the frictional stresses on the upper surface act in the backward direction and that on the lower surface act in the forward direction. In zone III, as the speeds of both the rolls are lower than the strip velocity, the frictional stresses at both the surfaces are in the backward direction.

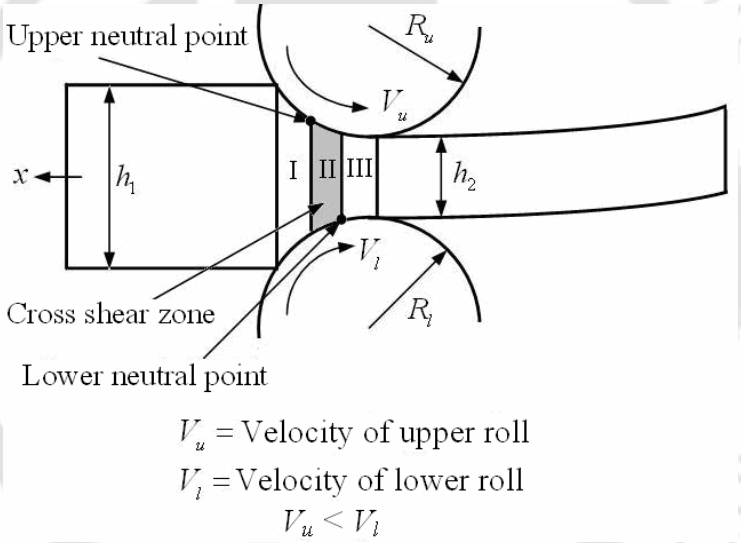

Figure 6.1. The schematic diagram of asymmetric rolling

A small slab element of length dx and the strip thickness h at a distance of x is chosen. For the equilibrium, net forces along the rolling direction, net forces along the normal direction and the net moments of the forces about any chosen point on the slab are equated to zero. This leads to the following set of equations:

$$\sum F_x = \left(\frac{p_u}{R_u} + \frac{p_l}{R_l}\right)x - \frac{x}{R_{eq}}(\sigma_u + \sigma_l) - (\tau_u + \tau_l) - \frac{h}{2}\left(\frac{\mathrm{d}\sigma_u}{\mathrm{d}x} + \frac{\mathrm{d}\sigma_l}{\mathrm{d}x}\right) = 0, \qquad (6.1)$$

$$\sum F_y = \frac{2x}{R_{eq}}\tau + (p_l - p_u) + \left(\frac{\tau_l}{R_l} - \frac{\tau_u}{R_u}\right)x + h\frac{\mathrm{d}\tau}{\mathrm{d}x} = 0\,, \tag{6.2}$$

$$\begin{aligned}\sum M_o = h\tau + \frac{xh}{2}\left(\frac{p_l}{R_l} - \frac{p_u}{R_u}\right) + \frac{xh}{2R_u}(\sigma_u + \sigma_l) + \frac{h}{2}(\tau_u - \tau_l) \\ - \frac{xh}{6R_{eq}}(\sigma_u + 5\sigma_l) + \frac{h^2}{12}\left(\frac{\mathrm{d}\sigma_u}{\mathrm{d}x} - \frac{\mathrm{d}\sigma_l}{\mathrm{d}x}\right) = 0,\end{aligned} \tag{6.3}$$

where R_u and R_l denote the radii of the upper and lower rolls and equivalent roll radius R_{eq} is given by

$$R_{eq} = \frac{2R_uR_l}{R_u + R_l}, \tag{6.4}$$

Rearranging the terms in Eqs. (6.1 and 6.3), we get

$$\left(\frac{\mathrm{d}\sigma_u}{\mathrm{d}x} + \frac{\mathrm{d}\sigma_l}{\mathrm{d}x}\right) = \frac{2x}{h}\left(\frac{p_u}{R_u} + \frac{p_l}{R_l}\right) - \frac{2x}{hR_{eq}}(\sigma_u + \sigma_l) - \frac{2}{h}(\tau_u + \tau_l) = A_1\,, \tag{6.5}$$

$$\begin{aligned}\left(\frac{\mathrm{d}\sigma_l}{\mathrm{d}x} - \frac{\mathrm{d}\sigma_u}{\mathrm{d}x}\right) = \frac{12}{h}\tau + \frac{6x}{h}\left(\frac{p_l}{R_l} - \frac{p_u}{R_u}\right) + \frac{6x}{hR_u}(\sigma_u + \sigma_l) \\ + \frac{6}{h}(\tau_u - \tau_l) - \frac{2x}{hR_{eq}}(\sigma_u + 5\sigma_l) = B_1.\end{aligned} \tag{6.6}$$

The normal pressures at the upper and lower rolls are denoted by p_u and p_l. τ_u and τ_l are the interfacial shear stresses at the upper and the lower interfaces, respectively. The average shear stress acting on the vertical surface of the material is τ. The longitudinal compressive stresses on the top and bottom rolls are denoted by σ_u and σ_l. For small bite angle, one can write [Salimi and Kadkhodaei, 2004]

$$\sigma_u = p_u - 2\sqrt{\frac{(\sigma_Y)^2}{3} - \tau_u^2}\,, \tag{6.7}$$

and

$$\sigma_l = p_l - 2\sqrt{\frac{(\sigma_Y)^2}{3} - \tau_l^2}\ . \tag{6.8}$$

For most of the strain hardening materials, the flow stress σ_Y can be given by (Eq. 3.8). Assumptions of volume constancy, plane strain and across the thickness uniform plastic strain in the thickness direction allow us to write the equivalent strain as

$$\tilde{\varepsilon} = \frac{2}{\sqrt{3}} \ln\left(\frac{h_1}{h_2}\right). \tag{6.9}$$

It is to be noted that although the present model accounts for an internal shear stress, yet in Eq. (6.9) the shear strain is neglected in the computation of overall strain. It was found that for the cases studied in this thesis, the shear strain was limited to a maximum 20% of overall equivalent strain in the most severe cases. This introduces less than 5% error in the estimation of flow stress because of the lower value of exponent *n*. Hence, for the estimation of flow stress, the approximate equivalent strain expression given by Eq. (6.9) is justified. Thus, the equation for the flow stress becomes

$$\sigma_Y = (\sigma_Y)_0 \left(1 + \frac{2}{\sqrt{3}} \frac{\ln\left(\frac{h_1}{h_2}\right)}{b}\right)^n . \tag{6.10}$$

(The above equation was used by Salunkhe [2006], but no justification for its suitability was provided.) As the strip thickness is a function of *x*, the above expression of flow stress is also a function of *x*. Differentiating Eq. (6.10) we obtain

$$\frac{\mathrm{d}\sigma_Y}{\mathrm{d}x} = C_1 \frac{\mathrm{d}h}{\mathrm{d}x}, \tag{6.11}$$

where

$$C_1 = -(\sigma_Y)_0 \frac{2/\sqrt{3}\, n}{bh}\left(1+\frac{2}{\sqrt{3}}\frac{\ln\left(\frac{h_1}{h_2}\right)}{b}\right)^{n-1}. \tag{6.12}$$

Differentiating Eq. (6.7–6.8) with respect to x, and substituting these derivatives as well as Eq. (6.11) in Eqs. (6.2, 6.5 and 6.6), the following system of equations is obtained.

$$\frac{\mathrm{d}p_u}{\mathrm{d}x} = \frac{(A_1 - B_1)}{2} - \frac{\tau_u}{R_u} - \frac{x}{R_u}\frac{\mathrm{d}\tau_u}{\mathrm{d}x} + \frac{3}{\sqrt{(\sigma_Y)^2 - 3\tau_u^{\,2}}}\left(\frac{4\sigma_Y C_1}{3R_{eq}}x - 2\tau_u\frac{\mathrm{d}\tau_u}{\mathrm{d}x}\right), \tag{6.13}$$

$$\frac{\mathrm{d}p_l}{\mathrm{d}x} = \frac{(A_1 + B_1)}{2} - \frac{\tau_l}{R_l} - \frac{x}{R_l}\frac{\mathrm{d}\tau_l}{\mathrm{d}x} + \frac{3}{\sqrt{(\sigma_Y)^2 - 3\tau_l^{\,2}}}\left(\frac{4\sigma_Y C_1}{3R_{eq}}x - 2\tau_l\frac{\mathrm{d}\tau_l}{\mathrm{d}x}\right), \tag{6.14}$$

$$\frac{\mathrm{d}\tau}{\mathrm{d}x} = \frac{x}{h}\left(\frac{\tau_u}{R_u} - \frac{\tau_l}{R_l}\right) + \left(\frac{p_u - p_l}{h}\right) - \frac{2x}{R_{eq}}\frac{\tau}{h}, \tag{6.15}$$

where A_1, B_1 and C_1 are defined as per Eqs. (6.5–6.6 and 6.12) respectively. These are system of three first order ordinary differential equations. A MATLAB function ODE45 is used to solve these differential equations. Solving these differential equations, the values of p_u, p_l and τ are obtained. The locations of two neutral points can be calculated using following relationship:

$$x_{nu} = \sqrt{V_A (x_{nl})^2 + R_{eq} h_2 (V_A - 1)}, \tag{6.16}$$

where, x_{nu}, x_{nl} are the distances of upper and lower neutral points from the centers of the roll, respectively and V_A is the speed ratio (*i.e.* the ratio of surface velocities of the lower roll to that of upper roll).

During rolling process, the rolls get elastically deformed. This roll flattening effect is taken into consideration using Hitchcock's formula [1935] that is discussed

in Eq. (3.17). It is to be mentioned that Hitchcock's formula is incapable of estimating roll deformation for rolling of thin and hard strips particularly at low reduction. However, for the cases examined in the present thesis, Hitchcock's formula is appropriate. This is supported by the work of Chandra and Dixit [2004], who have estimated the roll deformation by treating the roll as an elastic half space and using a theory of elasticity solution. The authors found that for moderate strip thickness, reduction, flow stress of the material and friction, their model provides almost same results as the model of Dixit and Dixit [1996], which uses Hitchcock's model. A more accurate roll deformation model will be needed for the studying the rolling of thin and hard strips at low reduction.

6.2.1 Roll Force, Roll Torque and Strip Curvature

The roll force per unit width can be calculated as [Salimi and Kadkhodaei, 2004]

$$F_u = \int_0^L \left(p_u + \frac{x}{R_u}\tau_u \right) \mathrm{d}x \text{ and } \quad F_l = \int_0^L \left(p_l + \frac{x}{R_l}\tau_l \right) \mathrm{d}x \,. \tag{6.17}$$

where L is the contact length. The converged solution is used for calculating the strip curvature. Taking moment about the center of roll, the rolling torque per unit width is given by

$$T_u = \int_0^L x p_u \mathrm{d}x \text{ and } T_l = \int_0^L x p_l \mathrm{d}x \,, \tag{6.18}$$

The asymmetry in the rolling process leads to produce an undesirable curvature to the rolled strip. There are two different types of effects that contribute to this curvature. The first is due to the difference in the axial strains at the upper and the lower surfaces and the second is due to the difference in the shear strains at the upper and the lower surfaces. The total curvature will be equal to the summation of the curvatures due to these two effects.

6.2.1.1 Strip Curvature Due to Difference in Axial Strains

Figure 6.2 (a) shows the rolled strip with a curvature. This type of curvature (convex upward) is considered negative in the sign convention adopted. Let l_1, l_2, and l_0 be

the lengths of the upper, lower and the neutral layer of the strip. From the geometry of the figure one can write,

$$\frac{1}{r_1} = -\frac{1}{h_2}\left(\frac{l_1 - l_2}{l_0}\right) = -\frac{1}{h_2}\left(\varepsilon_{x1} - \varepsilon_{x2}\right), \tag{6.19}$$

where r_1 is the radius of curvature due to difference in axial strains, h_2 is the outlet strip thickness and ε_{x1} and ε_{x2} are the axial strains at the upper and lower surfaces, respectively.

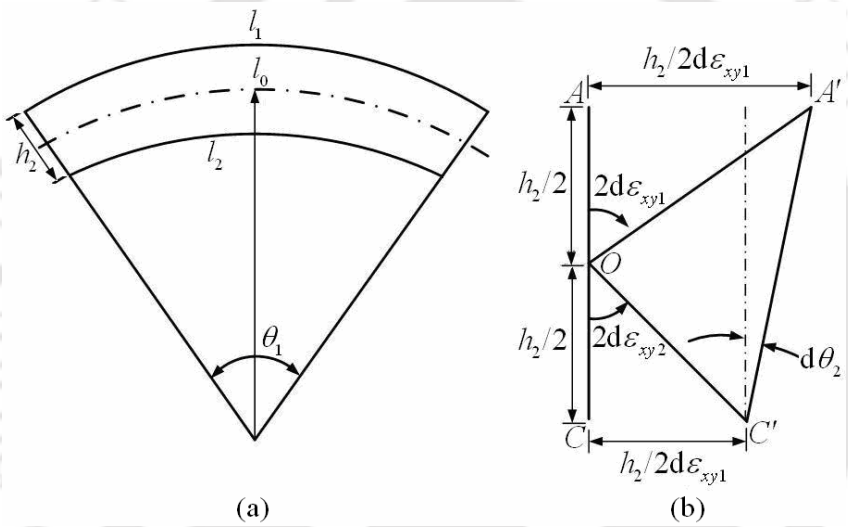

Figure 6.2. The strip curvature due to (a) difference in axial strains (b) difference in shear strains [Salunkhe, 2006]

6.2.1.2 Strip Curvature Due to Difference in Shear Strains

As the material undergoes deformation in the roll gap, the strip adopts a curvature due to the differential shear strains also. It is shown in Fig. 6.2 (b). The strip curvature due to difference in the shear strains is given by

$$\frac{1}{r_2} = -\frac{\int_0^L (\mathrm{d}\varepsilon_{xy1} - \mathrm{d}\varepsilon_{xy2})}{L}, \tag{6.20}$$

where the incremental shear strain at any point for the upper and lower surfaces is given by $\mathrm{d}\varepsilon_{xy1}$ and $\mathrm{d}\varepsilon_{xy2}$. Thus, the total curvature to the strip will be the summation

of the curvature due to the difference in the axial strains and curvature due to the difference in the shear strains. Thus, the resultant radius of curvature R_{curv} is given by

$$R_{curv} = \left(\frac{r_1 r_2}{r_1 + r_2} \right). \tag{6.21}$$

The curvature of the strip is the reciprocal of the resultant radius of curvature ($i.e. 1/R_{curv}$).

6.3 Validation and Parametric Study of the Model

Salunkhe [2006] compared the results of roll force and roll torque with the analytical model of Salimi and Kadkhodaei [2004] and reported that strain hardening and roll flattening increase the roll force and roll torque. However the author did not validate the model with that of experimental results. In the present thesis, validation with experimental results as well as detailed investigations of other parameters such as power dissipation in an asymmetric rolling, effect of friction mismatch and effect of strain hardening on the prediction of curvature *etc*. has been carried out. In the present thesis, results of the present model are compared with the experimental results of Hwang and Tzou [1997]. In the case of curvature, results are compared with the experimental results of Buxton and Browning [1972], Kennedy and Slammer [1958] as well as with finite element results of Shivpuri *et al*. [1988].

6.3.1 Roll Force and Roll Torque

Although the friction is modelled using Wanheim and Bay's friction model in the present thesis, for the sake of comparison with the available experimental and analytical results in the literature, a constant friction factor model is incorporated in the present model instead of Wanheim and Bay's model. In the constant friction factor model, the shear stresses at the roll-strip interface is given by

$$\tau = m \frac{\sigma_Y}{\sqrt{3}}, \tag{6.22}$$

where m is the friction factor.

Hwang and Tzou [1997] carried out experimental investigations considering asymmetry due to roll speed mismatch and different roll radius. The authors used alumunium as a material to be rolled. The present model is validated against the experimental results reported by Hwang and Tzou [1997]. The experimental results of roll torque have not been reported in the literature. Thus, only roll force values of the present model is compared with the experimental results. Figure 6.3 and 6.4 shows the results for different initial thickness of the strip. In Fig. 6.3 and 6.4, asymmetry is caused due to speed mismatch only whereas in Fig. 6.5, the asymmetry is caused due to speed mismatch as well as due to different roll radii. It is seen that in all cases, the predictions by the present model are in a close agreement with the experimental results. Thus, it is seen that the inclusion of strain hardening and roll flattening in the model provides closer values of roll force with the experimental values.

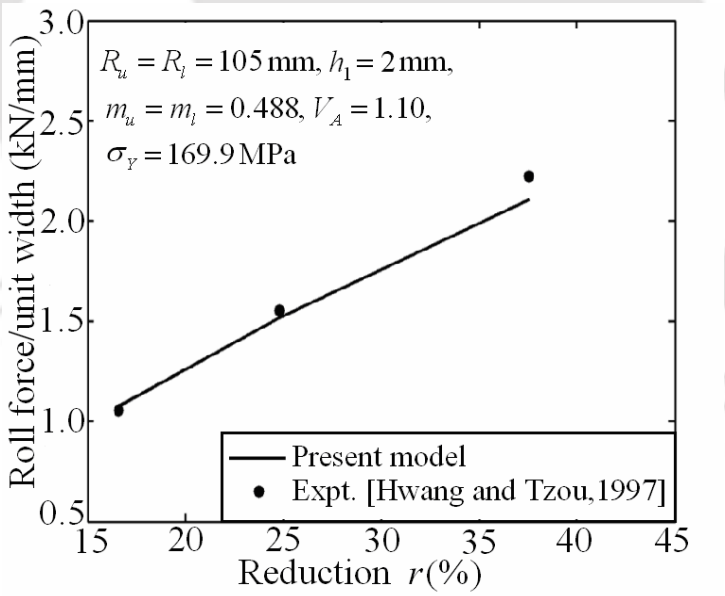

Figure 6.3. Comparison of experimental and analytical roll force for speed mismatch, (h_1 = 2 mm)

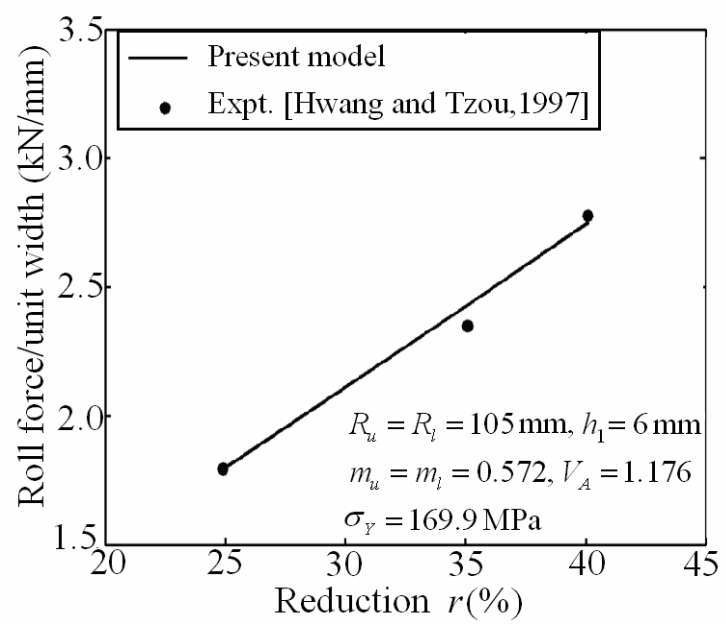

Figure 6.4. Comparison of experimental and analytical roll force for speed mismatch, ($h_1 = 6$ mm)

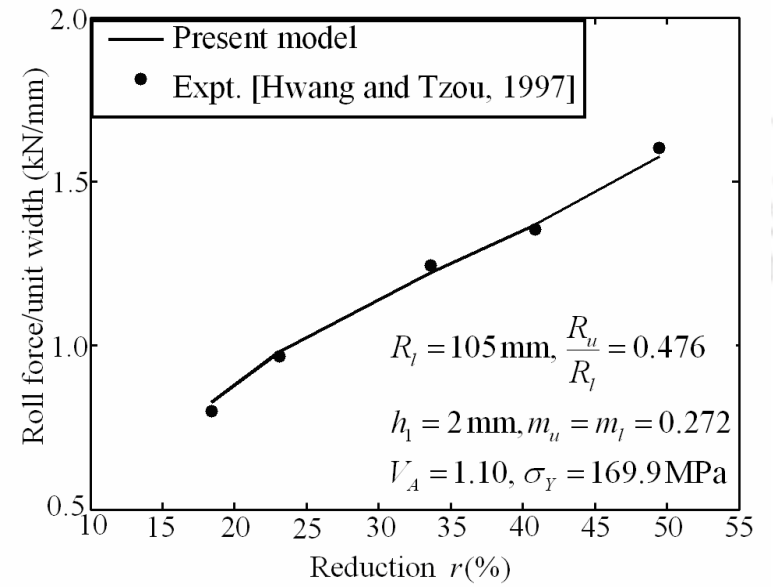

Figure 6.5. Comparison of experimental and analytical roll force for different roll radius

6.3.2 Effect of Friction Mismatch on Roll Force and Roll Torque Prediction

Effect of friction mismatch on the roll force and roll torque is also studied in the present thesis. Here, asymmetry is created due to different friction coefficients at the upper and lower rolls as well as roll speed mismatch.

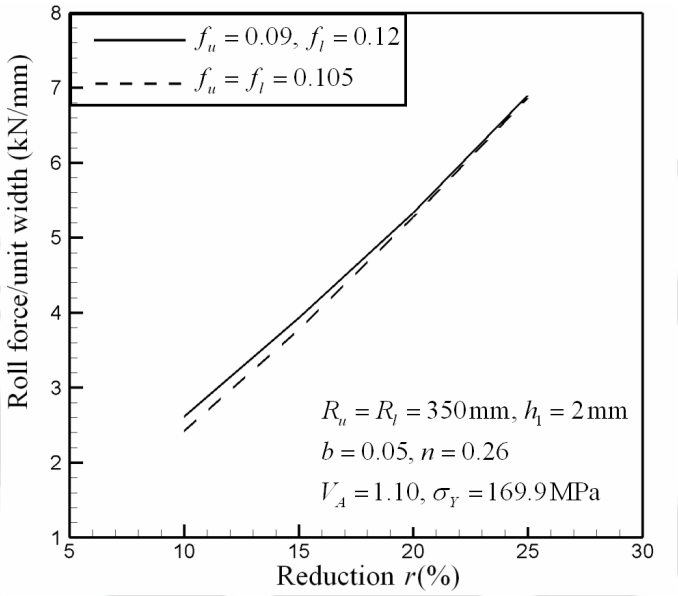

Figure 6.6. Variation of roll force with reduction for different and same frictions on upper and lower rolls

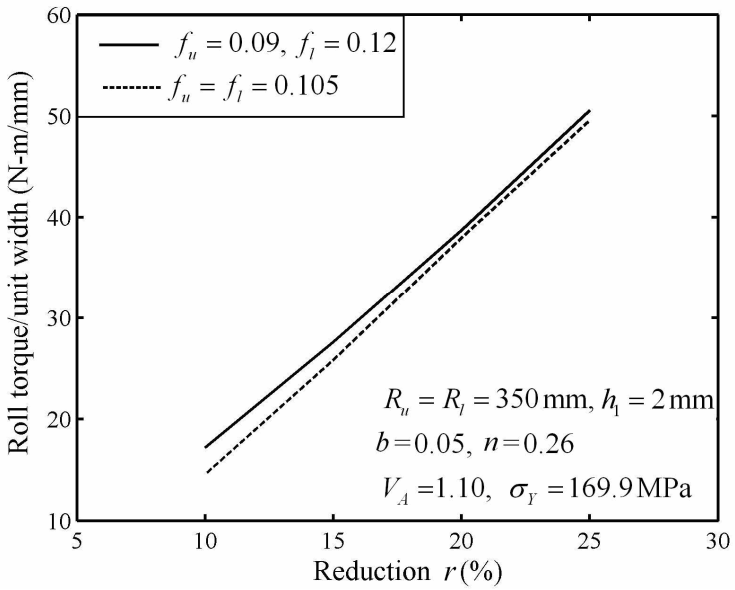

Figure 6.7. Variation of roll torque with reduction for different and same frictions on upper and lower rolls.

Figure 6.6 shows the roll force values for the case in which asymmetry is created due to different friction coefficients at the upper and lower rolls as well as roll speed mismatch. These roll forces are compared with the roll force values obtained by taking the average value of friction coefficient. It is observed that there is no significant difference in the roll force values when an average value of coefficient of friction is used. Thus, the lowering of roll force is mainly due to roll speed mismatch. Figure 6.7 shows the results for roll torque prediction. Here also, it is observed that there is no significant difference in the roll torque values when an average value of coefficient of friction is used.

6.3.3 Comparison of Roll Force and Roll Torque in Symmetric and Asymmetric Rolling

The roll force and roll torque calculated by present model for both asymmetric and symmetric cases are shown in Fig. 6.8 and 6.9. The roll force and roll torque is compared for three different speed ratios as shown in the figures. It is observed that speed mismatch causes more effect on roll force and roll torque than that of frictional asymmetry.

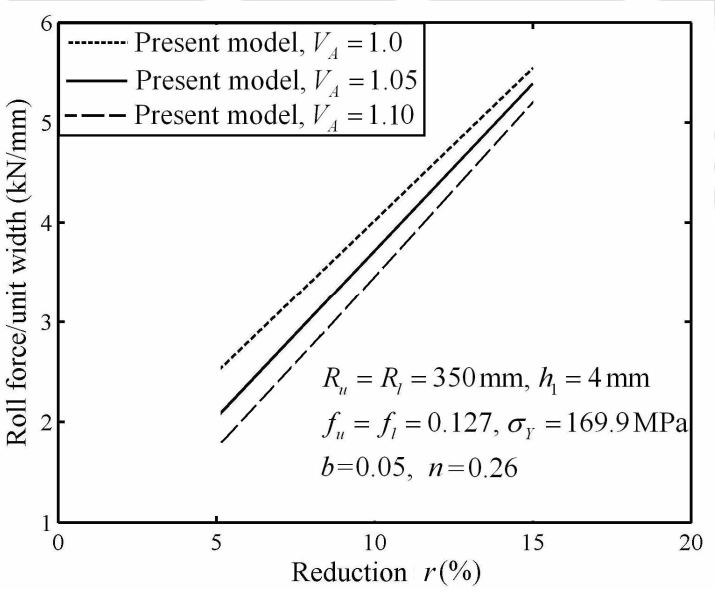

Figure 6.8. Comparison of symmetric and asymmetric roll force with different speed ratios

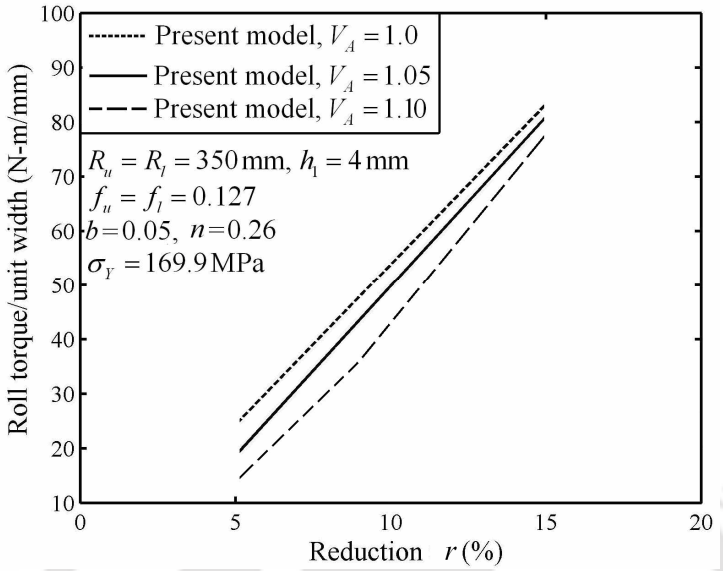

Figure 6.9. Comparison of symmetric and asymmetric roll torque with different speed ratios

It is observed that in symmetric rolling case, the roll force and roll torque values are higher than that of asymmetric rolling process. The difference in roll force and roll torque is more predominent at lower reductions. It is also observed that roll force and roll torque value decreases with increase in speed ratio V_A. The cause that reduces the roll torque during an asymmetric rolling process is further investigated by showing an illustration in Section 6.3.4.

6.3.4 Power Dissipation for Different Speed Ratios

The roll torque in an asymmetric rolling process is lesser as compared to that of symmetric rolling process. This characteristic is studied in detail by computing the power requirement in symmetric and asymmetric rolling process.

It is already explained in Section 6.2 that in an asymmetric rolling process, three zones are created. In zone II (Fig. 6.1), frictional stress points downstream on one side and upstream on the other side. Total power in the asymmetric rolling process is given by

$$P = P_p + P_f , \tag{6.23}$$

where power dissipation due to plastic deformation and frictional power dissipation are given by P_p and P_f respectively. The total power P can be calculated by multiplying the roll torque by the angular velocity of the roll (Eq. 3.21). The power dissipation due to friction P_f is computed as

$$P_f = \int_{\Gamma_u} \tau_u \left| \frac{1}{h_n} - \frac{1}{h} \right| V_2 h_2 \, d\Gamma_u + \int_{\Gamma_l} \tau_l \left| \frac{1}{h_n} - \frac{1}{h} \right| V_2 h_2 \, d\Gamma_l , \tag{6.24}$$

where h_n is the strip thickness at the neutral point and Γ_u and Γ_l are the upper and lower roll-work interface respectively. The power dissipation due to plastic deformation is then obtained by using Eq. (6.23).

The power dissipation is examined for a typical case with different speed ratios. For the case of $R_u = R_l =$ 350 mm, $f_u = f_l =$ 0.14, $b =$ 0.05, $n =$ 0.26, $\sigma_Y =$ 169.9 MPa, $h_1 =$ 4 mm and $r =$10 %. Total power dissipations with corresponding frictional power dissipation and plastic deformation power dissipation for different speed ratio are shown in Table 6.1.

Table 6.1. Comparison of plastic deformation and frictional power for symmetric and asymmetric rolling

Speed ratio V_A	Total power, P (kW)	Plastic deformation power, P_p (kW)	Frictional power, P_f (kW)
1.0	145.4206	79.0926	65.7816
1.01	131.5268	89.9389	41.5886
1.02	129.7112	96.1934	33.5953
1.05	126.0392	112.6071	13.4365

It is observed that, the internal power dissipation due to plastic deformation increases due to increased shear strains in an asymmetric rolling process. However, the friction power dissipation reduces drastically as the frictional stress points downstream on one side and upstream on the other side. As a result of this, the total power gets reduced, leading to reduced torque requirement. It is observed that as the asymmetry due to roll speed mismatch increases, the frictional power dissipation

reduces rapidly, whereas the plastic deformation power dissipation increases with slightly slower rate. The net effect is that with increasing roll speed mismatch, the total power keeps reducing. Thus, in an asymmetric rolling process roll torque reduces as compared with that of symmetric rolling process

6.3.5 Strip Curvature Analysis

In this thesis, the results of strip curvature is compared with the experimental results of Buxton and Browning [1972], Kennedy and Slammer [1958] and finite element analysis results of Shivpuri *et al*. [1988]. Figure 6.10 shows that the effect of roll speed ratio upon the strip curvature index. The strip curvature index is the ratio of length of the top surface of the sheet to the length of the bottom surface of the sheet. It is denoted as *K*.

$$K = \frac{R_{curv} - h_2/2}{R_{curv} + h_2/2}, \tag{6.25}$$

where R_{curv} is the resultant radius of curvature described in Eq. (6.21).

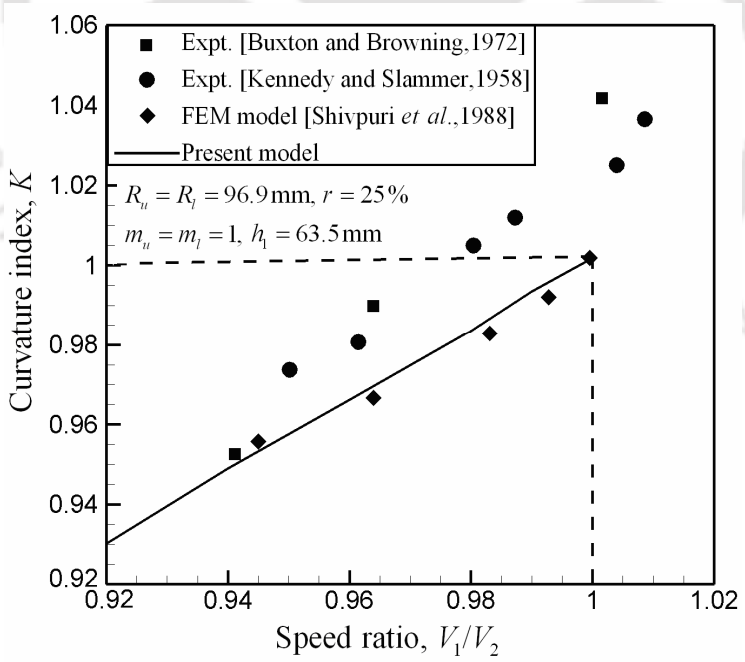

Figure 6.10. Comparison of experimental, finite element analysis and present method for strip curvature index

It is observed that results of the present model are in good agreement with the FEM results of Shivpuri *et al*. [1988]. There is a good qualitative agreement with the experimental results too. The variation with the experimental results may be due to statistical variation in material parameters, error in the measurement of speed ratio and due to the use of constant friction factor model. Moreover, the experimental results pertain to hot rolling, whereas the results of present model as well as FEM model of Shivpuri *et al*. [1988] have been obtained without considering the thermal effects.

6.3.6 Effect of Roll Flattening on the Strip Curvature

The effect of roll flattening on the curvature of the rolled product is also studied in the present thesis. As explained in Section 6.2, Hitchcock's formula is used for inclusion of roll flattening effect. Table 6.2 shows the comparison for different speed ratios. It is observed that in the absence of roll flattening, curvature is overestimated. However, at lower speed ratio, the roll flattening effect reduces the curvature of the rolled product by almost 6–7 %. Thus, it is concluded that the roll flattening effect plays a significant role on the estimation of curvature.

Table 6.2. Effect of roll flattening on the strip curvature for a case of. $R_u = R_l = 350$ mm, $f_u = f_l = 0.14$, $\sigma_Y = 169.9$ MPa, $h_1 = 4$ mm and r =20 %.

Speed ratio V_A	Radius of curvature, (m)		% deviation
	With roll flattening	Without roll flattening	
1.01	1.9807	1.8397	7.1180
1.03	0.6647	0.6176	7.0859
1.05	0.4648	0.4327	6.9061
1.07	0.3649	0.3504	3.9245
1.10	0.2672	0.2568	3.8922

6.4 Neural Network Model for the Prediction of Curvature

Salunkhe [2006] developed an inverse model for the estimation of friction based on measurement of curvature. The details are given in Appendix E. The curvature of the strip in the asymmetric rolling depends on the coefficient of friction for a given set of rolling conditions. This information is used to estimate the coefficient of

friction between the rolls and the strip in symmetric rolling situation. The method proposed by the author assumes same coefficient of friction for both the upper and lower rolls. Since there is a chance of having different friction coefficient at the upper and lower rolls for a given speed ratio, the appropriateness of the assumption needs to be checked before using the inverse modelling.

In the present thesis, neural network model is used for quicker prediction of radius of curvature. This NN model is used to ascertain the appropriateness of the methodology incorporated in the inverse model. Slab method model is used to generate the data required for NN model. For modelling of the radius of curvature as a function of seven-input parameters *i.e.* R/h_1, f_u, f_l, r, b, n and V_A, minimum 2^7=128 dataset are required in order to avoid extrapolation. These 128 datasets are obtained from the present slab method based code. The range for the selected data is as follows:

$$R/h_1: 50\text{-}100,\ f_u = f_l: 0.06\text{-}0.16,\ r: 10\text{-}20\%,\ b: 0.02\text{-}0.08,$$
$$n: 0.01\text{-}0.4,\ V_A: 1.02\text{-}1.10.$$

6.4.1 Study of Effect of Strain Hardening on the Curvature

In order to study the effect of input parameters (particularly strain hardening) on the prediction of curvature, an attempt has been made to use statistical analysis to determine the effect of input parameters on the curvature. However, due to highly non-linear relation between input-output parameters, statistical analysis using ANOVA and coefficients of correlation could not provide meaningful results. In view of this, a preliminary study was carried out to understand the effect of strain hardening on curvature at different conditions. The data are obtained for low and high cases of R/h_1 ratio, coefficient of frictions, reductions and speed ratio. The asymmetry is created by operating the upper and lower roll with different speeds ($i.e.\ V_A > 1.0$) only. Coefficient of friction at upper and lower roll is kept same. The strain hardening parameters b and n have been chosen to represent two cases– low strain hardening material (b= 0.08 and n= 0.01) and high strain hardening material (b= 0.02 and n= 0.4). Table 6.3 shows the results of radius of curvature for high and low cases discussed above. It is observed that the curvature is positive in all the cases and hence it curls towards the slower rotating upper roll. The

curvature goes on decreasing as the initial strip thickness increase. It is observed that for a smaller speed mismatch of 1.02, noticeable curvature can be seen. This trend is also observed by Shivpuri *et al.* [1988]. It is also observed that for moderate reductions and higher speed ratio V_A, curvature is insensitive to the strain hardening parameters.

Table 6.3. Effect of strain hardening on the strip curvature

R/h_1	$f_u = f_l$	r	V_A	b	n	Radius of curvature, (m)
50	0.06	10	1.02	0.08	0.01	2.8487
				0.02	0.4	1.9518
			1.1	0.08	0.01	0.6724
				0.02	0.4	0.6968
50	0.06	20	1.02	0.08	0.01	3.7459
				0.02	0.4	2.3654
			1.1	0.08	0.01	0.8883
				0.02	0.4	0.5948
50	0.16	10	1.02	0.08	0.01	0.7096
				0.02	0.4	0.5590
			1.1	0.08	0.01	0.2346
				0.02	0.4	0.2348
50	0.16	20	1.02	0.08	0.01	0.9040
				0.02	0.4	0.5905
			1.1	0.08	0.01	0.2964
				0.02	0.4	0.1667
100	0.06	10	1.02	0.08	0.01	2.1872
				0.02	0.4	1.3763
			1.1	0.08	0.01	0.4884
				0.02	0.4	0.5015
100	0.06	20	1.02	0.08	0.01	2.6385
				0.02	0.4	1.7609
			1.1	0.08	0.01	0.6790
				0.02	0.4	0.4221
100	0.16	10	1.02	0.08	0.01	0.4965
				0.02	0.4	0.4424
			1.1	0.08	0.01	0.1819
				0.02	0.4	0.1468
100	0.16	20	1.02	0.08	0.01	0.6539
				0.02	0.4	0.7069
			1.1	0.08	0.01	0.1654
				0.02	0.4	0.1238

6.4.2 Neural Network Model

Using the observations from Table 6.3, it is decided to construct the radial basis function neural network with five-input parameters only. The material to be rolled is treated as aluminium and the strain hardening parameters b and n are fixed as 0.05 and 0.26 respectively. In general, for a prediction over a wide range of materials, a network with material and hardening parameters should be used. The architecture of the RBF neural network used for the prediction of radius of curvature is shown in Fig. 6.11.

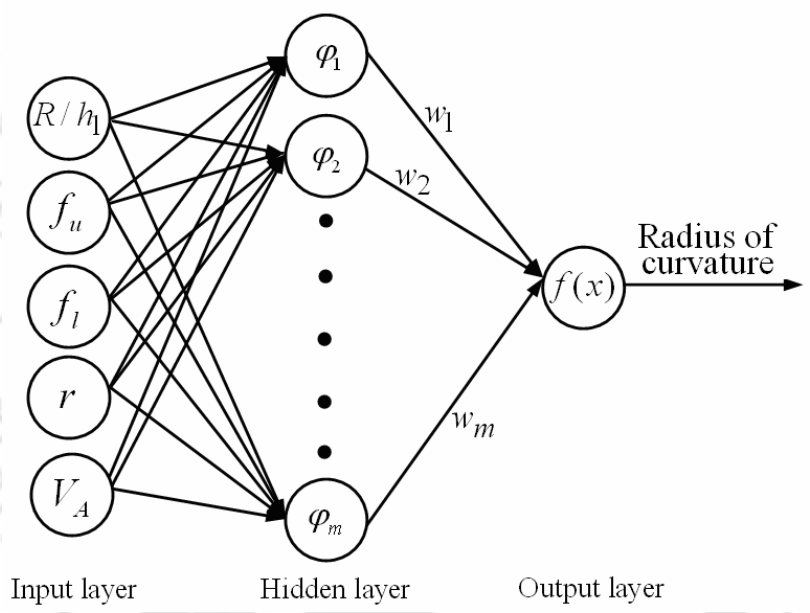

Figure 6.11. A typical RBF neural network architecture used in the present analysis

The radial basis function used in this work is a Gaussian function discussed in Subsection 3.3. The selection of training and testing data for the modelling of neural network is similar to the one explained in Chapter 4. The neural network is trained with 52 training data obtained by the slab method corresponding to the range of input parameters. The trained network is tested with 30 data points in the prescribed domain. The MATLAB function NEWRB is used for training of the network. Spread parameter is calculated using Eq. (3.28). The optimum value of constant factor that is to be multiplied with spread parameter β is obtained as 1.5. The output of the RBF neural network is approximated using Eq. (3.26). The

performance of the neural network is checked by determining the percentage root mean squared (*rms*) fractional error for training and testing datasets (Eq. 4.5).

Table 6.4. The final neural network parameters for radius of curvature prediction

Network parameters	for radius of curvature prediction
Error goal	0.0001
β	1.5
Number of centers	50
Number of training data	52
Number of testing data	30
$\%\ rms_{err}^{f}$ (training)	0.2339
$\%\ rms_{err}^{f}$ (testing)	2.5043

Table 6.4 shows the final neural network parameters for radius of curvature prediction. Once, the network is trained and tested for least error, the NN model is further used for sensitivity analysis of curvature with respect to friction.

The appropriateness of the assumption made by Salunkhe [2006] is validated using NN model as follows. Now, there may be the situation that one gets the same curvature as obtained by a particular friction coefficient in the case when the friction coefficients are different for upper and lower rolls. However, it will happen at a particular speed ratio V_A. If the speed ratio is changed, both the situations will provide different curvature. For example, Table 6.5 and 6.6 shows two typical cases of this type.

Table 6.5. Radius of curvature prediction for different friction and speed ratio ($R_u = R_l = 350\,\text{mm}$, $r = 10\,\%$, $\sigma_Y = 169.9\,\text{MPa}$, $h_1 = 7\,\text{mm}$)

f_u	f_l	Radius of curvature, (m)	
		$V_A = 1.04$	$V_A = 1.02$
0.10	0.10	0.9165	1.1996
0.06	0.143	0.9162	0.9239

Table 6.6. Radius of curvature prediction for different friction and speed ratio ($R_u = R_l = 350\,\text{mm}$, $r = 15\,\%$, $\sigma_Y = 169.9\,\text{MPa}$, $h_1 = 3.5\,\text{mm}$)

f_u	f_l	Radius of curvature, (m)	
		$V_A = 1.04$	$V_A = 1.02$
0.11	0.11	0.3306	0.1874
0.0925	0.14	0.3301	0.2583

Table 6.5 shows that at $V_A = 1.04$, the two different friction situations are providing same curvature, however, they provide different curvatures at $V_A = 1.02$. Similarly, Table 6.6 shows the results for a different case. Here also, at $V_A = 1.06$, two different friction situations are providing same curvature. At a different speed ratio *i.e.* $V_A = 1.10$, these two friction situations provide different curvature. Thus, it becomes easier to check the friction coefficient at the upper and lower rolls by carrying out the neural network based predictions at two or more speed ratios. Thus, the methodology proposed by Salunkhe [2006] for the estimation of coefficient(s) of friction in rolling can be effectively used with the assistance of a well-trained neural network. The neural network model can also be used for the estimation of curvature for controlling the curvature or imparting the desired curvature.

6.5 Effect of Frictional Asymmetry on the Curvature

In an actual rolling mill, maintaining the geometric and parametric symmetry at the mid-thickness of the sheet becomes difficult due to uncertain frictional condition at the upper and lower roll and lubrication mismatch. These differences lead to produce undesirable curvature in the rolled product. The minimization of the curvature in the rolled product is important from the point of view of quality. Considering the uncertainties and scatter in the experimental results available in the literature, Dixit and Dixit [1996] treated material and process parameters as fuzzy parameters for the validation of their FEM model. However, their study was focused on mainly estimation of roll force and roll torque. The authors did not include the estimation of the curvature of the rolled product that generates due to uncertain rolling conditions.

This section deals with the estimation of undesirable curvature due to uncertain frictional conditions at upper and lower rolls. A slab method is used for the estimation of the curvature. The material and process parameters are treated as fuzzy parameters for realistic rolling conditions. In the end, a methodology is proposed for the control of the undesired curvature based on the adjustment of roll velocities.

6.5.1 Fuzzy Modelling of Parameters

The inherent variation in the experimental investigation causes scatter in the experimental data. It causes large deviation with the analytical results also. Due to this, Dixit and Dixit [1996] considered the material and the process parameters as fuzzy parameters. Material and process parameters *i.e.* flow stress of the material σ_Y, strain hardening coefficients b and n, and coefficient of friction f are treated as fuzzy parameters which are characterized by their membership functions. The details of this fuzzy modelling of parameters are explained in Subsection 5.4.1. In this process of determining the fuzzy parameters, parameters are divided into three subsets such as low (optimistic estimate), most likely estimate and high (pessimistic estimate). It is shown in Fig. 6.12 that at α-cut of 0.5, we obtain two values of the corresponding parameters *i.e.*, low and high. Thus, instead of a single curve, band bounded by upper and lower estimation of curvature is generated.

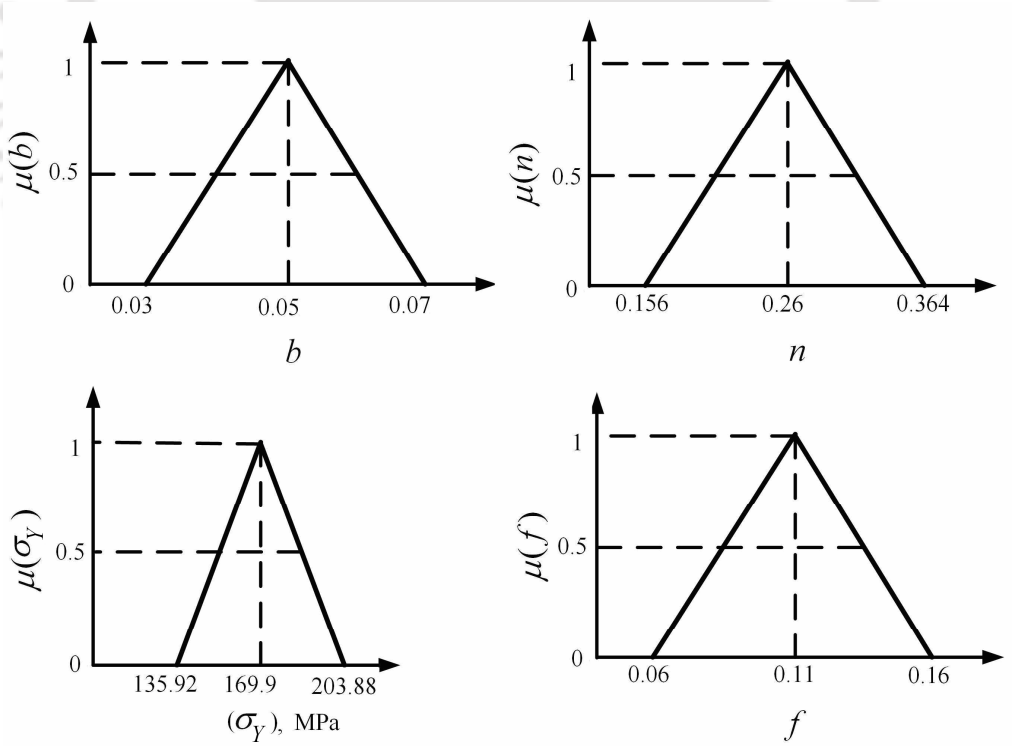

Figure 6.12. Membership functions of b, n, σ_Y and f

6.5.2 Simulations with Fuzzy Material and Process Parameters

In the process of predicting the curvature by considering fuzzy material and process parameters, three estimates of curvature are obtained as described in Subsection 6.5.1. In order to model the varying frictional conditions, different frictional conditions at upper and lower roll-work interfaces are considered. At α-cut of 0.5, friction at upper roll-work interface is considered as 0.085 where a friction at lower roll-work interface is assumed as 0.135. According to adopted sign convention, a positive radius of curvature indicates that the strip curls towards the upper roll whereas a radius of curvature with negative sign indicated that strip curls towards lower roll. It is observed that in the case of asymmetry due to friction, strip curls towards the roll having higher coefficient of friction at roll-work interface. In the past, Richelsen [1997] also observed this trend. Table 6.7 shows the results for optimistic, most likely and pessimistic estimates of radius of curvature. Similar trend was observed for all three set of estimates.

Table 6.7. Radius of curvature obtained due to friction mismatch at α-cut of 0.5 ($f_u = 0.085,\ f_l = 0.135,\ V_A = 1.0$)

R/h_1	r	Radius of curvature, (m)		
		Optimistic estimate σ_Y =152.91 MPa, b =0.06, n =0.208	Most likely estimate σ_Y =169.9 MPa, b =0.05, n =0.26	Pessimistic estimate σ_Y =186.89 MPa, b =0.04, n =0.286
50	10	-17.275	-8.6184	-5.5282
65	10	-5.2957	-3.5924	-2.6855
80	10	-2.8012	-2.0805	-1.6470
100	10	-1.6446	-1.2828	-1.0487
50	20	-1.3060	-0.9680	-0.7806
65	20	-0.7655	-0.5873	-0.4815
80	20	-0.5114	-0.4045	-0.3408
100	20	-0.3453	-0.2827	-0.2442

Simulations are also carried out for curvature prediction by considering variation in flow stress only. In this result, material hardening parameters b and n are kept fixed as 0.05 and 0.26 respectively. It is observed from Table 6.8 that variation of $\pm 10\%$ in the flow stress does not change the curvature drastically. Thus, it is observed that the curvature mainly depends on the plastic strains only. However,

type of material does play its role, because roll deformation is affected by the material. Change in roll deformation pattern influences the roll of friction and redundant deformation.

Table 6.8. Comparison of radius of curvature due to variation in flow stress at α-cut of 0.5 ($f_u = 0.085,\ f_l = 0.135,\ b$=0.05, n=0.26, $V_A = 1.0$)

R/h_1	r	Radius of curvature, (m)	
		for σ_Y =152.91 MPa	for σ_Y =186.89 MPa
50	10	-10.106	-8.1023
65	10	-3.9534	-3.4810
80	10	-2.2344	-2.0314
100	10	-1.3621	-1.2564
50	20	-1.0194	-0.9597
65	20	-0.6175	-0.5805
80	20	-0.4234	-0.4006
100	20	-0.2941	-0.2798

Results are generated for another set of uncertain frictional conditions. In this case, α-cut of 0.75 is created. At upper roll-work interface, coefficient of friction is considered as 0.0975 where coefficient of friction at lower roll-work interface is assumed as 0.1225. At the reduced frictional asymmetry, reduction in the curvature is observed for the same sets of flow stress, material parameters. Table 6.9 shows the results for optimistic, most likely and pessimistic estimates of radius of curvature at higher α-cut of 0.75.

Table 6.9. Radius of curvature obtained due to friction mismatch at α-cut of 0.75 ($f_u = 0.0975,\ f_l = 0.1225,\ V_A = 1.0$)

R/h_1	r	Radius of curvature, (m)		
		Optimistic estimate σ_Y =152.91 MPa, b =0.06, n =0.208	Most likely estimate σ_Y =169.9 MPa, b =0.05, n =0.26	Pessimistic estimate σ_Y =186.89 MPa, b =0.04, n =0.286
50	10	-32.762	-16.645	-10.875
65	10	-10.7550	-7.2410	-5.4235
80	10	-5.6767	-4.1882	-3.3210
100	10	-3.3084	-2.5703	-2.1077
50	20	-2.6168	-1.9361	-1.5685
65	20	-1.5316	-1.1750	-0.9672
80	20	-1.0238	-0.8080	-0.6809
100	20	-0.6882	-0.5608	-0.4846

6.5.3 Control of Undesired Curvature

In order to minimize the undesired curvature, the strategy proposed in the present work may be adopted. In this approach, the friction at upper roll-work interface is treated as lesser than the friction at lower roll-work interface. This asymmetry causes the different locations of neutral points as shown in Fig. 6.1. Now, along with this frictional asymmetry, if we operate the lower roll with the speed higher that that of the upper roll, the width of the shear zone (Zone II) decreases. This leads to reduce the effect of frictional asymmetry and results in the minimization of curvature of the rolled strip. In the present work, optimum speed ratio V_A is found out by using exhaustive search method. However, other search methods like golden section search method can also be implemented. Table 6.10 shows the results for the control of curvature with optimum speed mismatch. Column 4 and 5 represents the radius of curvature at optimum speed ratio V_A and at $V_A = 1.0$. It is observed that with optimum speed ratio, curvature can be minimized up to 90%. Thus, operating the rolls at different speeds helps to minimize the curvature that causes due to uncertain frictional conditions.

Table 6.10. Roll speed adjustment to minimize the curvature that causes due to friction mismatch ($f_u = 0.085$, $f_l = 0.135$, σ_Y =169.9 MPa, $b = 0.05$, $n = 0.26$)

R/h_1	r	Optimum V_A	Radius of curvature (m) at V_A =1.0	Radius of curvature (m) at optimum V_A	% deviation
50	10	1.006	-8.6184	-54.548	84.20
65	10	1.007	-3.5924	-38.125	90.57
80	10	1.009	-2.0805	-20.436	88.87
100	10	1.01	-1.2828	-5.6515	77.30
50	20	1.02	-0.9680	-3.2912	70.58
65	20	1.03	-0.5873	-2.9435	80.04
80	20	1.04	-0.4045	-1.8899	78.59
100	20	1.04	-0.2827	-0.6804	58.45

6.6 Summary

This chapter discusses various aspects of asymmetric rolling process. In this work, a slab method based model of [Salimi and Kadkhodaei [2004] modified by Salunkhe

[2006] to incorporate strain hardening behavior of the material and the roll flattening effect is used. Before using this model, the model is thoroughly studied. The validation of the model has been carried out by comparing the results of roll force, torque and curvature with the experimental and finite element based results available in the literature. (The comparison of present model with the FEM model of Salunkhe showing a close agreement between the two can be found in Salunkhe [2006] and is not included in this chapter). It is observed that the model is in good agreement with the experimental and analytical results available in the literature. It is also observed that roll force and roll torque in asymmetric rolling process will be lesser than symmetric rolling process. It is demonstrated that although the power dissipation due to plastic deformation increases due to increased shear strains in an asymmetric rolling, the friction power dissipation reduces drastically. As a result, total power gets reduced, leading to reduced torque requirement.

In the analysis of curvature, it is observed that roll flattening effect has influence on the prediction of curvature. It is also found that at moderate reductions and higher speed mismatch ratio, curvature is insensitive to the strain hardening parameters. It is demonstrated that NN model can be effectively used for assessing the sensitivity of the curvature towards the frictional conditions. The results obtained by neural network modelling are used to ascertain the appropriateness of the inverse model of friction identification proposed by Salunkhe [2006].

In the present work, a realistic situation of a rolling process is considered where geometric and parametric symmetry at the central mid-plane thickness of the sheet can not be ensured. The uncertain material and process parameters are treated as fuzzy. The estimation of curvature for uncertain material and process parameters are studied. A methodology based on speed control of upper and lower rolls is proposed for minimization of the curvature. It is shown by an illustration that proposed method of speed control can be effectively used for minimizing the undesired curvature. The method can enhance the quality of the rolled product to a greater extent and is suitable for flatness control of the rolled product.

7

Conclusions and Scope for Future Work

7.1 Conclusions

In this thesis, soft computing assisted modelling of symmetric and asymmetric rolling process has been carried out. Soft computing techniques (neural networks and fuzzy set theory) have been incorporated along with the previous established physics based techniques, *viz.* FEM, FDM and slab method, to alleviate the complexity of the process and for faster prediction of the parameters. This thesis is an attempt to demonstrate that the soft computing techniques and the physics based techniques can be complementary to each other and at the same time soft computing techniques can be implemented independently depending on the nature of the problem.

The important contributions of this thesis can be summarized as

- In the modelling of cold flat rolling process using radial basis function neural network (NN) assisted finite element method, it is observed that the neural network models can be used to reduce computational time significantly. Using traditional statistical analyses (coefficient of correlation and ANOVA), it is found that the velocity field is insensitive to the strain hardening parameters. Thus, strain hardening parameters can be ignored in the NN modelling of the velocity field which leads to reduce the total number of input parameters required to model neural networks. It is also observed that NN predicted velocity field is accurate enough to provide it as a guess to the finite element code. The neural network assisted finite element code requires 2-3 iterations only to provide the final velocity field. This is further used for post processing of other required parameters for detailed analysis of rolling

process. Thus, neural network assisted FEM provides accurate and faster analysis of the rolling process.

- In the TS fuzzy modelling of roll force and roll torque, it is observed that the coefficients of the crisp functions of the TS fuzzy inference can be used for sensitivity analysis of the roll force and roll torque with respect to the process variables. Radial basis function neural network can be used effectively for generating huge dataset required for constructing TS fuzzy model. The approximate method proposed in the present work can be utilized for finding out the roll force and roll torque of any material based on the values of roll force and roll torque for a given reference material. This method is suitable in actual rolling mills where a wide variety of rolled sheets made of different materials are produced by the same organization. The proposed method is an economical way to find out roll force and roll torque. Models based on soft computing techniques highly depend upon the accuracy of modelling data. In the present thesis, a methodology is proposed that identifies the outliers (faulty data) present in the modelling data and suppresses the effect of outliers on the model. Thus, prediction capability of the model can be enhanced. It is observed that the proposed methodology has good potential.
- In this thesis, a method of pressure field correction in the mixed pressure-velocity flow formulation of symmetric cold flat rolling process is proposed. Finite difference method and neural network models are used along with flow formulation in this approach. It is observed that for a high roll radius to thickness ratio, the results obtained from the present model differ with the finite element results available in the literature [Dixit and Dixit, 1996] and are closer to the experimental results of Shida and Awazuhara [1973]. At a low roll radius to thickness ratio, the hydrostatic stress plays less significant role in the computation of pressure and the proposed model is closer to finite element model of Dixit [1997] than experimental results of Al-Salehi *et al*. [1973]. The roll pressure distribution obtained by the proposed method is compared with that of finite element model as well as slab model. In the comparison, the set of process parameters for which the slab method is

justified, the present model found closer to the slab method than the result available in the literature [Dixit, 1997]. Thus, the proposed model developed in this thesis makes an improvement over the existing FEM flow formulations available in the literature. However, this strategy was not implemented in Chapter 3 and Chapter 4, because there the aim is to highlight the roll of neural network and fuzzy sets in the modelling of the process. Therefore, the existing FEM formulations have been taken as the basis for comparison. Moreover, the pressure correction methodology requires a significant computational time at this stage.

- In the analysis of asymmetric cold rolling process, it is observed that roll force and roll torque gets reduced as compared to that of symmetric rolling process. It is observed that lowering of roll force in an asymmetric rolling process is mainly due to speed mismatch. In the parametric study of the model, it is demonstrated that although the power dissipation due to plastic deformation increases due to increased shear strains in an asymmetric rolling, the friction power dissipation reduces drastically. As a result, total power gets reduced, leading to reduced torque requirement. It is observed that at moderate reduction and higher speed ratio, strain hardening does not make significant contribution towards curvature prediction. It is also observed that with the absence of roll flattening effect, curvature is over estimated. It is observed that neural network model can be effectively employed for quicker prediction of curvature. The neural network model can also be used for quicker analysis of the sensitivity of curvature towards the friction coefficients at upper and lower roll.
- In actual practice, friction varies in the roll gap. In the present thesis, the uncertain friction condition at upper and lower roll is modelled using fuzzy set theory. It is observed that uncertain frictional conditions lead to generate curvature to the rolled sheets. This undesired curvature hampers the quality of the product. Effect of flow stress and strain hardening parameters on the curvature prediction in a frictional asymmetry condition is also discussed. In the present thesis, a methodology is proposed to control this undesirable

curvature. The effectiveness of the proposed method is shown by an illustration. The results indicate better prospects of flatness control in actual rolling mills with the help of proposed strategy.

7.2 Scope for Future Work

- Till now, experimental investigations carried out by Shida and Awazuhara [1973] and Al-Salehi *et al*. [1973] are used as benchmark for validation of the models in the symmetric rolling process. Further experiments for symmetric cold rolling process may be carried out using different process conditions. It has been demonstrated by various researchers that in a rolling mill, friction varies at the roll-work interface. Experimental investigations may be carried out to study the effect of uncertain frictional conditions on the flatness of the rolled strips.
- Applications of pressure field correction model may be extended to other metal forming problems such as wire drawing. Experimental determination of pressure inside the material during its processing is a challenging task. Some thought may be given in that direction. Attempt should also be made to enhance the computational speed of the pressure correction algorithm.
- In the experimental investigations of asymmetric cold rolling process, estimation of curvature has been carried out using speed mismatch only. Further experiments may be carried out for the estimation of curvature by creating asymmetry due to different roll radii and different frictional condition at the upper and lower roll-work interface as well.
- Application of Takagi-Sugeno fuzzy model can be extended to analyze the roll force, roll torque and curvature in an asymmetric rolling process. The coefficients of crisp function in the TS model can be utilized for studying the sensitivity of these parameters with respect to input parameters. The information can be used to control the curvature/ reduce the roll force and roll torque.

- The inverse model for friction identification that is reported in the literature holds well with its assumptions in asymmetric rolling process. Still, a more robust inverse modelling of friction identification in an asymmetric rolling process is needed. For that purpose, a robust FEM model needs to be developed.
- The assistance of soft computing can be extended to the optimization of rolling processes. The soft computing can also be used for the updating of the material and process parameters. These techniques can also be used for controlling the process. For that purpose, robust algorithms need to be developed that utilize the sensory feedback in an optimum manner for process control.

References

- Abburi, N.R. and Dixit, U.S., (2006), A knowledge-based system for the prediction of surface roughness in turning process, Robotics and Computer-Integrated Manufacturing, **22**, pp. 363–372.

- Abo-Elkhier, M., (1997), Elasto-plastic finite element modelling of strip cold rolling using Eulerian fixed mesh technique, Finite Elements in Analysis and Design, **27**, pp. 323–334.

- Alexander, J.M., (1955), A slip line field for the hot rolling process, Proceedings of Institution of Mechanical Engineers, **169**, pp. 1021–1030.

- Alexander, J.M., (1972), On the theory of rolling, Proceedings of the Royal Society (London), A, **326**, pp. 535–563.

- Al-Salehi, F.A.R., Firbank, T.C. and Lancaster, P.R., (1973), An experimental determination for the roll pressure distributions in cold rolling, International Journal of Mechanical Sciences, **15**, pp. 693–710.

- Atreya, A. and Lenard, J.G., (1979), A study of cold strip rolling, Transactions of the American Society of Mechanical Engineers: Journal of Engineering Materials and Technology, **101**, pp. 129–134.

- Avitzur, B., (1964), An upper-bound approach to cold-strip rolling, Transactions of the American Society of Mechanical Engineers: Journal of Engineering for Industry, Series B., **86**, pp. 31–48.

- Avitzur, B., Gordon, B. and Talbert, W.S., (1987), Analysis of strip rolling by the upper bound approach, Transactions of the American Society of Mechanical Engineers: Journal of Engineering for Industry, **109**, pp. 338–346.

- Balagurusamy, E. (2004), Numerical methods, 13th edition, Tata Mcgraw-Hill, New Delhi.

- Basak, S., Dixit, U.S. and Davim, J.P., (2007), Application of radial basis function neural networks in optimization of hard turning of AISI D2 cold-worked tool steel with a ceramic tool, Proceedings of the Institution of Mechanical Engineers, Part B: Journal of Engineering Manufacture, **221**, pp. 987–998.

- Behzadipour, S., Khajepour, A., Lenard, J.G. and Biglou, J., (2004), A new shape change quantification method for estimation of power in shape rolling, Journal of Material Processing Technology, **148**, pp. 353–361.

- Bland, D.R. and Ford, H., (1948), The calculation of roll force and torque in cold strip rolling with tensions, Proceedings of Institution of Mechanical Engineers, **159**, pp. 144–163.

- Bland, D.R. and Ford, H., (1952), Cold rolling with strip tension, Part III: An approximate treatment of the elastic compression of the strip in cold rolling, Journal of the Iron and Steel Institute, **171**, pp. 245–249.

- Bland, D.R. and Sims, R.B., (1953), A note on the theory of rolling with tensions, Proceedings of Institution of Mechanical Engineers, **167**, pp. 371–372.

- Buxton, S.A. and Browning, S.C., (1972), Turn-up and turn-down in hot rolling: a study on a model mill using plasticine, Proceedings of the Institution of Mechanical Engineers, Part C: Journal of Mechanical Engineering Science, **14**, pp. 245–254.

- Cao, G.R., Hall, F.R., Hartley, P., Pillinger, I., Sturgess, E.N., Thompson, W. and Freshwater, I., (1993), Elastic plastic finite element analysis of asymmetric hot rolling, in: Proceedings of the 1st International Conference on Modelling of Metal Rolling Processes, London, pp. 542–552.

- Chandra, S. and Dixit, U.S., (2004), A rigid-plastic finite element analysis of temper rolling process, Journal of Material Processing Technology, **152**, pp. 9–16.

- Chakraborti, N. and Kumar, A., (2003), The optimal scheduling of a reversing strip mill: Studies using multipopulation genetic algorithms and differential evolution, 18/3, pp. 433–445.

- Chekmarev, A.P. and Nefedov, A.A., (1956), Obrabotka Metallov Davleniem, **4**, (British Library Translation R.T.S. 8939).

- Chen, J.C. and Black, J.T. (1997), A fuzzy-nets in-process (FNIP) system for tool-breakage monitoring in end-milling operations, International Journal of Machine Tools and Manufacture, **37**, pp. 783–800.

- Cho, S., Cho, Y. and Yoon, S., (1997), Reliable roll force prediction in cold mill using multiple neural networks, IEEE Transactions: Neural Networks, **8**, pp. 874–882.

- Cho, S., Jang, M., Yoon, S., Cho, Y. and Cho, H., (1997), A hybrid neural network/mathematical prediction model for tandem cold mill, Computers and Industrial Engineering, **33**, pp. 453–456.

- Christensen, P., Everfelt, K. and Bay, N., (1986), Pressure distributions in plate rolling, Annals of CIRP, **35**, pp. 141–146.

- Chun, M., Biglou, J., Lenard, J. and Kim, J., (1999), Using neural networks to predict parameters in the hot working of aluminum alloys, Journal of Material Processing Technology, **86**, pp. 245–251.

- Collins, I.F., (1968), The algebraic-geometry of slip line fields with applications to boundary value problems, Proceedings of the Royal Society (London), A, **303**, pp. 317–338.

- Collins, I.F., (1969), The upper bound theorem for rigid-plastic solids generalized to include Coulomb friction, Journal of the Mechanics and Physics of Solids, **17**, pp. 323–338.

- Collins, I.F., (1969), Slip-line field solution for compression and rolling with slipping friction, International Journal of Mechanical Sciences, **11**, pp. 971–978.

- Collins, I.F. and Dewhurst, P., (1975), A slipline field analysis of asymmetrical hot rolling, International Journal of Mechanical Sciences, **17**, pp. 643–651.

- Crane, F.A.A. and Alexander, J.M., (1968), Slip-line fields and deformation in hot rolling strip, Journal of the Institute of Metals, **96**, pp. 289–300.

- Dawson, P.R. and Thompson, E.G., (1978), Finite element analysis of steady-state elasto-plastic flow by the initial stress-rate method, International Journal for Numerical Methods in Engineering, **12**, pp. 47–57.

- Dewhurst, P, Collins, I.F. and Johnson, W., (1973), A class of slip-line field solutions for the hot rolling of strip, Proceedings of the Institution of Mechanical Engineers, Part: C, Journal of Mechanical Engineering Science, **15**, pp. 439–447.

- Dewhurst, P., Collins, I.F. and Johnson, W., (1974), A theoretical and experimental investigation into asymmetrical hot rolling, International Journal of Mechanical Sciences, **16**, pp. 389–397.

- Dieter, G.E., (1991), Engineering Design: A Materialistic and processing approach, 2nd edition, McGraw-Hill, New York.

- Dixit, P.M. and Dixit, U.S., (2008), Modeling of metal forming and machining processes: By finite element and soft computing methods, Springer-Verlag, London.

- Dixit, U.S. and Chandra, S., (2003), A neural network based methodology for the prediction of roll force and roll torque in fuzzy form for cold flat rolling process, International Journal of Advanced Manufacturing and Technology, **22**, pp. 883–889.

- Dixit, U.S., and Dixit, P.M., (1995), An analysis of the steady-state wire drawing of the strain hardening materials, Journal of Material Processing Technology, **47**, pp. 201–229.

- Dixit, U.S. and Dixit, P.M., (1996), A finite element analysis of flat rolling and applications of fuzzy set theory, International Journal of Machine Tools and Manufacture, **36**, pp. 947–969.

- Dixit, U.S. and Dixit, P.M., (1997), A study on residual stresses in rolling, International Journal of Machine Tools and Manufacture, **37**, pp. 837–853.

- Dixit, U.S. and Dixit, P.M., (2000), Application of fuzzy set theory in the scheduling of a tandem cold-rolling mill, Transactions of the American Society of Mechanical Engineers: Journal of Manufacturing Science and Engineering, **122**, pp. 494–500.

- Dixit, U.S., Robi, P.S. and Sarma, D.K., (2002), A systematic procedure for the design of a cold rolling mill, Journal of Material Processing Technology, **121**, pp. 69–76.

- Doğruoğlu, A.N., (2001), On constructing kinematically admissible velocity fields in cold sheet rolling, Journal of Material Processing Technology, **110**, pp. 287–299.

- Domanti, S.A. and McElwain, D.L.S., (1998), Cold rolling of flat metal products: Contribution of mathematical modelling, Proceedings of the Institution of Mechanical Engineers, Part B: Journal of Engineering Manufacture, **212**, pp. 73–86.

- Drucker, D.C., (1954), Coulomb friction, plasticity and limit loads, Transactions of the American Society of Mechanical Engineers: Journal of Applied Mechanics, **21**, pp. 71–74.

- Dyja, H. and Pietrzyk, M., (1983), On the theory of the process of hot rolling of bimetal plate and sheet, Journal of Mechanical Working Technology, **8**, pp. 309–325.

- Ekelund, E., (1933), The analysis of factors influencing rolling pressure and power consumption in the hot rolling of steel, Steel, pp. 8–14, (Translated from Jerkontorets Ann. Feb. 1927, by B. Blomquist).

- Firbank, T.C. and Lancaster, P.R., (1965), A suggested slip-line field for cold rolling with slipping friction, International Journal of Mechanical Sciences, **7**, pp. 847–852.

- Firbank, T.C. and Lancaster, P.R., (1966), Note: On some aspects of the cold rolling problem, International Journal of Mechanical Sciences, **8**, pp. 653–656.

- Firbank, T.C. and Lancaster, P.R., (1967), A proposed slip-line field for lubricated cold rolling, International Journal of Mechanical Sciences, **9**, pp. 65–67.

- Ford, H., Ellis, F. and Bland, D.R., (1951), Cold rolling with strip tension, Part I: A new approximate method of calculation and a comparison with other methods, Journal of the Iron and Steel Institute, **168**, pp. 57–72.

- Gao, H., Ramalingam, S.C., Barber, G.C. and Chen, G., (2002), Analysis of asymmetrical cold rolling with varying coefficient of friction, Journal of Material Processing Technology, **124**, pp. 178–182.

- Garg, S., Pal, S.K. and Chakraborty, D., (2007), Evaluation of the performance of back-propagation and radial basis function neural networks in predicting the drill flank wear, Neural Computing & Applications, **16**, pp. 407–417.

- Gelton, C.J.M., Koter, A.W.A., (1982), Application of mesh rezoning in the updated Lagrangian method to metal forming analysis, In: J.F.T. Pittman (Eds.), Numerical Methods in Industrial Forming Processes, pp. 511–521.

- Geerdes, W.M., Alvarado, M.Á.T., Cabrera-Ríos, M. and Cavazos, A. (2008), An application of physics-based and artificial neural networks-based hybrid temperature prediction schemes in a hot strip mill, Transactions of the American Society of Mechanical Engineers: Journal of Manufacturing Science and Engineering, **130**, 014501, pp. 1–5

- Ghobrial, M.I., (1989), A photoelastic investigation on the contact stresses developed in rolls during asymmetrical fiat rolling, International Journal of Mechanical Sciences, **31**, pp. 751–764.

- Goldberg, D.E., (1989), Genetic algorithms in search, optimization and machine learning, Addison-Wesley, Reading, Massachusetts.

- Gorni, A.A., (1997), The application of neural networks in the modelling of plate rolling processes, Journal of Metals, **49/4**, pp. 1–9.

- Gratacos, P., Montmitonnet, P., Fromholz, C. and Chenot, J.L., (1992), A plane-strain elastoplastic finite-element model for cold rolling of thin strip, International Journal of Mechanical Sciences, **34**, pp. 195–210.

- Green, J.W. and Wallace, J.F., (1962), Estimation of load and torque in the hot rolling process, Journal of Mechanical Engineering Science, **4**, pp. 136–142.

- Green, J.W., Sparling, L.G.M. and Wallace, J.F., (1964), Shear plane theories of hot and cold rolling, Journal of Mechanical Engineering Science, **6**, pp. 219–235.

- Gunasekera, J.S. and Alexander, J.M., (1987), Analysis of Rolling, Annals of CIRP, **36**, pp. 203–206.

- Gunasekera, J.S., Jia, Z., Malas, J.C. and Rabelo, L., (1998), Development of a neural network model for a cold rolling process, Engineering Applications of Artificial Intelligence, **11**, pp. 597–603.

- Ham, F. and Kostanic, I., (2001), Principles of neurocomputing for science and engineering, Mcgraw-Hill, New York.

- Hartley, P., Sturgess, C.E.N., Liu, C. and Rowe, G. W., (1989), Experimental and theoretical studies of work-piece deformation, stress and strain during flat rolling, International Materials Reviews, **34**, pp. 19–34

- Hashemolhosseini, H., Dalayeli, H. and Farzin, M., (2002), Correction of hydrostatic pressure obtained by finite element flow formulation using moving least square method, Journal of Material Processing Technology, **125/126**, pp. 588–593.

- Haykin, S., (1996), Adaptive Filter Theory, 3rd edition, Prentice-Hall, New Jersey.

- He, H.T., Zhang, L., (2007), The research on the model of flatness control based on the optimized RBF fuzzy neural network, International Conference on Machine Learning and Cybernetics, **1**, pp. 472–476.

- Hill, R., (1963), A general method of analysis for metal-working processes, Journal of the Mechanics and Physics of Solids, **11**, pp. 305–326.

- Hitchcock, J.H, (1935), Elastic deformation of rolls during cold rolling, American Society of Mechanical Engineers: Report of special research committee on roll neck bearings, pp. 33–41.

- Holbrook, R.L. and Zorowski, C.F., (1966), Effects of non-symmetry in strip rolling on single-roll drive mills, Transactions of the American Society of Mechanical Engineers: Journal of Engineering for Industry, pp. 401–409.

- Holland, J.H., (1975), Adaptation in natural and artificial systems, University of Michigan Press, Ann Arbor.

- Hwang, Y.M. and Chen, T.H., (1996), Analysis of asymmetrical sheet rolling by stream function method, Japan Society of Mechanical Engineers, Series A, **39**, pp. 598–605.

- Hwang, S.M. and Joun, M.S., (1992), Analysis of hot-strip rolling by a penalty rigid-viscoplastic finite element method, International Journal of Mechanical Sciences, **34**, pp. 971–984.

- Hwang, Y.M. and Tzou, G.Y., (1997), Analytical and experimental study on asymmetrical sheet rolling, International Journal of Mechanical Sciences, **39**, pp. 289–303.

- Hwu, Y.J. and Lenard, J.G., (1988), A finite element study of flat rolling, Transactions of the American Society of Mechanical Engineers: Journal of Engineering Materials and Technology, **110**, pp. 22–27.

- Iguchi, T. and Yarita, I., (1991), Three-dimensional analysis of flat rolling by rigid-plastic FEM considering sticking and slipping frictional boundary, Transactions of the Iron and Steel Institute of Japan, **31**, pp. 559–565.

- Jeswiet, J., Arentoft, M. and Henningsen, P., (2006), Methods and devices used to measure friction in rolling, Proceedings of the Institution of Mechanical Engineers, Part B: Journal of Engineering Manufacture, **220**, pp. 49–57.

- Jeswiet, J. and Cao, X., (1994), The effect of aspect ratio upon friction and normal forces in strip rolling, Journal of Material Processing Technology, **45**, pp. 99–104.

- Jeswiet, J. and Greene, P.G., (1998), Experimental measurement of curl in rolling, Journal of Material Processing Technology, **84**, pp. 202–209.

- Jiang, Z.Y. and Tieu, A. K., (2001), A simulation of three-dimensional metal rolling processes by rigid-plastic finite element method, Journal of Material Processing Technology, **112**, pp. 144–151.

- Johnson, W. and Kudo, H., (1960), The use of upper-bound solutions for the determination of temperature distributions in fast hot rolling and axi-symmetric extrusion processes, International Journal of Mechanical Sciences, **1**, pp. 175–191.

- Johnson, G. and Needham, W., (1966), Further experiments in asymmetrical rolling, International Journal of Mechanical Sciences, **8**, pp. 443–455.

- Jortner, D., Osterle, J.F. and Zorowski, C.F., (1959), An analysis of the mechanics of cold strip rolling, Iron and Steel Engineering Year Book, pp. 403–411.

- Jortner, D., Osterle, J.F. and Zorowski, C.F., (1960), An analysis of cold strip rolling, International Journal of Mechanical Sciences, **2**, pp. 179–194.

- Jung, J.Y. and Im, Y.T., (2000), Fuzzy algorithm for calculating roll speed variation based on roll separating force in hot rolling, International Journal of Mechanical Sciences, **42**, pp. 249–272.

- Jung, J.Y., Im, Y.T. and Lee-Kwang, H., (1996), Fuzzy-control simulation of cross-sectional shape in six-high cold-rolling mills, Journal of Material Processing Technology, **62**, pp. 61–69.

- Jung, J.Y. and Im, Y.T., (1997), Simulation of fuzzy shape control for cold-rolled strip with randomly irregular strip shape, Journal of Material Processing Technology, **63**, pp. 248–253.

- Kadkhodaei, M., Salimi, M. and Poursina, M., (2007), Analysis of asymmetrical sheet rolling by a genetic algorithm, International Journal of Mechanical Sciences, **4**, pp. 622–634.

- Kalpakjian, S. (1989), Manufacturing Engineering and Technology, Addison-Wesley, London.

- Karman, T.von., (1925), On the theory of rolling, L Angew. Math. Mech., **5**, pp. 139–141.

- Kennedy, G.E. and Slamar, F., (1958), Turn-up and turn-down in hot rolling. Iron and Steel Engineer, **35**, pp. 71–79.

- Kim, N., Kobayashi, S. and Altan, T., (1991), Three–dimensional analysis and computer simulation of shape rolling by the finite and slab element method, International Journal of Mechanical Sciences, **31**, pp. 553–563.

- Kiuchi, M.M. and Hsiang, S., (1986), Analytical model of asymmetrical rolling process of sheets, Proceedings of the 14th NAMRC, Society of Manufacturing Engineers, Minneapolis, pp. 384.

- Knight, C.W., Hardy, S.J., Lees, A.W. and Brown, K.J., (2003), Investigations into the influence of asymmetric factors and rolling parameters on strip curvature during hot rolling, Journal of Material Processing Technology, **134**, pp. 180–189.

- Kobayashi, S., Oh, S. and Altan, T. (1989), Metal forming and the finite-element method, Oxford University Press, New York.

- Kobayashi, S. and Li, G.J., (1982), Rigid-plastic finite element analysis of plane strain rolling, Transactions of the American Society of Mechanical Engineers: Journal of Engineering for Industry, **104**, pp. 55–64.

- Kohli, A. and Dixit, U.S., (2004), A neural network based methodology for prediction of surface roughness in turning process, International Journal of Advanced Manufacturing and Technology, **25**, pp. 118–129.

- Kumar, D. and Dixit, U.S., (2006), A slab method study of strain hardening and friction effects in cold foil rolling process, Journal of Material Processing Technology, **171**, pp. 331–340.

- Kusiak, J., Lenard, J.G. and Dudek, K., (1999), Intelligent processing and manufacturing of materials, International Conference on Intelligent Processing and Manufacturing of Materials, pp. 543–547.

- Lahoti, G.D., Akgerman, N., Oh, S.I. and Altan, T., (1980), Computer-aided analysis of metal flow and stresses in plate rolling, Journal of Mechanical Working Technology, **4**, pp. 105–l19.

- Larkiola, J., Myllykoski, P., Nylander, J. and Korhonen, A.S., (1996), Prediction of rolling force in cold rolling by using physical models and neural computing, Journal of Material Processing Technology, **60**, pp. 381–386.

- Le, H.R. and Sutcliffe, M.P.F., (2001), A robust model for rolling of thin strip and foil, International Journal of Mechanical Sciences, 43, pp. 1405–1419.

- Lee, C.H. and Kobayashi, S., (1973), New solutions to rigid–plastic deformation problems using a matrix method, Transactions of the American Society of Mechanical Engineers: Journal of Engineering for Industry, **95**, pp. 865–873.

- Lee, J.D., (1998), A large-strain elastic-plastic finite element analysis of rolling process, Computer Methods in Applied Mechanics and Engineering, **161**, pp. 315–347.

- Lee, D.M. and Choi, S.G., (2004), Application of on-line adaptable neural network for the rolling force set-up of a plate mill, Engineering Applications of Artificial Intelligence, **17**, pp. 557–565.

- Lee, D. and Lee, Y., (2002), Application of neural-network for improving accuracy of roll force model in hot-rolling mill, Control Engineering Practice, **10**, pp. 473–478**.**

- Lenard, J.G., (1991), Measurement of friction in cold flat rolling, Journal of Material Shaping Technology, **9**, pp. 171–180.

- Lenard, J.G., (1992), Friction and forward slip in cold strip rolling, Transactions of the American Society of Mechanical Engineers: Journal of Tribology, **35**, pp. 423–428.

- Li, G.J. and Kobayashi, S., (1982), Rigid plastic finite element analysis of plane strain rolling, Transactions of the American Society of Mechanical Engineers: Journal of Engineering for Industry, **104**, pp. 55–64.

- Lim L.S. and Lenard J.G., (1984), Study of friction in cold rolling, Transactions of the American Society of Mechanical Engineers: Journal of Engineering Materials and Technology, **106**, pp. 139–146.

- Lindgren, L.E. and Edberg, J., (1990), Explicit versus implicit finite element formulation in simulation of rolling, Journal of Material Processing Technology, **24**, pp. 85–94.

- Liu, C., Hartley, P., Sturgess, C.E.N. and Rowe, G.E., (1985), Elastic-plastic finite element modelling of cold rolling of strip, International Journal of Mechanical Sciences, **27**, pp. 531–541.

- Liu, Y.J., Tieu, A.K., Wang, D.D. and Yuen, W.Y.D., (2001), Friction measurement in cold rolling, Journal of Material Processing Technology, **111**, pp. 142–145.

- Lu, C., (1998), Application of ANN in combination with mathematical models in prediction of rolling load of the finishing stands in hsm, Proceedings of Steel Rolling, **98**, pp. 206–209.

- Lu, J.S., Harrer, O.K., Schwenzfeier, W. and Fischer, F.D., (2000), Analysis of the bending of the rolling material in asymmetrical sheet rolling, International Journal of Mechanical Sciences, **42**, pp. 49–61.

- Malinowski Z. and Lenard, J.G., (1992), A study of the state of stress during cold strip rolling, Journal of Material Processing Technology, **33**, pp. 273–288.

- Malvern, L.E., (1969), Introduction to the mechanics of a continuous medium, Chap.6, Sect. 6.5 and 6.6., Prentice-Hall, Englewood Cliffs, New Jersey.

- Mamdani, E.H., (1976), Advances in linguistic synthesis of fuzzy controllers, International Journal of Man Machine Studies, **8**, pp. 669–678.

- Maniatty, A.M, (1994), Predicting residual stresses in steady-state forming processes, Computing Systems in Engineering, **5**, pp. 171–177.

- Marques Barata, M.J.M. and Martins, P.A.F., (1990), A solution to plane strain rolling by the weighted residuals method, International Journal of Mechanical Sciences, **32**, pp. 817–827.

- McCulloch W.S. and Pitts, W., (1943), A logical calculus of the ideas immanent in nervous activity, Bulletin of Mathematical Biology, **5**, pp. 115–133.

- Mischke, J., (1996), Equations of strip equilibrium during asymmetrical flat rolling, Journal of Material Processing Technology, **61**, pp. 382–394.

- Montmitonnet, P. and Buessler, P., (1991), A review on theoretical analyses of rolling in Europe, Transactions of the Iron and Steel Institute of Japan, **31**, pp. 525–538.

- Mori, K., Osakada, K. and Oda, T., (1982), Simulation of plane strain rolling by rigid-plastic finite element method, International Journal of Mechanical Sciences, **24**, pp. 519–527.

- Myllykoski, P., Larkiola, J., Korhonen, A.S. and Cser, L., (1998), The role of neural networks in the optimization of rolling processes, Journal of Material Processing Technology, **80/81**, pp. 6–23.

- Nadai, A., (1939), The forces required for rolling steel strip under tension, Transactions of the American Society of Mechanical Engineers: Journal of Applied Mechanics, A, pp. 54–62.

- Nandan, R., Rai, R., Jayakanth, R., Moitra, S., Chakraborti, N. and Mukhopadhyay, A., (2005), Regulating crown and flatness during hot rolling: A multiobjective optimization study using genetic algorithms, Materials and Manufacturing Processes, **20/3**, pp. 459–478.

- Nandi, A.K. and Pratihar, D.K., (2004), Automatic design of fuzzy logic controller using a genetic algorithm-to predict power requirement and surface finish in grinding, Journal of Material Processing Technology, **148**, pp. 288–300.

- Nepershin, R.I., (1999), Plane strain hot rolling of slab and strip, International Journal of Mechanical Sciences, **41**, pp. 1401–1421.

- Nolle, L., Armstrong, D.A., Ware, J.A. and Biegler-Konig, F., (1997), Optimization of roll profiles in the hot rolling of wide steel strip genetic algorithm in engineering systems: Innovations and Applications, Proceedings of the 5th International Mendel Conference, pp. 133–138.

- Orowan, E., (1943), The calculation of roll pressure in hot and cold flat rolling, Proceedings of Institution of Mechanical Engineers, **150**, pp. 140–167.

- Pan, D. and Sansome, D.H., (1982), An experimental study of the effect of roll-speed mismatch on the rolling load during the cold rolling of the strip, Journal of Mechanical Working Technology, **6**, pp. 361–377.

- Panda, S.S., Charkraborty, D. and Pal, S.K., (2008), Flank wear prediction in drilling using back propagation neural network and radial basis function network, Applied Soft Computing, **8**, pp. 858–871.

- Park, B.H. and Hwang, S.M., (1997), Analysis of front end bending in plate rolling by the finite element method, Transactions of the American Society of Mechanical Engineers: Journal of Manufacturing Science and Engineering, **119**, pp. 314–323.

- Park, B.H., Hwang, S.M. and Kim, J.G., (1993), Finite element modelling of front end bending due to roll speed difference in plate rolling, in: Proceedings of the 1st International Conference on Modelling of Metal Rolling Processes, London, pp. 553–557.

- Park, J.J. and Kobayashi, S., (1984), Three-dimensional finite element analysis of block compression, International Journal of Mechanical Sciences, **26**, pp. 165–176.

- Pedrycz, W. (1994), Why triangular membership functions? Fuzzy Sets and Systems, **64**, pp. 21–30.

- Philipp, M., Schwenzfeier, W., Fischer, F.D., Wödlinger, R. and Fischer, C., (2007), Front end bending in plate rolling influenced by circumferential speed mismatch and geometry, Journal of Material Processing Technology, **184**, pp. 224–232.

- Pican, N., Alexandre, F. and Bresson, P., (1996), Artificial neural networks for the presetting of a steel temper mill, IEEE Transactions: Expert, **11**, pp. 22–27.

- Pietrzyk, M., Wilk, K. and Kusiak, H., (1993), Steady state FEM simulation of the strip bending in asymmetrical rolling process, In Proceedings of Metal Forming, Krynica, pp. 50–55.

- Pospiech, J., (1987), A note on the influence of some factors affecting curvature in the flat rolling of strip, Journal of Mechanical Working Technology, **15**, pp. 69–80.

- Prakash, R.S., Dixit P.M. and Lal, G.K., (1995), Steady-state plane-strain cold rolling of a strain-hardening material, Journal of Material Processing Technology, **52**, pp. 338–358.

- Pratihar, D.K., Deb, K. and Ghosh, A., (1999), A genetic-fuzzy approach for mobile robot navigation among moving obstacles, International Journal of Approximate Reasoning, **20**, pp. 145–172.

- Rao, R.S. and Lee, H.Y., (1989), A finite element solution of strip rolling, Journal of Mechanical Working Technology, **20**, pp. 453–461.

- Rao, S.S. and Kumar, A., (1977), Finite element analysis of cold strip rolling. International Journal of Machine Tool Design and Research, **17**, pp. 157–168.

- Reddy, D.M. and Verduzco, M.A., (1972), Effect of asymmetry in cold rolling of thin strip, Proceedings of 3rd Inter–American Conference on Material Technology, Rio de Janiero, pp. 3.

- Richelsen, A.B., (1991), Viscoplastic analysis of plane-strain rolling using different friction models, International Journal of Mechanical Sciences, **33**, pp. 761–774.

- Richelsen, A.B., (1994), Interface element modelling of friction in rolling, Journal of Material Processing Technology, **42**, pp. 209–216.

- Richelsen, A.B., (1997), Elastic-plastic analysis of the stress and strain distributions in asymmetric rolling, International Journal of Mechanical Sciences, **39**, pp. 1199–1211.

- Roberts, W.L., (1965), A simplified cold rolling model, Iron and Steel Engineer Year Book, pp. 925–937.

- Roberts, W.L., (1976), Computing the coefficient of friction in the roll bite from mill data, Blast Furnace and Steel Plant, **55**, pp. 499–508.

- Roberts, W.L., (1978), Editor, Cold rolling of steel. New York, Marcel Dekker.

- Rodríguez-Rodríguez, M.G., Valdés-Covarrubias, E., Zambrano, P.C., Guerrero-Mata, M.P. and Colás, R, (2001), Visioplastic analysis of experimental rolling of steel, Proceedings of the Institution of Mechanical Engineers, Part L: Journal of Materials: Design and Applications, **215**, pp. 155–163.

- Rooyen, G.T.V. and Bachofen, W.A., (1957), Friction in cold rolling, Journal of the Iron and Steel Institute, **6**, pp. 235–244.

- Roychoudhari, R. and Lenard, J.G., (1984), A mathematical model for cold rolling-Experimental substantiation, Proceedings of 1st International Conference on Technology and Plasticity, Tokyo, pp. 1138–1143.

- Sachs, G. and Klinger, L.J., (1947), The flow of metals through tools of circular contour, Transactions of the American Society of Mechanical Engineers: Journal of Applied Mechanics, **69**, pp. 88–98.

- Salimi, M. and Kadkhodaei, M., (2004), Slab analysis of asymmetrical sheet rolling, Journal of Material Processing Technology, **150**, pp. 215–222.

- Salimi, M. and Sassani, F., (2002), Modified slab analysis of asymmetrical plate rolling, International Journal of Mechanical Sciences, **44**, pp. 1999–2023.

- Salunkhe, M.A., (2006), Analysis of cold flat asymmetric rolling process, M. Tech. Thesis, Indian Institute of Technology Guwahati.

- Samanta, B., (2004), Artificial neural networks and genetic algorithms for gear fault detection, Mechanical Systems and Signal Processing, **18**, pp. 1273–1282.

- Sarma D.K. and Dixit, U.S., (2007), A comparison of dry and air-cooled turning of grey cast iron with mixed oxide ceramic tool, Journal of Material Processing Technology, **190**, pp. 160–172.

- Sbarbaro-Hofer, D., Neumerkel, D. and Hunt, K., (1993), Neural control of a steel rolling mill, IEEE Transactions: Control Systems, **13**, pp. 69–75.

- Setnes, M., Babuˇska, R. and Verbruggen, H. B., (1998), Rule-based modelling: Precision and transparency, IEEE Transactions: Systems, Man and Cybernetics, Part C: Applications and Reviews, **28**, pp. 165–169.

- Sezek, S., Aksakal, B. and Can, Y. (2008), Analysis of cold and hot plate rolling using dual stream functions, Materials and Design, **29**, pp. 584–596.

- Shangwu, X., Rodrigues, J.M.C. and Martins, P.A.F., (2003), Three–dimensional modelling of the vertical-horizontal rolling process, Finite Elements in Analysis and Design, **39**, pp. 1023–1037.

- Shida, S. and Awazuhara, H., (1973), Rolling load and torque in cold rolling, The Japan Society for Technology of Plasticity, **14**, pp. 267–278.

- Shima, S., Mori, K., Oda, T. and Osakada, K., (1982), Rigid-plastic finite element analysis of strip rolling, Proceedings on 4th International Conference in Production Engineering, Tokyo, pp. 82–87.

- Shivpuri, R. and Chou, P.C., (1989), A comparative study of slab, upper bound and finite element methods for predicting force and torque in cold rolling, International Journal of Machine Tools and Manufacturing, **29**, pp. 305–322.

- Shivpuri, R., Chou, P.C. and Lau, C.W., (1988), Finite element investigations of curling in non-symmetric rolling of flat stock, International Journal of Mechanical Sciences, **30**, pp. 625–635.

- Siebel, E., (1930), Resistance and deformation and the flow material during rolling, Stahl und Eisen., **50**, pp. 1769–1775.

- Siebel, E., (1941), The theory of rolling processes between unequally driven rolls, Archiv fur Eisenhuttenwesen, **15/9**, pp. 125-128.

- Siebel, E. and Lueg, W., (1933), Investigations into the distribution of pressure at the surface of the material in contact with rolls, Mitteilungen aus dem Kaiser-Wilhem-Institut für Eisenforschung, **15**, pp. 1–15.

- Sims, R.B., (1954), Calculation of roll force and torque in cold rolling by graphical and experimental methods, Journal of the Iron and Steel Institute, **178**, pp. 19–34.

- Sims, R.B., (1954), Calculation of roll force and torque in hot rolling mills, Proceedings of Institution of Mechanical Engineers, **168**, pp. 191–200.

- Ŝkrjanc, I., Blažič, S., and Agamennoni, O. (2005), Interval fuzzy model identification using l_∞ –norm, IEEE Transactions: Fuzzy Systems, **13**, pp. 561–568.

- Son, J.S., Lee, D.M., Kim, I.S. and Choi, S.K., (2004), A study on genetic algorithm to select architecture of a optimal neural network in the hot rolling process, Journal of Material Processing Technology, **153/154**, pp. 643–648.

- Son, J.S., Lee, D.M., Kim, I.S. and Choi, S.G., (2005), A study on on-line learning neural network for prediction for rolling force in hot-rolling mill, Journal of Material Processing Technology, **164/165**, pp. 1612–1617.

- Sonar, D.K., Dixit, U.S. and Ojha, D.K., (2005), The application of a radial basis function neural network for predicting the surface roughness in a turning process, International Journal of Advanced Manufacturing Technology, **27**, pp. 661–666.

- Stephenson, D.A., (1983), Friction in cold strip rolling, Wear, **92**, pp. 293–311.

- Tamano, T., (1973), Finite element analysis of steady flow in metal processing, Journal of Japan Society of Technical Plastics, **14**, pp. 766–769.

- Tamano, T. and Yangimoto, S., (1975), Finite element analysis of steady metal flow problems. Journal of the Japan Society of Mechanical Engineers, **41**, pp. 1130–1135.

- Tanaka, E., Tsunokawa, K. and Fukuda, T., (1963), Curling and bowing of rolled strips, Transactions of Japan Institute of Metals, **4/3**, pp. 124–133.

- Tieu, A.K. and Liu, Y.J., (2004), Friction variation in the cold-rolling process, Tribology International, **37**, pp. 177–183.

- Tirosh, J., Iddan, D. and Pawelski, O., (1985), The mechanics of high speed rolling of viscoplastic materials, Transactions of the American Society of Mechanical Engineers: Journal of Applied Mechanics, **52**, pp. 309–318.

- Thompson, E.G., (1982), Inclusion of elastic strain rate in the analysis of viscoplastic flow during rolling, International Journal of Mechanical Sciences, **24**, pp. 655–659.

- Thompson, E.G. and Berman, H.M., (1984), Steady-state analysis of elasto-viscoplastic flow during rolling, Numerical analysis of forming process (Edited by Pittman *et al.*), pp. 269–283, Wiley, New York.

- Thomsen, E.G., Yang, C.T and Bierbower, J.B., (1954), An experimental investigation of the mechanics of plastic deformation of metals, university of California Press, Berkeley, **5**, pp. 89–144.

- Thomson, P.F., (1982), A combined visioplasticity and finite element analysis of cold rolling, Numerical Methods in Industrial Forming Processes, pp. 757–765.

- Thomson, P.F. and Brown, J.H., (1982), A study of deformation during cold rolling using visioplasticity, International Journal of Mechanical Sciences, **24**, pp. 559–576.

- Tuncer, C. and Dean, T.A., (1987), A new pin design for pressure measurements in metal forming processes, International Journal of Machine Tools and Manufacture, **27**, pp. 325–331.

- Tselikov, A.I., (1939), Effect of external friction and tension on the pressure of the metal on the rolls in rolling, Metallurg, **6**, pp. 61–76.

- Utsunomiya, H., Ueno, T. and Sakai, T., (2007), Improvement in the *r*-value of aluminum sheets by differential-friction rolling, Scripta Materialia, **57**, pp. 1109–1110.

- Venter, R. and Abd-Rabbo, A., (1980), Modeling of the rolling process-I, Inhomogeneous deformation model, International Journal of Mechanical Sciences, **22**, pp. 83–92.

- Venter, R. and Abd-Rabbo, A., (1982), Modelling of the rolling process-II, Evaluation of the stress distribution in the rolled material, International Journal of Mechanical Sciences, **22**, pp. 93–98.

- Wang, D.D., Tieu, A.K., Boer, F.G.D., Ma, B. and Yuen, W.Y.D., (2000), Toward a heuristic optimum design of rolling schedules for tandem cold rolling mills, Engineering Applications of Artificial Intelligence, **13/4**, pp. 397–406.

- Wang, D.D., Tieu, A.K. and D'Alessio, G., (2005), Computational intelligence-based process optimization for tandem cold rolling, Materials and manufacturing Processes, **20/3**, pp. 479–496.

- Wanheim, T. and Bay, N., (1978), A model for friction in metal forming processes, Annals of CIRP, **27**, pp. 189–194.

- Yamamoto, H. and Kawanami, T., (1982), Study on asymmetrical strip rolling (plasticine strain analysis), Proceedings-57, Special Conference of Japan Society for Technology of Plasticity, **65**, (In Japanese).

- Yang, Y.Y., Linkens, D.A., Talamantes-Silva, J. and Howard, I.C., (2003), Roll force and torque prediction using neural network and finite element modeling, Transactions of the Iron and Steel Institute of Japan, **43**, pp. 1957–1966.

- Yang, Y.Y., Linkens, D.A. and Talamantes-Silva, J., (2004), Roll load prediction-data collection, analysis and neural network modelling, Journal of Material Processing Technology, **152**, pp. 304–315.

- Yarita, I., Mallett, R.L. and Lee, E.H., (1988), Stress and deformation analysis of plane strain rolling process, Steel Research, **56**, pp. 231–255.

- Ying, H. (1998), General Takagi–Sugeno fuzzy systems with simplified linear rule consequent are universal controllers, models and filters, Journal of Information Sciences, **108**, pp. 91–107.

- Zadeh, L. A., (1965), Fuzzy sets, Information and Control, **8**, pp. 338–353.

- Zhang, W. and Bay, N., (1997), Numerical analysis of cross shear plate rolling, Annals of CIRP, **46/1**, pp. 195–200.

- Zhu, H.T., Jiang, Z.Y., Tieu A.K. and Wang, G.D., (2003), A fuzzy algorithm for flatness control in hot strip mill, Journal of Material Processing Technology, **140**, pp. 123–128.

- Zienkiewicz, O.C. and Godbole, P.N., (1974), Flow of plastic and visco-plastic solids with special reference to extrusion and forming processes, International Journal of Numerical Methods in Engineering, **8**, pp. 3–16.

- Zienkiewicz, O.C., Jain, P.C. and Onate, E., (1978), Flow of solids during forming and extrusion: some aspects of numerical solution, International Journal of Solids and Structures, **14**, pp. 15–38.

- Zorowski, C.F. and Shutt, A., (1963), Analysis of the load and torque characteristics of single-roll drive mills, International Research in Product Engineering, Pittsburgh, pp. 380–387.

- Zuperl, U., Cus, F. and Milfelner, M., (2005), Fuzzy control strategy for an adaptive force control in end-milling, Journal of Material Processing Technology, **164/165**, pp. 1472–1478.

Appendix

Appendix A

Formulation for Strain Hardening

The equivalent strain at a point is obtained by the time integration of the equivalent strain rate along the particle path, as given by Eq. (3.9). Construction of the particle path or flow lines is the first step in the determination of the equivalent strain field. The slope of a flow line is given by

$$\frac{\mathrm{d}x_2}{\mathrm{d}x_1} = \frac{v_2}{v_1}. \tag{A.1}$$

Given a point $(x_{1i},\ x_{2i})$ on a flow line, the coordinates $(x_{1i+1},\ x_{2i+1})$ of the adjacent point are found by using the relationship

$$x_{2i+1} = x_{2i} + (x_{1i+1} - x_{1i})\frac{v_2}{v_1}, \tag{A.2}$$

where $(x_{2i+1} - x_{1i})$ is chosen sufficiently small so that the path between the two points may be approximated by a straight line. In this manner, flow lines of various points on the inlet boundary can be found. Now, along a flow line,

$$\mathrm{d}t = \frac{\mathrm{d}s}{v_s} = \frac{\mathrm{d}x_1}{v_1} = \frac{\mathrm{d}x_2}{v_2}. \tag{A.3}$$

Thus, substitution of this expression for $\mathrm{d}t$ in Eq. (3.9) gives the following expression for the equivalent strain:

$$\tilde{\varepsilon} = \int_0^t \frac{\dot{\tilde{\varepsilon}}}{v_2} \mathrm{d}x_2 \,. \tag{A.4}$$

The equivalent strain is zero at the first plastic boundary. However, this boundary is not known a priory, therefore, the equivalent strain is taken as zero on the inlet boundary. This is acceptable, since the strains it give rises to at the first plastic boundary are quite small. Then integrating expression (A.4) by Simpson's scheme, equivalent strains are found at various points along the flow lines. Nine points in each element are selected and the equivalent strain values at these points are interpolated to obtain the equivalent strains at the Gauss points. These values are then substituted into Eq. (3.8) to update the values of σ_Y for further iteration.

Appendix B

1) Galerkin Formulation

In this work, Galerkin weak formulation has been used. Let v_1, v_2 and p be the functions that satisfy all essential boundary conditions exactly, thus the equations will become

$$\int_A \left[-\left(\dot{\varepsilon}_{11} + \dot{\varepsilon}_{22}\right) w_p + \left(\frac{\partial \sigma_{11}}{\partial x_1} + \frac{\partial \sigma_{12}}{\partial x_2} \right) w_1 + \left(\frac{\partial \sigma_{21}}{\partial x_1} + \frac{\partial \sigma_{22}}{\partial x_2} \right) w_2 \right] \mathrm{d}x_1 \mathrm{d}x_2 = 0 , \tag{B.1}$$

where A denotes domain of a typical area element. The above expression can be written in index form as:

$$\int_A \left[-\dot{\varepsilon}_{ii} w_p + \sigma_{ij,j} w_i \right] \mathrm{d}x_1 \mathrm{d}x_2 = 0 . \tag{B.2}$$

Using the divergence theorem, second integral can be simplified as

$$\begin{aligned} \int_A \sigma_{ij,j} w_i \, \mathrm{d}A = \int_A \left(\sigma_{ij} w_i\right)_{,j} \mathrm{d}A - \sigma_{ij}, w_{i,j} \mathrm{d}A = \oint_\Gamma \sigma_{ij} w_i n_i \mathrm{d}\Gamma - \int_A \sigma_{ij}, w_{i,j} \mathrm{d}A \\ = \oint_\Gamma t_i w_i \mathrm{d}\Gamma - \int_A \sigma_{ij}, w_{i,j} \mathrm{d}A. \end{aligned} \tag{B.3}$$

By the theorem that any matrix can be decomposed into a symmetric and anti-symmetric part:

$$w_{i,j} = \frac{1}{2}\left[\left(w_{i,j} + w_{j,i} \right) + \left(w_{i,j} - w_{j,i} \right) \right]. \tag{B.4}$$

The symmetric part can be denoted as $\dot{\varepsilon}_{ij}(w)$. Thus the governing equation will become

$$\int_A \dot{\varepsilon}_{ii} w_p \, \mathrm{d}A + \int_A \sigma_{ij} \dot{\varepsilon}_{ij} \left(w \right) \mathrm{d}A - \int_{\Gamma_i} t_i w_i \mathrm{d}\Gamma = 0. \tag{B.5}$$

Equation (B.5) can be written as

$$\int_A \left(\sigma_{ij}, w_{i,j}\right) \mathrm{d}A = \int_A \sigma_{ij}\dot{\varepsilon}_{ij}\left(w\right) \mathrm{d}A \ . \tag{B.6}$$

Equation (B.5) has all terms in first order derivatives of velocity component, thus the weak form has been obtained for further finite element modelling. This equation can be further expanded as

$$\begin{aligned}\sigma_{ij}\dot{\varepsilon}_{ij}\left(w\right) = &- p\left[\dot{\varepsilon}_{11}\left(w\right) + \dot{\varepsilon}_{22}\left(w\right)\right] \\ &+ 2\mu\left[\dot{\varepsilon}_{11}\dot{\varepsilon}_{11}\left(w\right) + 2\dot{\varepsilon}_{12}\dot{\varepsilon}_{12}\left(w\right) + \dot{\varepsilon}_{22}\dot{\varepsilon}_{22}\left(w\right)\right].\end{aligned} \tag{B.7}$$

Thus, the entire weak formulation will be

$$\int_A I_1 \, \mathrm{d}A + \int_A I_2 \, \mathrm{d}A - \int_{\Gamma_1} I_3 \, \mathrm{d}\Gamma - \int_{\Gamma_2} I_4 \, \mathrm{d}\Gamma = 0 \ , \tag{B.8}$$

where

$$\begin{aligned} I_1 &= \int_A \left[\dot{\varepsilon}_{11} + \dot{\varepsilon}_{22}\right] w_p \, , \\ I_2 &= \int_A - p\left[\dot{\varepsilon}_{11}\left(w\right) + \dot{\varepsilon}_{22}\left(w\right)\right] + 2\mu\left[\dot{\varepsilon}_{11}\dot{\varepsilon}_{11}\left(w\right) + 2\dot{\varepsilon}_{12}\dot{\varepsilon}_{12}\left(w\right) + \dot{\varepsilon}_{22}\dot{\varepsilon}_{22}\left(w\right)\right], \\ I_3 &= \int_{\Gamma_1} t_1 w_1 \, , \\ I_4 &= \int_{\Gamma_2} t_2 w_2 \, . \end{aligned} \tag{B.9}$$

Γ_1 and Γ_2 are respectively those parts of the boundary where tractions t_1 and t_2 are specified.

2) Finite Element Approximation

In the weak form of the governing equation, as velocity is of first order derivative and pressure is of zero order, C^0 continuity is sufficient. For velocity, bi-quadric approximation has been chosen and for pressure, bilinear approximation has been selected. The approximation for v_1 and v_2 will be

$$\begin{Bmatrix} v_1 \\ v_2 \end{Bmatrix} = [N_v]\{v^e\}. \tag{B.10}$$

Here, weight functions for velocity and pressure are approximated using same shape functions as that of velocity and pressure respectively.

$$\{w_v\} = [N_v]\{w_v{}^e\}. \tag{B.11}$$

The approximation for pressure will be

$$p = \{N_p\}^{\mathrm{T}}\{p^e\}. \tag{B.12}$$

The weight function for pressure will be

$$\{w_p\} = [N_v]\{w_p{}^e\}. \tag{B.13}$$

The expressions of Lagrangian shape functions N_i can be obtained from any standard text book of FEM. The geometry is also approximated by the same shape functions as that used for velocities. Therefore,

$$\{x_1\} = [N]\{x_1{}^e\} \quad \text{and} \quad \{x_2\} = [N]\{x_2{}^e\}. \tag{B.14}$$

As the boundary of the element consists of three nodes, evaluation of the integrals over the boundaries Γ_i will be

$$w_1 = [N_b]\{w_1{}^b\}, \quad w_2 = [N_b]\{w_2{}^b\}. \tag{B.15}$$

Further t_1 and t_2 are approximated as

$$t_1 = [N_b]\{t_1{}^b\}, \qquad t_2 = [N_b]\{t_2{}^b\}, \tag{B.17}$$

where t_1 and t_2 are the vectors of the nodal value of the traction.

$$N_1^b = \frac{1}{2}(\zeta^2 - \zeta), \quad N_2^b = \frac{1}{2}(\zeta^2 + \zeta), \quad N_3^b = \frac{1}{2}(1 - \zeta^2), \tag{B.19}$$

where ζ is the natural coordinate on the boundary.

3) Finite Element Equations

The above all derivations described in (B.9) can be expressed in matrix form to obtain the solution. For that purpose

$$\{\dot{\varepsilon}\} = \begin{Bmatrix} \dot{\varepsilon}_{11} \\ \dot{\varepsilon}_{22} \\ \sqrt{2}\,\dot{\varepsilon}_{12} \end{Bmatrix} = \begin{Bmatrix} \dfrac{\partial v_1}{\partial x_1} \\ \dfrac{\partial v_2}{\partial x_2} \\ \dfrac{1}{\sqrt{2}}\left(\dfrac{\partial v_1}{\partial x_2} + \dfrac{\partial v_2}{\partial x_1} \right) \end{Bmatrix}, \tag{B.20}$$

$$\{\dot{\varepsilon}(w)\} = \begin{Bmatrix} \dot{\varepsilon}_{11}(w) \\ \dot{\varepsilon}_{22}(w) \\ \sqrt{2}\,\dot{\varepsilon}_{12}(w) \end{Bmatrix} = \begin{Bmatrix} \dfrac{\partial w_1}{\partial x_1} \\ \dfrac{\partial w_2}{\partial x_2} \\ \dfrac{1}{\sqrt{2}}\left(\dfrac{\partial w_1}{\partial x_2} + \dfrac{\partial w_2}{\partial x_1} \right) \end{Bmatrix}. \tag{B.21}$$

Using the approximations (B.10-B.11), the strain rate vector $\{\dot{\varepsilon}\}$ and $\{\dot{\varepsilon}(w)\}$ becomes

$$\{\dot{\varepsilon}\} = [B]\{v^e\} \quad \text{and} \quad \{\dot{\varepsilon}(w)\} = [B]\{w_v^e\}, \tag{B.22}$$

where

$$[B] = \begin{bmatrix} \dfrac{\partial N_1}{\partial x_1} & 0 & \dfrac{\partial N_2}{\partial x_1} & 0 & ----- & \dfrac{\partial N_9}{\partial x_1} & 0 \\ 0 & \dfrac{\partial N_1}{\partial x_1} & 0 & \dfrac{\partial N_2}{\partial x_1} & ----- & 0 & \dfrac{\partial N_9}{\partial x_1} \\ \dfrac{1}{\sqrt{2}}\dfrac{\partial N_1}{\partial x_2} & \dfrac{1}{\sqrt{2}}\dfrac{\partial N_1}{\partial x_1} & \dfrac{1}{\sqrt{2}}\dfrac{\partial N_2}{\partial x_2} & \dfrac{1}{\sqrt{2}}\dfrac{\partial N_2}{\partial x_1} & --- & \dfrac{1}{\sqrt{2}}\dfrac{\partial N_9}{\partial x_2} & \dfrac{1}{\sqrt{2}}\dfrac{\partial N_9}{\partial x_1} \end{bmatrix} \tag{B.23}$$

Here

$$\dot{\varepsilon}_{11} + \dot{\varepsilon}_{22} = \{1 \quad 1 \quad 0\}\{\dot{\varepsilon}\} = \{m\}^{\mathrm{T}}[B]\{v^e\}, \tag{B.24}$$

where

$$\{m\} = \begin{Bmatrix} 1 \\ 1 \\ 0 \end{Bmatrix}. \tag{B.25}$$

Similarly,

$$\dot{\varepsilon}_{11}(w) + \dot{\varepsilon}_{22}(w) = \{m\}^{\mathrm{T}}[B]\{w_v^e\}. \tag{B.26}$$

Using all above expressions (B.10-B.26) in Eq. (B.9) in the following manner;

$$\begin{aligned} &\int_A -\left[w^p\right]\{N^p\}\{m\}^{\mathrm{T}}[B]\{v^e\}\mathrm{d}x_1\mathrm{d}x_2 + \int_A -\left[w_v^e\right]\{N^p\}\{m\}^{\mathrm{T}}[B]\{p^e\}\mathrm{d}x_1\mathrm{d}x_2 \\ &+\int_A 2\mu\left[w_v^e\right]\{B\}[B]^{\mathrm{T}}\{v^e\}\mathrm{d}x_1\mathrm{d}x_2 = \int_{\Gamma_1} t_1 w_1 \mathrm{d}\Gamma + \int_{\Gamma_2} t_2 w_2 \mathrm{d}\Gamma, \end{aligned} \tag{B.27}$$

where

$$\begin{aligned} \{K_{pv}^e\} &= \int_A -\{N^p\}\{m\}^{\mathrm{T}}[B]\mathrm{d}x_1\mathrm{d}x_2, \\ \{K_{vp}^e\} &= \{K_{pv}^e\}^{\mathrm{T}} \quad \text{and} \quad \{K_{vv}^e\} = \int_A 2\mu\{B\}[B]^{\mathrm{T}}\mathrm{d}x_1\mathrm{d}x_2. \end{aligned} \tag{B.28}$$

Thus the finite element equation in local variable form will be

$$\sum_{e=1}^{ne}\{w^e\}^{\mathrm{T}}\{K^e\}\{\delta^e\} = \sum_{b=1}^{nb_1}\{w_1^b\}^{\mathrm{T}}\{f_1^b\} + \sum_{b=2}^{nb_2}\{w_2^b\}^{\mathrm{T}}\{f_2^b\}, \tag{B.29}$$

where

$$\{f_1^b\} = \int_{\Gamma_1^b}\{N_b\}\{N_b\}^{\mathrm{T}}\{t_1^b\}\mathrm{d}\Gamma, \quad \{f_2^b\} = \int_{\Gamma_2^b}\{N_b\}\{N_b\}^{\mathrm{T}}\{t_2^b\}\mathrm{d}\Gamma. \tag{B.30}$$

Here ne is the number of area elements, nb_1 and nb_2 are the number of boundary elements on Γ_1 and Γ_2. Similarly,

$$\{w^e\} = \begin{Bmatrix} \{w_p^e\} \\ \{w_v^e\} \end{Bmatrix}, \quad \{\delta^e\} = \begin{Bmatrix} \{p^e\} \\ \{v^e\} \end{Bmatrix} \quad \text{and} \quad [K^e] = \begin{bmatrix} [0] & [K_{pv}^e] \\ [K_{vp}^e] & [K_{vv}^e] \end{bmatrix}, \quad \text{(B.31)}$$

For numerical evaluation, the variables of the area integrals in (B.35) are transformed to the natural coordinates (ξ, η) using the following transformation:

$$\int_{A^e} (---)\mathrm{d}x_1\mathrm{d}x_2 = \int_{-1}^{+1}\int_{-1}^{+1} (---)\,|J|\,\mathrm{d}\xi\,\mathrm{d}\eta, \quad \text{(B.32)}$$

$$|J| = \begin{bmatrix} \dfrac{\mathrm{d}x_1}{\mathrm{d}\xi} & \dfrac{\mathrm{d}x_1}{\mathrm{d}\eta} \\ \dfrac{\mathrm{d}x_2}{\mathrm{d}\xi} & \dfrac{\mathrm{d}x_2}{\mathrm{d}\eta} \end{bmatrix}, \quad \text{(B.33)}$$

where $|J|$ is the elemental Jacobian matrix. Similarly, the boundary integrals are transformed by the relation

$$\int_{\Gamma} (---)\,\mathrm{d}\Gamma = \int_{-1}^{+1} (---)\,|J|\,\mathrm{d}\zeta\,, \quad \text{(B.34)}$$

where $|J_b|$ is the Jacobian for boundary element and is given by

$$|J_b| = \sqrt{\left(\frac{\partial x_1}{\partial \zeta}\right)^2 + \left(\frac{\partial x_2}{\partial \zeta}\right)^2}\,. \quad \text{(B.35)}$$

Along the boundary the coordinates (x_1, x_2) are approximated using 1-D quadratic shape functions. All elemental matrices are evaluated using 3×3 Gauss quadrature. Similarly the elemental vectors are evaluated using 3 point gauss quadrature. The assembled finite element can be written as

$$\{W\}[K]\{\Delta\} = \{W\}^{\mathrm{T}}\{F\}. \quad \text{(B.36)}$$

where $\{W\}$, $[K]$ and $\{\Delta\}$ are the global vector of nodal values of weight function, global coefficient matrix and global vector of nodal values of pressure and

velocity. The global right hand side vector is $\{F\}$. Since weight functions are arbitrary, final finite element expression will be

$$[K]\{\Delta\} = \{F\}. \tag{B.37}$$

4) Application of Boundary Conditions

The friction condition at a typical node on the roll-work interface is shown in Fig. B.1.

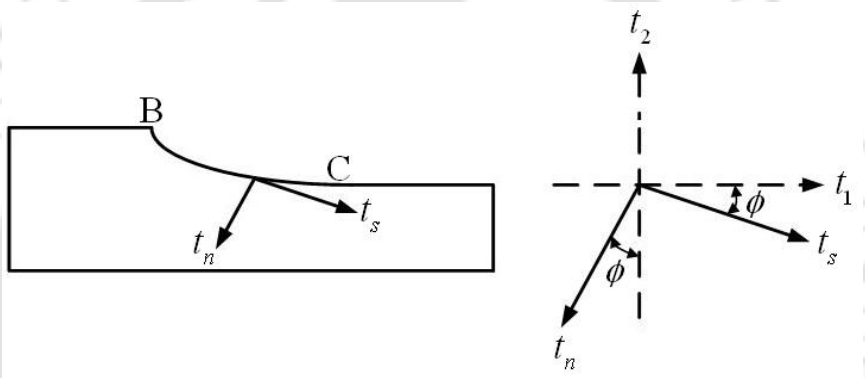

Figure B.1. Shear and normal components of traction at roll-work interface

Using Eq. (3.15), we can we can express t_s and t_n in the form of t_1 and t_2 as follows:

$$|t_s| = t_1 \cos\phi - t_2 \sin\phi \quad \text{and} \quad |t_n| = -t_1 \sin\phi - t_2 \cos\phi. \tag{B.38}$$

Thus putting the decomposed form t_s and t_n into Eq. (B.38) we get,

$$t_1(\cos\phi + f \sin\phi) - t_2(\sin\phi + f \cos\phi) = 0. \tag{B.39}$$

Replacing $f = ck_s$ in the above Eq. (B.39) where k_s is -1 before neutral point and +1 after neutral point. In the case of Coulomb's model, c is equal to friction coefficient f. Equation (B.39) can be modified as

$$t_1(1 - ck_s \tan\phi) - t_2(\tan\phi + ck_s) = 0. \tag{B.40}$$

The above expression for an element can be written as

$$\begin{Bmatrix} \left(t_b^1\right)_1 \\ \left(t_b^2\right)_1 \\ \left(t_b^3\right)_1 \end{Bmatrix} (1 - ck_s \tan\phi) - \begin{Bmatrix} \left(t_b^1\right)_2 \\ \left(t_b^2\right)_2 \\ \left(t_b^3\right)_2 \end{Bmatrix} (\tan\phi + ck_s) = 0 \,. \qquad \text{(B.41)}$$

After multiplying the above equation by

$$\int_{-1}^{+1} \{N_b\}\{N_b\}^{\mathrm{T}} \mid J_b \mid \mathrm{d}\zeta \,. \qquad \text{(B.42)}$$

It becomes

$$\left\{f_1^b\right\}(1 - ck_s \tan\phi) - \left\{f_2^b\right\}(\tan\phi + ck_s) = \{0\} \,. \qquad \text{(B.43)}$$

This above equation holds good at all nodes of the element. At the middle node say '*k*' (global node number), there is no contribution from the neighbouring elements and therefore, in terms of the global right hand side of the vector, Eq. (B.43) can be expressed as

$$\{F\}_{(d_p+2k-1)} (1 - ck_s \tan\phi) - \{F\}_{(d_p+2k)} (\tan\phi + ck_s) = \{0\}, \qquad \text{(B.44)}$$

where d_p is the total number of pressure variables. This Eq. (B.44) holds good at the end node also. Procedure for applying the condition (B.44) at the node '*k*' is as follows:

- Replace $(d_p + 2k - 1)^{\text{th}}$ row of global coefficient matrix [*K*] by the following linear combination: $(1 - ck_s \tan\phi)$ times $(d_p + 2k - 1)^{\text{th}}$ row of [*K*] – (tanα + ck_s) times $(d_p + 2k)^{\text{th}}$ row of [*K*].
- Make the $(d_p + 2k - 1)^{\text{th}}$ row of global right hand vector {*F*} zero.
- The velocity boundary condition at the node is applied by replacing $(d_p + 2k)^{\text{th}}$ row of [*K*] by Eq. (3.13).
- Make $(d_p + 2k)^{\text{th}}$ row of [*K*] zero.
- Set $(d_p + 2k, d_p + 2k - 1)^{\text{th}}$ element of [*K*] to $\tan\phi(d_p + 2k,\ d_p + 2k)^{\text{th}}$ element of [*K*] to 1.

- Make $(d_p + 2k)^{th}$ row of $\{F\}$ to zero.

The essential boundary conditions at the other boundaries are applied as follows:

- In the stiffness matrix, all the elements of row and columns corresponding to the specified degree of freedom excepting the diagonal term are made equal to zero.
- The diagonal term is replaced by unity.
- The right hand side vector element corresponding to the specified degree of freedom is replaced by the specified value and other elements are modified by subtracting from them the products of corresponding coefficient element and specified value.

After imposing the boundary condition as discussed above section, the final matrix equation (B.37) is solved iteratively by the Householder method, because the resulting matrix of the mixed formulation is ill-conditioned. Once the solution is obtained in the form of primary variables for nodal pressure and velocity for any assumed position of neutral point, the secondary variables like roll force, roll torque can be calculated. This calculation is termed as post-processing of the finite element method.

Appendix C

Procedure for Computing the Step Size (*h*)

The step size used in Eq. (4.11) is calculated using the procedure available in standard textbooks *viz*. [Balagurusamy, 2004]. In a quadratic approximation, using three neighbouring points x_0, x_1 and x_2, a function F_r can be expresses as

$$F_r = a_0 + a_1(x - x_0) + a_2(x - x_0)(x - x_1) + R_2 , \tag{C.1}$$

where R_2 is the reminder term given by

$$R_2 = \frac{f'''(\theta)}{3!}(x - x_0)(x - x_1)(x - x_2) . \tag{C.2}$$

where θ is the coordinate of some point in the interval containing x_0, x_1, x_2 and x. For $x_0 = x$, $x_1 = x+h$ and $x_2 = x+2h$, the truncation error in the derivative is given by

$$e_t = \frac{\mathrm{d}R_2}{\mathrm{d}x} = \frac{h^2 f'''(\theta)}{3}, \quad x \le \theta \le (x + h) , \tag{C.3}$$

The worst case round-off error is computed using Eq. (4.11) as

$$e_r = \frac{8e}{2h} = \frac{4e}{h} . \tag{C.4}$$

where e is the magnitude of the error. The worst case total error in the derivative, E_T is given by

$$E_T = \frac{h^2}{3} f'''(\theta) + \frac{4e}{h} . \tag{C.5}$$

The error will be the minimum when

$$\frac{\mathrm{d}E_T}{\mathrm{d}h} = \frac{2h}{3} f'''(\theta) - \frac{4e}{h^2} = 0. \tag{C.6}$$

Thus,

$$h^3 = \frac{6e}{f'''(\theta)}. \tag{C.7}$$

In the present thesis, initially the value of roll force is computed for three nearest points x_0, x_1 and x_2 using FEM code [Dixit and Dixit, 1996]. At a point $(x_0 + x_1)/2$, the value of roll force is obtained using FEM code and quadratic approximation method (Eq. C.1). Using the values of roll force obtained by these two methods, R_2 is computed as

$$R_2 = (F_r)_{\text{FEM}} - (F_r)_{\text{Quadratic approximation}}. \tag{C.8}$$

Using this R_2, the value of $f'''(\theta)$ in Eq. (C.2) is computed. Considering the 5% accuracy in the estimation of the roll force, error e may be assumed as

$$e = 0.05F_r \tag{C.9}$$

where F_r is the value of roll force (by quadratic approximation method) at a point $(x_0 + x_1)/2$. Thus, Eq. (C.7) may be written as

$$h^3 = \frac{6 \times 0.05F_r}{f'''(\theta)}. \tag{C.10}$$

Using Eq. (C.10), value of step size h is calculated. Same procedure is adpoted for computing partial derivative of roll torque with respect to to R/h_1, f and r. Note that $f'''(\theta)$ itself may depend on the step size *h*. Hence, a trial and error procedure may be required. The following example illustrates how $f'''(\theta)$ and finally step size may be calculated.

Example:

In the computation of step size for determining partial derivative of roll force with respect to R/h_1, first the values of roll force is obtained using the FEM code at three neighbouring points of R/h_1 as shown in Table C.1. In this computation of roll force

at different R/h_1, the values of friction and reduction are kept as 0.04 and 24 respectively. Note that here the assumed step size is 10.

Table C.1. The values of roll force at three different intervals of R/h_1

For reductions	Roll force by FEM (MN/m)
10	0.9060
20	1.2366
30	1.8629

Using the values from Table C.1, roll force at $R/h_1 = 15$ is computed by the quadratic approximation method and FEM code.

$$F_r = 1.0391 \text{ MN/m} \quad \text{(by approximation method).}$$

$$F_r = 1.0645 \text{ MN/m} \quad \text{(by FEM).}$$

Using Eq. (C.8), the reminder R_2 comes out as

$$R_2 = 0.0254 .$$

It was verified that this the maximum truncation error in the domain of interest. Putting this value of R_2 in Eq. (C.2), $f'''(\theta)$ is calculated as

$$0.0254 = \frac{f'''(\theta)}{3!}(15-10)(15-20)(15-30) .$$

Thus,

$$f'''(\theta) = 4.064 \times 10^{-4} .$$

Using this estimate of $f'''(\theta)$ in Eq. (C.9), optimum step size is computed.

$$h^3 = \frac{6 \times 0.05 \times 1.0391}{4.064 \times 10^{-4}},$$

This gives $h = 9.1541$ for R/h_1. It is very close to assumed step size of 10. Hence, based on the computations, optimum step size for R/h_1 is taken as 10. (If the assumed and obtained step sizes differ, the whole procedure is repeated with modified assumed step size. Thus, the procedure for obtaining the step size is

iterative. However, if a proper guess is used based on the experience, very few iterations are needed.) Similarly, the optimum value of step size for f and r is taken as 0.02 and 4 respectively.

Appendix D

Wanheim and Bay's Friction Model

In a non-sticking zone, the general relationship between interfacial shear stress and roll pressure can be expressed as,

$$\tau = f\ p\,. \tag{D.1}$$

In the case of Coulomb model, the coefficient of friction f is assumed to be constant. However, in the case of Wanheim and Bay's model, f depends on the normal pressure. The Wanheim and Bay's model is as follows [Wanheim and Bay, 1978]:

$$\tau = \begin{cases} f\ p & \text{for } p \le p' \\ \tau' + \left(m\sigma_Y/\sqrt{3} - \tau'\right)\left(1 - \exp\left(\dfrac{\left(p' - p\right)\tau'}{\left(m\sigma_Y/\sqrt{3} - \tau'\right)p'}\right)\right) & \text{for } p > p' \end{cases} \tag{D.2}$$

where τ' and p' are the tangential and the normal stresses at the limit of proportionality given by [Christensen *et al*., 1986]

$$\frac{\tau'}{\sigma_Y} = \frac{\left(1 - \sqrt{1-m}\right)}{\sqrt{3}}, \tag{D.3}$$

$$\sigma_Y = \frac{1 + \dfrac{\pi}{2} + \cos^{-1} m + \sqrt{1-m^2}}{\sqrt{3}\left(1 + \sqrt{1-m}\right)}, \tag{D.4}$$

and m is the friction factor related to the coefficient of friction by the relation:

$$f = \frac{m}{1 + \dfrac{\pi}{2} + \cos^{-1} m + \sqrt{1-m^2}}, \tag{D.5}$$

where σ_Y is the flow stress of the strip material.

Appendix E

Estimation of Friction Based on Measurement of Curvature

Salunkhe [2006] developed the inverse model of estimation of friction based on measurement of curvature. It is briefly described here. Let R be the measured radius of curvature, f^* be the coefficient of friction to be estimated, R_1 and R_2 be the radii of curvature corresponding to the lower and upper estimates of friction, f_1 and f_2 respectively. The radius of curvature is found to decrease with increasing coefficient of friction. The procedure consists of calculating the radius of curvature for a coefficient of friction, $f_m = (f_1 + f_2)/2$. Let this value of radius of curvature be equal to R_m. If $R_m > R$ then f^* must be lying between f_m and f_2, otherwise f^* lies between f_m and f_1. Again the new limits are set and the procedure is repeated in iterative manner till the required accuracy is obtained.

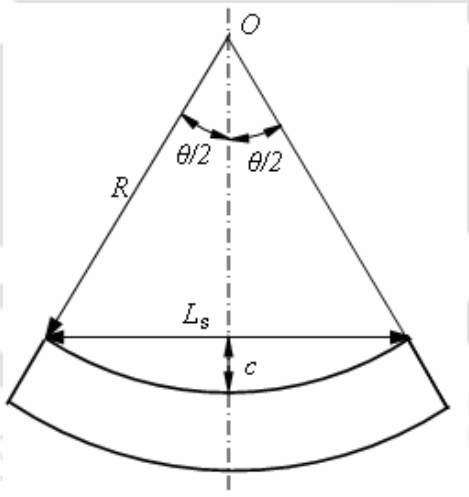

Figure E.1. Geometry of a curved strip

The value of the radius of curvature can be calculated by using the following relation [Knight *et al*., 2006]

$$R = \left(4c^2 + L_s^2\right)/8c, \tag{E.1}$$

where L_s and c are defined as shown in Fig. E.1. It is obvious that the value of radius of curvature depends on the accuracy to which c and L_s are calculated. Assuming that typically the value of L_s will be less than 0.3 m to accommodate the strip in a measuring table, and c to be more than 2 mm for ensuring proper accuracy in its measurement the radius of curvature should be less than 5.6 m. The speed mismatch should be decided accordingly.

In the simulation, the upper and lower roll radii are fixed at 350 mm. The material for the sheet to be rolled is assumed to be aluminium. An asymmetry in speed mismatch, of the order of V_A = 1.01 to V_A = 1.02 is created. The parameters varied are coefficient of friction and percentage reduction. The author reported that 8-10 iterations of the bisection method are required to get the coefficient of friction with an accuracy of 5×10^{-4}.

Publications from the Present Thesis Work

1. Gudur, P.P. and Dixit, U.S., (2008), A neural network-assisted finite element analysis of cold flat rolling, Engineering Applications of Artificial Intelligence, **21/1**, pp. 43–52.

2. Gudur, P.P. and Dixit, U.S., An application of fuzzy inference for studying the dependency of roll force and roll torque on process parameters in cold flat rolling, International Journal of Advanced Manufacturing, In Press, DOI 10.1007/s00170-008-1574-6.

3. Gudur, P.P. and Dixit, U.S., (2008), A combined finite element and finite difference analysis of cold flat rolling, Transactions of the American Society of Mechanical Engineers: Journal of Manufacturing Science and Engineering, **130**, **011007**, pp.1–6.

4. Gudur, P.P. and Dixit, U.S., Estimation and control of curvature of cold flat rolled sheets, 2nd International & 23rd All India Manufacturing Technology, Design and Research Conference, AIMTDR, Dec. 2008.

5. Gudur, P.P., Salunkhe, M.A. and Dixit, U.S., (2008), A theoretical study on the application of asymmetric rolling for the estimation of friction, International Journal of Mechanical Sciences, **50/2**, pp. 315–327. [Part of the work in this paper has been taken from Salunkhe, M.A., (2006), Analysis of cold flat asymmetric rolling process, M. Tech. Thesis, Indian Institute of Technology Guwahati].